Topographically enhanced cell culture systems to induce and monitor mechanobiology

Topographically enhanced cell culture systems to induce and monitor mechanobiology

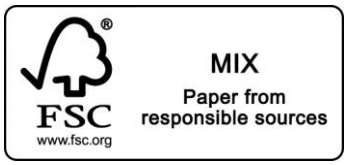

ISBN | 978-90-825680-6-6

Print | Gildeprint

Layout | NRM Beijer

The research presented in this dissertation was performed at the Department of Cell Biology-Inspired Tissue Engineering (cBITE), MERLN Institute for Technology-Inspired Regenerative Medicine, Maastricht University, The Netherlands.

This research was funded by the province of Limburg and the European Union´s Seventh Framework Program (FP7/2007-20013) STELLAR (Grant agreement no. 305436).

The printing of this dissertation was sponsored in part by the Netherlands society for Biomaterials and Tissue Engineering (NBTE).

Topographically enhanced cell culture systems to induce and monitor mechanobiology

DISSERTATION

to obtain the degree of Doctor at Maastricht University on the authority of the Rector Magnificus prof. dr. Rianne M. Letschert in accordance with the decision of the Board of Deans, to be defended in public on Friday the 13th of April 2018, at 16:00 hours

by

Nick Ronaldus Maria Beijer

Born on the 10th of April 1989 in Zaanstad

Promotor
Prof. Dr. Jan de Boer

Co-promotor
Dr. Roman Truckenmüller

Assessment committee

Prof. Dr. Pamela Habibović (voorzitter)

Prof. Dr. Marileen Dogterom (Technische Universiteit Delft)

Prof. Dr. Pascal Jonkheijm (Universiteit Twente)

Dr. Tim Welting

PARANIMFEN

Emo van Halsema

Marloes Kamphuis

Contents

⠠⠞⠓⠑ ⠠⠟⠥⠊⠉⠅ ⠃⠗⠕⠺⠝ ⠋⠭ ⠚⠥⠍⠏⠎ ⠕⠧⠑⠗ ⠞⠓⠑ ⠇⠁⠵⠽ ⠙⠕⠛

Chapter 1

General introduction

From the native microenvironment of cells *in vivo* towards artificial conditions *in vitro*

Cells in the human body are situated in a three dimensional microenvironment which is full of stimuli and tissue specific features. Here, cells can sense many different aspects of this unique surrounding, upon which they can change functions and processes. They can e.g. sense the chemical composition of the host extra cellular matrix, the factors secreted by neighboring cells or delivered via the vascular system, and the mechanical properties of their direct surrounding[1,2]. Stimuli from the extra cellular space can be roughly divided into two groups of triggers: chemical or mechanical. Chemical factors are e.g. cytokines, growth factors, drugs, metabolites and extra cellular matrix components. Mechanical properties that can stimulate cells include tissue stiffness, shear stress and cellular confinement.

To study – and manipulate – molecular processes in cells, scientist strive for a fully controlled cell culture environment. For adherent cell types, such an *ex vivo* environment is often created by culturing cells on tissue culture plastics in the presence of metabolic precursors, growth factors and small molecules. Some growth factors or small molecules can initiate signal transduction cascades with a very specific effect, depending on the cell type. For instance, dexamethasone can induce the expression of the early osteogenesis marker alkaline phosphatase in human mesenchymal stem cells[3], gadolinium can affect the activity of stretch-activated channels[4], and blebbistatin inhibits myosin, thus disrupting cytoskeletal processes[5]. Pharmaceutical activation of signal transduction cascades or activation and inhibition of specific processes in cells are at the root of the pharmaceutical sciences and has given a tremendous amount of control in the culture of (stem) cells.

Engineered biomaterials to control cell behavior

Besides control of cell physiology by chemical compounds, it became evident over the past 30 years that the materials on which cells grow can influence cell behavior as well[6,7]. So far, cell behavior has been correlated to multiple biomaterial properties. As seen in the native microenvironment of cells, the chemistry of substrates[8], its stiffness[9] and surface structure[10], and resulting cellular confinement[11] are found to instruct cell behavior *in vitro*. The past decade, cell-material interaction became of great interest and the field of mechanobiology specifically studied cell behavior which is controlled by physical stimuli. Seminal papers in this field exemplify the effect of different types of triggers in strong phenotypic changes. Engler et al. described that soft gels induce neurogenic differentiation of hMSCs, whereas stiff gels induce osteogenesis[12]. McBeath et al. demonstrated that hMSCs on small adhesive islands remain rounded and favor adipogenesis over osteogenesis, a trend which was found *vice versa* on large adhesive islands which created flat cells[13]. Mei et al. showed the effect of polymer chemistry on clonal growth of human pluripotent stem cells[14]. And Dalby et al. used

a defined surface structure to induce osteogenic differentiation[10]. All these manuscripts point at a precise correlation between material parameters and cell differentiation. The vast majority of papers published on cell-material interaction describe how materials induce alterations in cell phenotypes, but little is known about underlying molecular mechanisms of action. To look into this in more detail, it is important to realize that the signal from the biomaterials can enter cells through several initial responses (Figure 1). For example, materials may act through differential cell adhesion complex composition and clustering, through altered gating of stretched activated channels but may also act through receptor availability. These events can subsequently initiate a variety of molecular processes, in the form of altered protein activity and translocation, and significant changes in the cell cytoskeleton. Importantly, all these signaling cascades are induced at the same time and to make it even more complex, extensive crosstalk exists between signaling cascades. To conclude, one is not able to model a canonical pathway of mechanotransduction at this moment, with the knowledge currently available. Or in other words: unlike growth factor mediated signal transduction cascades which act through a canonical, standard, relay of molecular signals, mechanotransduction is a combinatorial signal input in cells.

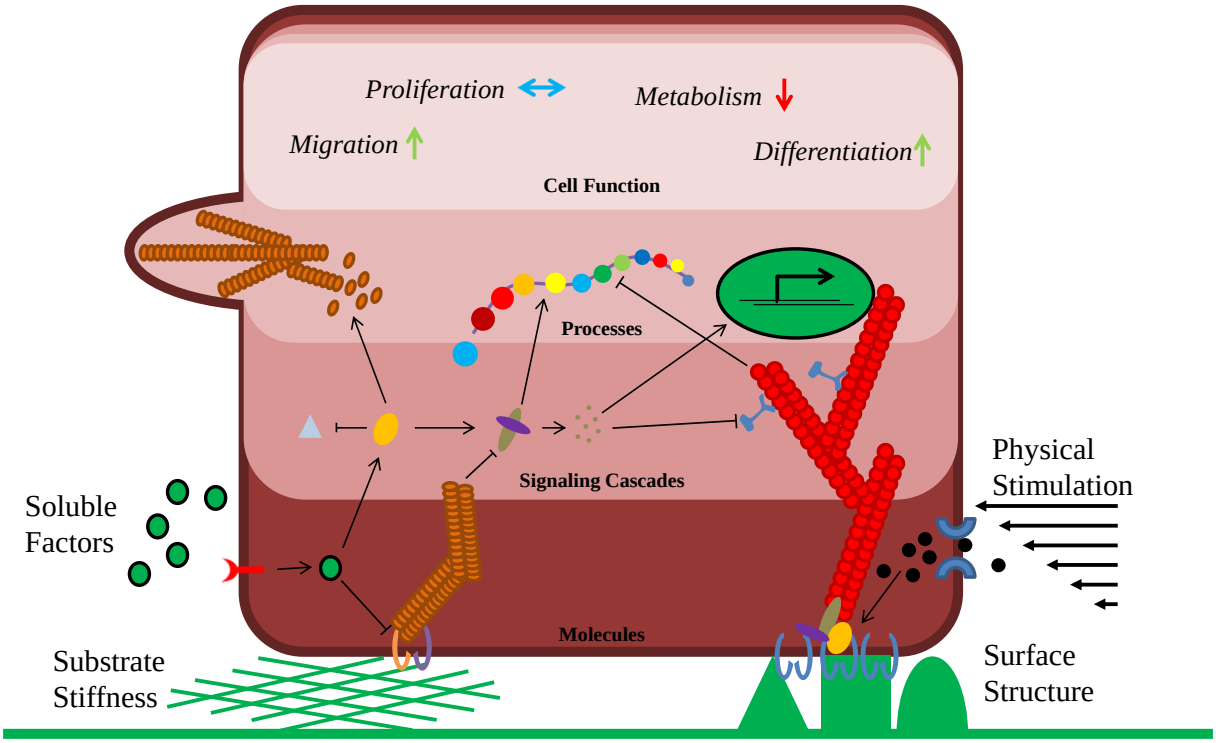

Figure 1: Canonical pathway of mechanotransduction. The physical environment of cells contains many different properties which can be sensed by cells. Cell-material interactions initiate possibly a wide variety of molecular signaling cascades which can result in dramatic changes of cellular functions.

Screening bioactive surface topographies

Our group studies the effect of surface topography on cell behavior and tries to unravel the underlying mechanisms of mechanotransduction. To do so, we developed a high-throughput screening tool, designated the TopoChip[15]. Using the TopoChip we can screen micrometer-scale defined surface topographies for their cell instructive potency[16–19]. Furthermore, the TopoChip platform allows us to discover bioactive surface topographies, and more importantly, by exploring the full design space, it allows us to study the interaction with the underlying molecular mechanisms.

Surface topographies on the TopoChip are created by combining circles, squares and rectangles (Figure 2A) into topographical features (Figure 2B) that vary in size, density and roundness. These topographical features are placed in an arrayed order in 290 × 290 µm TopoUnits (Figure 2C). In total, 2176 TopoUnits with unique surface topographies are placed in duplicate on a 2 × 2 cm polymer based chip to create the TopoChip (Figure 2D). So far, we observed dramatic changes in cell morphology and behavior of cells that were cultured on topographically enhanced substrates. However, similar to other material platforms, the underlying molecular mechanisms behind these phenotypes remain to be elucidated. In this thesis, we use the TopoChip platform to study the underlying processes in mechanotransduction. Furthermore, we introduce additional cell culture tools within the TopoChip platform in order to obtain different and valuable data on cell-material interaction.

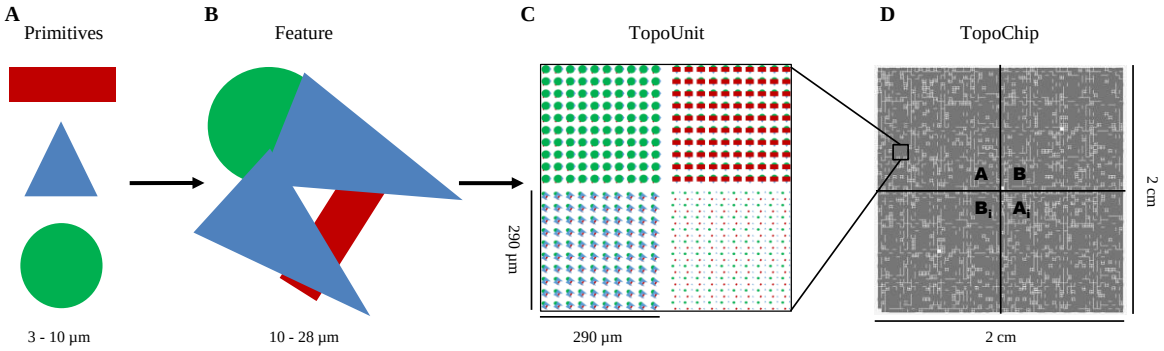

Figure 2: The TopoChip platform. A) Primitive shapes used to create the (B) topographical features which will create the (C) TopoUnits when distributed in an arrayed manner. D) The TopoChip contains 2176 unique surface topographies in duplicate and 4 unpatterned TopoUnits.

Outline of this thesis

The most efficient mechanobiological systems are found in nature, in a wide variety of appearances. Using such powerful mechanobiological principles as examples can give rise to great inspiration in the development of engineered biomaterials. **Chapter 2** leads biomedical

engineers through the great variety of systems "ready-to-react to mechanical stimuli" by using a colorful selection of natural systems. Furthermore, state-of-the-art technologies will be highlighted and linked to the natural mechanobiological systems in terms of opportunities for meaningful read-outs and material development.

Designing biomaterials to fully control cell behavior requires a thorough understanding of the underlying mechanisms of action. Stimuli received by cells via cell-material interactions are diverse and can result in a great variety of complex molecular signaling cascades. In order to unravel these mechanisms, *in vitro* cell culture systems are needed which allow a high degree of control over very specific material properties. So far, taking full advantage of state-of-the-art technologies allowed biomedical engineers to develop magnificent biomaterials, however, continuation of innovation is essential to obtain an even greater level of control over the material properties. Similarly important is the translation of the material advancements into insightful mechanobiological research. The goal should be to gain detailed knowledge on acting mechanisms, and not settle with proof of principle experiments or generic phenotypic observations.

The first experimental chapter in this thesis, **chapter 3**, touches upon the underlying mechanisms of mechanotransduction induced by surface topography. In previous work using the TopoChip, we identified a surface topography characterized by its osteogenic effect on human bone marrow-derived mesenchymal stem cells[17]. This defined titanium coated surface topography was found to stimulate both the expression of early osteogenesis marker alkaline phosphatase, and mineralization of the secreted extra cellular matrix. We used a holistic approach to reveal the mechanobiology-based underlying mechanisms by which physical stimuli from the defined surface topography induces osteogenesis. Using various molecular tools, we studied the effect of the osteogenic topography on focal adhesion complex formation and cytoskeleton remodeling, the early activation of mechanosensitive proteins, the gene expression profiles, and epigenetic component in differentiation in those cells.

Dramatic changes in cell morphology and behavior, as observed in cells exposed to TopoChip-derived surface topographies, occur immediately upon cell attachment. During the first 24 hours of cell-material interaction, the cells actively adapt to their new environment. In **chapter 4**, we followed the adaptation of cells based on basic cellular functions, such as: cell size regulation, metabolic activity, and cell cycle progression. Furthermore, we were able to link this adapted phenotype with the reactivity on anti-cancer drugs.

Besides the TopoChip platform, numerous other tools have been developed to study cell-material interaction. These platforms can be roughly divided in two types: high-throughput and low-throughput. Both groups have their inseparable positive and negative features. While low-throughput systems allow the usage of a wealth of molecular tools, they cannot be used to generalize the design space of the studied material properties due to the relative small variations. On the other hand, high-throughput platforms allow studying the full design space,

however, are often limited to less informative imaging-based read-outs. Therefore, the need for a tool to study cell-material interaction in a rational set-up in high-throughput available for all molecular biology assays was evident. The TopoWellPlate offers this potential. In **chapter 5**, we developed the TopoWellPlate in a multistep cleanroom process and show its potency as a screening tool available for molecular biology using a proof of principle assay on metabolic activity.

The next step was to introduce the TopoWellPlate in a clinically more relevant context and to test its potential as screening tool. Mesenchymal stem cells from different sources are used – or assessed for potential usage – for transplantation purposes in various disease models. One example is the application of kidney derived cells in chronic kidney diseases, where these stromal cells are used for their trophic activity. We envisioned a pre-transplantation cultivation of these cells on surface topographies in order to 'train' the cells for specific secretion profiles desirable in the context of its application. In **chapter 6**, we used the TopoWellPlate to screen surface topographies for differential cytokine secretion profiles. Using both kidney and bone marrow derived stromal cells, we studied the effect of surface topography induced differences in secretion profiles.

Biomaterials enhanced with micrometer-scale surface topographies manipulate cells in various ways. Eye-catching changes in cell morphology are already intriguing in itself; however, this comes with e.g. dramatic changes in membrane stretch and protein distribution. Scaling down from micrometer towards nanometer-scaled surface topographies will introduce a complete new way of cell-material interactions. Here, sub-micrometer-sized defined surface topographies are able to manipulate cells more on a molecular level directly. In **chapter 7**, we introduce the NanoTopoChip, a similar high-throughput screening tool as the normal TopoChip, only using nanometer-scale defined surface topographies instead of micrometer-scale. Using the NanoTopoChip we screened U2OS cells to study the potency of these miniature versions of the TopoChip platform surface topographies to change their behavior. **Chapter 8** contains a general discussion on cell-material interaction research. Here, we discuss a variety of topics as covered in this thesis, and furthermore discuss the development of novel materials and analytic tools as envisioned future directions for cell-surface topography research.

One of the novelties introduced in this thesis is the surface topography enhanced cell culture plate. Where *in vitro* well-plate-based cell cultures are normally performed on unpatterned – flat – polystyrene tissue culture plastics, we have shown the potential of surface topography in various cell models. In **chapter 9**, we discuss the potential societal impact and valorization opportunities of topographically enhanced cell culture plates in laboratories around the globe.

References

1. Watt, F. M. Out of Eden: Stem Cells and Their Niches. *Science* **287,** 1427–1430 (2000).

2. Discher, D. E. Tissue Cells Feel and Respond to the Stiffness of Their Substrate. *Science* **310,** 1139–1143 (2005).

3. Jaiswal, N., Haynesworth, S. E., Caplan, A. I. & Bruder, S. P. Osteogenic Differentiation of Purified , Culture-Expanded Human Mesenchymal Stem Cells In Vitro. *J. Cell. Biochem.* **64,** 295–312 (1997).

4. Hamill, O. P. & McBride, D. W. J. The pharmacology of mechanogated membrane ion channels. *Pharmacol Rev* **48,** 231–252 (1996).

5. Straight, A. F. *et al.* Dissecting Temporal and Spatial Control of Cytokinesis with a Myosin II Inhibitor. *Science* **299,** 1743–1747 (2003).

6. Watt, F. M., Jordant, P. W. & Neillt, C. H. O. Cell shape controls terminal differentiation of human epidermal keratinocytes. *Proc Natl Acad Sci U S A* **85,** 5576–5580 (1988).

7. Curtis, A. & Wilkinson, C. Topographical control of cells. *Biomaterials* **18,** 1573–1583 (1997).

8. Lutolf, M. P. *et al.* Synthetic matrix metalloproteinase-sensitive hydrogels for the conduction of tissue regeneration: engineering cell-invasion characteristics. *Proc. Natl. Acad. Sci. U. S. A.* **100,** 5413–8 (2003).

9. Swift, J. *et al.* Nuclear lamin-A scales with tissue stiffness and enhances matrix-directed differentiation. *Science* **341,** 975–990 (2013).

10. Dalby, M. J. *et al.* The control of human mesenchymal cell differentiation using nanoscale symmetry and disorder. *Nat. Mater.* 997–1003 (2007). doi:10.1038/nmat2013

11. Ermis, M., Akkaynak, D., Chen, P., Demirci, U. & Hasirci, V. A high throughput approach for analysis of cell nuclear deformability at single cell level. *Sci. Rep.* **6,** 36917 (2016).

12. Engler, A. J., Sen, S., Sweeney, H. L. & Discher, D. E. Matrix Elasticity Directs Stem Cell Lineage Specification. *Cell* **126,** 677–689 (2006).

13. Mcbeath, R., Pirone, D. M., Nelson, C. M., Bhadriraju, K. & Chen, C. S. Cell Shape , Cytoskeletal Tension , and RhoA Regulate Stem Cell Lineage Commitment. *Dev. Cell* **6,** 483–495 (2004).

14. Mei, Y. *et al.* Combinatorial development of biomaterials for clonal growth of human pluripotent stem cells. *Nat. Mater.* **9,** 768–778 (2010).

15. Unadkat, H. V *et al.* An algorithm-based topographical biomaterials library to instruct cell fate. *Proc. Natl. Acad. Sci.* **109,** 5905–5905 (2012).

16. Reimer, A., Vasilevich, A., Hulshof, F. & Viswanathan, P. Scalable topographies to support proliferation and Oct4 expression by human induced pluripotent stem cells. *Sci. Rep.* 1–8 (2016). doi:10.1038/srep18948

17. Hulshof, F. F. B. *et al.* Mining for osteogenic surface topographies: In silico design to in vivo osseo-integration. *Biomaterials* **137,** 49–60 (2017).

18. Hulsman, M. *et al.* Analysis of high-throughput screening reveals the effect of surface topographies on cellular morphology. *Acta Biomater.* **15,** 29–38 (2015).

19. Le, B. Q. *et al.* Micro-Topographies Promote Late Chondrogenic Differentiation Markers in the ATDC5 Cell Line. *Tissue Eng Part A* **23,** 458–469 (2017).

⠞⠕⠏⠕⠛⠗⠁⠏⠓⠊⠉⠁⠇⠇⠽ ⠑⠝⠓⠁⠝⠉⠑⠙ ⠉⠑⠇⠇ ⠉⠥⠇⠞⠥⠗⠑ ⠎⠽⠎⠞⠑⠍⠎ ⠞
⠕⠏⠕⠛⠗⠁⠏⠓⠊⠉⠁⠇⠇⠽ ⠑⠝⠓⠁⠝⠉⠑⠙ ⠉⠑⠇⠇ ⠉⠥⠇⠞⠥⠗⠑ ⠎⠽⠎⠞⠑⠍⠎ ⠞⠕
⠏⠕⠛⠗⠁⠏⠓⠊⠉⠁⠇⠇⠽ ⠑⠝⠓⠁⠝⠉⠑⠙ ⠉⠑⠇⠇ ⠉⠥⠇⠞⠥⠗⠑ ⠎⠽⠎⠞⠑⠍⠎ ⠞⠕
⠕⠛⠗⠁⠏⠓⠊⠉⠁⠇⠇⠽ ⠑⠝⠓⠁⠝⠉⠑⠙ ⠉⠑⠇⠇ ⠉⠥⠇⠞⠥⠗⠑ ⠎⠽⠎⠞⠑⠍⠎ ⠞⠕ ⠊
⠗⠁⠏⠓⠊⠉⠁⠇⠇⠽ ⠑⠝⠓⠁⠝⠉⠑⠙ ⠉⠑⠇⠇ ⠉⠥⠇⠞⠥⠗⠑ ⠎⠽⠎⠞⠑⠍⠎ ⠞⠕ ⠊⠝⠙
⠏⠓⠊⠉⠁⠇⠇⠽ ⠑⠝⠓⠁⠝⠉⠑⠙ ⠉⠑⠇⠇ ⠉⠥⠇⠞⠥⠗⠑ ⠎⠽⠎⠞⠑⠍⠎ ⠞⠕ ⠊⠝⠙⠥⠉
⠊⠉⠁⠇⠇⠽ ⠑⠝⠓⠁⠝⠉⠑⠙ ⠉⠑⠇⠇ ⠉⠥⠇⠞⠥⠗⠑ ⠎⠽⠎⠞⠑⠍⠎ ⠞⠕ ⠊⠝⠙⠥⠉⠑
⠁⠇⠇⠽ ⠑⠝⠓⠁⠝⠉⠑⠙ ⠉⠑⠇⠇ ⠉⠥⠇⠞⠥⠗⠑ ⠎⠽⠎⠞⠑⠍⠎ ⠞⠕ ⠊⠝⠙⠥⠉⠑ ⠁⠝
⠇⠇⠽ ⠑⠝⠓⠁⠝⠉⠑⠙ ⠉⠑⠇⠇ ⠉⠥⠇⠞⠥⠗⠑ ⠎⠽⠎⠞⠑⠍⠎ ⠞⠕ ⠊⠝⠙⠥⠉⠑ ⠁⠝⠙
⠽ ⠑⠝⠓⠁⠝⠉⠑⠙ ⠉⠑⠇⠇ ⠉⠥⠇⠞⠥⠗⠑ ⠎⠽⠎⠞⠑⠍⠎ ⠞⠕ ⠊⠝⠙⠥⠉⠑ ⠁⠝⠙ ⠍
⠑⠝⠓⠁⠝⠉⠑⠙ ⠉⠑⠇⠇ ⠉⠥⠇⠞⠥⠗⠑ ⠎⠽⠎⠞⠑⠍⠎ ⠞⠕ ⠊⠝⠙⠥⠉⠑ ⠁⠝⠙ ⠍⠕⠝
⠓⠁⠝⠉⠑⠙ ⠉⠑⠇⠇ ⠉⠥⠇⠞⠥⠗⠑ ⠎⠽⠎⠞⠑⠍⠎ ⠞⠕ ⠊⠝⠙⠥⠉⠑ ⠁⠝⠙ ⠍⠕⠝⠊⠞
⠝⠉⠑⠙ ⠉⠑⠇⠇ ⠉⠥⠇⠞⠥⠗⠑ ⠎⠽⠎⠞⠑⠍⠎ ⠞⠕ ⠊⠝⠙⠥⠉⠑ ⠁⠝⠙ ⠍⠕⠝⠊⠞⠕⠗
⠑⠙ ⠉⠑⠇⠇ ⠉⠥⠇⠞⠥⠗⠑ ⠎⠽⠎⠞⠑⠍⠎ ⠞⠕ ⠊⠝⠙⠥⠉⠑ ⠁⠝⠙ ⠍⠕⠝⠊⠞⠕⠗ ⠍
⠉⠑⠇⠇ ⠉⠥⠇⠞⠥⠗⠑ ⠎⠽⠎⠞⠑⠍⠎ ⠞⠕ ⠊⠝⠙⠥⠉⠑ ⠁⠝⠙ ⠍⠕⠝⠊⠞⠕⠗ ⠍⠑⠉
⠑⠇⠇ ⠉⠥⠇⠞⠥⠗⠑ ⠎⠽⠎⠞⠑⠍⠎ ⠞⠕ ⠊⠝⠙⠥⠉⠑ ⠁⠝⠙ ⠍⠕⠝⠊⠞⠕⠗ ⠍⠑⠉⠓⠁
⠇ ⠉⠥⠇⠞⠥⠗⠑ ⠎⠽⠎⠞⠑⠍⠎ ⠞⠕ ⠊⠝⠙⠥⠉⠑ ⠁⠝⠙ ⠍⠕⠝⠊⠞⠕⠗ ⠍⠑⠉⠓⠁⠝⠕
⠉⠥⠇⠞⠥⠗⠑ ⠎⠽⠎⠞⠑⠍⠎ ⠞⠕ ⠊⠝⠙⠥⠉⠑ ⠁⠝⠙ ⠍⠕⠝⠊⠞⠕⠗ ⠍⠑⠉⠓⠁⠝⠕⠃
⠥⠇⠞⠥⠗⠑ ⠎⠽⠎⠞⠑⠍⠎ ⠞⠕ ⠊⠝⠙⠥⠉⠑ ⠁⠝⠙ ⠍⠕⠝⠊⠞⠕⠗ ⠍⠑⠉⠓⠁⠝⠕⠃⠊⠕
⠞⠥⠗⠑ ⠎⠽⠎⠞⠑⠍⠎ ⠞⠕ ⠊⠝⠙⠥⠉⠑ ⠁⠝⠙ ⠍⠕⠝⠊⠞⠕⠗ ⠍⠑⠉⠓⠁⠝⠕⠃⠊⠕⠇⠕
⠗⠑ ⠎⠽⠎⠞⠑⠍⠎ ⠞⠕ ⠊⠝⠙⠥⠉⠑ ⠁⠝⠙ ⠍⠕⠝⠊⠞⠕⠗ ⠍⠑⠉⠓⠁⠝⠕⠃⠊⠕⠇⠕⠛⠽

Chapter 2

Mechanobiology for engineers:

Taking a closer look at natural systems

Nick R.M. Beijer & Jan de Boer

Abstract

Nearly every cell, tissue and organism is able to respond to physical forces, however, this knowledge is hardly used when studying mechanobiology for tissue engineering. In this chapter we sketch parallels between molecular engineering of mechanoactive materials and natural biological systems. By looking at ready-to-respond mechanoresponsive systems and underlying mechanisms we illustrate nature's solutions for mechanobiological problems at multiple length scales. There is a fast growing body of literature on biomaterial induced mechanotransduction, however, the biological meaning of the created phenotypes remains often unclear. Pharmacology often tries to interfere with the molecular pathology, e.g. produces small molecules that inhibit the enzymatic activity of a tumor inducing kinase by binding to its enzymatic pocket. In mechanobiology, such biomimetic approaches are rare, often because the underlying mechanisms are unknown but also because mechanotransduction occurs at different length scales. Here, we propose to use the wealth of mechanobiological examples from nature as example to further develop state-of-the-art technological platforms used to study cell-biomaterial interaction. In this way, materials can be created in which specific technological principles serve as a base for specific interactions with biologically systems and meaningful read-outs. We expect the combination of both technology and biological models to fuel development of next-generation, out-of-the-box cell culture platforms to study mechanobiology.

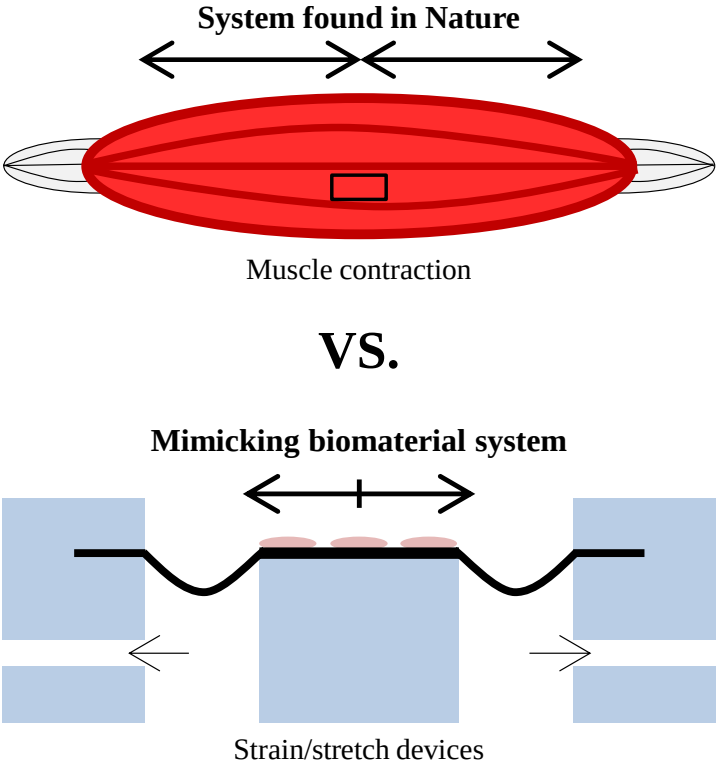

Introduction

The major issue dealt with in this chapter is: "How to take inspiration from natural mechanical molecular mechanisms and use microfabrication and chemistry to create mechanically bioactive biomaterials?" Stunning technological advancements in the modern world around us find applications in numerous research fields, including the field of mechanobiology. A wide variety of cell culture platforms have been developed to mimic the directive microenvironments of cells *in vivo*, or at least, to allow researchers to fully control one parameter in the system. Unfortunately, the relation between the biomaterial design parameter used and the biological read-out measured are often very remote and appear as a black box. For instance, stiffness relates to stem cell differentiation[1]. But which molecular interactions within the polymer define this stiffness and to which cellular components is this biomaterial property transferred to elicit a response, which ultimately results in differentiation? Therefore, we propose to open our eyes again for the wonderful nature around us. Nearly all living entities have mechanisms able to react to mechanical stimuli from their direct environment. Proteins, cells and tissues are often able to sense the mechanical properties of its surrounding, which can subsequently trigger processes across all these different length scales (Figure 1). The underlying mechanisms are often initiated at the molecular level, typically in the shape of protein structures (e.g. stretch-activated calcium channel) or supramolecular structures (e.g. hairs in the ears responding to sounds waves).

The first biomaterial pioneers started working on mechanobiology around 30 years ago, and used materials that were poorly characterized in terms of the cells' microenvironment[2,3]. Today, technological advancements brought us biomaterials with complex sets of properties, however, at the cellular interface often chemically and mechanically still poorly defined. A major deliverable in the field of mechanobiology is to design biomaterials potent to direct tissue regeneration. In most cases this means that the engineered biomaterial should provide specific cues to cells and its surrounding tissue which results in desired cell behavior for regeneration of damaged tissue.

Material platforms are often engineered from the perspective of 'pushing the boundaries of technical possibilities', and only broadly justified in biological terms. Typically, these platforms are tested by exposing cells to the materials, and the phenotypic tests which are performed do not strictly relate to the design itself at the molecular level. This approach led already to the observation of numerous potential changes in cell behavior. Many comprehensive reviews[4–6] cover these findings (coming from selections of biomaterial platforms), in order to create a coherent story of cellular responses to mechanical stimuli. However, only very little is currently known about the underlying molecular mechanisms of mechanotransduction activated by these biomaterials. Overall, many uncertainties remain about the specific parameters that result in a phenotypic change and involved molecular signaling cascades. Inspired by the successes in bioactive material engineering, we hope that nature's colorful ways of dealing with mechanical stimuli can be used as a source of

inspiration for further development of biomaterial systems. Mechanotransduction found in nature gives a wealth of examples on processing a wide variety of mechanical stimuli. Here, a tremendous number of specifically targeted molecular mechanisms result in effective solutions to mechanobiological challenges.

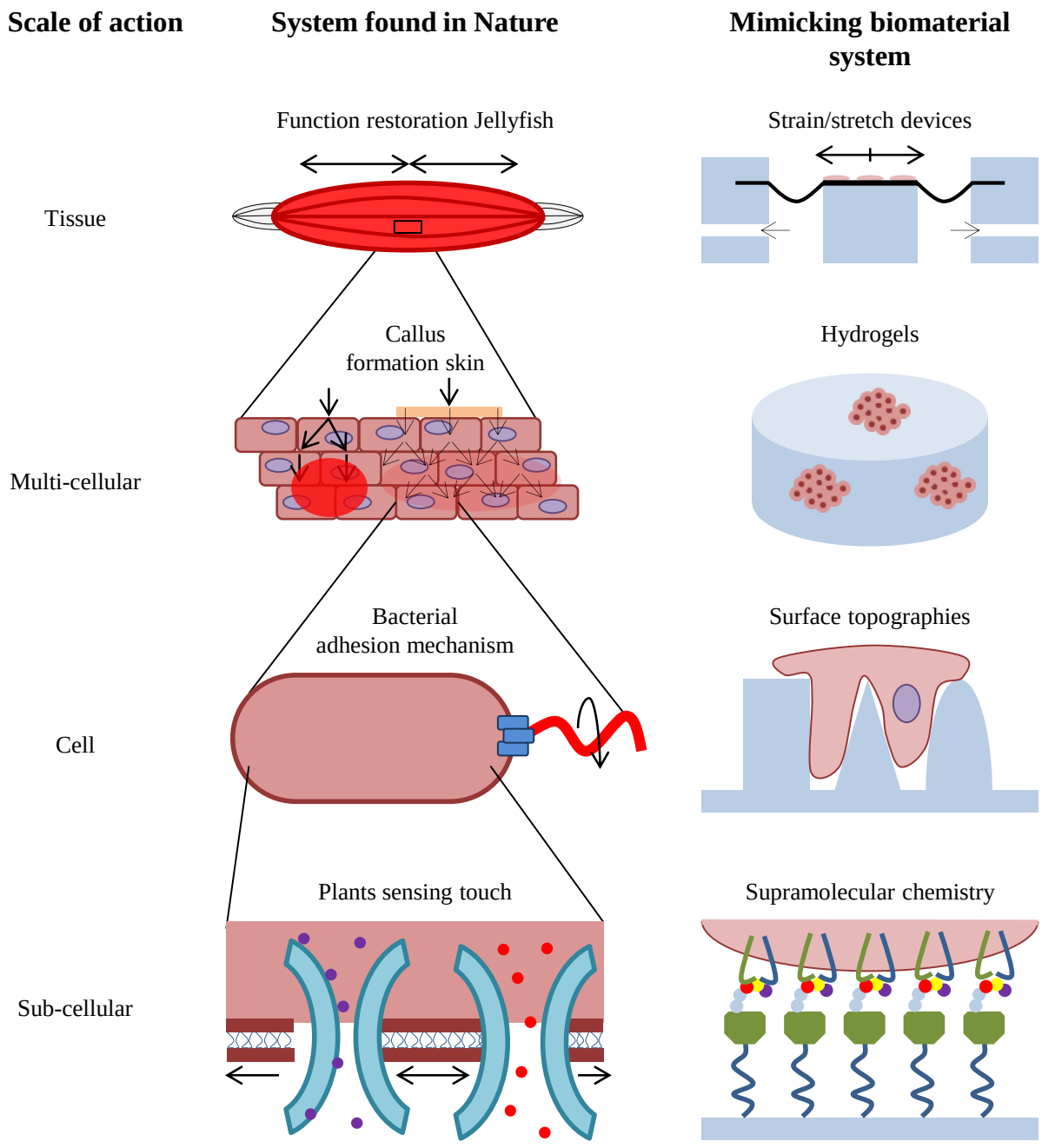

Figure 1: Mechanical forces act on all living entities, and on different length scales such as: tissues, multicellular organizations, individual cells and specific molecules. Besides the stunning examples from nature (middle column), in which mechanical stimulation acts on these different scales, we also see engineered biomaterials (right column) interacting at the same levels.

In this chapter we sketch parallels between molecular engineering of mechanoactive materials and natural biological systems with a well-described function to illustrate how nature has solved the mechanical demands at multiple length scales. We aim to look outside the framework of the current usage of state-of-the-art biomaterial platforms, and describe an approach on how to use these systems to study biological more meaningful mechanobiological models.

Mechanobiological models found in nature

As material engineers, we investigate the response of cells and tissues to mechanical signals induced by e.g.: fluid flow[7], hydrostatic pressure[8], stretching[9], substrate surface organization[10,11] or material stiffness[1]. Many of these phenomena are relevant in normal physiology of organisms. Think for instance about Wolff's law on remodeling of bone in response to mechanical loading[12], or the formation of callus on the palm of your hands when frequently used[13]. To be able to fine-tune our material systems, we have to understand *what* a cell actually feels and *how* it does it. Which cells feel the mechanical load in the palm of your hand, does it feel hydrostatic pressure or sheer, and which molecule is able to sense this? Relevant questions if we want to mimic nature on a chip.

Sensing the environment

The mechanical nature of the direct environment of organisms has a great impact on their interactions: from basic support towards complete control over behavior, and on a scale from meters to micrometers. The information relayed by a mechanical stimulus greatly depends on the mechanisms by which it is detected and processed. These mechanisms take mainly place on a molecular level, and there are numerous models known to describe the effect of the stimulus on the transducing receptor. Membrane stretching, intercellular fluid pressure, receptor-ligand binding, enzymatic activity and conformational changes of cellular antennae are physiological phenomena initiating signal transduction upon mechanical stimulation.

The human body

In daily life, we are constantly moving and purposely positioning our body parts. Within the musculoskeletal system there are various receptors to monitor this activity. The feedback provided to the central nervous system creates a sense of movement and position (proprioception). This, for instance, allows us to walk on ice. Mechanical information is generated and processed in the same way as the other signals processed by the somatosensory system, e.g.: mechanical deformation, pressure, temperature, sound, and light. The

somatosensory system perceives a signal and is linked, via neurons, to the central nervous system[14]. Activation of these specialized cells often starts with the initiation of an action potential. Molecular and cellular cognition starts with a physical or chemical stimulus that manipulates specialized protein-based receptors in order to create a chemical (neurotransmitters) or electrical (action potential) signal to be interpreted for feedback by the brain.

Multiple types of mechanoreceptors are known within the somatosensory system and can be found all over the body. Within muscles two specialized types of receptors are known: (i) the muscle spindle and (ii) the Golgi tendon organ (n.b.: Nobel Prize winner Camillo Golgi (1824-1936) was active in many aspects of biology. Besides working on the central nervous system, he is best-known from his work on the Golgi apparatus). Only together, the muscle spindles and the Golgi tendon organs – that are situated around joints – gather enough information to enable the central nervous system to exactly place the body part of interest. Moreover, both passive and active muscle movements are measured by the designated specialized and well placed mechanoreceptors. But how does it work?

Passive movement of the joint causes elongation of the muscle, which is captured by the muscle spindle. Wrapped around the intrafusal muscle fiber lays the annulospiral sensory neuron which is activated upon stretching the sensory endings of the afferent axons. In un-stretched conditions, mechanosensitive membrane pore protein complexes have a closed configuration within the cell membrane. Three major families of channels are proposed to be mechanosensory in the muscle spindle: degenerin epithelial Na^+ channels (DEG/ENaC), transient receptor potential (TRP), and piezos[15]. Upon elongation of the muscle, the cell membrane of the sensory axon is stretched, causing a conformational change in the tertiary structure of the membrane pore proteins. By altering the protein structure the membrane pore opens, allowing the influx of Na^+ and Ca^+ ions. This ion influx causes a depolarization of the terminal and spreads electrotonically towards the narrower nerve region where it opens voltage-activated channels (Na^+, Ca^+, K^+), leading to increased action potential firing[16,17]. This signal is conveyed to, and processed by the brain.

A similar sensing mechanism is used by the Golgi tendon organ, only the activation is different here. Active movement of joints occurs as a result of muscle fiber contractions. The force generated by the muscle fibers is transmitted via the musculo-tendinous boundaries into the tendon tissue. Tendon tissue is rich in collagen fibers which are loosely configured in rest, but directionally moved into straight stretched bundles upon muscle contraction. Within the tendon tissue - in between the woven collagen fibers - are the Golgi tendon organs. These mechanosensory cells are providing information on active muscle movement to the central nervous system. Stretching of collagen fibers by muscle contraction will tighten the woven collagen structure which results in an increased pressure on the Golgi tendon organ. Thus, a different trigger (stretching versus squeezing) leading to the activation of the same

responder[18–20]. The combination of both specialized sensors provides information to the brain on both position and movement, and are thus solely triggered by mechanical cues.

It is important to realize that the mechanoactive effect is initiated by activation of the stretch activated channels, but leading to a cascade of signaling. As such, the whole system is 'ready-to-react'. This is typical for biological systems and can be used as a design principle. For example, in previous work, we used embryonic stem cells (ESCs) for bone tissue engineering, but noticed that the cells failed to form bone tissue, even though we successfully differentiated them in to osteoblast. However, when we differentiated ESCs into chondrocytes *in vitro* prior to implantation, the construct was able induce bone formation. In this case, the cells needed a tweak – chondrogenesis – before they were able to execute the rest of their morphogenetic program[21].

Plants closing upon touch

Many plants are known to respond to mechanical stimulation, and environmentally altered morphogenesis in plants is seen widely. For example, shorter and more robust plants with increased quantities of support tissue will be developed when exposed to mechanical stimuli such as wind. Furthermore, roots will change direction of growth once an obstacle blocks their path, and by this, find their way around rocks in soil[22]. Mechanoperception in plants is known for more than a century already, however, only recently the underlying mechanisms became of more interest. Here, "movement upon touch" is an extraordinary example which is only observed in a few species.

The fast folding of the leaflets of the *Mimosa Pudica*, alias the shy plant (https://www.youtube.com/watch?v=g0LFBM3hOLs), can startle herbivores and make it seem less appealing to eat. Mechanoperception at the leaflets is proposed to occur via similar mechanisms as described above in animal cells, but the molecular mechanism it actuates is very different. Upon touching, plant homologues of stretch activated channel families (TRP-channels, the DEG/ENaC voltage-independent Na^+ channel family, and the TREK K^+ channel family) are thought to be activated. Here, the mechanoresponsive channel of small conductance (MscS), found in bacteria, is the strongest starting point for unravelling the precise underlying mechanisms since homologues of these protein complexes (MLS-genes) are also found in plant genomes[23]. These channels allow ions to transfer past the plasma membrane, creating a depolarization which leads to an action potential. The created action potential progresses through the plants phloem until it reaches the pulvinar cells (cells situated in a thickening (pulvinus) at the base of leaflets and responsible for growth-independent movement). These cells are responsible for creating the shape change of the plants, and therefore, classified as 'motor organ'. Once the electrical signal reaches the pulvini, it activates the voltage-gated ion channels which lead to H^+, Ca^{2+}, Cl^- and K^+ redistribution[24]. The created osmotic disbalance between the cell and its surrounding potently affects the water

flux via aquaporin gating. The sudden depletion of calcium-ions from the cytosol decreases the activity of calcium-depended kinases which can phosphorylate the c-terminus of aquaporin, causing an inhibition of the membrane-pore closure. Once the action potential pulse has faded away, ions are actively transported into the cells again, restoring the function of the calcium-depended kinases that close the aquaporin membrane-pores[25,26]. Besides calcium-depended kinases, multiple other mechanisms are known to be able to regulate aquaporin gating, such as the collapsing open-pore-structure by osmotic pressure. While a complete overview of action remains to be elucidated, already multiple molecular mechanisms are known to be possibly involved in ion and water distribution.

The aquaporin mediated transport of water leads to a rapid and bulky loss of water. The water loss which compensates the ion efflux can cause cells to lose up to 25% of their volume. Since the pulvinar cells are situated at the base of the leaflets, the drop in hydrostatic pressure results in a conformation change visible as rapid folding. Recovering of the hydrostatic pressure occurs as ions are actively pumped back into the pulvinar cells, while maintaining the osmotic balance by the uptake of water. Obviously, this defense mechanism of plants requires a strong energy source within the pulvinar cells, since H^+ATPase activity is needed to sustain the ion flux[23,27].

As observed before, this system exists of a multi-step mechanism before the final state is reached. While the initial reaction occurs in mechanoresponsive cells which are able to sense the touch as trigger, these first steps do not directly show the resulting phenotype of the tissue. Here, subsequent signaling – the secondary reaction – results in the changes on the tissue level.

At the scale of bacteria

Bacteria are found in the most diverse conditions (under which some extreme circumstances), and both situated free-floating in water as well as attached to surfaces. The viscosity of a medium is an important parameter to describe the physical surrounding of swimming bacteria since this is a relatively large force on entities in the size range of 1 µm. An important descriptor for the mechanical properties of fluids is the dimensionless quantity called Reynolds number. The Reynolds number is a: "dimensionless value that measures the ratio of inertial forces to viscous forces and describes the degree of laminar or turbulent flow" (concept introduced by George Stokes: On the effect of the internal friction of fluids on the motion of pendulums (1851)). For example, laminar flows are described by a low Reynolds numbers and turbulent flows by high values. Typically Reynolds numbers faced by humans are around 10^4, whereas orders of magnitude smaller bacteria deal with 10^{-3} at most. Therefore, bacteria experience completely different mechanical cues from their environment, where the bacteria-surface interaction is of great importance. In a low Reynolds environment, viscous drag will increase in close proximity of a stiffer material. The increased mechanical

forces in close proximity of a substrate surface causes increasing mechanical loads on the flagellar rotation machinery. The mechanical load slows the flagellar system down. At the same time, the mechanical loading initiates a response in which extracellular polymeric substances (EPS) are secreted. Reduced speed in combination with the secreted adhesion promoting substance ultimately results in surface attachment.

An exact mechanism of mechanosensing for flagellar movement is not elucidated yet. However, a central role is proposed for stator elements. This protein is part of the flagellar machinery, and is located at its plasma membrane base. With increased viscosity, more torque is needed in order to keep the flagella rotating. The stators are proteins responsible for this torque generation, and known to be able to adapt to the changing force needed to keep the motor running efficiently. A stator-motor protein-complex will generate higher torques upon an increased viscosity of the surrounding medium. It is proposed that higher torque from the stators modulates an availability of cryptic binding sites for attachment of new stator-units, resulting in more stator recruitment at the flagellar base[28]. Together these stators use more energy which creates a shift in the proton economy[29]. Both proton motive force and sodium motive force are suggested to be involved in sensing flagellum obstruction[30]. Downstream of this mechanosensing is secretion of EPS. EPS is a secreted mixture of proteins, polysaccharides, and DNA which creates a distinct environment for attached bacterial cells. The viscous and elastic properties of the EPS depend on the specific composition and can be used to alter cell attachment, migration and proliferation. Multicellular organizations, including biofilms, can be created in this way and adapt actively to the external mechanical loading such as fluid flows[31].

Meeting physical boundaries

When organisms face an environment that contains physical boundaries, it can be forced to modify its shape accordingly. While this may seem like a purely morphological change, it can also heavily influence ongoing processes and behavior. Culturing cells in a restricted three-dimensional (3D) microenvironment can for instance have a pronounced effect on molecular signaling cascades and affiliated protein distributions. For *E. coli*, it is shown that cell morphology influences cell division. When grown within physical boundaries – by which the cell morphology can be dramatically altered – the axis of cell division is affected.

The location on which an actin ring will appear in order to start the cell division depends on the organization of oscillating Min-proteins. With Min-proteins oscillating from pole to pole, there is information available on cell size and symmetry. Under normal conditions, *with E. coli* being rod-shaped, the spatial-temporal Min concentration is the lowest in the middle of the longitudinal symmetrical axis. Once the bacterial cell is large enough, the concentration of the division inhibiting Min-proteins reaches a threshold-level which allows for the cell division machinery to assemble. By changing the morphology of the cells, Min-proteins adapt

their trajectory, and by this redefine axis of symmetry used for cell division[32]. While this system might not fit exactly in the classical mechanobiological pathways, it is a major effector of cell behavior initiated by the physical organization of the microenvironment. In many cases, mechanical loading of a tissue leads to morphological cell changes. The basic reaction-diffusion mechanism as in the described Turing-rings is a basics physics phenomenon underlying Min pattern formation, and is important for possible molecular interactions occurring in cells. The influence of the laws of physics on systems able to respond to mechanical stimuli was highlighted by D'Arcey Thompson (On growth and form, 1917) one century ago. He stated the importance of the physical environment of organisms on its structure and organization. This influence is of great importance during development, however, it also plays a major role during regeneration.

Mechanical stimuli for tissue homeostasis

Besides sensing the surrounding environment in order to adapt behavior, mechanical stimuli are also known to start processes for repair and regeneration. Upon injury, many organisms can start a variety of mechanisms to repair damaged or replace lost tissue. Numerous mechanisms are known for tissue/function regeneration, for example: blood platelet clotting in mammals to cover a wound and attracting building blocks to initiate skin repair[33], regeneration of complete limbs without any scar tissue formation as seen in *Axolotl*[34], and acute liver injury repaired by hypertrophy of hepatocytes[35]. The influence of mechanical stimuli on regeneration is evident in multiple cases. Patients suffering from tendinopathy need mechanical loading of the tendon tissue to produce tensile-stretch on tenocytes to stimulate regeneration[36]. Another well-known illustration of tissue homeostasis relying on mechanical stimulation is the loss in bone density in astronauts. A bone density loss of approximately 1% per month under zero gravity conditions results from an unbalanced bone production and resorption ratio[37]. Osteoclasts and osteoblasts, mainly responsible for bone-tissue homeostasis, are mechanosensitive and weightlessness affects their overactive and/or underactive behavior.

Nature teaches us to think out-of-the-box. Regeneration is not always needed to regain full tissue function since the remaining site might already consist of all ingredients needed. For instance, multiple species of jellyfish respond to arm amputation by reorganizing the remaining parts in order to recover a functional swim apparatus. Once an arm is amputated, a misbalance occurs within the remaining arms which cause inefficient swim movements. Compensation of this misbalance does not occur – unlike in other species – via altered proliferation or apoptotic programs. Instead, mechanical loading of the viscous body deforms by propulsion muscle contractions. This results in a re-centration of the manubria (n.b.: the manubrium is a muscular channel that connects the mouth of the jellyfish to the gastrovascular cavity), and subsequently, the muscular network will regenerate and complete

tissue function. Regaining full swim functionality is observed to be completed between 12 and 40 hours after amputation in young *Aurelia aurita*[38]. This activity on the tissue level is ideal to create an *in silico* model to capture the forces which act upon the system and the accompanying results in reorganization. Within the human body, the heart valves have been subject of many modeling studies to create an overview of the needs for engineered valves able to replace the malfunctioning tissue. Mechanical needs to deal with the forces that act on the system and cellular ingrowth of the implanted materials over time are important parameters in these models.

Mechanical stimuli can also initiate a defense mechanism in order to protect the subjected tissue. A well-known example is the formation of a callus layer after repeated pressure on the skin. Even though the incidence of (harmless) callused skin is very high, little is known about the underlying mechanisms of mechanotransduction. Various processes occurring subsequently during callus formation have been proposed as mechanism. In short, mechanical stress on cells in the dermis initiates secretion of inflammatory factors which causes hyper proliferation and incomplete keratinocyte differentiation into corneocytes. Subsequently, corneocytes migrate towards the outer layer of the dermis (stratum corneum), and increase the production of keratin and collagen rich extra cellular matrix (ECM). This process is often referred to as hypertrophy of stratum corneum or hyperkeratosis[39]. The increased production of ECM, which is containing a greater number of strongly attached cells, decreases the rate of desquamation. This results in thickening of the skin. The formed callus layer will disperse the mechanical load over a larger area and volume of skin, and thus decrease the intensity of the mechanical stimulation of underlying tissue. This enforced additional skin layer thus reduces the external mechanical loading of skin cells, and by this, inactivates the hyperkeratosis.

Whilst the major processes occurring during this skin transformation are already known for decades, it remains unclear how the system is exactly triggered on a molecular level. It is proposed that there is much overlap with alternative models which are popular topics of study. Here, mechanoresponsive Ca^{2+} channels might play an important role again as well as focal adhesion complex mediated signaling which is hypothesized to be involved in keratinocyte mechanotransduction. This can either progress via molecular signaling (e.g. via focal adhesion kinase (FAK), or extracellular signal-regulated kinases (ERK) signaling) or via a direct physical link with the cell cytoskeleton (e.g. via talin/paxilin binding of the actin cytoskeleton)[40]. Even though many steps of the involved molecular signaling remain to be elucidated, Kim et al. proposed a set of genes downstream of mechanosensing. Gene expression analysis suggests a role for such genes (CDSN, DSG1, DSC1, KLK5, KLK7, KLK14, LEKTI, LEKTI2 and a2ML1) in various processes in callus formation, such as: epidermal proliferation, dermal cornification, and increased adhesion in the stratum corneum[41].

State-of-the-art technologies used to study cell-material interaction

Scientists working in the highly interdisciplinary field of mechanobiology are often inspired by nature in their quest to create instructive biomaterials. For example, the functionality of a natural material can be as effective as an engineered supramolecular chemistry, or a defined surface structure on a substrate surface as material functionalization. The leaves of the lotus flower contain such a surface structure. The micrometer-scale protrusions create a hydrophobic surface where water droplets remain rounded, role down from the leaves, and by this, take all dirt particles along. Furthermore, the microscopic structure that resembles the skin of a shark was found to be antibacterial due to its specific micrometer-scale configuration of surface topography which inhibits bacterial attachment[42]. The diversity of material properties of natural materials extends far beyond bioactive surface structure. Biomimetic materials are engineered for mechanical characteristics, specific chemistries and even optical/photonic properties. For example, the cuticle gyroid structure found in the wings of *Parides Sesostris* butterflies (which give rise to their striking green metallic patch, visible from broad angles), are explored to create inorganic photonic crystals with tunable mechanical properties[43]. Or recreating the silk spun by spiders is found to be tough as Kevlar and strong like steel, and furthermore, this natural protein biomaterial is six times lighter[44]. During the development of a *de novo* biomaterial it is important to realize that material properties are a sum of the structures on all length scales. Ranging from the chemical composition of a microscopic polymer backbone, to the anisotropic arrangement of macroscopic fibers.

Technological advancements allowed the development of numerous platforms to study mechanobiology on a next level. Substrates are created, for example, with the highest control over chemistry and organization, and sensitive to its environment as triggered by e.g. light or heat. All material properties will influence cell behavior, however, the full design space of a material needs to be understood in order to achieve full control.

Controlled microenvironments

Many properties of biomaterials used as microenvironment for cells arise from the material specific chemical composition. For example: the mechanical parameters of the material, possibility for cells to alter its surrounding, manipulation of its direct environment, and the degree of bio-integration. To study cell-material interactions, typically a single or maybe only a few material properties are altered. Such an alteration leads in most cases to accompanying changes of other material properties as well, which also influence cell behavior, only here uncontrolled. Nevertheless, some platforms have been created that allow alterations to solely the envisioned changes.

Surface structure

A two-dimensional (2D) biomaterial-cell interface provides great control over cues in cell-material interactions. Here, both physical and chemical properties can be controlled, as well as the spatial configuration of the substrate surface the cells are exposed to. Applying a structure on the biomaterial surface can be a powerful tool to influence cell behavior. Coming from the classical 2D cell culture plastics, this is the first step in increasing the dimensionality of cell-material interaction towards a full surrounding microenvironment. Often, such a surface structure is referred to as a two-and-a-half dimensional cell-material interface. Within many tissues, cells are in contact with tissue specific ECM. The specific chemical composition of different types of ECM give – besides chemical stimulation – rise to a typical structural organization. Together with the accompanying mechanical character of the ECM, it is of great importance for its instructive nature. Furthermore, we find large differences in terms of physical properties between tissues. Where collagens are often important building blocks of ECM, we see for instance a 60% (dry weight) inorganic calcium phosphate fraction in bones. This causes an increase in elastic moduli which can strongly influence cell behavior[1,45]. Furthermore, this difference in chemical composition also effects the structural organization. In contrast to collagen bundles, the presence of calcium phosphates e.g. creates a crystallite structure. These specific surface structures are known to effect cell behavior, as seen when decoupled from a specific chemistry[46].

As described above, collagen bundles play a dominant role in the mechanobiological model of the Golgi tendon organ. Embedded in interwoven collagen bundles, the sensory axon terminal will be subjected to an increased forced upon muscle contraction. Current 3D printing methods explore the use of electrospinning of polymer fibers in order to create 3D meshes. The diameters can go down to the nanometer range, and polymers as well as e.g. collagen based materials can be used. Using this strategy, we can in theory fairly easily mimic the native Golgi tendon organ activity. Trapping cells within the interwoven fibers and mechanically stimulating them in order to study their behavior and initiate desired mechanisms.

Where the field of mechanobiology started with micrometer sized structures to manipulate cell behavior, it scaled down to nanometer sized structures. Using nanoimprint technologies, cell culture substrates can be enhanced with complex surface structures with very high reproducibility. With this broad variety of structural feature sizes, many types of cell-material interactions can be addressed. The micrometer-scale features are able to cause dramatic changes in cell and nuclear morphologies. As described above, differential cell spreading can influence multiple cellular components, and by this, alter molecular cell signaling cascades[47]. Material induced differences in cell morphology can be accompanied by differential cell spreading of the whole cell, or more locally, on a sub-cellular level. Furthermore, strongly deformed cells can experience e.g.: shifts in protein distributions and local concentrations, being abandoned from cell-cell contact, and changed nuclear morphologies resulting in

differential epigenetic states. Biomaterials enhanced with nanometer-scale structural features will manipulate cells by addressing completely different cellular components. For example: altered clustering of cell adhesion receptors which can cause extreme differences is the polymerization of cytoskeletal components, increased formation of filopodia, and even initiation of podosome activity[48]. The scale at which such engineered biomaterial systems can interact with cells is very similar to many of the natural mechanosensitive systems described above, and are found to induce similar molecular reactions.

The instructive capacity of natural substances such as tissue specific ECM or calcium phosphate ceramics can be – at least partly – assigned to its structural organization this molecular level. The building blocks of the tissue specific collagen fibers have a size of around 300 by 1.5 nm. This is at the scale at which cell adhesion molecules can start clustering into focal adhesion complexes. The same goes for the microstructure of many calcium phosphate ceramics which contain a porous structure at a sub-micrometer scale.

No material in nature is completely flat on a nanometer scale. Often, this surface structure doesn't immediately lead to an insight of its direct function. However, taking a closer look to nature can show us numerous examples of very useful material surface structures. These functionalities are not always directly applicable in biomedical research as seen in for example: self-cleansing lotus leafs, sticky gecko setae, and adhesive frog toe pads[49]. However, in the wealth of nature's diversity, there must be more examples like antibacterial micropattern as found on shark skin[42], or osteoinductive nacre as found in oyster shells[50]. Expeditions in regions containing a high biodiversity can give us the opportunity to find remarkable results of millions of years of material surface engineering, or at least systems that evolved to respond to these mechanical stimuli.

Supramolecular chemistry

Besides a more physical driven cell-material interaction, it is also possible to target mechanosensitive proteins more directly by specific designed chemistries. Using a bottom-up approach it is possible to compose the exact chemical composition of the desired substrate material. Supramolecular chemistry is already explored in other fields of research for decades. It finds e.g. application in many types of sensors for organic and inorganic analytes, drug delivery, crystal engineering, photodynamic therapy and within the textile industry by odor absorbing materials[51].

Supramolecular chemical strategies allow for combining chemically defined building blocks – in a LEGO-like manner – in order to create a highly controlled cell-biomaterial interface. The used molecular building blocks often interact via non-covalent bonds and can be very diverse in nature. Important when used as cell culture substrate is the availability of RGD-peptides for integrin binding. However, besides the RGD-containing blocks one can play with parameters

such as elasticity, hydrophobicity, and attachment/detachment upon trigger. It allows to interact with cells on a functional scale, with molecular precision, and in a spatial and temporal controlled manner[52].

Creating a well-defined 2D cell-material interface using supramolecular chemistry enables great control over numerous important mechanoresponsive components of cells. For example, tweaking the number of available cell adhesive peptide sequences can be used to promote very strong cell attachment and spreading. Within the spectrum of cell spreading, many important organizational changes can be addressed. The degrees of spreading can lead to distinct differences in stress fibers formation of the actin cytoskeleton. This will influence many cellular processes. Actin is one of the most abundant proteins in cells and whether it is polymerized as filamentous actin in stress fibers, or remained as a monomeric globular actin in the cytosol, greatly changes its availability to interact with other proteins. These formed stress fibers build a cytoskeletal tension within cells which can trigger specialized mechanoresponsive proteins to initiate more molecular signaling pathways. Furthermore, extensive cell spreading leads to the activation of stretched-activated-channels in the cell membrane. As described before, these channels are important regulators of ion-fluxes and can alter numerous cell signaling cascades.

Besides influencing cells based on spreading, supramolecular chemistry can be used to create many other substrate surface properties. Specific patterning of cell adhesive add-on units can be used to control the size of cell adhesion receptor clusters which leads to differences in focal adhesion complex maturation. Varying lengths of molecular backbones can be used to create a difference in rigidity of the cell-material interface. Controlled detachment of certain chemical groups (based on electrical current for example) can be used to even create a dynamic system, to follow processes over controlled measures of time, and tune the directionality of ongoing processes.

As described above for the mechanosensitive motor machinery of the bacterial flagellum, bacterial cell function dramatically changes upon substrate attachment. Creating a material that can bind flagella in a controlled manner should allow a closer observation of underlying mechanisms of action. Besides bacterial cells, many other cell types possess cilia. Immotile cilia often serve as mechanosensors of cells and can have distinct functions within highly specialized tissues. For example, the primary cilia on renal epithelial cells sense fluid flows which leads to the uptake of calcium ions by these cells[53]. Motile cilia – as flagella are – can be found in human trachea where they serve to transport mucus out of the lungs.

Besides electrical stimulation of supramolecular chemistry dynamics in e.g. peptide release, one can envision the use of a chemical feedback system towards the engineered material upon cell derived action potentials. Initiating a series of material changes purely based on cellular output can be used to create an intelligent material which is able to modify itself upon cellular requests. So far, we have seen various biological models in which mechanical stimulation

resulted in activation of stretch activated ion-channels which are causing cell depolarization and the start of an action potential. Once this electrical signal reaches the electro-sensitive supramolecular composed material, it triggers the system by which, for example, the elasticity, hydrophobicity, recruitment of specific proteins, or release of compounds can be altered. Following such a cascade of cellular induced changes in material and microenvironmental properties can potentially lead to enough feedback mechanisms to constantly optimize cell culture conditions.

Dynamic materials

Obviously, cells encounter a complex 3D surrounding *in vivo*. Here, every tissue contains a specific cocktail of growth factors and cytokines, various specialized cell types, and a tissue specific ECM composition with accompanying mechanical and structural properties. The overwhelming number of parameters that are possibly involved in cell function currently makes designing instructive biomaterials an educated guess. Step-by-step materials are developed which induce desired cellular reactions, however, it is difficult to translate the data obtained in one system towards another.

Currently, it is hard to create a hydrogel which is able to maintain the bioactivity of proteins and allows creating 3D structures at the same time. However, Lutolf et al. developed a hydrogel system in which stiffness, degradability and biochemical composition can be altered. Such a system allows to systematically test the influence of the individual parameters, without changing the other properties. In their system, pluripotency of induced pluripotent stem cells (iPSCs) is maintained by making use of the synergistic effect of the fine-tuned individual parameters. Confinement of the 3D microenvironment of iPSCs was found to be a major player in this process[54]. Furthermore, they developed a hydrogel system which is able to overcome difficulties in maintaining bioactive proteins while creating 3D structures for cell culture. Photolabile cage groups protect bioactive peptides until they are released using photopatterning. This dynamic system creates a possibility to spatiotemporally control the hydrogel properties which can e.g. lead to controlled migration of human mesenchymal stem cells[55].

In vivo the mechanical properties from the direct environment of a cell, tissue or organism changes constantly. These changes can occur with repetitive rhythms as experienced by cardiomyocytes in heart tissue, or it can be more incidental or constant as attached bacterial cells experience in a fluid flow. Such dynamic natures of mechanical stimulation are explored in a number of experimental set-ups to study effects on cell behavior. Multiple properties of the biomaterials can be changed within such switchable systems, with changing surface structures and material stiffness as two well-known examples[56,57]. By using a large variety of stimuli in those systems, one could obtain various degrees of control over different length scales.

A relatively simple way to create a dynamic system can be achieved by the mechanical stretching of a biomaterial. In such a system, the changes in biomaterial structure are created by a direct mechanical load on the biomaterial. This force can be created by different sources, in many biologically relevant magnitudes, having the desired directionalities. Multiple tools have been developed to introduce mechanical stretching both *in vitro* and *in vivo*, from stretching membranes to manipulating cells and mechanical loading of complete ligament tissues. Furthermore, we have seen the reorganization of jellyfish arms under physical forces derived from the swim-apparatus. Here, repetitive muscle contraction caused physical forces on the arms of the jellyfish resulting in step-by-step reorganization of the remaining arms. Where jellyfish exist of tissues with very low elastic moduli, analogies could be drawn towards dynamic hydrogels systems in which multicellular complexes organize under mechanical loads.

Besides deformation using direct mechanical loading, biomaterials properties can be changed in an indirect way using other sources of stimulation. In the last decade, elegant systems have been developed to alter properties based on changes in temperature, electrical current or upon excitation by light[58]. Photo-degradable and photo-crosslinkable polymers can serve as a base material for light induced dynamic biomaterial systems. Recently, a biomaterial system has been described which allowed very precise photothermal activation. As a result, micrometer scale areas of the materials shrink and cause the incorporated micro pillars to bend, resulting in subcellular stretching of the cell membranes[59].

The growing number of opportunities to control the properties of biomaterials enables to study its effect on cell behavior in a parameter precise and dynamic way. Using such systems, we can alter ongoing cellular processes, study dynamic processes real time upon initiation, and address interesting research questions on e.g. the memory of cells.

Discussion and future outlook

Even though every living organism interacts with its physical environment, it only became a widely studied phenomenon in the past three decades. During this time, more emphasis was placed on unraveling the molecular mechanisms which are triggered upon mechanical stimulation. In more recent years, numerous biological models were added to the research portfolio as well as a continuous exploration of novel experimental set-ups and read-outs. The vast majority of the work resulted in phenotypical observations, and up till now lacked a proper elucidation of the underlying mechanisms of mechanotransduction.

Tremendous effort has been put in the development of platforms that are able to change the physical environment of cells in a controlled manner. This enables precise control over mechanical stimulation on a wide variety of length scales, ranging from full tissue scale down to molecular interactions. However, sketching the clinically relevant context of the studied

system and the obtained data are often not tightly coupled to meaningful biology. Nevertheless, nature does provide numerous of such examples for many centuries already, ranging from plant morphogenesis under the influence of wind, all the way down to altered ion-fluxus due to cell membrane stretched channels. Thus, reconsidering the use of the engineered biomaterials in terms of meaningful read-outs could greatly improve our understanding of mechanobiology and the use of smart biomaterial systems for future usage.

Further development of the currently available biomaterials is desirable in order to tweak functionality by impinging on mechanoresponsive molecular mechanisms. At the same time, material scientists outside of the biotech world are constantly developing new materials which include most certainly material properties beneficial for studying cell-material interactions at some point in future. In this chapter, we have speculated on potential developmental directions of biomaterials. For example, the option to mimic the Golgi tendon organ/collagen fibers interaction using electrospun fibers, creating reactive intelligent materials made via supramolecular chemistries and inducing tissue reorganization in dynamic hydrogel systems.

Equally important is the need for assays which allows us to measure cellular responses to particular mechanical stimulation in a quantitative way. What do we need to quantify in order to measure mechanotransduction? Can we measure certain cellular components or processes instead of phenotypes? A possibility could be the use of förster resonance energy transfer (FRET) microscopy in order to measure e.g. talin interactions with focal adhesions and quantification of the involved forces within this system.

With a substantial increase in high-throughput platforms used to study cell-material interaction, the amount of data produced began to give rise to new challenges and opportunities. In most cases, micrographs depicting cells on materials can provide enormous datasets. Such data can be used to create models which can greatly improve our insights in occurring processes and the influence of external factors on the system.

To control cell behavior by creating a specific microenvironment for cells and tissues, we need to understand the mechanisms underlying mechanobiology (exemplified in this work). However, it is very important to realize that the system we want to affect needs to be able to act accordingly. There is a need for recreating interactions provided by engineered biomaterials on levels and with entities as we find in nature. But after all, nature itself has taught us that regenerating functionality does not require an exact restoration of the initial situation.

References

1. Engler, A. J., Sen, S., Sweeney, H. L. & Discher, D. E. Matrix Elasticity Directs Stem Cell Lineage Specification. *Cell* **126,** 677–689 (2006).

2. Watt, F. M., Jordant, P. W. & Neillt, C. H. O. Cell shape controls terminal differentiation of human epidermal keratinocytes. **85,** 5576–5580 (1988).

3. Curtis, A. & Wilkinson, C. Topographical control of cells. *Biomaterials* **18,** 1573–1583 (1997).

4. Crowder, S. W., Leonardo, V., Whittaker, T., Papathanasiou, P. & Stevens, M. M. Material Cues as Potent Regulators of Epigenetics and Stem Cell Function. *Cell Stem Cell* **18,** 39–52 (2016).

5. Watt, F. M. & Huck, W. T. S. Role of the extracellular matrix in regulating stem cell fate. *Nat. Rev. Mol. Cell Biol.* **14,** 467–473 (2013).

6. Yao, X., Peng, R. & Ding, J. Cell-material interactions revealed via material techniques of surface patterning. *Adv. Mater.* **25,** 5257–5286 (2013).

7. Voyvodic, P. L., Min, D. & Baker, A. B. A multichannel dampened flow system for studies on shear stress-mediated mechanotransduction. *Lab Chip* **12,** 3322–30 (2012).

8. Wang, E., Truschel, S. & Apodaca, G. Analysis of hydrostatic pressure-induced changes in umbrella cell surface area. *Methods* **30,** 207–217 (2003).

9. Sinha, R. *et al.* A medium throughput device to study the effects of combinations of surface strains and fluid-flow shear stresses on cells. *Lab Chip* **15,** 429–39 (2014).

10. Dalby, M. J. *et al.* The control of human mesenchymal cell differentiation using nanoscale symmetry and disorder. *Nat. Mater.* 997–1003 (2007). doi:10.1038/nmat2013

11. Mcbeath, R., Pirone, D. M., Nelson, C. M., Bhadriraju, K. & Chen, C. S. Cell Shape , Cytoskeletal Tension , and RhoA Regulate Stem Cell Lineage Commitment. **6,** 483–495 (2004).

12. Robling, A. G. & Turner, C. H. Mechanical Signaling for Bone Modeling and Remodeling. *Crit Rev Eukaryot Gene Expr* **19,** 319–338 (2013).

13. Freeman, D. B. Corns and calluses resulting from mechanical hyperkeratosis. *Am. Fam. Physician* **65,** 2277–2280 (2002).

14. Shaffer, S. W. & Harrison, A. L. Aging of the Somatosensory System: A Translational Perspective. *Phys. Ther.* **87,** 193–207 (2007).

15. Nilius, B. & Honoré, E. Sensing pressure with ion channels. *Trends Neurosci.* **35,** 477–486 (2012).

16. Bewick, G. S. & Banks, R. W. Mechanotransduction in the muscle spindle. *Pflugers Arch. Eur. J. Physiol.* **467,** 175–190 (2014).

17. Windhorst, U. Muscle proprioceptive feedback and spinal networks. *Brain Res. Bull.* **73,** 155–202 (2007).

18. Jami, L. Golgi tendon organs in mammalian skeletal muscle: functional properties and central actions. *Physiol. Rev.* **72,** 623–66 (1992).

19. Watanabe, T. *et al.* Morphological study of the Golgi tendon organ in equine superficial digital flexor tendon. *Okajimas Folia Anat. Jpn.* **81,** 33–37 (2004).

20. Woo, S.-H. *et al.* Piezo2 is the principal mechanotransduction channel for proprioception. *Nat. Neurosci.* **18,** 1756–1762 (2015).

21. Jukes, J. M. *et al.* Endochondral bone tissue engineering using embryonic stem cells. *Proc. Natl. Acad.*

Sci. **105,** 6840–6845 (2008).

22. Monshausen, G. B. & Gilroy, S. Feeling green: mechanosensing in plants. *Trends Cell Biol.* **19,** 228–235 (2009).

23. Monshausen, G. B. & Haswell, E. S. A force of nature: Molecular mechanisms of mechanoperception in plants. *J. Exp. Bot.* **64,** 4663–4680 (2013).

24. Volkov, A. G., Foster, J. C., Baker, K. D. & Markin, V. S. Mechanical and electrical anisotropy in *Mimosa pudica* pulvini. *Plant Signal. Behav.* **5,** 1211–1221 (2010).

25. Maurel, C. Plant aquaporins: Novel functions and regulation properties. *FEBS Lett.* **581,** 2227–2236 (2007).

26. Zhao, C. X., Shao, H. B. & Chu, L. Y. Aquaporin structure-function relationships: Water flow through plant living cells. *Colloids Surfaces B Biointerfaces* **62,** 163–172 (2008).

27. Braam, J. & Braam, J. In touch - plant responses to mechanical stimuli (2004) NP . *New Phytol.* **165,** 17 (2004).

28. Chawla, R., Ford, K. M. & Lele, P. P. Torque, but not FliL, regulates mechanosensitive flagellar motor-function. *Sci. Rep.* **7,** 5565 (2017).

29. Lele, P. P., Hosu, B. G. & Berg, H. C. Dynamics of mechanosensing in the bacterial flagellar motor. *Proc. Natl. Acad. Sci.* **110,** 11839–11844 (2013).

30. Ellison, C. & Brun, Y. V. Mechanosensing: a regulation sensation. *Curr. Biol.* **25,** R113-5 (2015).

31. Persat, A. *et al.* The mechanical world of bacteria. *Cell* **161,** 988–997 (2015).

32. Wu, F., Schie, B. G. C. Van, Keymer, J. E. & Dekker, C. shaped bacterial sculptures. *Nat. Nanotechnol.* (2015). doi:10.1038/nnano.2015.126

33. Coller, B. S. Historical perspective and future directions in platelet research. *J. Thromb. Haemost.* **9,** 374–395 (2011).

34. Kragl, M. *et al.* Cells keep a memory of their tissue origin during axolotl limb regeneration. *Nature* **460,** 60–65 (2009).

35. Miyaoka, Y. *et al.* Hypertrophy and Unconventional Cell Division of Hepatocytes Underlie Liver Regeneration. *Curr. Biol.* **22,** 1166–1175 (2012).

36. Wang, T. *et al.* Cyclic mechanical stimulation rescues achilles tendon from degeneration in a bioreactor system. *J. Orthop. Res.* **33,** 1888–1896 (2015).

37. Iwamoto, J., Takeda, T. & Sato, Y. Interventions to prevent bone loss in astronauts during space flight. *Keio J. Med.* **54,** 55–59 (2005).

38. Abrams, M. J., Basinger, T., Yuan, W., Guo, C.-L. & Goentoro, L. Self-repairing symmetry in jellyfish through mechanically driven reorganization. *Proc. Natl. Acad. Sci.* **112,** E3365–E3373 (2015).

39. Hashmi, F., Nester, C., Wright, C., Newton, V. & Lam, S. Characterising the biophysical properties of normal and hyperkeratotic foot skin. *J. Foot Ankle Res.* **8,** 35 (2015).

40. Reichelt, J. Mechanotransduction of keratinocytes in culture and in the epidermis. *Eur. J. Cell Biol.* **86,** 807–816 (2007).

41. Kim, S. H. *et al.* Callus formation is associated with hyperproliferation and incomplete differentiation of keratinocytes, and increased expression of adhesion molecules. *Br. J. Dermatol.* **163,** 495–501 (2010).

42. May, R. M. *et al.* An engineered micropattern to reduce bacterial colonization, platelet adhesion and

fibrin sheath formation for improved biocompatibility of central venous catheters. *Clin. Transl. Med.* **4,** 9 (2015).

43. Pouya, C. *et al.* Characterization of a Mechanically Tunable Gyroid Photonic Crystal Inspired by the Butterfl y Parides Sesostris COMMUNICATION. 99–105 (2016). doi:10.1002/adom.201500436

44. Qin, Z., Compton, B. G., Lewis, J. A. & Buehler, M. J. spider webs for high strength. *Nat. Commun.* **6,** 1–7 (2015).

45. Swift, J. *et al.* Nuclear lamin-A scales with tissue stiffness and enhances matrix-directed differentiation. *Science* **341,** 1240104 (2013).

46. Groen, N. *et al.* Linking the Transcriptional Landscape of Bone Induction to Biomaterial Design Parameters. *Adv. Mater.* **29,** (2017).

47. Dalby, M. J., Gadegaard, N. & Oreffo, R. O. C. Harnessing nanotopography and integrin-matrix interactions to influence stem cell fate. *Nat. Mater.* **13,** 558–69 (2014).

48. Hulshof, F. F. B. *et al.* NanoTopoChip: High-throughput Nanotopographical Cell Instruction. *Acta Biomater.* (2017). doi:10.1016/j.actbio.2017.08.023

49. Crawford, N., Endlein, T., Pham, J. T., Riehle, M. & Barnes, W. J. P. When the going gets rough - studying the effect of surface roughness on the adhesive abilities of tree frogs. *Beilstein J. Nanotechnol.* **7,** 2116–2131 (2016).

50. Alakpa, E. V *et al.* Nacre Topography Produces Higher Crystallinity in Bone than Chemically Induced Osteogenesis. *ACS Nano* acsnano.7b01044 (2017). doi:10.1021/acsnano.7b01044

51. Lüning, U. Applications of Supramolecular Chemistry. Edited by Hans-Jörg Schneider. *Angew. Chemie Int. Ed.* **52,** 4724–4724 (2013).

52. Brinkmann, J. *et al.* About supramolecular systems for dynamically probing cells. *Chem. Soc. Rev.* **43,** 4449–69 (2014).

53. Satir, P., Pedersen, L. B. & Christensen, S. T. The primary cilium at a glance. *J Cell Sci* **123,** 499–503 (2010).

54. Caiazzo, M. *et al.* boost induction of pluripotency. **15,** (2016).

55. Mosiewicz, K. A. *et al.* hydrogel photopatterning. **12,** (2013).

56. Yang, C., Tibbitt, M. W., Basta, L. & Anseth, K. S. Mechanical memory and dosing influence stem cell fate. *Nat. Mater.* **13,** 645–52 (2014).

57. Le, D. M., Kulangara, K., Adler, A. F., Leong, K. W. & Ashby, V. S. Dynamic topographical control of mesenchymal stem cells by culture on responsive poly(????-caprolactone) surfaces. *Adv. Mater.* **23,** 3278–3283 (2011).

58. Kim, J. & Hayward, R. C. Mimicking dynamic in vivo environments with stimuli-responsive materials for cell culture. *Trends Biotechnol.* **30,** 426–439 (2012).

59. Sutton, A. *et al.* Photothermally triggered actuation of hybrid materials as a new platform for in vitro cell manipulation. *Nat. Commun.* **8,** 14700 (2017).

topographically enhanced cell culture systems t
opographically enhanced cell culture systems to
ographically enhanced cell culture systems to i
raphically enhanced cell culture systems to ind
phically enhanced cell culture systems to induc
hically enhanced cell culture systems to induce
cally enhanced cell culture systems to induce a
lly enhanced cell culture systems to induce and
y enhanced cell culture systems to induce and mo
enhanced cell culture systems to induce and mon
nhanced cell culture systems to induce and moni
anced cell culture systems to induce and monito
ced cell culture systems to induce and monitor
d cell culture systems to induce and monitor me
cell culture systems to induce and monitor mec
ell culture systems to induce and monitor mecha
l culture systems to induce and monitor mechano
culture systems to induce and monitor mechanobi
ulture systems to induce and monitor mechanobiol
ture systems to induce and monitor mechanobiolo
re systems to induce and monitor mechanobiology

Chapter 3

The mechanobiological imprint on osteogenesis

Nick R.M. Beijer[1], Aysegul Dede-Eren[1], Rika Reihs[1], Dennie G.A.J. Hebels[1], Jeroen van der Peppel[2], Zarina M. Nauryzgaliyeva[1], Steven Vermeulen[1], Marloes M.J. Kamphuis[1], Daniel Pereira[3], Aliaksei S. Vasilevich[1], Shantanu Singh[4] & Jan de Boer[1]

[1] Laboratory of Cell Biology Inspired Tissue Engineering, MERLN Institute, Maastricht University, the Netherlands. [2] Department of Internal Medicine, Erasmus MC, Rotterdam, the Netherlands. [3] Department of Instructive Biomaterial Engineering, MERLN Institute, Maastricht University, the Netherlands. [4] Imaging Platform, Broad institute of MIT and Harvard, Cambridge, MA, USA.

Abstract

The role of mechanotransduction in normal tissue homeostasis and development is increasingly evident, and spatial confinement is one of the parameters that feed into cell physiology *in vivo*. The signal transduction cascades involved in sensing confinement are not well defined although adhesion and actin cytoskeleton are known to be affected. In this manuscript, we analyzed cells on a library of topographies with an array of different confinement-induced cell shapes. Actin organization was described by high content imaging and related to osteogenic differentiation of mesenchymal stem cells (MSCs). Based on this data, we selected a defined surface topography, which together with MSCs, was characterized as a mechanobiological osteogenic system. On these topographically enhanced substrates, MSCs showed strong differences in the number and size of focal adhesions, as well as in the activity of mechanosensitive proteins, such as YAP (yes-associated protein), EGR1 (early growth response protein 1), and SRF (serum response factor). Next, we used a transcriptomics approach to identify molecular signaling underlying the mechanotransduction that led to osteogenesis. 2, 24 and 72 hours after seeding on topographically enhanced substrates, we observed strong effects of confinement on activation of HIF (hypoxia induced factor) target genes. Furthermore, database analysis revealed a gene expression signature comparable to exposure of cells to the histone deacetylation inhibitor trichostatin A. The evidence for a role of epigenetics in this mechanobiological osteogenic response was further strengthened by dramatic nuclei deformations, DNA condensation, and differential lamin A and C expression.

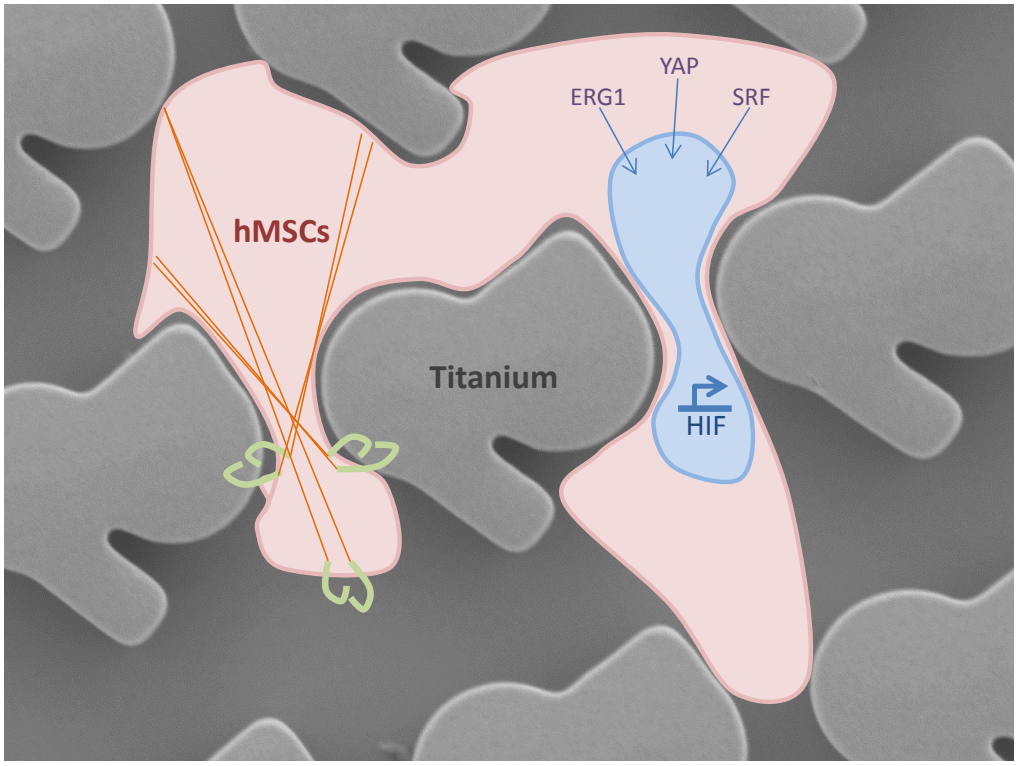

Introduction

The majority of cells in the human body are situated either within extra cellular matrix (ECM) or are in direct cell-cell contact in a three dimensional (3D) microenvironment[1,2]. Cells receive chemical signals from their surrounding in the shape of hormones, metabolites, oxygen level or pH, but cells experience many physical cues as well[3,4]. For instance, osteocytes are surrounded by the calcified ECM of bone and are under the control of both hormones and mechanical loading[5]. Biomaterials engineering tries to recapitulate the mechanical component of the cells' niche. To optimize this, first there is the need to understand the underlying mechanisms of mechanotransduction which covers a great portion of the material-induced changes in phenotype. For this, a wide variety of materials are developed to create a controlled environment in which the influence of individual material design parameters can be assessed. For example, cell-regulated degradation of hydrogels caused a significant increase in tension in the cytoskeleton of mesenchymal stem cells (MSCs), resulting in the initiation of osteogenic differentiation[6]. However, the complex interplay of environmental stimuli that lead to the abundance of molecular processes involved in osteogenesis elapse by mechanisms which remain to be fully elucidated. Genomics is one strategy to unravel this.

We previously used gene expression profiles of MSCs stimulated with dexamethasone to induce osteogenic differentiation and discovered three separate phases in the differentiation process, each with their specific regulators[7]. We also primed MSCs *in vitro* to activate the protein kinase A (PKA) signaling cascade using cyclic AMP. Stimulation of PKA signaling pathway results in an increased expression of the bone related cytokines BMP-2, IGF-1, and IL-11, and results in enhanced bone formation in vivo[8]. Others investigated the influence of vitamin D3 and bone morphogenetic protein 2 (BMP2) addition and reported that c-myc accelerates dexamethasone-induced osteoprogenitor commitment of MSCs[9]. These studies showcase the power of the holistic approach of transcriptomics for the investigation of signal transduction.

Besides bone formation induced by molecules, there are also a few characterized bone inducing materials known. Porous calcium phosphates ceramics are applied in the clinics as bone void fillers for many years already. After parameterization of the materials, we created a gene network for calcium-phosphate ceramic induced osteogenesis, with a decisive role for genes that regulate ECM deposition[10]. Similarly, the mechanism underlying cell-material interactions that lead to osteogenesis of MSCs by nanometer-scale pits in the substrate were explored using transcriptomics by Dalby and co-workers. They observed that MSCs which were exposed to nanopits have a distinct differentiation profile compared with those treated with dexamethasone supplemented culture medium[11]. In contrast to chemically-induced osteogenesis, the molecular targets of osteo-inductive materials are not known.

The cytoskeleton plays a role in mechanotransduction, and more specifically, there is an evident role for the remodeling of the actin cytoskeleton in transmitting mechanical signals into the nucleus. External mechanical stimulation induces cytoskeletal reorganization which can lead to MSC differentiation[12]. Such stimuli can e.g. be initiated by growing cells in defined shapes using printed adhesive islands, by growing them under fluid flow-induced shear stress or by via material vibration[13–15]. MSCs on culture plastic contain a large number of thin, parallel actin filaments across the entire cytoplasm. However, the actin-cytoskeleton is remodeled into only a few, but very thick actin bundles during osteogenic differentiation, which are located at the cell's periphery[16]. Filamentous actin is the main structural component of the cytoskeleton, and tension in it is generated via myosin. The MAPK/ERK and RhoA/ROCK signaling pathways play an important role in myosin mediated mechanotransduction. Downstream of this, the yes-associated protein (YAP) functions as a nuclear switch of extracellular mechanical signals. Activation of YAP requires e.g. adhesion initiated Rho-GTPase activity, myosin-induced tension on actin fibers, and remodeling of the cytoskeleton[17–19]. As a co-transcription factor, YAP regulates osteogenic differentiation, for instance by promoting RUNX2-dependent gene transcription[20]. The link between YAP-mediated mechanotransduction and osteogenesis is supported by studies on a variety of engineered biomaterial systems[17,21].

Besides cell adhesion receptor regulated cytoskeletal remodeling and myosin dependent tension, mechanotransduction leading to osteogenesis can follow multiple different routes of signaling. Cells are e.g. able to sense mechanical stimuli via mechanosensitive ion-channels. Gating of these stretch activated channels (SACs) can create an ion flux, and activation of the mechanosensitive channel TRPM7 can lead to osteogenesis in MSCs[22–24]. As a result of all afore mentioned mechanotransduction signaling pathways, it is observed that gene expression is altered which leads to a change in cell phenotype. The mechanical load cells experience in these systems impact the nuclear structure as well. Within the nucleus, the lamin protein family is responsible for structural integrity, and an important role is described for lamins in mechanotransduction[25]. It is hypothesized that deformation and size reduction of the nucleus under mechanical loading might alter the epigenetic state of cells which results in differential gene expression. Downing et al. observed reduced histone deacetylase activity and increase in H3 methyltranferase activity, induced by substrates which are enhanced with micro-grooves. This significantly altered the epigenetic state of mouse fibroblasts by increased acetylation and methylation of histone H3[26]. Furthermore, it has been reported that fluid flow can decrease DNA methylation in the promotor region of three osteogenic genes (osteocalcin, osteopontin, collagen type 1) in MSCs[27]. Under cyclic mechanical stretch, MSCs show osteogenic differentiation by downregulation of HDAC1 which affects matrix mineralization via JAG1-mediated Notch signaling[28].

In previous work, we identified a defined surface topography that was able to induce osteogenic differentiation[29,30]. In this manuscript, we use this osteogenic system to induce the

osteogenic process and used transcriptomics to reveal signaling pathways which are involved in mechanotransduction in MSCs.

Materials and methods

Topography enhanced polystyrene film fabrication process

Titanium covered TopoChips were used to screen for the osteogenic differentiation marker alkaline phosphatase (ALP). As a hit topography from this screen we selected T2_TI_0304 and validated its osteogenic potential both *in vitro* and *in vivo*[30]. The T2_TI_0304 topography pattern was placed in a 15 mm circle format as the lay-out of the chromium masks for photolithography. The micrometer-scale patterns were etched from the silicon wafer by directional reactive ion etching (DRIE), generating a silicon master mould. These silicon master moulds contained the inverse topography patterns. A three-replication process was used to fabricate the surface topography enhanced polystyrene films. In these three replications, we subsequently used silicon moulds, PDMS moulds and Ormostamp moulds.

Topography number used in this manuscript, T2_TI_0304, was derived from the second generation TopoChip[29] (T2) coated with titanium (TI). The last 4 digits are built-up as followed: the first two digits represent the row number counted from the top, and the second two digits represent the column number.

Silicon master mould fabrication

Si <100> wafer was prepared with positive photo resist (907-16, Olin) by spin-coating at 4000 rpm for 30 minutes. The prepared substrate was patterned using the designed masks in conventional UV lithography (EVG 620). After development (OPD 4262) and hard baking on a hotplate at 120 °C for 30 minutes, we etched the wafer by directional reactive ion etching (DRIE, Adixen AMS 100 SE) using a Bosch process of SF6/C4F8, with a flow of 250/200 sccm (3/1 seconds), inductively coupled plasma of 1500 W, capacitive coupled plasma of 80 W and a substrate temperature of 80 °C for 3 minutes and 18 seconds. By this, we obtained a feature depth of 10 µm. The photo resist was then stripped in O_2 plasma.

PDMS mould fabrication

The silicon master mould was first cleaned in Piranha solution (H_2SO_4 : H_2O_2 = 3:1 v/v) for 30 minutes at 95 °C, rinsed with deionized water, spin dried with N_2 and coated with a monolayer of trichloro(1H, 1H, 2H, 2H-perfluorooctyl)silane (FOTS, Sigma-Aldrich) in the gas phase under vacuum in a desiccator. Degassed PDMS (curing agent : base = 1:10 w/w,

Sylgard 184 silicone elastomer kit, Dow Corning Corporation) was cast on the full 100 mm silicon master mould to create a 1-2 mm thick PDMS mould, and cured on a leveled hotplate at 80 °C for at least 8 hours. After curing, the PDMS film was peeled from the silicon mould and ready to be used for the next replication cycle.

Ormostamp mould fabrication

Due to thermal expansion and mechanical properties of PDMS, the obtained PDMS mould could not be used as a direct template for hot embossing. Therefore, a second replication step was needed using a much harder polymer. For this, we used Ormostamp (OrmoStamp, Micro Resist Technology GmbH, Germany), a UV-curable inorganic-organic hybrid polymer. A layer of Ormoprime (OrmoPrime08, Micro Resist Technology GmbH, Germany) was applied on a clean support Borofloat wafer (Borofloat 33 of 100 mm diameter and 500 µm thickness, Schott) via spin-coating for 30 seconds at 4000 rpm followed by 5 minutes on a hot plate at 150 °C. This layer promotes adhesion of the Ormostamp and was prepared immediately before application. 1.5 mL Ormostamp was slowly dispensed in the middle of the PDMS mould and carefully brought into contact with the Borofloat wafer with the Ormoprime coating. The gap between the two substrates was completely filled by capillary force after 30 minutes. The PDMS/Ormostamp/Borofloat sandwich was exposed to 365 nm UV light for 300 seconds with a light intensity of 12 W/cm^2 (EVG 620 i-line exposure system), after which the PDMS mould was peeled from the Ormostamp mould. UV curing was followed by a hard bake process on a hot plate at 130 °C for 30 minutes (ramping up from RT at a ramping speed of 5 °C/min) to finalize this replication cycle.

Polystyrene hot embossing and titanium sputter coating

Before the third replication step, the Ormostamp mould was treated with a gentle O_2-plasma (reactive ion etching (RIE, home-build) at 10 °C, 50 sccm oxygen flow, 75 mTorr pressure and 50 W CCP power for 30 seconds) and FOTS coated as described earlier. Commercially available bi-axially oriented 190 µm thick polystyrene films (Goodfellow, United Kingdom) were used as substrate material for hot embossing (Obducat Eitre 6 Nano Imprint Lithography system, Obducat, Sweden) the inverse ORMO stamp template at 140 °C and 10 bar for 5 minutes. The replication process was finalized by separating the Ormostamp template from the 10 µm high topographical features enhanced polystyrene films at 95 °C. Untreated polished silicon wafers were used for embossing unpatterned substrates, which serve as a reference condition for the topographically enhanced substrates. After embossing, the embossed polystyrene films were coated with 200 nm titanium by sputter coating at a sputtering rate of 6 nm/min. All surfaces were pre-treated with medium overnight before adding hMSCs for cell culture.

Cell culture of hMSCs

Human bone marrow-derived mesenchymal stem cells (hMSCs) were derived as described previously[31]. hMSCs were expanded in basic hMSC medium that consisted of α-minimal essential medium (α-MEM, Life Technologies), supplemented with 10% foetal bovine serum (FBS, Sigma), 2 mM L-glutamine (Thermo Fisher Scientific), 0.2 mM ascorbic acid, 100 U/ml penicillin, and 100 mg/ml streptomycin (Thermo Fisher Scientific). To investigate the effect of surface T2_TI_0304 on hMSCs (passage number 5), cells were seeded at densities of 30,000 (microarray), 15,000 (western blot), and 10,000 (imaging) cells/cm^2 on both flat titanium (ti-flat) and surface T2_TI_0304 (ti-topography) and grown for the designated times in a humidified incubator with 5% CO_2 at 37 °C. Chemically induced osteogenesis served as a control for the microarray, were 10^{-8} M dexamethasone was added to the medium on the 24 and 120 hour time points on ti-flat.

RNA isolation and cRNA synthesis

Total RNA was isolated using the Qiagen RNeasy Mini Kit, following the manufacturer's instructions. RNA quantity and purity was measured with a BioDrop µLITE and RNA quality with an Agilent BioAnalyzer 2100. All samples had RNA integrity of >9. From 100 ng RNA, cRNA was synthesized using the Illumina TotalPrep RNA amplification Kit (Ambion), according to the manufacturer's instructions. The quality of the cRNA was verified on a Bioanalyzer 2100 (Agilent).

Microarray-based gene expression profiling

The Illumina HT-12 v4 expression Beadchip platform was used for gene expression profiling. Briefly, 750 ng of cRNA was hybridized on the microarray overnight, after which the array was washed and blocked. By addition of streptavidin Cy-3, a fluorescent signal was developed. Arrays were scanned on an Illumina Beadarray reader and raw intensity values were background corrected in BeadStudio (Illumina). Further data processing and statistical testing were performed using the R-based online gene expression analysis tool ArrayAnalysis (http://arrayanalysis.org/)[32]. Probe-level raw intensity values were quantile normalized and transformed using variance stabilization (VSN). A linear modeling approach with empirical Bayesian methods, as implemented in the Limma package, was applied for differential expression analysis of the resulting probe-level expression values. P-values were corrected for multiple testing using the Benjamini and Hochberg method. Genes were considered differentially expressed at a corrected p-value of <0.05 and an absolute fold change >1.5.

Pathway and network analysis

Pathway over-representation analysis was performed using the web-tool ConsensusPathDB (CPDB), which provides a comprehensive pathway analysis covering most public resources for interactions[33]. Over-representation analysis was performed on a set of differentially expressed genes (DEGs), and a background list containing all measured genes was used to improve the statistical evaluation of the pathways. Pathways with a false discovery rate-corrected p-value <0.05 were considered significant.

Network analysis was carried out in two steps. CPDB contains an induced network module which uses the interactions described in all the public resources to build a network based on a list of input genes. At first a network was generated on the same list of DEGs as used for pathway analysis using a z-score threshold of 18. Only binary protein interactions of low, medium, and high confidence were selected, and intermediate genes were allowed to be added to the network in order to improve inter-gene connectivity. The resulting network was subsequently imported into CytoScape and the plugin CyTargetLinker was used to extend the CPDB network by adding transcription factors (TFs) from the TF-target database TFe (Transcription Factor encyclopedia)[34–36]. TFe is a small-scale manual literature curation project containing 1,531 human TF-target interactions.

Fluorescent staining and microscopy

For fluorescence microscopy, cells were fixated in freshly prepared 3.7% paraformaldehyde for 10 minutes at room temperature, permeabilized by 1% Triton-x (Sigma) in phosphate buffered saline (PBS) for 10 minutes and blocked for a-specific binding by 1% bovine serum albumin (BSA, sigma Aldrich) in PBS for 30 minutes at room temperature. Primary antibody incubation of YAP (dilution 1:500, YAP1, SC-101199 Santa Cruz,), EGR1 (dilution 1:200, T.126.1 Thermo Fisher Scientific), SRF (dilution 1:200, SRF (G-20), SC-335 Santa-Cruz), and Vinculin antibodies (dilution 1:200, AB18058 Abcam) over night at 4 °C was followed by secondary antibody incubation, goat-anti-mouse Alexa fluor 488 (dilution 1:500, Life technologies) for 1.5 hours at room temperature in the dark.

The actin cytoskeleton was labeled with phalloidin 488 (1:80, A12379, Thermo Fisher Scientific) for 40 minutes and DNA with 4',6-diamidino-2-phenylindole (DAPI, 14.3 µM, D1306 Invitrogen) for 5 minutes both in the dark and at room temperature.

The Cell Paint protocol stained a variety of cellular entities using a pallet of fluorescent dyes. Here, DNA (Hoechst, 385 nm, H3570 Thermo Fisher Scientific), nucleoli (SYTO 14 green fl nucleic acid stain, S7576 Invitrogen), endoplasmatic reticulum (concanavalin A AF488, C11252 Invitrogen), f-actin (Phalloidin AF568, 10135092 Thermo Fisher Scientific), cell membrane (WGA AF594, W11262 Invitrogen), and mitochondria (MitoTracker deep red FM

AF647, M22426 Invitrogen) were stained following an established protocol[37]. Fluorescence micrographs of hMSCs were obtained using a Nikon A1 epifluorescence set-up.

Imaging, data extraction and analysis

hMSCs on eight titanium-coated TopoChips in basic medium were fixed after 5 days of culture and stained for their nucleus actin cytoskeleton and alkaline phosphatase as described previously[30]. Fluorescence micrographs were obtained for all individual TopoUnits using the BD-Pathway (BD) high content microscope and analyzed using an in-house developed Matlab scripts[38] to correct for imaging artifacts and to remove out-of-focus images. Subsequently, morphological and intensity features were measured using CellProfiler image analysis software[39]. The relationship between ALP expression and shape and intensity parameters was estimated using linear regression, as implemented in R[40] (R version 3.3.2 (2016-10-31)). The clustering of features was obtained using hierarchical clustering, using the hclust function in R.

Western Blotting

After 24 hours exposure to ti-flat and ti-topography, hMSCs were lysed using a lysis buffer cocktail containing RIPA buffer (Cat no. C999K75, Amresco), cOmplete™ Mini EDTA-free Protease Inhibitor Cocktail (7x stock, Cat no. 11836170001, Sigma-Aldrich), and Halt™ Phosphatase Inhibitor Cocktail (Cat no. 10668304, Fisher Scientific). The protein concentration was determined using Pierce™ BCA Protein Assay Kit (Cat no. 23227, Thermo Fisher Scientific).

For each sample, 30 µg protein was loaded on an SDS-PAGE gel (4–15% Mini-PROTEAN TGX Stain-Free Gel, Cat no. 4568084, Bio-Rad) and separated for 90 minutes at 100 volts. Next, the proteins were transferred from the gel to the PVDF membrane (Trans-Blot® Turbo™ Mini PVDF Transfer Packs, Cat no. 1704156, Bio-Rad) using the high-molecular weight proteins program (1.3mA, 25V, 10 minutes, Trans-Blot® Turbo™ Transfer System, Cat no. 1704150, Bio-Rad). After transferring, PVDF membranes were blocked in 5% non-fat dried bovine milk (Blotting-Grade Blocker, Cat no. 1706404, Bio-Rad) in Tris-buffered saline (10x Tris Buffered Saline, Cat no. 1706435) with Tween-20 (Cat no.437082Q, VWR) for one hour. Primary antibodies used for blotting were pFAK (120 kDa, 1:500, ab81298, Abcam), FAK (120 kDa, 1:500, ab40794, Abcam), HIF1α (120 kDa, 1:100, Cat no. 610958, BD Biosciences), and Lamin A+C (63 kDa, 1:100, ab108595, Abcam). As loading control, we used β-actin (42 kDa, 1:2000, Cat no. A2228, Sigma) and TBP (40 kDa, 1:2000, ab51841, Abcam). All membranes were incubated with primary antibodies at 4°C on a rotator shaker overnight. The secondary antibodies used for blotting were goat anti-mouse HRP (Cat no. 10494932, Fisher Scientific) and goat anti-rabbit HRP (Cat no. 10696113, Fisher Scientific)

and incubated one hour at room temperature. MSCs incubated in medium with 200 mM phenanthroline (Cat no. P9375-5g, Sigma-Aldrich) were used as positive control for HIF1α stabilization. Membranes were incubated with a chemilumescent signal enhancing substrate (ECL, Bio-Rad) according to manufacturer's protocol, after which the chemiluminescence signal was detected using the Gel imager Biorad ChemiDoc MP (Bio-Rad).

Metabolic activity

MSCs cultured on ti-flat and ti-topography were assessed for their metabolic activity after 2, 24 and 72 hours using the Presto Blue assay (A13261 Invitrogen) according to the manufacturer's protocol. In brief, at the designated time points we replaced basic hMSC culture medium by Presto Blue medium (1x concentrated in basic hMSC medium), and incubated the cells for 1 hour at 37 ˚C in a humid environment. Equal amounts of supernatant were subsequently transferred to a black/black bottom 96-well plate, followed by quantification of the fluorescent signal measured at 590 nm using a plate reader (Clariostar).

Reactive oxygen species

After 24 hours on ti-flat and ti-topography, MSCs were incubated with 10 µM CM-H_2DCFDA (C6827 Invitrogen) for 1 hour at 37 °C to visualize reactive oxygen species. As a positive control, we exposed MSCs on ti-flat for 2 hours to 200 µM H_2O_2. After incubation, the cell containing substrates were washed with PBS, and transferred to new well-plates for trypsinization. Cells were collected in FBS containing medium, centrifuged for 5 minutes at 300 g, and resuspended in PBS before flow cytometry using the BD Acurri C6.

Statistical analyses

Experiments were carried out in triplicate. Bar-graphs represent the mean ± standard deviation. Boxplots include the median values with 95% confidence interval notches, the boxes covering the 1^{st} and 3^{rd} quantile, the whiskers the highest and lowest values, and the dots the outliers. Variation of the mean values between samples were compared using Students t-test, with $P<0.05$. Statistics used during gene expression analysis are explained in detail in the respective subsection on gene expression profiling.

Results

Surface topographies influence hMSC shape, cytoskeletal organization and ALP expression

To define a mechanobiologically based osteogenic system to study underlying signaling pathways, we analyzed high-throughput imaging data from a previously performed TopoChip screen for the osteogenic differentiation of hMSCs on titanium-coated surface topographies[30]. Using CellProfiler software[39] we derived per cell quantitative data on cell shape and size, the actin cytoskeleton, and alkaline phosphatase expression. We observed that diverse topographies induced diverse cellular phenotypes (Figure 1). For example, we identified topographies which were able to either strongly alter cell size, affect the abundance of filamentous actin, and interestingly, altered the expression of early osteogenic differentiation marker ALP, as compared to a flat reference substrate.

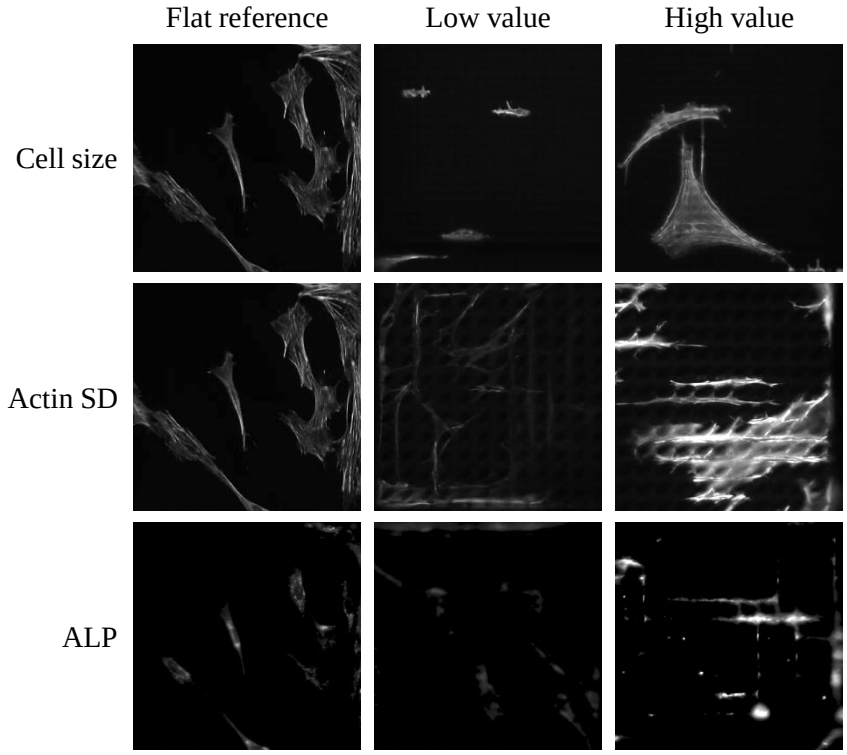

Figure 1: Surface topography has diverse effects on hMSCs. A selection of micrographs of hMSCs cultured on the titanium-coated TopoChip for 5 days to show the large variety in shape, actin architecture and ALP expression, as compared to cells cultured on ti-flat substrates. Individual images are 290 by 290 µm.

Quantification of these cellular responses allowed us to measure correlations between morphological features and the expression levels of ALP. Here, we found that actin, nuclear architecture and the number of cells each strongly correlated with ALP expression (Figure 2A). Further clustering of ALP-correlating features grouped cell shape and size parameters,

the interaction with neighbors, and the actin organization in separate groups, indicating that there are three distinct groups of features that correlate with ALP expression (Figure 2B). For instance, several actin features correlated with ALP expression, such as a feature describing differences in actin filament formation, and a feature describing accumulation of actin in the cell's periphery (Figure 2C). Together, these data suggest a functional relationship between actin organization and ALP expression.

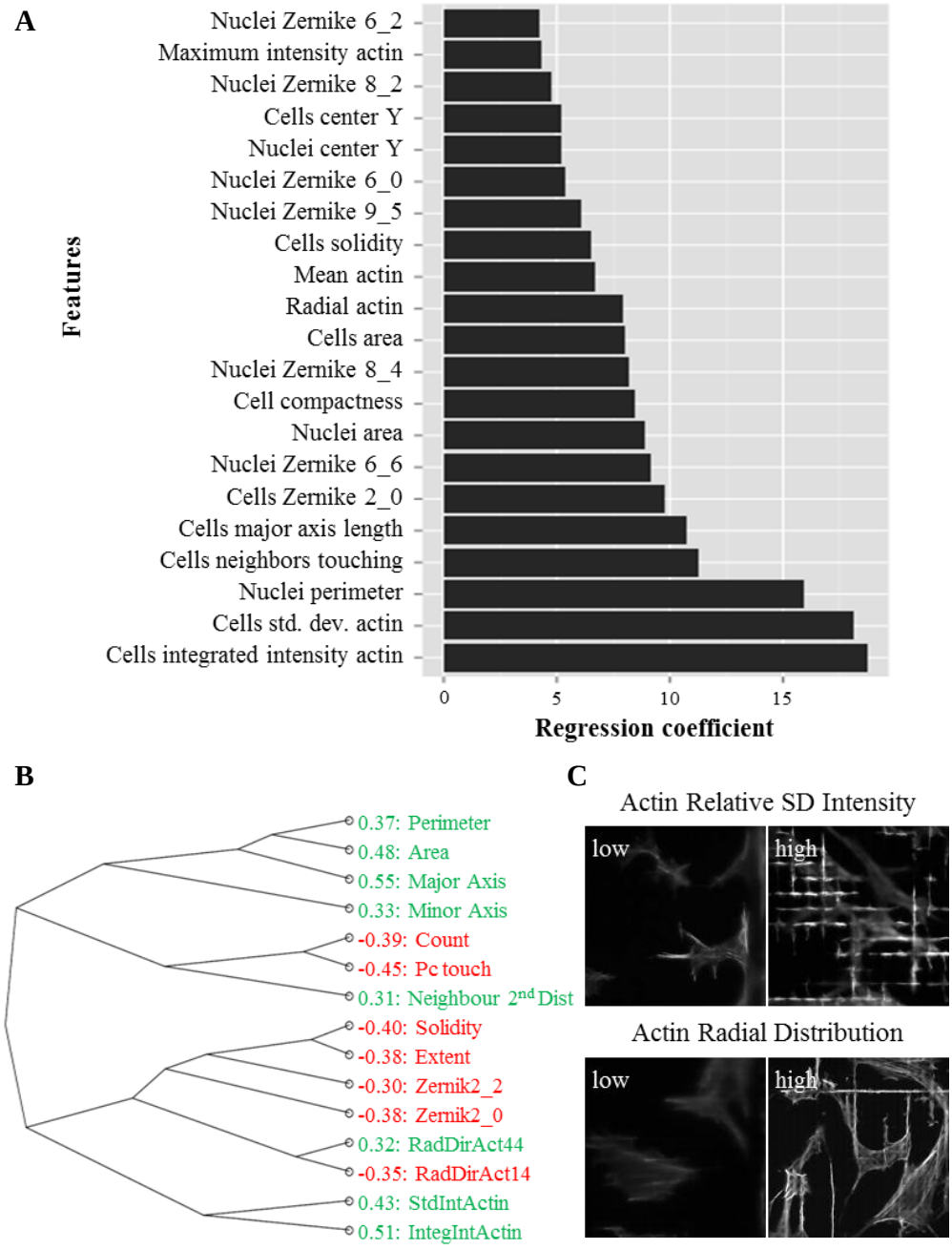

Figure 2: ALP expression correlates to cell shape features, actin and cell number. A) Regression coefficients of morphological features and intensity measurements from the actin cytoskeleton as predictors for ALP expression. B) Clustering analysis showing the similarities between the different descriptors, and their role in the prediction of ALP expression. C) High and low scoring examples for the two parameters most correlated to ALP expression.

Based on previous validation studies on osteogenic potential and the matching correlations from current image analysis, we selected topography T2_TI_0304 (Figure 3A, further referred to as ti-topography, and unpatterned titanium coated reference substrates as ti-flat), as mechanobiology-based osteogenic system to study underlying mechanisms of mechanotransduction. Here, ti-topography was found to induce osteogenic differentiation – as based on ALP expression (Figure 3B) – solely by this unique defined surface topography.

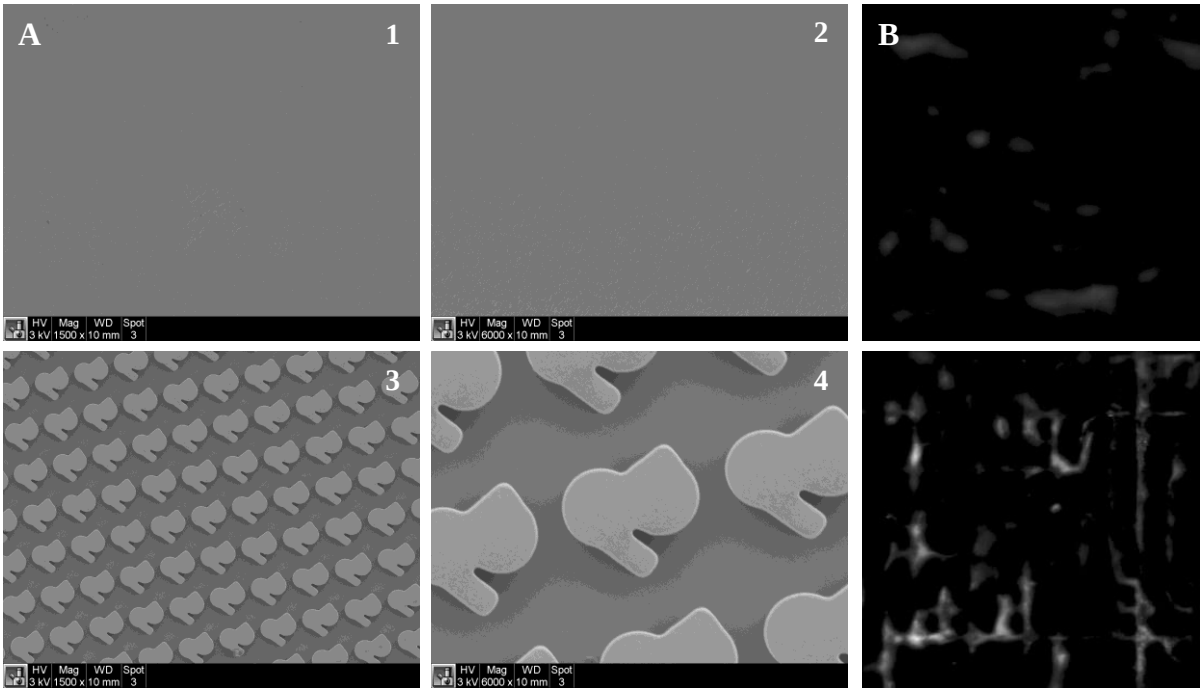

Figure 3: TopoChip-derived topography potent to induce osteogenic differentiation. A) SEM images of cell culture substrates: unpatterned (1. 1500x magnification and 2. 6000x magnification) and topographically enhanced (3. 1500x magnification and 4. 6000x magnification). B) Micrographs of ALP expression after 5 days on ti-flat and hit surface ti-topography, each 290 × 290 µm.

The identification of the osteogenic ti-topography allowed us to study the biological model in which MSCs initiate their osteogenic program as a response to mechanical stimuli. The first striking effect of ti-topography on cells, compared to flat substrates, is the dramatically altered cell and nucleus shape. Within 24 hours after seeding, the cells adapted their shape due to the confinement by the topographical features of ti-topography. This resulted in a strongly compressed and elongated cell morphology, compared to the typical spindle-shaped spreading of hMSCs on flat materials. Besides the clear changes in total cell morphology, we also observed significant changes in sub-cellular traits such as the cell nucleus, endoplasmic reticulum, actin cytoskeleton, and the mitochondria (Figure 4). Here, the strong spatial confinement to which the cells adapted resulted in a condensation of cell organelle distribution. For example, whereas the mitochondria were homogenously distributed throughout the cell when cultured on ti-flat, we observed a strong signal from the region of the cell nucleus on ti-topography. Furthermore, we did not observe any F-actin stress fiber formation on ti-topography, whereas these fibers were present in MSCs on ti-flat.

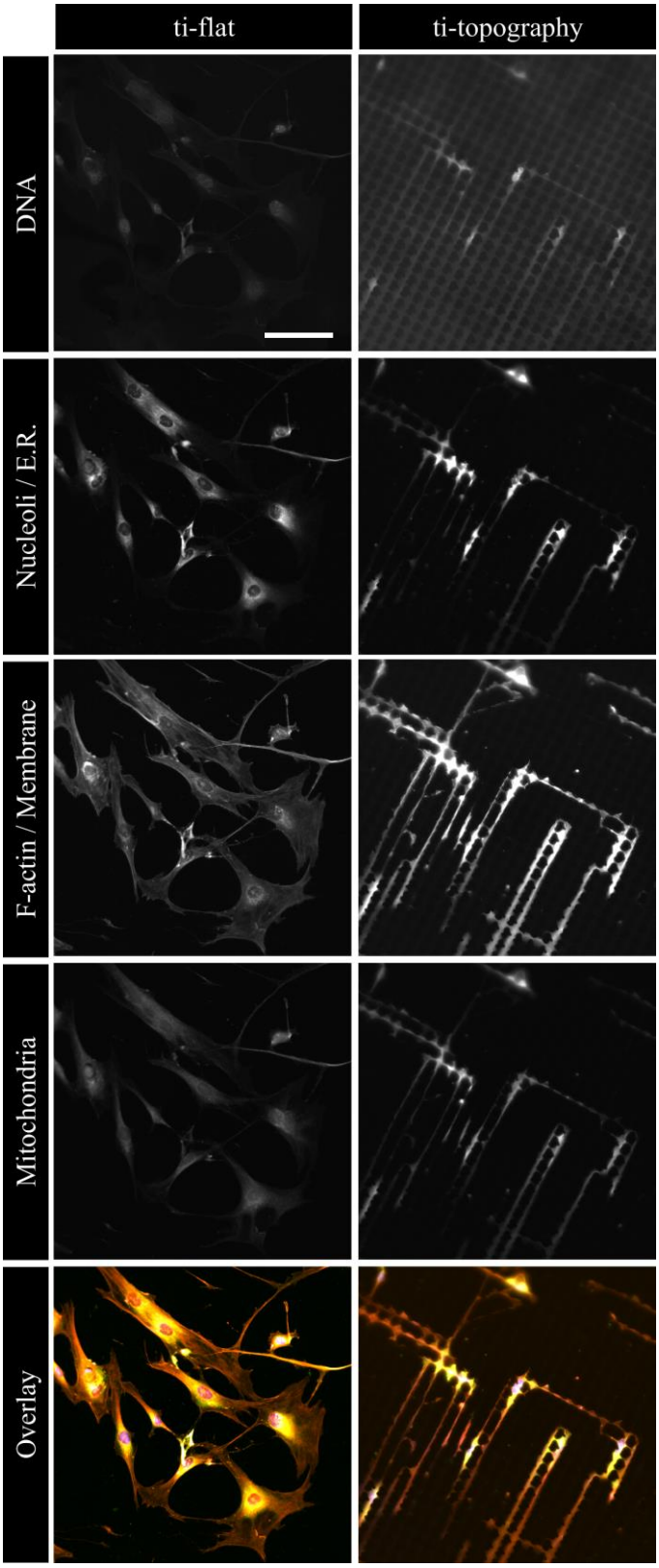

Figure 4: Surface topography alters subcellular traits. MSCs cultured for 24 hours on ti-flat and the osteogenic ti-topography substrate before fluorescently labeling various cellular entities as shown in the panel. Scale bare represents 100 µm. The overlay contains the four different channels: DNA (blue), nucleoli and endoplasmic reticulum (green), F-actin and plasma membrane (yellow), and mitochondria (red).

Mechanobiological signaling is initiated upon cell attachment

The dramatic cellular deformation reached its most spread status after 24 hours, and is expected to activate mechanosensitive signaling cascades. However, the cells start adapting to their environment directly upon attachment where there is immediately some level of confinement. These initial physical stimuli will be decisive for early responses, and therefore we assessed the topographically guided development of morphology within this adhesion period. As expected, MSCs attached to the flat substrates within 4 hours and reach a completely spread morphology with many thin actin fibers within 24 hours (Figure 5 top). A similar regime was observed for MSCs that attached to topographically enhanced substrates, however, they immediately adapted to the surrounding topographical features. Directly from the earliest time point, distinct differences in both cell and nucleus morphology were observed (Figure 5 bottom).

Integrins are transmembrane adhesion receptors and play an important role in cellular attachment onto materials. Typically, the activation of these cell adhesion receptors leads to the formation of focal adhesion complexes, a cluster of proteins connected with the actin cytoskeleton. Since there is an evident role for the modeling of the cytoskeleton in osteogenesis, we hypothesized that MSCs create their focal adhesion complexes differently on ti-topography compared to the flat reference. To assess this, we stained the focal adhesion protein vinculin 2 and 24 hours after cell seeding. After 2 hours, the MSCs were attached with a circular morphology in both conditions and were still actively spreading in order to reach their final state. At this point, we observed pronounced matured focal adhesion complexes on ti-flat which were mainly situated at the cell's periphery in structures resembling lamellopodia. In contrast, only few focal adhesion complexes were observed on ti-topography and all of them were significantly smaller in size. Again, these adhesion sides were located at the cell's periphery, and interestingly not around the topographical features (Figure 6A). The intensity of the vinculin staining appears more intense on ti-topography but image analysis revealed that integrated intensity, representing the total signal per cell does not differ between surfaces. After 24 hours of culture, the significant differences in complex maturation remained, while the cellular morphology had changed completely by this time. Where we observed large focal adhesion complexes in the periphery of the MSCs on ti-flat, vinculin was distributed homogenous throughout the cells on ti-topography (Figure 6B). These observations suggest differences in focal adhesion formation and perhaps in focal adhesion mediated signaling. To investigate this, we quantified the amount of focal adhesion kinase (FAK, another key component of the focal adhesion complex) and the phosphorylated FAK by Western blot analysis. Interesting, no difference was observed between MSCs cultured on either ti-flat or ti-topography after 24 hours (Figure 6C).

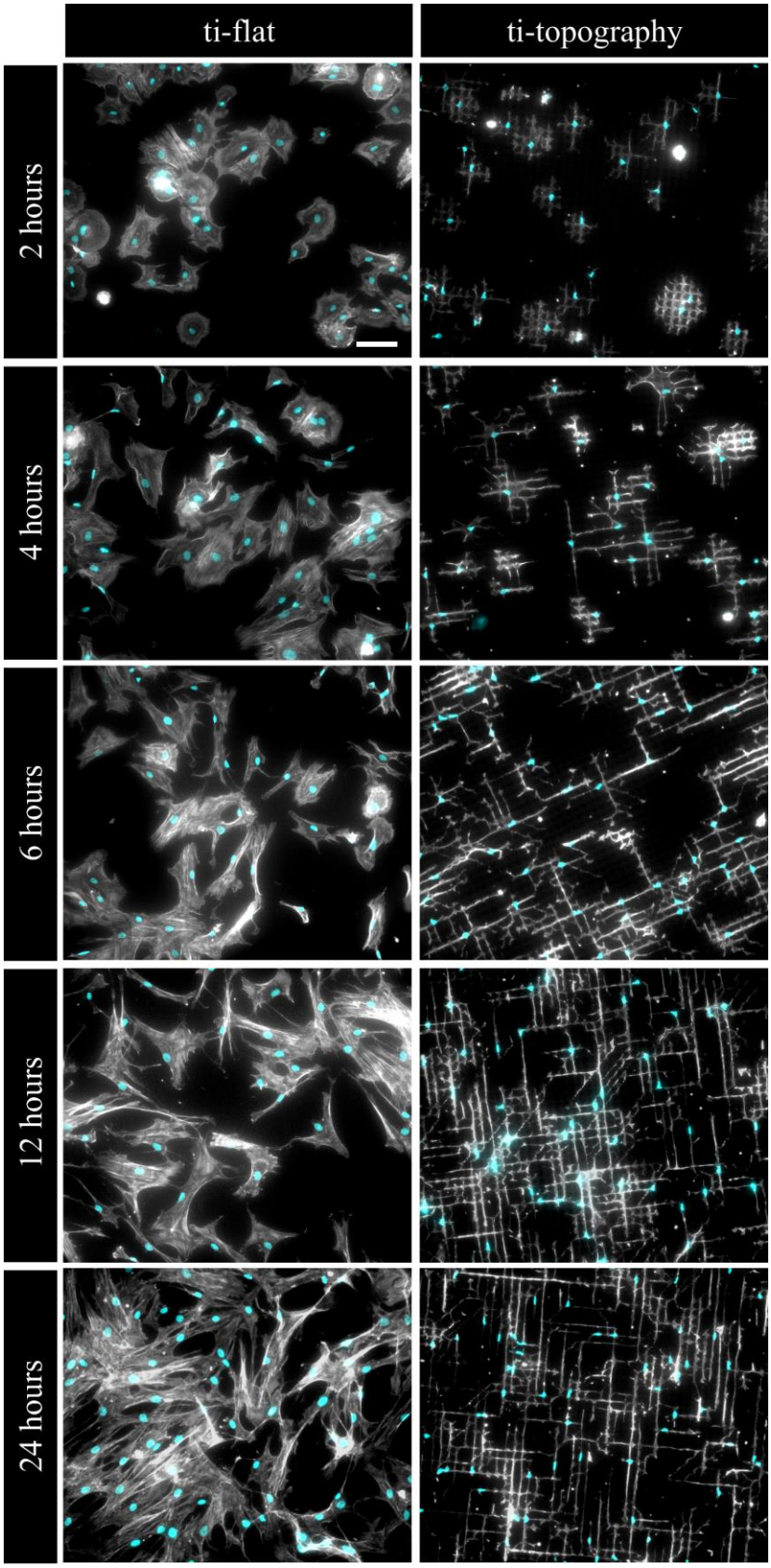

Figure 5: Differential hMSCs attachment to osteogenic surface topography. MSC morphology on ti-flat and ti-topography substrates 2, 4, 6, 12, and 24 hours after seeding. Micrographs include F-actin (gray) and DNA (blue) staining, and the scale bar represents 100 µm.

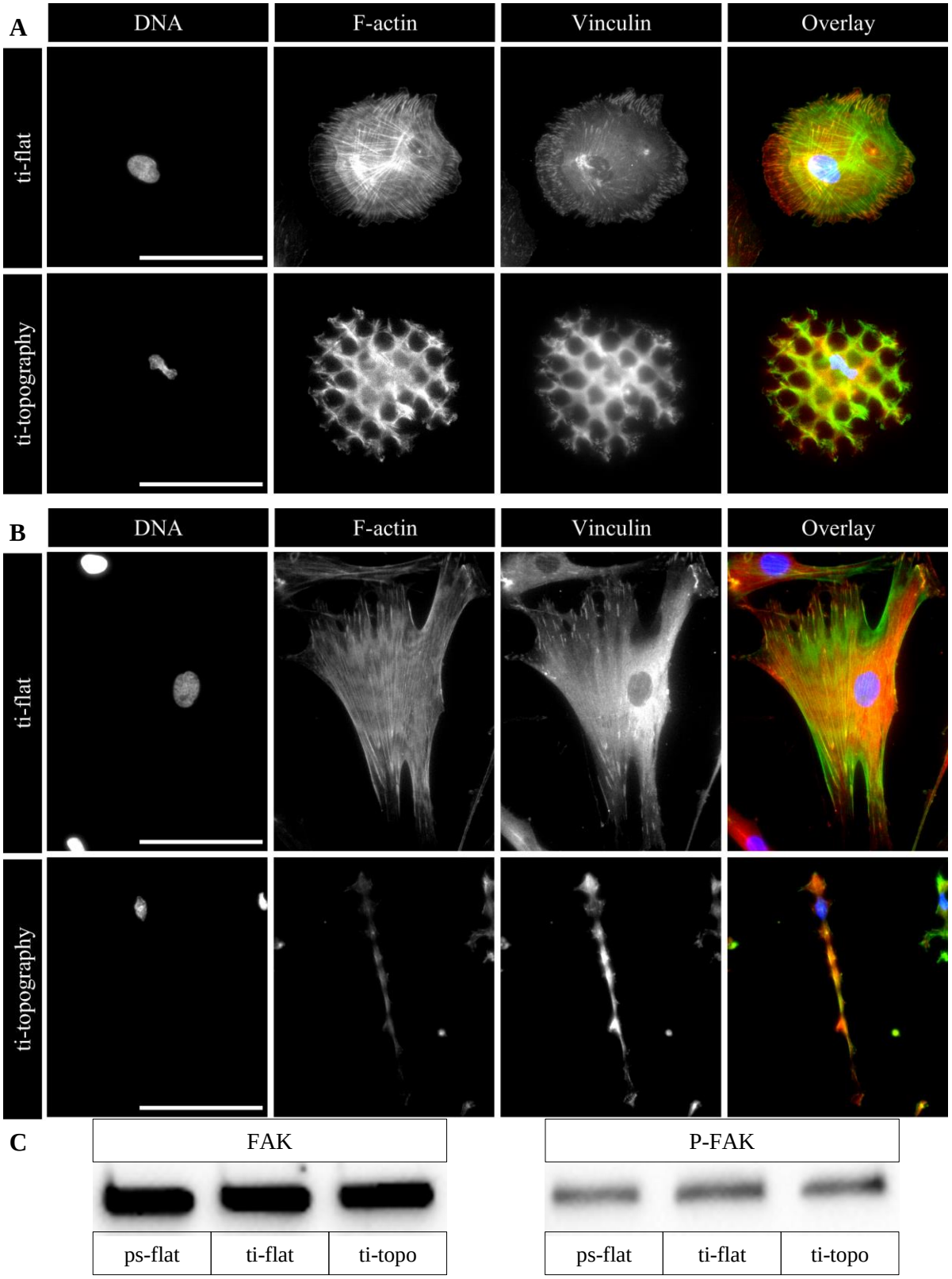

Figure 6: Differential focal adhesion complex formation on topographically enhanced surfaces. Vinculin expression in hMSCs exposed to ti-flat and ti-topography substrates for (A) 2 and (B) 24 hours. The overlay image shows the stain for DNA (blue), F-actin (green), and vinculin (red). The scale bar represents 100 µm. C) Western blot analysis of focal adhesion kinase (total and mount and phosphorylation specific) abundance after 24 hours of culture.

The clear differences in cell morphology and adhesion complexes which regulate the cytoskeleton are already apparent after 2 hours, indicating an early physical stimulation. Therefore, we wanted to investigate a potential role of known mechanosensitive proteins and early responder proteins YAP, EGR1 (early growth response protein 1) and SRF (serum response factor). As actin remodeling plays an important role in YAP activity, we quantified its translocation at multiple time points within the first 24 hours of attachment, in which we observed the largest changes in the cellular morphology. Consistent with early differences in focal adhesions formation, during the first 4 hours, MSCs experienced the strongest difference in YAP localization between ti-flat and ti-topography (Figure 7A). Here, we observed more nuclear YAP (un-phosphorylated, active) in MSCs exposed to ti-topography (Figure 7C) compared to the flat reference (Figure 7B). This difference diminished over time, and reached similar levels after 24 hours. We observed a similar trend for EGR1 and SRF, in which a pronounced difference in nuclear localization was observed after 3 hours, fading away after 24 hours (Figure 7D). The early response of this selection of mechanosensitive proteins points-out that potential key triggers are given to the cells already within this first period of attachment.

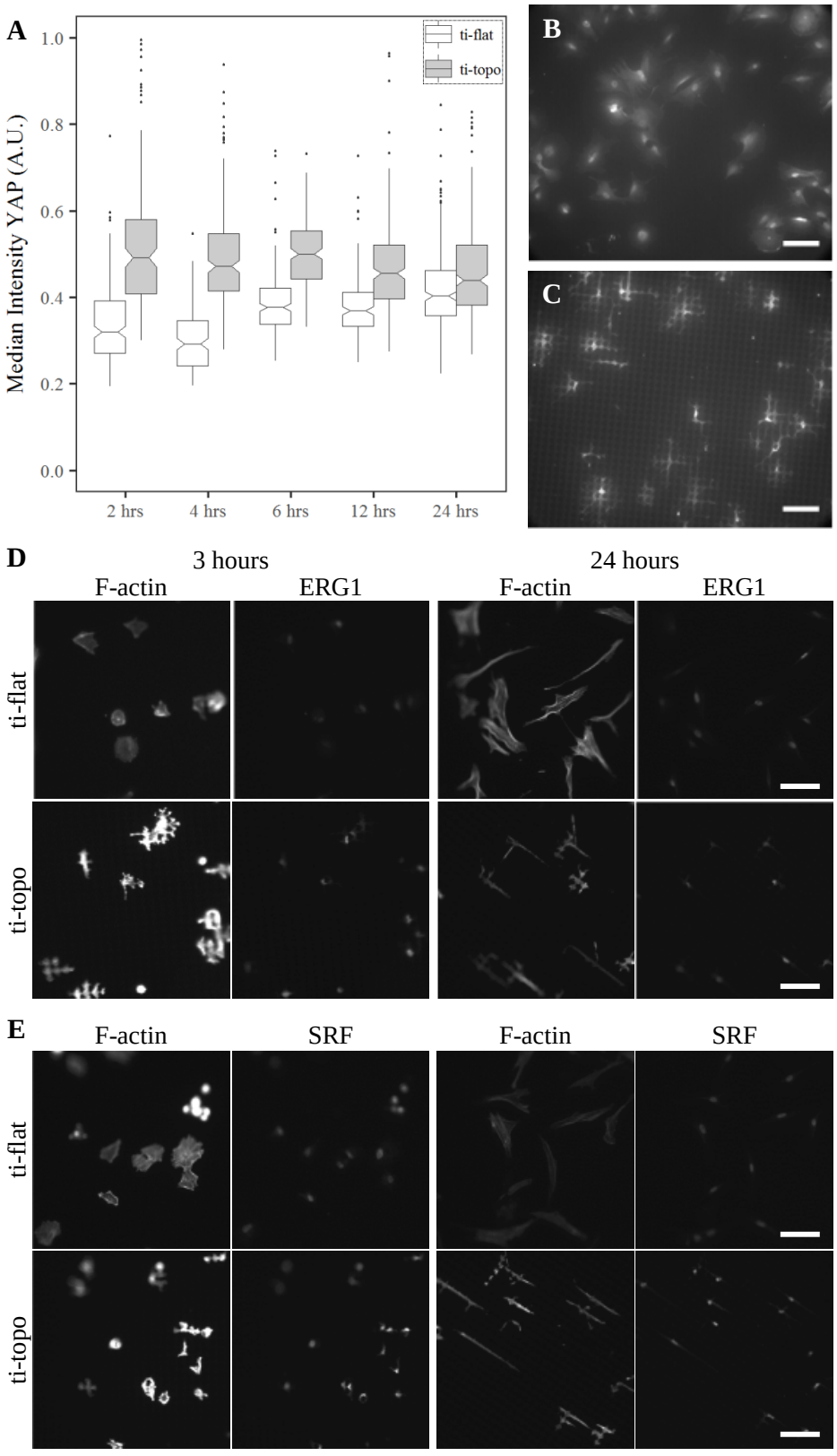

Figure 7: Topography induced differential YAP translocation. hMSCs were exposed to ti-flat and ti-topography substrates and stained for YAP. A) Quantification of per cell YAP translocation after 2, 4, 6, 12 and 24 hours of culture. Representative micrograph of YAP translocation after 2 hours on (B) ti-flat and (C) ti-topography substrates. Micrographs of (D) EGR1 and (E) SRF expression after 3 and 24 hours on ti-flat and ti-topography. All scale bars represent 100 µm.

Hypoxia response-like gene expression profiles are involved in mechanotransduction

The activation of YAP, EGR-1, and SRF showed clearly that MSCs on ti-topography experience mechanobiological stimuli. However, in order to obtain a broader overview of involved signaling pathways, we assessed topographically-induced alterations in gene expression profiles. We exposed MSCs to ti-flat and ti-topography for 2, 24 and 120 hours and assessed whole transcriptome profiles. We observed significant changes, as quantified by up and down-regulated genes of at least a 1.5 times difference. Using these cut-off criteria, we identified the differential expression of hundreds of genes between flat and topographically enhanced substrates on all time points (Table 1). Furthermore, for 24 and 120 hours we included a condition in which osteogenesis was induced by dexamethasone. Interestingly, we also found hundreds of genes to be differentially expressed between the chemical and the physically induced osteogenesis.

Table 1: Topography induced differential gene expression. Microarray analysis of hMSCs exposed to ti-flat and ti-topography substrates for 2, 24 and 120 hours (24 and 120 hours included an additional conditions with dexamethasone). Both up and down regulated genes are identified, for subtle differences (p-value <0.05 / fold change >1.5) as well as more stringent criteria (p-value <0.05 / fold change >2).

Time Point	Comparison	Nr. of DEGs (subtle)	Total	Nr. of DEGs (stringent)	Total
2 hrs	ti-flat vs ti-topo	110 up / 128 down	238	14 up / 25 down	39
24 hrs	ti-flat vs ti-flat + dex	113 up / 163 down	276	29 up / 38 down	67
	ti-flat vs ti-topo	253 up / 98 down	351	42 up / 3 down	45
	ti-flat + dex vs ti-topo	447 up / 389 down	836	71 up / 65 down	136
120 hrs	ti-flat vs ti-flat + dex	281 up / 255 down	536	93 up / 81 down	174
	ti-flat vs ti-topo	99 up / 124 down	223	14 up / 26 down	40
	ti-flat + dex vs ti-topo	436 up / 517 down	953	119 up / 153 down	272

To identify the pathways which were affected strongest by surface topography, we narrowed the list of differential expressed genes down based on a fold change cut-off of 2. These genes were used to identify pathways in which a significant fraction of the DEGs was present according to gene ontology analysis. Comparing gene expression profiles of cell populations exposed for 2 hours to ti-flat and ti-topography revealed a substantial overlap with genes

reported to be involved in striated muscle contraction. For the 24 and 120 hour time points we did not find strong correlations or biologically meaningful results (Table 2).

Since known pathways did not show strong correlations with the DEGs related to topography, we wanted to look in more detail at the possible relations between the individual genes. Therefore we used the DEGs from the three different time points to create gene networks, based on interactions that are known from literature (Figure 8). Most of the DEGs were included in networks, demonstrating a strong functional connection between the DEGs. Interestingly, for all time points, we observed a series of genes related to hypoxia signaling. Various genes regulated by the transcription factor HIF1α were found to be differentially expressed, and HIF1α became a prominent hub in all three networks. For example, VEGF-A and B were found to be differentially expressed, genes known to be involved in angiogenesis under hypoxic conditions. Furthermore, we found stanniocalcin-1, another gene which is upregulated in MSCs under hypoxia, to be differentially expressed.

Based on these strong HIF-related gene expression signatures in cells cultured on ti-topography across multiple time points, we hypothesized that cells on topographies stabilize HIF1α via known regulators. To test this, we explored the mitochondrial activity, accumulation of reactive oxygen species, and stabilization of HIF1α, as key-aspects of HIF1α regulation[42]. First, we measured the mitochondrial activity after 2, 24 and 72 hours. Cells cultured on ti-topography reduced their mitochondrial activity significantly after 72 hours, but not after 2 and 24 hours (Figure 9A). Furthermore, MSCs cultured for 24 hours on ti-flat and ti-topography did not accumulate different amounts of reactive oxygen species (Figure 9B). The final regulator assessed was HIF1α itself. Under normoxia HIF1α is degraded in the cytoplasm and only under hypoxic conditions, HIF1α is stabilized and translocates into the nucleus. Since our gene expression profiles showed many genes which could be regulated via HIF1α, we assessed HIF1α levels in MSCs on ti-flat and ti-topography. Interestingly, we did not observe stabilization of HIF1α on both substrates (Figure 9C). Together, we see a clear HIF1α-related gene network but did not find evidence for the molecular mechanism resulting in the expression of the genes.

Table 2: Gene expression based changes in phenotype induced by topography. Gene ontology analysis of the gene expression profiles of hMSCs after 2, 24, 120 hours on ti-flat and ti-topography.

	Pathway	Positive (r)	Measured (n)	Total	Overlap (%)
2 hrs	Striated muscle contraction	3	15	39	20.00
	Myometrial relaxation and contraction pathw.	4	109	161	3.67
	Calcium regulation in the cardiac cell	3	88	163	3.41
	Primary focal segmental glomerulosclerosis	2	52	78	3.85
	Hypertrophy model	1	18	21	5.56
	Common pathways in drug addiction	1	25	49	4.00
	Senescence and autophagy in cancer	2	94	112	2.13
	Preimplantation embryo	1	30	60	3.33
24 hrs	Cytoplasmic ribosomal proteins	3	87	89	3.45
	Oncogenic pathways as metastatic traits	1	15	18	6.67
	Canonical and non-canonical TGF-B signal.	1	15	18	6.67
	Parkin-ubiquitin proteasomal system pathway	2	62	75	3.23
	Apoptosis modulation by HSP70	1	17	22	5.88
	miRNA targets ECM and membrane recept.	1	20	46	5.00
	Inflammatory response pathway	1	22	34	4.55
	Pathw. pathogenesis of cardiovasc. Disease	1	24	27	4.17
	Alpha 6 Beta 4 signaling pathway	1	30	34	3.33
	Lung fibrosis	1	39	83	2.56
	Focal adhesion	2	151	192	1.32
120 hrs	Deregulation of Rab and Rab effector genes	1	9	17	11.11
	Blood clotting cascade	1	11	25	9.09
	Senescence and autophagy in cancer	3	94	112	3.19
	Osteopontin signaling	1	12	14	8.33
	Hypertrophy model	1	18	21	5.56
	Photodyn.-induced unfolded protein response	1	24	28	4.17
	Insulin-like growth factor-Akt signaling	1	25	34	4.00
	Adipogenesis	2	98	132	2.04
	Preimplantation embryo	1	30	60	3.33
	Complement and coagulation cascades	1	35	63	2.86
	Lung fibrosis	1	39	83	2.56
	PPAR signaling pathway	1	41	75	2.44

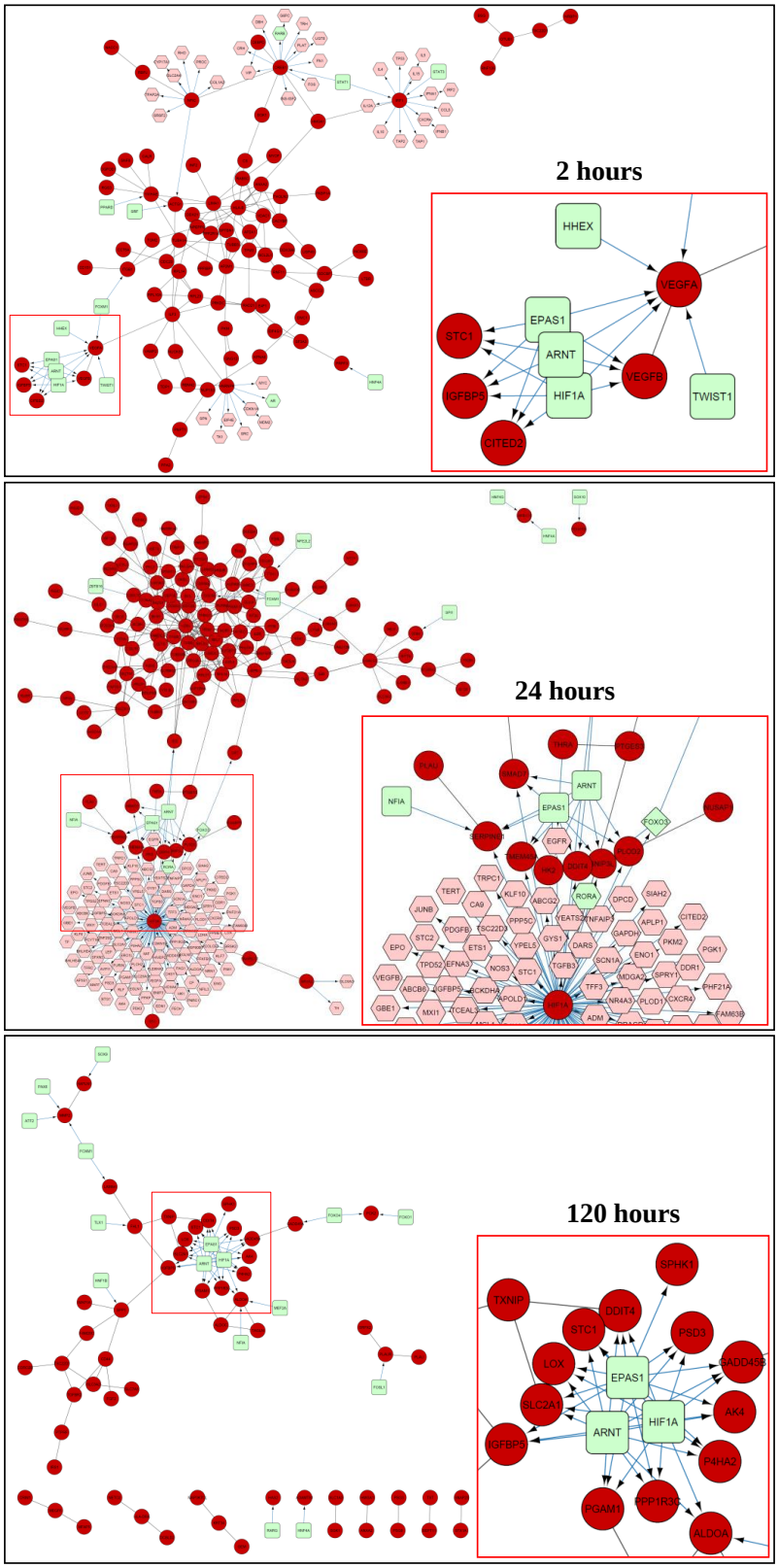

Figure 8: Topography induced strongly connected gene networks. Visualization of the interactions between the DEGs (ti-flat vs. ti-topography) of hMSCs after 2, 24 and 120 hours. The gene hubs revolving around the HIF-pathway are highlighted in the red squares. Red circles represent microarray identified DEGs, green squares represent CyTargetLinker added transcription factors, and pink hexagons represent CyTarget linker added genes used to create the networks.

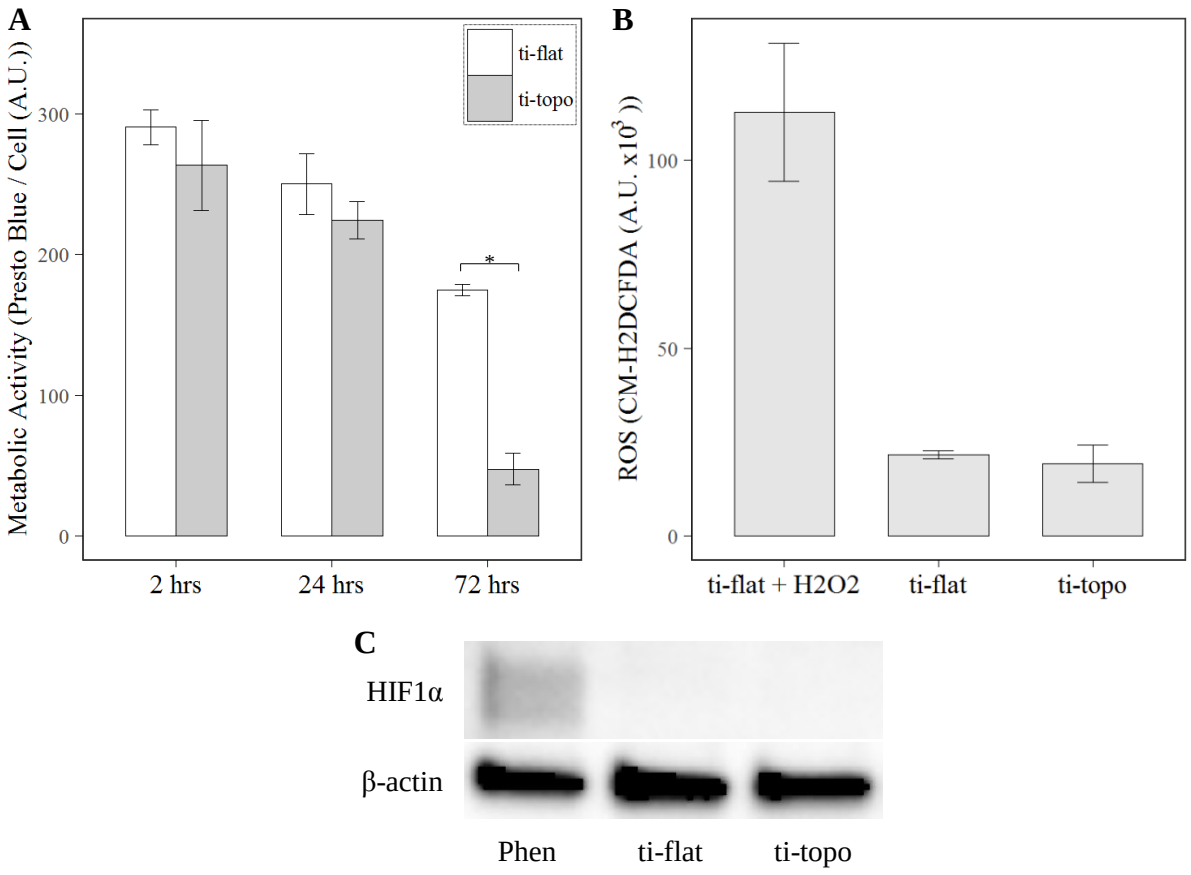

Figure 9: Topography does not act along hypoxia induced signaling. A) Mitochondrial activity per cell in MSCs using Presto Blue at 2, 24 and 73 hours of culture on ti-flat and ti-topography. B) Intercellular reactive oxygen species after 24 hours of culture on ti-flat and ti-topography using CM-H_2DCFDA for flow cytometry, using H_2O_2 as a positive control for ROS accumulations. C) Western blot of HIF1α stabilization after 24 hours of culture on ti-flat and ti-topography, with phenanthroline as a positive control for HIF1α stabilization.

A potential role for epigenetics in mechanotransduction.

Next, we compared the topography induced DEG set with gene expression profiles induced by chemical compounds using the Connectivity Map database[43]. All genes measured with at least a 1.5 times difference between ti-flat and ti-topography after 24 hours were included in this analysis. Interestingly, we found a strong correlation between our list of DEGs and that of multiple gene expression profiles which were based on an induction by trichostatin A (Table 3). Trichostatin A is a drug known to regulate the acetylation of histones. Therefore, we wanted to explore the possible influence of epigenetic components on the altered mechanobiological processes as found on ti-topography. Furthermore, we identified an overlap with a HSP90 inhibitor which is applied in cancer treatment (tanespimycin), all-trans retinoic acid (tretinoin) which has a great overlap with epigenetics again, and a PI3K inhibitor (LY-294002).

Table 3: Topography induced gene expression profiles resemble compound genotypes. Connectivity map comparison for the overlap of the differential expressed genes of hMSCs after 24 hours on ti-topography (vs. ti-flat) with various compound induced gene expression profiles.

Reference set name	Biological process	Set size	Query length
Trichostatin A 0.1 μM MCF7	Histone acetylation	69	332
Trichostatin A 0.1 μM PC3	Histone acetylation	39	332
Trichostatin A 0.1 μM HL60	Histone acetylation	31	332
Trichostatin A 1 μM MCF7	Histone acetylation	23	332
Tanespimycin 1 μM PC3	HSP90 inhibitor	12	332
Tretinoin 1 μM MCF7	All-trans retinoic acid	11	332
LY-294002 10 μM PC3	PI3K inhibitor	10	332

Acetylation of histones influences DNA condensation, which can influence the size and morphology of the nucleus. As described above, the nuclei of cells cultured on ti-topography are dramatically deformed immediately after cell attachment. Assessment of this nucleus deformation by quantitative image analysis revealed a strong alteration in both size and shape (Figure 10A). With an average 2-fold size reduction, the nuclei of cells exposed to ti-topography were significantly smaller. Furthermore, we quantified elongation of the nuclei on ti-topography which were more ellipse-shaped compared with the rounder oval nuclei as found on ti-flat (Figure 10B). Of note, we observed bright DAPI staining in regions of the nuclei on ti-topography, which points at differences in DNA condensation (Figure 10C). Within the nucleus, lamins are important structural proteins which are located at the nuclear envelope in order to create the stiffness needed to maintain its shape. It is known that lamin expression is affected by physical stimulation, e.g the abundancy of lamin A and its splice-variant C is known to increase on stiffer substrates[25]. We confirmed a mechanobiological aspect in lamin regulation by a reduction of lamin A and C abundance in cells which are exposed to surface topography. Whereas cells cultured for 24 hours on ti-flat expressed both lamin A and C, it was undetectable in cell cultured on ti-topography (Figure 10D). Interestingly, the role of substrate chemistry also greatly impacted the expression of lamin A and C. We observed a ten-fold higher lamin A and C expression in cells on regular flat tissue culture plastic compared to ti-flat, which shows the potential synergy of substrate chemistry and surface topography in influencing molecular mechanisms.

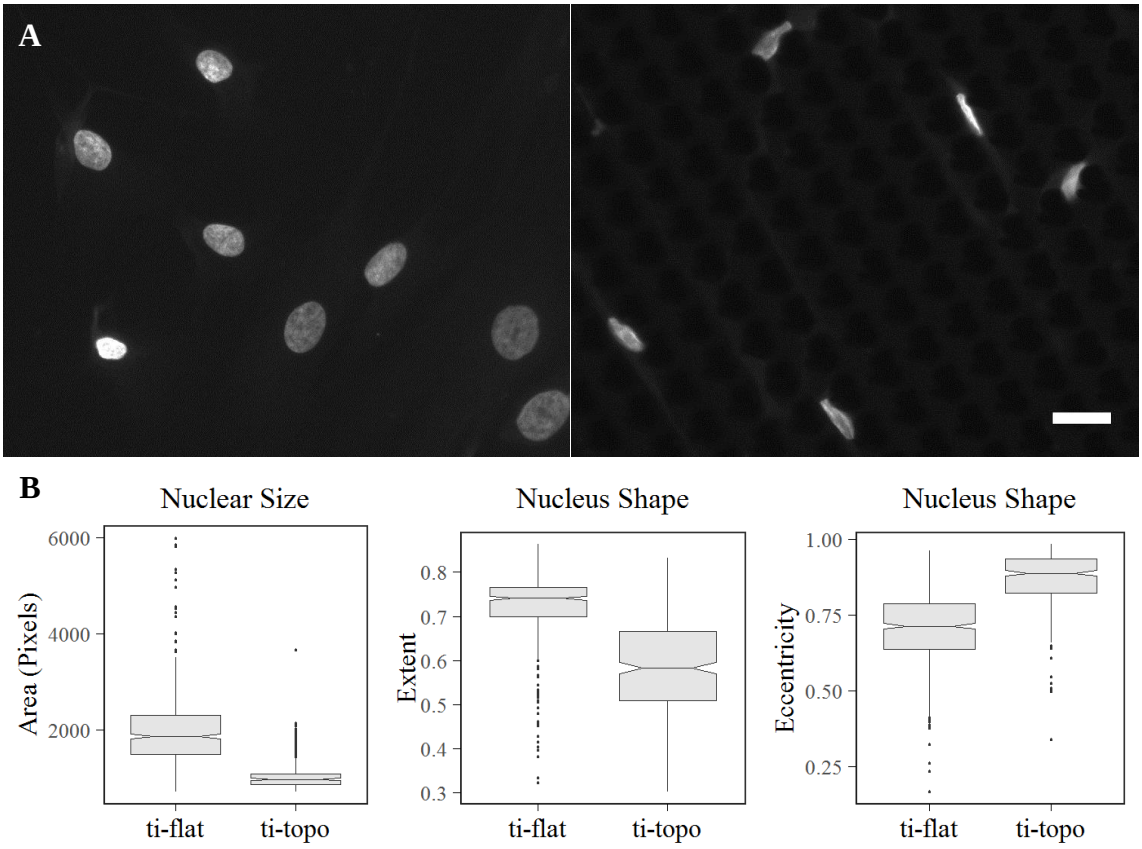

	TCP	ti-flat	ti-topo
Lamin A	931	95	NAN
Lamin C	2377	295	NAN
B-actin	34490	30065	26185

Figure 10: Topography induced differences in epigenetic factors. A) Representative micrographs of nuclei of cells cultured on ti-flat (left) and ti-topography (right). B) Morphological quantifications showed significant differences between ti-flat (N=543) and ti-topography (N=383) in a variety of size and shape descriptors. C) Representative micrographs cells cultured on ti-flat (top left) and ti-topography in which DNA condensation can be appreciated. D) Western blot analysis of lamin A and C expression in cells cultured on flat TCP, ti-flat, and ti-topography for 24 hours and signal intensity quantifications. In the micrographs, the DNA is stained with DAPI, and the scale bar represents 25 µm (A) and 10 µm (C).

Discussion

In this manuscript we used a mechanotransduction-based osteogenic system to study the underlying mechanisms of surface topography induced mechanotransduction in MSCs. This surface topography was previously described to induce ALP expression, without the addition of any chemical osteogenic compounds, express late markers for osteogenic differentiation together with matrix mineralization in an osteogenic environment and improve bone bonding in vivo[30]. However, the underlying signaling pathways which are activated leading to this osteogenic phenotype remained to be elucidated. We used a holistic approach in which transcriptomics was used to provide more insight in pathway activity via topographically induced gene expression profiles.

Differential focal adhesion complex formation and actin configuration, together with an early response in the translocation of the mechanosensitive YAP, EGR1, and SRF showed a clear mechanobiological response of MSCs on ti-topography compared to ti-flat. Interestingly, the formed focal adhesion complexes differed in maturation, but not in quantity. After activation upon cell attachment, the difference in activity of these mechanosensory proteins leveled out within the first 24 hours. Nevertheless, it is very well possible that key signaling pathways for mechanical induced osteogenesis were already activated within this timeframe. Moreover, re-activation of this family of transcription factors may occur after mitosis, when the round-up cells have to re-adhere to the underlying surface.

Transcriptomics analysis of MSCs exposed for various periods of time revealed a strong and compact network of interactions between DEGs. Interestingly, we observed a recurring signature of HIF signaling for all three assessed time points. A HIF signaling induced gene expression profile was found before in MSCs on osteoinductive ceramics[10]. Differential gene expression of e.g. STC1 and VEGF is known to occur under hypoxic conditions[44,45]. Therefore, we tested known components involved in the hypoxia response of MSCs, such as mitochondrial activity, oxidative stress, and HIF1α stabilization[42]. Interestingly, we did not observe a correlation between these components of a hypoxia response in MSCs in our system. Perhaps, a non-canonical pathway leads to hypoxia related gene expression. More experiments are needed to unravel such a pathway.

Comparing the differential gene expression between ti-flat and ti-topography with drug-induced gene expression profiles revealed a strong correlation with trichostatin A. Trichostatin A is known to manipulate the epigenetics of cells by inhibiting the activity of HDACs (histone deacetylases[46]. Besides this strong fingerprint of trichostatin A induced gene expression, we observed dramatic changes in nucleus size and shape. In line with our observations, it is known that material induced nuclear deformations have an effect on the cell's epigenetics and the reprogramming[26]. Future investigations should reveal how mechanotransduction can feed into epigenetic regulation of osteogenesis. Interestingly, we previously demonstrated that administration of TSA induces osteogenesis of MSCs[47].

The holistic approach to find the underlying mechanisms of mechanotransduction in MSCs – in a validated mechanobiological-based osteogenic system – confirmed three important players as known from literature. We found differential focal adhesion complex formation and cytoskeleton remodeling accompanied by early activation of mechanosensitive proteins, a hypoxia signature on a gene expression level, and the epigenetic state of the cells to be pronounced in MSCs exposed to our defined surface topography. Once more we show the potency of surface topography to control cell behavior, and demonstrate that ti-topography can be used to further explore the underlying mechanisms. It would be of great interest to link YAP translocation, non-canonical HIF1α-induced gene expression and the regulation of epigenetic processes resulting in osteogenic differentiation.

References

1. Charras, G. & Sahai, E. Physical influences of the extracellular environment on cell migration. *Nat. Rev. Mol. Cell Biol.* **15,** 813–824 (2014).

2. Ladoux, B. & Mège, R.-M. Mechanobiology of collective cell behaviours. *Nat. Rev. Mol. Cell Biol.* (2017). doi:10.1038/nrm.2017.98

3. Watt, F. M. Out of Eden: Stem Cells and Their Niches. *Science (80-.).* **287,** 1427–1430 (2000).

4. Discher, D. E. Tissue Cells Feel and Respond to the Stiffness of Their Substrate. *Science (80-.).* **310,** 1139–1143 (2005).

5. Palumbo, C., Palazzini, S. & Marotti, G. Morphological study of intracellular junctions during osteocyte differentiation. *Bone* **11,** 401–406 (1990).

6. Khetan, S. *et al.* Degradation-mediated cellular traction directs stem cell fate in covalently crosslinked three-dimensional hydrogels. *Nat. Mater.* **12,** 458–465 (2013).

7. van de Peppel, J. *et al.* Identification of Three Early Phases of Cell-Fate Determination during Osteogenic and Adipogenic Differentiation by Transcription Factor Dynamics. *Stem Cell Reports* **8,** 947–960 (2017).

8. Siddappa, R. *et al.* cAMP / PKA pathway activation in human mesenchymal stem cells in vitro results in robust bone formation in vivo. *Proc. Natl. Acad. Sci.* **105,** 7281–7286 (2008).

9. Piek, E. *et al.* Osteo-transcriptomics of human mesenchymal stem cells: Accelerated gene expression and osteoblast differentiation induced by vitamin D reveals c-MYC as an enhancer of BMP2-induced osteogenesis. *Bone* **46,** 613–627 (2010).

10. Groen, N. *et al.* Linking the Transcriptional Landscape of Bone Induction to Biomaterial Design Parameters. *Adv. Mater.* **29,** (2017).

11. Dalby, M. J. *et al.* The control of human mesenchymal cell differentiation using nanoscale symmetry and disorder. *Nat. Mater.* 997–1003 (2007). doi:10.1038/nmat2013

12. Pongkitwitoon, S., Uzer, G., Rubin, J. & Judex, S. Cytoskeletal Configuration Modulates Mechanically Induced Changes in Mesenchymal Stem Cell Osteogenesis, Morphology, and Stiffness. *Sci. Rep.* **6,** 1–12 (2016).

13. Arnsdorf, E. J., Tummala, P., Kwon, R. Y. & Jacobs, C. R. Mechanically induced osteogenic differentiation - the role of RhoA, ROCKII and cytoskeletal dynamics. *J. Cell Sci.* **122,** 546–553 (2009).

14. Kilian, K. A., Bugarija, B., Lahn, B. T. & Mrksich, M. Geometric cues for directing the differentiation of mesenchymal stem cells. *Proc. Natl. Acad. Sci.* **107,** 4872–4877 (2010).

15. Uzer, G., Pongkitwitoon, S., Ete Chan, M. & Judex, S. Vibration induced osteogenic commitment of mesenchymal stem cells is enhanced by cytoskeletal remodeling but not fluid shear. *J. Biomech.* **46,** 2296–2302 (2013).

16. Rodríguez, J. P., González, M., Ríos, S. & Cambiazo, V. Cytoskeletal organization of human mesenchymal stem cells (MSC) changes during their osteogenic differentiation. *J. Cell. Biochem.* **93,** 721–731 (2004).

17. Dupont, S. *et al.* Role of YAP/TAZ in mechanotransduction. *Nature* **474,** 179–183 (2011).

18. Reddy, P., Deguchi, M., Cheng, Y. & Hsueh, A. J. W. Actin Cytoskeleton Regulates Hippo Signaling. *PLoS One* **8,** e73763 (2013).

19. Zhao, B. *et al.* Cell detachment activates the Hippo pathway via cytoskeleton reorganization to induce

anoikis. *Genes Dev.* **26,** 54–68 (2012).

20. Yagi, R., Chen, L. F., Shigesada, K., Murakami, Y. & Ito, Y. A WW domain-containing Yes-associated protein (YAP) is a novel transcriptional co-activator. *EMBO J.* **18,** 2551–2562 (1999).

21. Tang, Y. *et al.* MT1-MMP-Dependent Control of Skeletal Stem Cell Commitment via a ??1-Integrin/YAP/TAZ Signaling Axis. *Dev. Cell* **25,** 402–416 (2013).

22. Clapham, D. E. TRP channels as cellular sensor. *Nature* **426,** 517–524 (2003).

23. Xiao, E. *et al.* TRPM7 Senses Mechanical Stimulation Inducing Osteogenesis in Human Bone Marrow Mesenchymal Stem Cells. *Stem Cells* 1–9 (2014). doi:10.1002/stem.1858

24. Tsimbouri, P. M. *et al.* Stimulation of 3D osteogenesis by mesenchymal stem cells using a nanovibrational bioreactor. *Nat. Biomed. Eng.* **1,** 758–770 (2017).

25. Swift, J. *et al.* Nuclear Lamin-A Scales with Tissue Stiffness and Enhances Matrix-Directed Differentiation. *Science (80-.).* **341,** 1240104–1240104 (2013).

26. Downing, T. L. *et al.* Biophysical regulation of epigenetic state and cell reprogramming. *Nat. Mater.* **12,** 1154–1162 (2013).

27. Arnsdorf, E. J., Tummala, P., Castillo, A. B., Zhang, F. & Jacobs, C. R. The epigenetic mechanism of mechanically induced osteogenic differentiation. *J. Biomech.* **43,** 2881–2886 (2010).

28. Wang, J. *et al.* Mechanical stimulation orchestrates the osteogenic differentiation of human bone marrow stromal cells by regulating HDAC1. *Cell Death Dis.* **7,** e2221 (2016).

29. Unadkat, H. V *et al.* An algorithm-based topographical biomaterials library to instruct cell fate. *Proc. Natl. Acad. Sci.* **109,** 5905–5905 (2012).

30. Hulshof, F. F. B. *et al.* Mining for osteogenic surface topographies: In silico design to in vivo osseo-integration. *Biomaterials* **137,** 49–60 (2017).

31. Both, S. K., van der Muijsenberg, A. J. C., van Blitterswijk, C. A., de Boer, J. & de Bruijn, J. D. A rapid and efficient method for expansion of human mesenchymal stem cells. *Tissue Eng.* **13,** 3–9 (2007).

32. Eijssen, L. M. T. *et al.* User-friendly solutions for microarray quality control and pre-processing on ArrayAnalysis.org. *Nucleic Acids Res.* **41,** 71–76 (2013).

33. Kamburov, A., Stelzl, U., Lehrach, H. & Herwig, R. The ConsensusPathDB interaction database: 2013 Update. *Nucleic Acids Res.* **41,** 793–800 (2013).

34. Kutmon, M., Kelder, T., Mandaviya, P., Evelo, C. T. A. & Coort, S. L. Cytargetlinker: A Cytoscape app to integrate regulatory interactions in network analysis. *PLoS One* **8,** 1–9 (2013).

35. Shannon, P. *et al.* Cytoscape: a software environment for integrated models of biomolecular interaction networks. *Genome Res.* 2498–2504 (2003). doi:10.1101/gr.1239303.metabolite

36. Yusuf, D. *et al.* The Transcription Factor Encyclopedia. *Genome Biol.* **13,** R24 (2012).

37. Bray, M.-A. *et al.* Cell Painting, a high-content image-based assay for morphological profiling using multiplexed fluorescent dyes. *Nat. Protoc.* **11,** 1757–1774 (2016).

38. Hulsman, M. *et al.* Analysis of high-throughput screening reveals the effect of surface topographies on cellular morphology. *Acta Biomater.* **15,** 29–38 (2015).

39. Carpenter, A. E. *et al.* CellProfiler: image analysis software for identifying and quantifying cell phenotypes. *Genome Biol.* **7,** R100 (2006).

40. R Core team. R. A Language and environment for statistical Computing. (2014).

41. Kuhn, M. Building Predictive Models in R Using the caret Package. *J. Stat. Softw.* **28,** 1–26 (2008).

42. Movafagh, S., Crook, S. & Vo, K. Regulation of hypoxia-inducible Factor-1a by reactive oxygen species: New developments in an old debate. *J. Cell. Biochem.* **116,** 696–703 (2015).

43. Lamb, J. *et al.* The Connectivity Map : Using Gene-Expression Signatures to Connect Small Molecules, Genes, and Disease. *Science (80-.).* **313,** 1929–1936 (2006).

44. Ohnishi, S., Yasuda, T., Kitamura, S. & Nagaya, N. Effect of Hypoxia on Gene Expression of Bone Marrow-Derived Mesenchymal Stem Cells and Mononuclear Cells. *Stem Cells* **25,** 1166–1177 (2007).

45. Doorn, J. *et al.* A small molecule approach to engineering vascularized tissue. *Biomaterials* **34,** 3053–3063 (2013).

46. Teven, C. M. *et al.* Epigenetic Regulation of Mesenchymal Stem Cells: A Focus on Osteogenic and Adipogenic Differentiation. *Stem Cells Int.* **2011,** 1–18 (2011).

47. de Boer, J. *et al.* Inhibition of Histone Acetylation as a Tool in Bone Tissue Engineering. *Tissue Eng.* **12,** 2927–2937 (2006).

⠠⠞⠓⠑ ⠠⠟⠥⠊⠉⠅ ⠃⠗⠕⠺⠝ ⠋⠭ ⠚⠥⠍⠏⠎ ⠕⠧⠑⠗ ⠞⠓⠑ ⠇⠁⠵⠽ ⠙⠕⠛

Chapter 4

Dynamic adaptation of mesenchymal stem cell physiology upon exposure to surface micropatterns

Nick R.M. Beijer[1], Zarina M. Nauryzgaliyeva[1], Estela M. Arteaga[1], Laurent Pieuchot[2], Karine Anselme[2], Jeroen van de Peppel[3], Aliaksei S. Vasilevich[1], Nathalie Groen[1], Nadia Roumans[1], Dennie G.A.J. Hebels[1] & Jan de Boer[1]

[1] Department of Cell Biology Inspired Tissue Engineering, MERLN Institute for Technology-Inspired Regenerative Medicine, Maastricht University, Maastricht, the Netherlands. [2] Institut de Science des Materiaux de Mulhouse, University of Haute-Alsace, CNRS, IS2M UMR7361, F-68100 Mulhouse, France. [3] Department of Internal Medicine, Erasmus University Medical Center, Rotterdam, the Netherlands.

Abstract

Human mesenchymal stem cells (hMSCs) are defined as multi-potent cells expressing a specific subset of plasma membrane markers grown on flat polystyrene. However, as soon as hMSCs are used for transplantation, they are exposed to a 3D environment, which can strongly impact cell physiology and influence proliferation, differentiation and metabolism. Strategies to control *in vivo* cell behavior, for instance for stem cell transplantation or cancer treatment, are skewed by the un-physiological flatness of the standard well plates. We used micrometer-scale defined surface topographies as model to describe the phenotype of hMSCs during adaptation to their new environment. Compared to hMSCs cultured on flat polystyrene, we observed dramatically changed cell morphologies accompanied by shrinkage of cytoplasm and nucleus, a decreased overall cellular metabolism, and a slower cell cycle progression resulting in a lower proliferation rate in cells exposed to surface topographies. We hypothesized that this reduction in proliferation rate models an anti-cancerous state, which was confirmed by higher survival rate of hMSCs cultured on topographies after treatment with the anti-cancer drug paclitaxel. Thus, micro-topographies can be used as a model system to mimic the natural cell micro-environment, and be a powerful tool to optimize cell treatment *in vitro*.

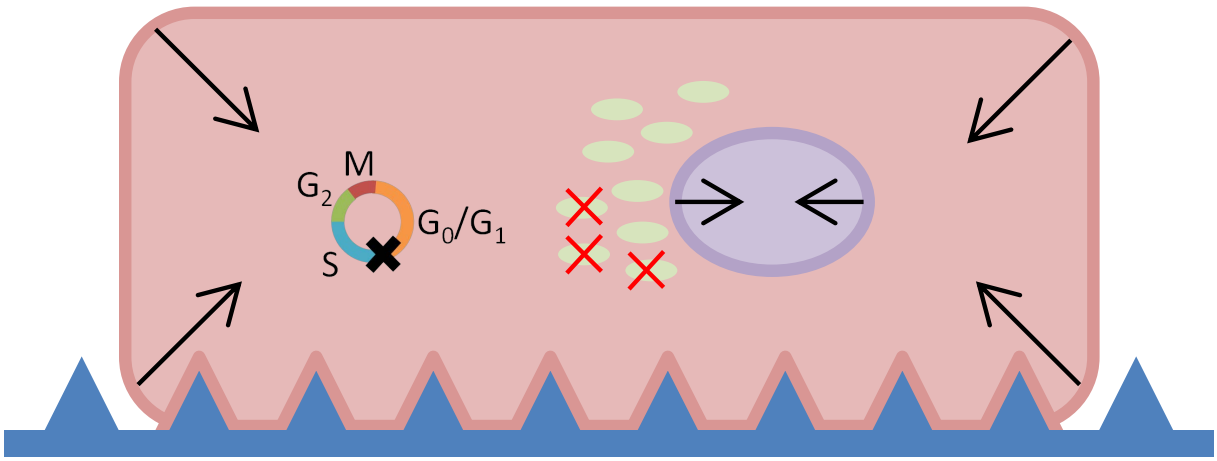

Introduction

Human mesenchymal stem or stromal cells (hMSCs) have a spherical morphology *in vivo,* display a quiescent phenotype and their biological function centers around paracrine communication with the surrounding tissue. hMSCs are exposed to flat tissue culture polystyrene (TCP) the moment they are harvested from the human body and cultured *in vitro*. The cells rapidly adhere and spread in a two dimensional plain, and are exposed to cell culture medium containing fetal bovine serum. hMSCs are defined as plastic-adherent clonogenic cells which are multipotent, express CD73, CD90 and CD105 on their cell plasma membrane and lack expression of CD34, CD45, CD11b, CD14 and CD79[1]. hMSCs lack expression of telomerase and the majority of the bone marrow derived hMSC population is β-galactosidase positive after approximately 25 population doublings (this number is donor dependent), indicating that they have reached replicative senescence and thus lack self-renewal capacity[2]. During *in vitro* cultivation, hMSCs also change their cell morphology towards larger and wide spread, and lose their multipotency[3]. For this reason, hMSCs are used for *in vitro* experimental work typically within the first 5 passages, and in this window, their response to a wide variety of small molecules and cytokines is known. A clear example of such a well-known response is the elevated expression of alkaline phosphatase after 5 days of incubation with dexamethasone[4].

The influence that culture conditions can have on cell behavior is notoriously known among cell culture laboratories around the world. For instance, clear differences in proliferation rate and differentiation capacity are two of parameters closely monitored when a new batch of serum is purchased. There is also growing awareness on the effect of the cell culture substrate on cell behavior. Here, substrates are explored which differ from TCP in both chemical and physical appearance in order to mimic the *in vivo* situation more closely. For example, hydrogels are orders of magnitude softer than TCP[5], exotic mixtures of monomers can create unique chemical compositions[6], and material surface structures can be modified on the nanometer-scale[7] and micrometer-scale to provide cells a more physiological environment[8]. We and other have used micro-fabrication technologies to design and engineer surface topographies eliciting very defined cellular responses. Depending on the type of surface topography and cell type, induced changes in cell behavior range from initiation of osteogenic differentiation of hMSCs[9], induced clonogenicity of induced-pluripotent stem cells, adaptation of an anti-inflammatory M2 phenotype of macrophages to enhanced induction of IPSCs formation. Cell phenotypes are often correlated to more basal cell parameters. For instance, multi-potency of hMSCs correlates to their size and metabolic profile, and survival of cancer cells is strongly correlated to their mitotic profile. Microfabrication platforms are able to influence these basal phenotypes, as e.g. surface structure induced shifted cell cycle distribution[10] and water flux controlled cell volume as a response to differential cell spreading[11]. In this manuscript, we used topographically-defined substrates to map surface topography induced changes in cellular state compared to hMSCs cultured on flat substrates.

For this, we follow the adaptation of hMSC phenotype within the first hours after contact up to a few days, in terms of changes in cell and nucleus shape and volume, metabolism and cell cycle progression. We were able to correlate micro-topography-induced quiescence to increased resistance to anti-cancer drugs.

Materials and methods

Topographically enhanced substrate production

TopoChip-derived surface topographies, selected based on topographical feature size and the cell morphology they induce, were placed in 15 mm circle format as the lay-out of a chromium masks for photolithography. Topographies used in this manuscript were patterns derived from the second generation TopoChip[8], produced in polystyrene (PS). Topography nomenclature is based on the relative size of the topographical features, and is formulated as follows: Medium (M) = T2-PS-0304, Large (L) = T2-PS-1642, Small (S) = T2-PS-3240, and Extra Small (XS) = T2-PS-1901. T2 stands for the second TopoChip design as described in Unadkat et al, PS stands for polystyrene, the first two digits represent the row number counted from the top, and the second two digits represent the column number. The micrometer-scale patterns were etched from the silicon wafer by directional reactive ion etching (DRIE), generating a silicon master mould, and thus containing the inverse topography patterns. A three-replication process was used to fabricate the surface topography enhanced polystyrene films, using sequentially silicon, PDMS and Ormostamp moulds, as described before[12]. The Ormostamp moulds were for used for imprinting (Obducat Eitre 6 Nano Imprint Lithography system, Obducat, Sweden) into bi-axially oriented 190 µm thick polystyrene films (Goodfellow, United Kingdom) at 140 °C and 10 bar for 5 minutes. Untreated polished silicon wafers were used for embossing the unpatterned substrates. To increase hydrophilicity, we treated the topographically enhanced polystyrene films with a gentle O_2-plasma (reactive ion etching home-build) at 10 °C, 50 sccm oxygen flow, 75 mTorr pressure and 50 W CCP power for 30 seconds). All surfaces were pre-treated with medium overnight before adding the hMSCs for cell culture.

Cell culture

Mesenchymal stem cells (hMSCs) from a human donor (female, 74 years-old) were expanded in basic hMSC medium consisting of α-minimal essential medium (a-MEM, Life Technologies) supplemented with 10% foetal bovine serum (FBS, Sigma), 2 mM L-glutamin (Fisher Scientific), 0.2 mM ascorbic acid (Sigma), 100 U/ml penicillin, and 100 mg/ml streptomycin (Fisher Scientific). To investigate the effect of surface topography on hMSCs (passage number 5), seeding densities of 10,000 cells/cm^2 were used on both flat and

topographically enhanced surfaces and grown for the designated times in a humidified incubator with 5% CO_2 at 37 °C. Prior to experiments on cell size, protein synthesis, cell cycle distribution, proliferation, and chemotoxins, hMSCs were synchronized by serum depletion for 48 hours. hMSCs were incubated with paclitaxel (300 - 0.3 µM, Sigma) for 44 hours, starting with an initial cell density of 7,500 cell/cm^2.

Fluorescence staining and microscopy

For fluorescence microscopy, cells were fixated in freshly prepared 3.7% paraformaldehyde (Sigma) for 10 minutes at room temperature, permeabilized by 1% Triton-X (Sigma) in phosphate buffered saline (PBS) for 10 minutes and blocked for a-specific binding by 1% bovine serum albumin (BSA, Sigma Aldrich) in PBS for 30 minutes at room temperature. The actin cytoskeleton was stained with Phalloidin 488 (1:80, A12379 Thermo Fisher Scientific) for 40 minutes and DNA stained with 4',6-diamidino-2-phenylindole (DAPI, 14.3 µM, D1306 Invitrogen) for 5 minutes both in the dark and at room temperature. Epifluorescent micrographs were obtained using a Nikon A1 microscope, while confocal micrographs for nucleus volume quantification were obtained using a Leica SP8. For time lapse imaging of fluorescently labeled U2OS cells (GFP-Actin) on topographically enhanced substrates, z-stacks of confocal images were taken every 5 minutes. Here, the three-dimensional reconstructed time lapse confocal images were obtained using an upright Carl Zeiss LSM 700 with a humidified 5% CO_2 chambers at 37 °C. Time resolved three-dimensional reconstructions of cells on topography M were created using Fiji[13].

Cell and nucleus size and shape analysis

Image analysis was performed using CellProfiler[14]. Analysis pipelines were customized for each dataset, and included background correction, cell identification and segmentation, and measurements on shape and size. We highlighted two shape descriptors, extent and eccentricity to quantify cellular and nuclear deformation. Cells with a relatively large extent, i.e. segmented cell area divided by the area of the bounding box, are circular or elliptical and have no protrusions. Nuclei with eccentricity (ratio of the distance between the foci of the ellipse and its major axis length) of 0 represent a circle, while an eccentricity of 1 represents a line. The volumes of the nuclei were quantified using FIJI, and based of the measurements of the three dimensional reconstructions. To quantify cell volume, hMSCs were trypsinized after 24 hours of culture, and quickly washed before direct measurements in the flow cytometer (BD Accuri C6). Cell size was measured using the forward scatter.

Gene expression analysis

hMSCs were cultured for 7 days on the topographies and flat control surfaces before total RNA was isolated after a freeze thaw cycle using the Nucleospin RNA isolation kit (MarchereyNagel) according to the manufacturer's protocol. cRNA was synthesized from 350 ng RNA using the Illumina TotalPrep RNA Amplification Kit. RNA and cRNA quality were verified on a Bioanalyzer 2100 (Agilent). The microarray analysis was performed using HT-12 v4 expression Beadchips (Illumina). According to the manufacturer's protocol, 750 ng of cRNA was hybridized on the array overnight and the fluorescent signal was developed by adding streptavidin Cy-3. The bead chips were scanned on an Illumina Beadarray reader and the measured raw intensity values were background corrected in BeadStudio (Illumina). Further data processing and statistical testing was performed in R[15] (R version 3.3.2 (2016-10-31)) using the Bioconductor statistical software. The probe-level raw intensity values were quantile normalized and transformed using variance stabilization (VSN). A linear modeling approach with empirical Bayesian methods, as implemented in the Limma package[16], was applied for differential expression analysis of the resulting probe-level expression values. Genes were considered differentially expressed between flat and topography surfaces at a p-value <0.05 and an absolute fold change >1.5. The list of differentially expressed gene which overlapped in the expression profiles on all three topographies relative to the flat control surface was used for functional classification using PANTHER (http://pantherdb.org/)[17]. Using this database, the gene ontology terms associated with the list of differentially expressed genes were grouped by biological process.

Metabolic activity

HMSCs cultured on the flat and topographically enhanced substrates were assessed for their metabolic activity after 1, 3, 5, and 7 days, using the Presto Blue assay (A13261 Invitrogen) according to the manufacturer's protocol. In brief, at the designated time points we replaced basic hMSC culture medium by Presto Blue medium (1x concentrated in basic hMSC medium), and incubated for 1 hour at 37 ˚C in a humid environment. Equal amounts of supernatant were subsequently transferred to a black/black bottom 96-well plate (Nunc, Fisher Scientific) and followed by the quantification of the fluorescent signal measured at 590 nm using a plate reader (Perkin Elmer, Victor3). After 72 hours of culture on topography XS, mitochondria were stained by incubating the samples with 25 nM MitoTracker deep red FM (AF647, M22426 Invitrogen) in basic medium for 15 minutes at 37 °C. Subsequently, cells were collected from the substrates and measured directly using the flow cytometer (BD Accuri C6).

Cell proliferation

Newly synthesized DNA was detected using a live cell incorporation kit (Click-iT™ EdU Alexa Fluor™ 488 Imaging Kit, C10337 Invitrogen) according to the manufacturer's protocol. In brief, after cell cycle synchronization by serum depletion for 48 hours, hMSCs were seeded on the flat control surface and topography XS where they were allowed to re-enter the cell cycle by addition of 10% serum in the culture medium. 10 µM EdU in basic medium was incubated for 40 hours before cells where fixed with 3.7% paraformaldehyde for 15 minutes. Next, cells were stained using the Click-it reaction buffer, and counterstained using Hoechst before fluorescent imaging.

For cell cycle measurement, hMSCs where cultured on flat and topography XS for 24 hours, and after trypsinization rersuspended in ice cold MilliQ water. Subsequently, ice cold absolute ethanol was added to the cell suspension to obtain a 70:30 ethanol:MilliQ mixture, in which the cells were fixed for 1 hour at 4 °C while shaking. After fixation, cells were washed with PBS and resuspended in a mixture of propidium iodide and RNAse (FxCycle™ PI/RNase Staining Solution, F10797 Invitrogen) and incubated for 30 minutes at room temperature. Finally, the DNA content was quantified by flow cytometry (BD Accuri C6). Cell cycle distribution analysis was performed with the FlowJo software, using the univariate fitting model for DNA content.

Statistical analyses

Experiments were carried out in triplicate with three independent samples. Bar-graphs represent the mean ± standard deviation. Boxplots include the median values, with the boxes covering the 1^{st} and 3^{rd} quantile, the whiskers the highest and lowest values, and the dots the outliers. Samples were compared using the students t-test, with $P<0.05$. Statistics used during gene expression analysis are explained in detail in the respective subsection on gene expression profiling.

Results

Cells actively remodel their shape to adapt to surface topographies

Cell shape is the most eye-catching effect of micro-topography on cells and a clear example of cell adaptation. We selected three different TopoChip-derived topographies based on the confinement they will offer the cells. Besides a flat reference surface, we included substrates that were enhanced with large, medium, and small topographical features (see inserts figure 1A). After seeding, hMSCs mostly adhere to the valleys, and are thus surrounded by 10 µm high topographical features. hMSCs changed both their cell and nuclear morphology

dramatically compared to the flat reference as seen after 3 days of culture. (Figure 1A) We observed strongly elongated cells with nuclei which seemed to be compressed and smaller in size. On topo M, cell shape was defined by long perpendicular structures, whereas cells on topo L displayed a wave like pattern but in one direction. Cells on surface S however tended to produce structures into multiple directions. The width of the cell body correlated with the distance between the topographical features. Quantitative imaging of cells cultured on flat and the three topographies revealed a two-fold reduction of cell area as well as the nuclear area (Figure 1B).

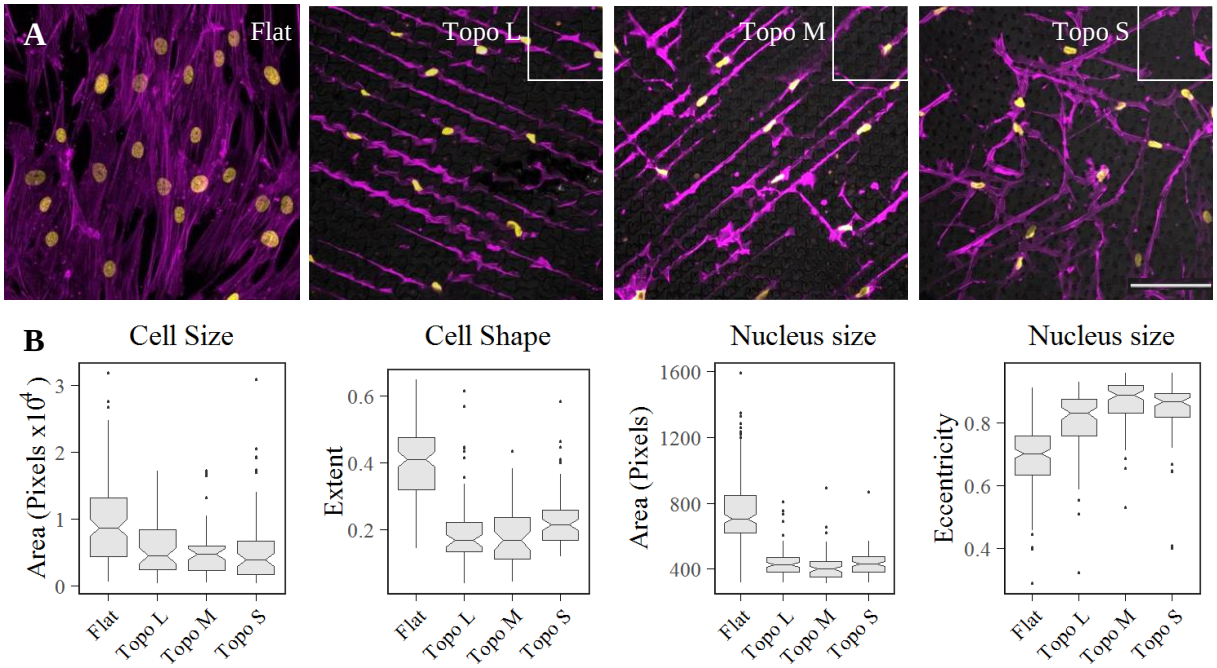

Figure 1: Surface topography induced changes in morphology A) hMSCs cultured for 3 days on flat and topographically enhanced substrates (flat and topography M, L and S) show clear differences in both nuclear and cellular morphology. The inserts show the topographical feature designs of topography M,L and S, and each insert represents 50 by 50 µm. B) Quantification of morphological descriptors Area and Extent for cells (N>48), and Area and Eccentricity for nuclei (N>75). In the micrographs, the nuclei are stained in yellow using DAPI and the actin cytoskeleton in purple using phalloidin. The scale bar represents 100 µm.

To assess very early responses in terms of topography-induced cell shape deformation, and follow them over time, we seeded fluorescently labeled GFP-actin transgenic U2OS cells and imaged them from attachment to 24 hours on topography M (Figure 1, video in Supplementary figure 1). As shown in supplemental video 1, the rounded cells in suspension touch the top of the topographical features but immediately start to descend to the valleys and start spreading within minutes. In video 2, one cell is followed for 5 hours and it is interesting to see how the cell continuously retracts and redirects cellular protrusions, as if it is sensing

its environment. The cell shows no directionality, which we confirmed for other U2OS cells, but which is different for hMSCs which do show directional movement on topographies (data not shown). Video 3 shows how one cell divides. First, the cell rounds up, sits on top of the topography and then divides to immediately spread and adhere again to the valley. Similar to U2OS cells, hMSCs actively adapt to their environment by constantly remodeling their shape and size. A distinct difference in cell morphology between hMSCs on flat substrates and topographies is clearly visible after 1 hour (Figure 2). The deformation increases over the course of the following 24 hours, and hMSCs seemed to have found a state of maximum spreading by then. Besides the changes in total cell morphology and size, cells also actively deform their nucleus within a similar timeframe. These images demonstrate highly adaptive cells which remodel their shape relative to the micropattern to which they are exposed.

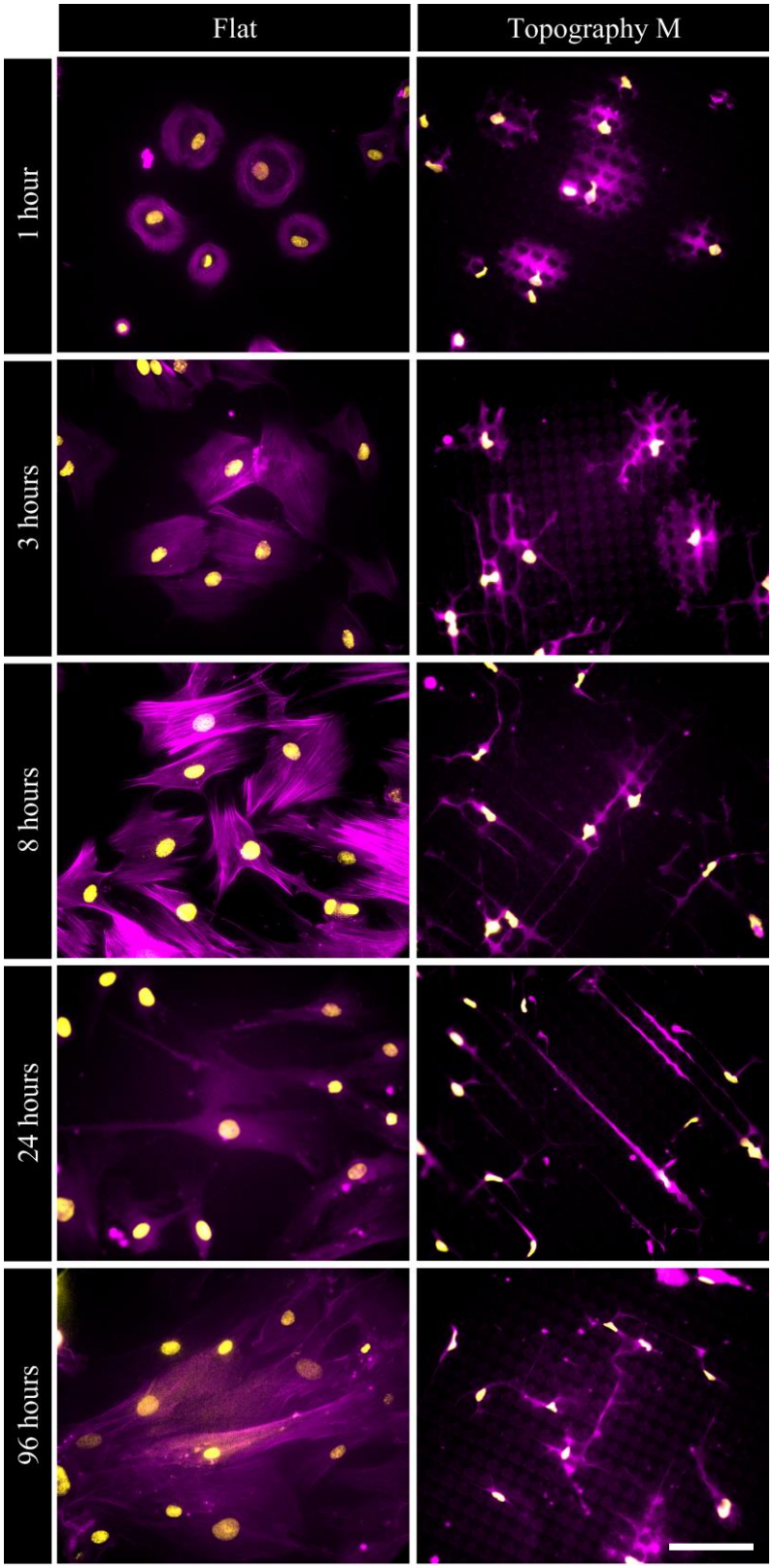

Figure 2: hMSCs adapt cell and nucleus morphology within the first hours after attachment to topographically enhanced substrates. hMSCs after 1, 3, 8, 24, and 96 hours of exposure to flat and topography M. The changes in cell and nucleus morphology between flat and topography are growing over time. Nuclei (yellow) are stained using DAPI and the actin cytoskeleton (purple) using phalloidin, the scale bar represents 100 µm.

Cells decrease their nucleus and total cell volume under topographical confinement

Next, we wanted to assess if the compacted nuclei, as seen on the xy-plane (Figure 1B), have a smaller volume as well. In previous work, we described that cells which are confined in the xy-plane become larger in the z-direction[9]. This suggests that confined cells change their shape, however, we assumed this would not give rise to a significant difference in the total cellular volume. To quantify the volumes of the nuclei we used three dimensional (3D) reconstructions of cells cultured on flat and surface topographies using confocal imaging. In order to capture the dynamics of the deformation, we assessed the nuclei after 1, 3, 8, 24 and 96 hours of exposure to flat and topography M (Figure 3A). Here, we observed a highly dynamic adaptation of the nuclear volume. For both conditions, a two-fold increase in nuclear volume was observed during the first eight hours of culture. During the next 16 hours, the nuclei shrunk significantly and volumes dropped three-fold for both conditions. After 96 hours, we observed a two-fold difference between the volumes of nuclei on flat substrates compared to topography M. The significant differences in nuclear volumes quantified for nuclei on flat substrates after 1 and 8 hours are originating from a size increase in the xy-plane, and not from an increase in the z-direction. The difference in nucleus volume between cells on flat and topography M after 96 hours did show an increase in the z-direction on topography, however, the difference in the xy-plane is significantly larger (Figure 3B). Next, we wanted to see if such significant differences in nuclear volumes hold true for more topographies as well. Therefore, we assessed the deformation of the nuclei on the three topographies with varying topographical feature size (S, M, and L) after 72 days of culture. Again, we observed a strong adaptation of cells on the different topographies. For all three assessed topographies, cells reduced the volumes of their nuclei up to 2.5-fold (Figure 3C).

From literature it is known that the size of the nucleus correlates with the size of the cytoplasm[18]. While the underlying mechanisms for this karyoplasmic ratio regulation are not completely elucidated yet, it is conserved across a wide variety of species. Since we observed that the cells decrease their nucleus size as a reaction to surface topographies, we wondered if this correlated with the total cell size. To assess the cellular reaction in terms of total cell volume, we performed flow cytometry. Forward scatter is a measure for the diameter of the spherical cells which we harvested from the flat and topographically enhanced substrates. In line with the karyoplasmic ratio theory, we found that hMSCs significantly reduce their total cell volume after 3 days of culture (Figure 3D).

Cells under confinement lower their metabolism

Next, we wondered whether the strongly deformed and smaller nuclei also displayed different transcriptional activity. Here, we hypothesized that a nucleus deformation induced overlap in gene expression profiles which might indicate a difference in the cell's basic physiology. For this, we compared gene expression profiles of hMSCs which were cultured on flat and the

three topographically enhanced substrates for seven days. The differentially expressed genes (DEGs) on the three topographies, compared to the flat reference, revealed genes which were unique for one specific topography, genes that had an overlap with two topographies and DEGs that were found for all three topographies (Figure 4A). The overlapping DEGs between the three topographies are thus typical for hMSCs which are adapting to a topographically enhanced microenvironment. Among the 34 overlapping DEGs there were 13 probes which do not have a protein product. These DEGs were not included in further analysis. The 21 genes used for further analysis showed all a similar trend in their expression compared to the flat reference conditions (Figure 4B).

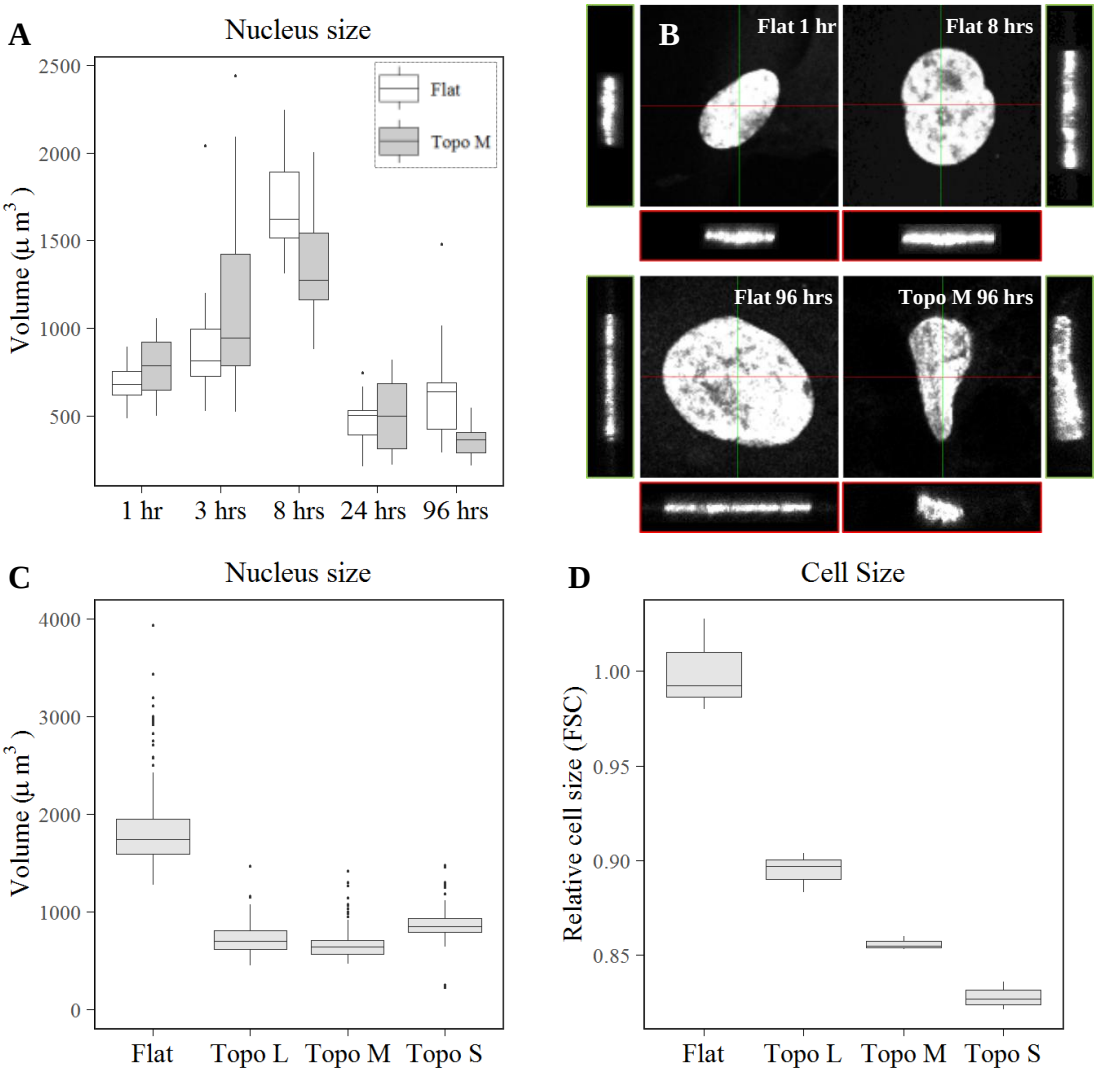

Figure 3: Topographical induced decrease in both nucleus and total cell size. A) Dynamic change of nucleus volume (N>11) in hMSCs cultured on flat and topography M after 1, 3, 8, 24, and 96 hours as quantified using confocal micrographs. B) Volume views of representative nuclei after 1 and 8 hours on flat, and after 96 hours on flat and topography M. C) Confocal micrograph quantification of nucleus volumes of cells on topographies with varying topographical feature size (S, M, and L) after 72 hours. D) Flow cytometer measurements of relative cell size after 72 hours on topographies with varying topographical feature size (S, M, and L).

A functional classification of the overlapping DEGs revealed that 9 out of these 21 genes were related to metabolic processes as defined by GO-term annotations (Figure 4C). Among these 9 genes involved in metabolism, a selection was found that encodes for ribosomal proteins (RPS24, RPL26, and RPS27a) involved in protein synthesis, and in lipid metabolism (UGCG and SPTLC1). We found that the Deleted in Liver Cancer-1 (DLC1) gene was expressed higher in cells cultured on topographies. As stated in the gene-name, this gene acts as a tumor suppressor since it inhibits cell growth and proliferation[19]. Besides liver cancer, it is involved in various other types of cancer, such as kidney, breast, lung, and prostate amongst others[20]. Furthermore, DLC1 activated GTP-bound GTPases to convert GTP into GDP (and thus inactivate them) in e.g. RhoA and Cdc42[21]. Elevated DLC1 levels as measured on topographies might therefore be associated with cytoskeleton organization and additionally, cell cycle regulation.

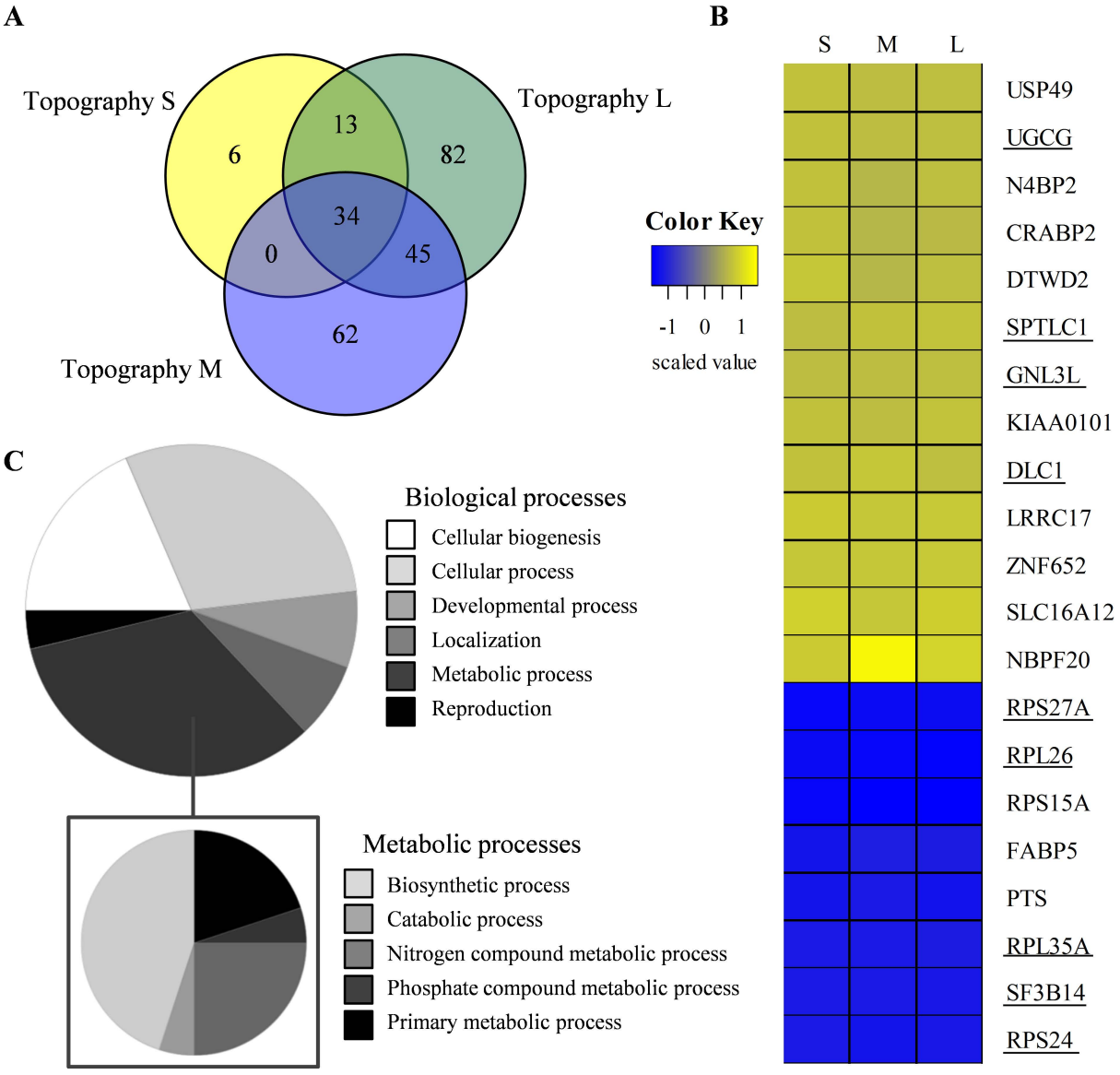

Figure 4: Topography induced differences in gene expression profiles. Microarray analyses of hMSCs after 7 days on topographically enhanced (S, M, and L) substrates compared to flat. A) Venn diagram represents the number of DEGs which were unique for the topography conditions or which overlapped with the other condition(s). B) Z-score scaled heatmap with DEGs, for each topography (S, M, and L), which were found in all three topographies. Underlined genes are involved in metabolic processes. C) Panther gene ontology classification analysis grouped DEGs to biological processes based on their gene ontology annotation. The list of DEGs linked to metabolic processes was specified further.

To validate enrichment of metabolic processes, we exposed cells to non-fluorescent resazurin, which is converted into fluorescent resorufin in the reducing environment of mitochondria. Fluorescence intensities measured in this assay thus represent the mitochondrial metabolic activity. Additionally we quantified the number of cells to normalize the measured metabolic activity. Using this method, we observed a lower metabolic activity already after 24h on all three topographies relative to flat (Figure 5). Where the metabolism of cells on flat surfaces remained constant, the metabolism was lowered three-fold in cells exposed to topographies over a period of 7 days.

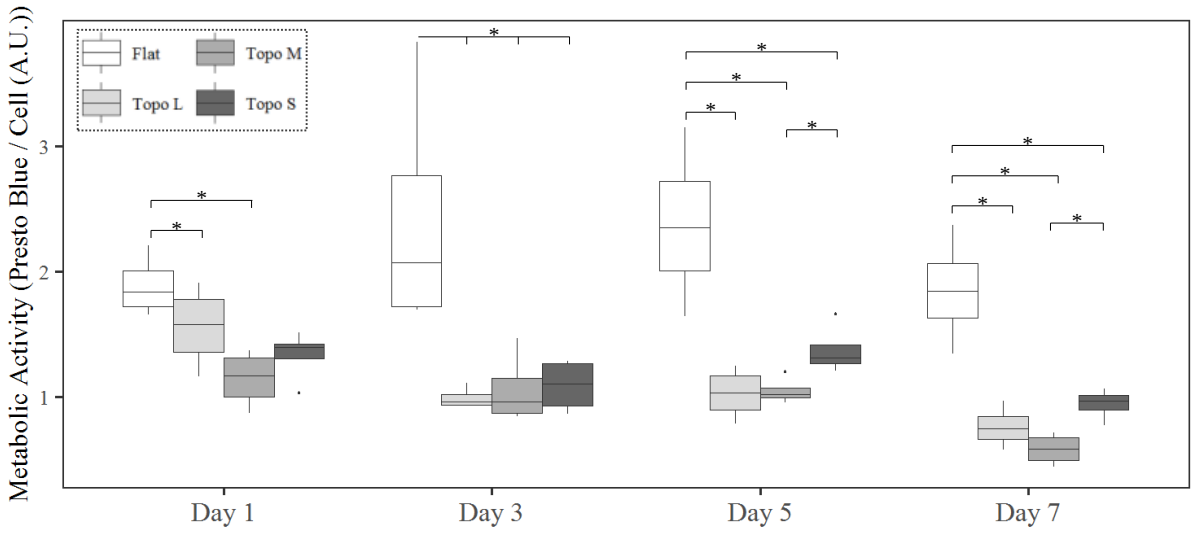

Figure 5: Topographical induced difference in metabolic activity develops over time. Mitochondrial activity, as quantified using Presto blue, differs significantly in hMSCs between flat and topography culture conditions. Stars represent statistical significance $P < 0.05$.

Decrease in metabolic activity is not dependent on the degree of cellular confinement

The phenotypic changes observed so far are induced by surface topographies that cause strong confinements for cells, as seen by the dramatically changed morphologies. Cells needed to adapt their total and nucleus morphology, and such strong deformations might have caused an intense membrane stretch and possibly damage to the nuclear envelope[22,23]. In order to assess

the effect of a less confining topography on the degree of cellular adaptation, we screened for a TopoChip-derived surface topography which allowed hMSCs to maintain their spread morphology. hMSCs grown on topography XS displayed a mild level of cell confinement, which resulted in a classification 'normal' in a supervised clustering approach[24] (Figure 6a). Interestingly, even though the cells have the option to remain in the wide valleys between topographical features, we did occasionally observe strongly deformed nuclei indicating that the cells did migrate through the small pores. We also noted that cells used the topographies as anchor points.

Interestingly, hMSCs exposed to low confinement surface topographies still significantly reduced their overall cellular metabolism by two-fold within three days (Figure 6b). Since metabolism is measured as mitochondrial activity, we hypothesized this difference might depend on the number of mitochondria. To measure this, we fluorescently stained the mitochondria in living cells and quantified the total number of mitochondria using flow cytometry. We observed a significant decrease in abundance of mitochondria in hMSCs exposed to topography XS for 3 days compared to hMSCs cultured on flat substrates (Figure 6c).

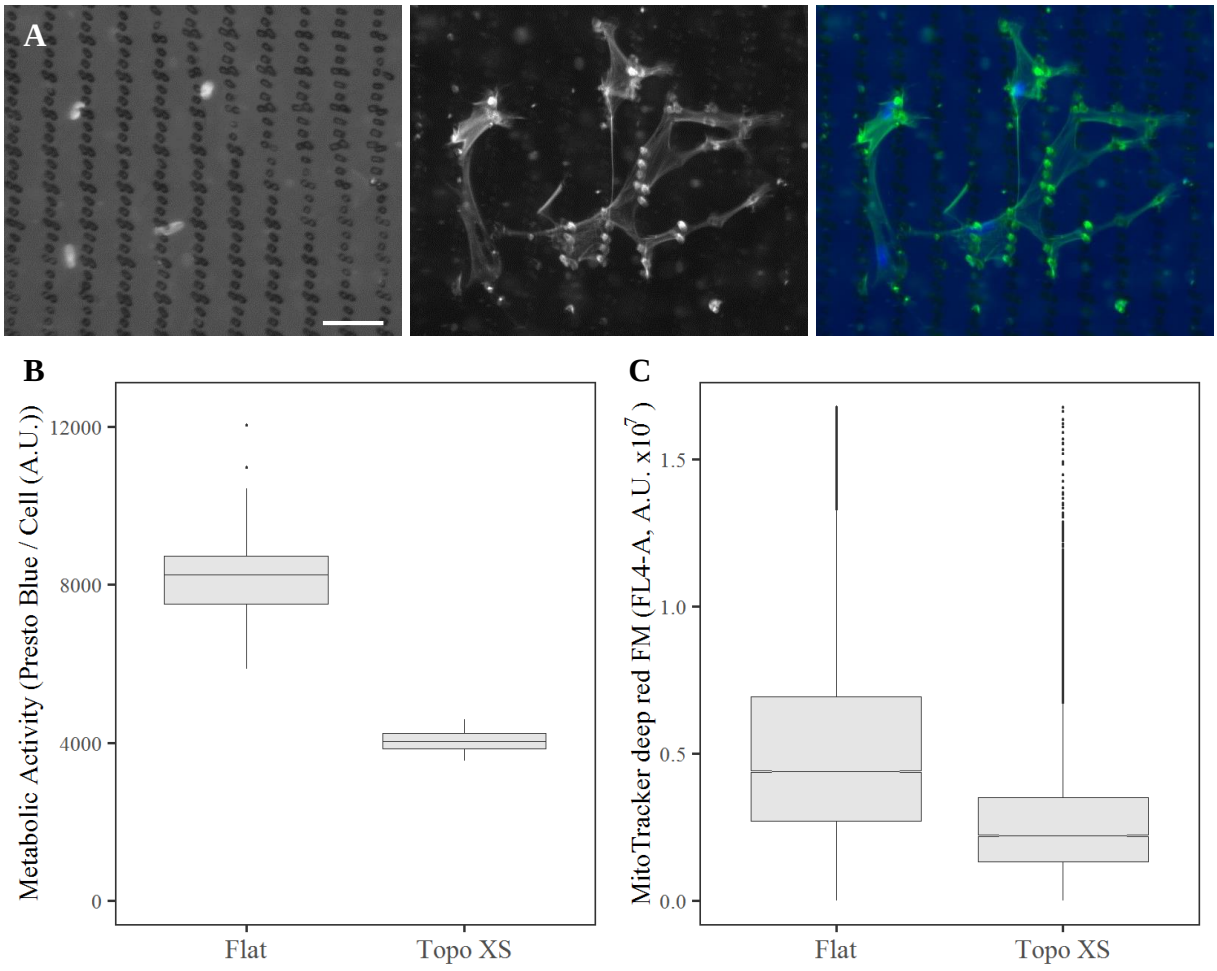

Figure 6: Mild cellular confinement leads to decreased metabolic activity. A) hMSCs exposed for 72 hours to topography XS show mild confinement in morphology. Left shows DNA stained with DAPI, middle shows the actin cytoskeleton stained with phalloidin, right is a merge of both channels. Notes: left, one can appreciate the surface topographical features as darker spots. Middle, light captured from outside of the cellular boundaries comes from auto-fluorescence of the polystyrene. Scale bar represents 50 μm. B) Presto Blue analysis for mitochondrial activity in hMSCs after 72 hours of culture on flat and topographically enhanced (XS) substrates. C) Flow cytometer quantification of the mitochondrial abundance in hMSCs cultured after 72 hours on topography XS compared to flat polystyrene.

Cell cycle progression slows down in response to surface topography

It is well-known that both cell and nuclear size increase during cell cycle progression[25]. While preparing for cell division, cells copy their DNA and multiply their organelles, which inevitably lead to an increase in volume[26]. However, cells cultured on topographically enhanced substrates are smaller and contain less organelles (in the form of mitochondria), and therefore we hypothesized a slower cell cycle progression. Consistent with the link between cell cycle progression and growing cell volume, we observed a 2.5-fold decrease in proliferation rates in the smaller cells which were cultured on surface topographies (Figure 7a). Furthermore, assessment of the cell cycle distribution revealed an increase in the G_0/G_1-phase accompanied by a decrease in the S-phase for cells cultured on surface topographies (Figure 7b). Interestingly, the fraction of the cell population which were in the G_2/M-phase of both flat and topographically enhanced conditions remained the same, indicating a block to enter into the G_2/M phase.

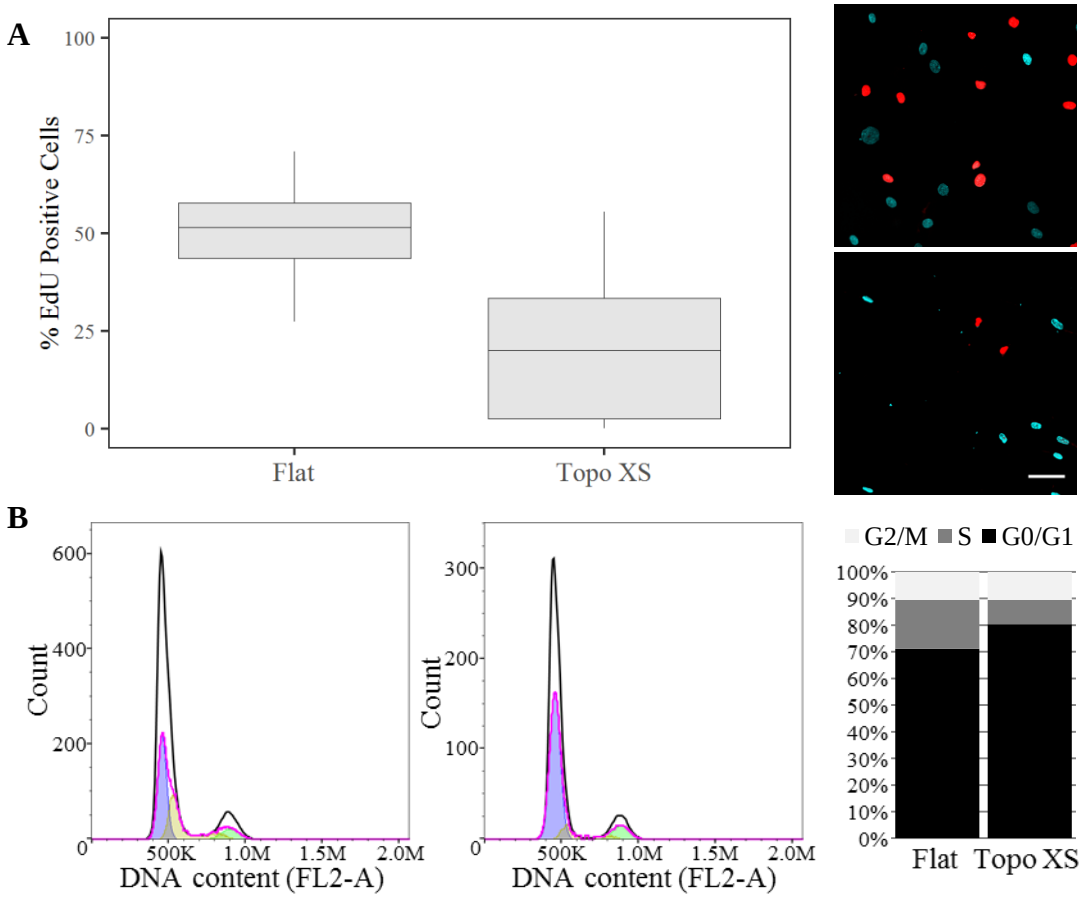

Figure 7: Surface topography inhibits cell cycle progression. A) EdU-positive fraction of hMSCs exposed to flat and topography XS after 40 hours. Representative micrographs showing the difference in quantity of EdU-positive cells on flat (top image) and surface topography (bottom image). Scale bar represents 100 µm. B) Quantification of cellular DNA content (FL2-A) using flow cytometry revealed a shift in the cell cycle distribution between the flat and topography conditions after 24 hours of culture.

hMSCs on topographies are less sensitive to cancer drugs

Cancer therapies often target metabolically active, dividing cells. The cancer drug paclitaxel increases stability of the microtubules and thus interferes with mitosis, resulting in G_2/M cell cycle arrest and apoptosis[27,28]. Based on the lower level of metabolism and cell cycle, we reasoned that cells on topographies are less sensitive paclitaxel. We exposed hMSCs for 44 hours to a range of paclitaxel concentrations and chose 300 µM paclitaxel, which resulted in a 75% reduction of cell number compared to hMSCs cultured in basic medium after 44 hours (Figure 8A). Next, compared cell survival between a flat control surface and hMSCs cultures on topography M, and observed that two times more cells remained alive after the paclitaxel treatment when being exposed to surface topography (Figure 8B and C).

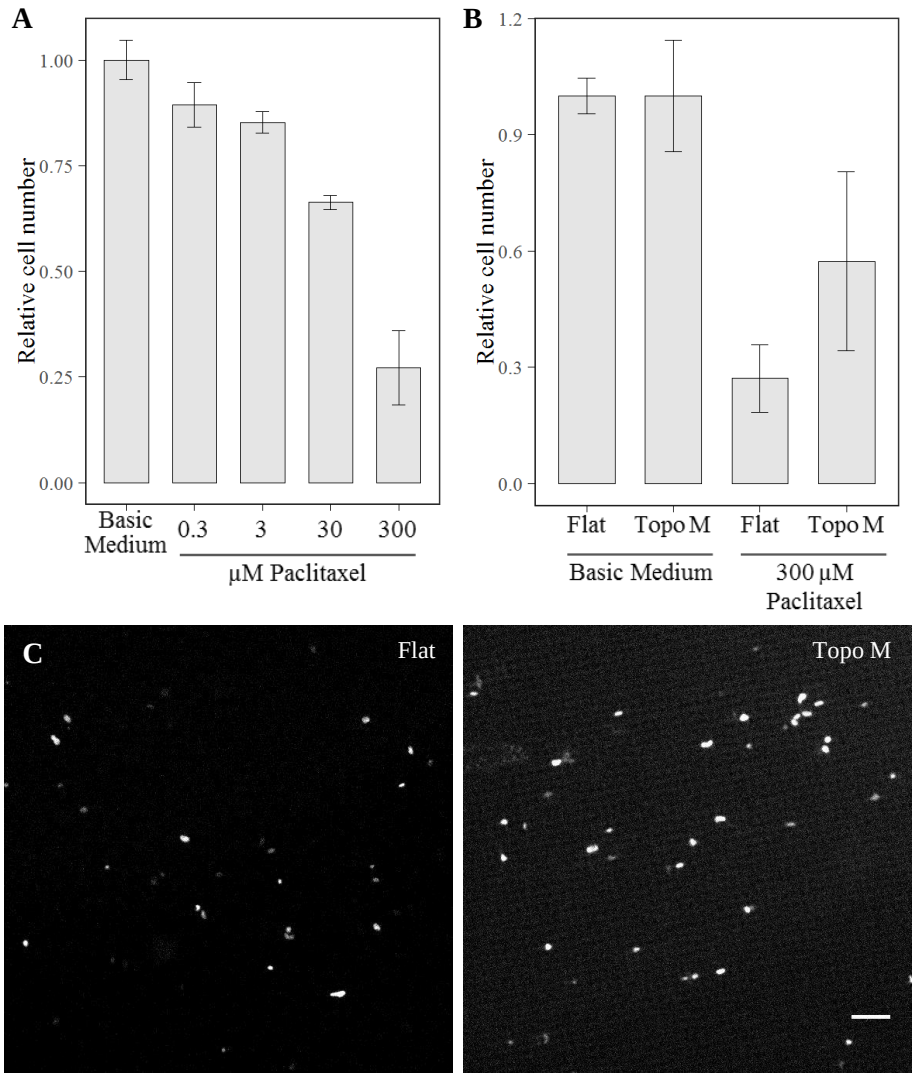

Figure 8. Surface topography adapted hMSCs are more resistant to anti-cancer drugs. A) dose-response curve of MSC survival after a 44 hours paclitaxel treatment. B) Differential resistance to paclitaxel of MSC cultured on flat of topographically enhanced substrates after 44 hours. Cell counts are normalized to the basic medium condition. C) Representative micrographs of nuclei staining after 44 hours of exposure to 300 µM paclitaxel on flat (left) and topography M (right). Scale bar represents 50 µm.

Discussion and conclusion

The in house developed TopoChip platform is used for screening of algorithm generated surface topographies for their influence on cell phenotype, and typically in terms of differentiation[8]. However, besides differential expression of differentiation markers we often observed changes in other cellular functions as well compared to cells cultured on flat TCP. These changes occur upon cell attachment to topographically enhanced substrates, where cells become physically confined by the topographical features. Within the first 24 hours cells adapt to their new environment and from there continue to reach equilibrium in their cellular

state. Compared to cells that attach to flat tissue culture plastic, we observed topographically-induced changes in cell and nucleus morphology and volume, mitochondria abundance causing a lower overall metabolism; and reduced cell cycle progression in cells on our topographically enhanced substrates (Figure 9).

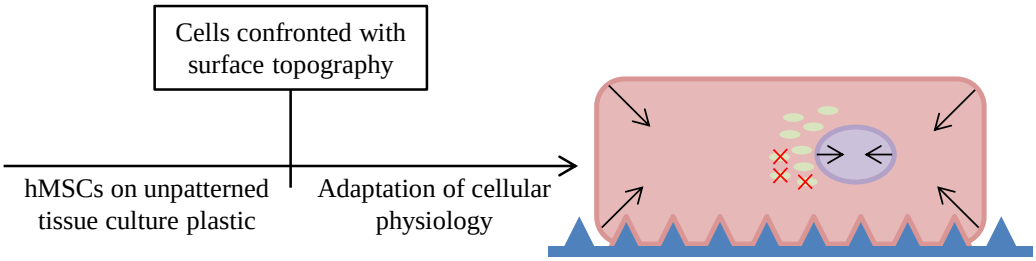

Figure 9: Timeline of topography induced cell behavior adaptation. After initial cell-surface topography contact, cells quickly respond and create an adapted cellular state. Here, we observe shrinkage of cell and nucleus sizes, condensation of proteins, reduction in mitochondria abundance, and cell cycle arrest.

Cell-material interaction – from which the behavior controlling mechanotransduction arises – initiates upon cell attachment. Already in 1964, Adam Curtis used interference reflection microscopy to assess the shape of cells and the proximity towards the adhesive substrate after cellular attachement[29]. More recently, Pierres et al. showed – using a similar microscopy technique– that cells first attach with only small protrusions in a 'tiptoe-like' manner, after which complete cell attachment occurs during the following tens of seconds[30]. Other studies – in which biomaterials with modified surfaces are used – showed that contact guidance comes in play immediately after initial attachment, with fibroblasts elongating along linear patterned fibronectin within 30 minutes[31]. Furthermore, guided by surface structure, significant differences in morphology are typically observed within minutes to hours, with total cellular areas remaining similar between surface structure and flat conditions[32]. Using human osteosarcoma-derived cells (SaOs-2), Davidson et al. observed full deformation of both total cells and nucleus after 24 hours, but not yet after 6 hours, as a reaction to 7 by 7 µm sized 4 µm tall micropillars[33]. This is in line with our findings, in which we observed cellular deformation immediately after attachment and continued until around 24 hours later where we observed a maximum deformation state. Also for this period after the first 24 hours, it is known that both total cell and nucleus shape are constantly changing, with e.g. clear differences in elongation. Interestingly, the magnitude of deformations is found to decrease around 14 days of continues exposure to micropillars[34].

For nucleus deformation in particular, we observed an increase in nucleus size between 1 and 8 hours after initial attachment, on both flat and patterned surfaces. In terms of deformation (not volume), Lui et al. observed a maximum around 8 hours of exposure to micropillars, in

line with our observed maximum volume. In the hours following, this deformation partially recovered[35]. Moreover, this recovery process was not completed and micropillar-induced deformations persisted over longer periods of time[36]. For mouse embryonic fibroblasts that detach from their substratum, it has been measured that both total cell and nucleus volumes reduce by 50%[37]. We hypothesize that the maximum nucleus volume, measured around 8 hours on our substrate, might be the end stage of nucleus volume increase that occurs when cells attach. It has to be noted that as seen for total cell morphology[38], observed trends in nucleus deformation are dynamics and highly depended on cell type[39,40].

Cell attachment and spreading are accompanied by water efflux, resulting in reduction of cell volume. This reduction in cell volume was found to be linearly correlated with their nucleus volume, and holds true for multiple cell types[11], and seems to correlate to the strength of attachment. Spreading controlled reduction in cellular volume was amplified by our topographies with an extra 15% reduction in cell diameter after 24 hours. With cell deformation, as e.g. elongation, it is reported that the nucleus elongates as well, guided by the cytoskeletal organization, and reduces its volume[41]. In both examples from literature, cells attached to adhesion promoting surfaces which resulted in a maximum amount of cell spreading and reduction of cellular volume. In contrast, we observed lower adherence of hMSCs to patterned than flat surfaces, while cells had a smaller volume (manuscript in prep.). Based on this contradiction, we hypothesize that in addition to adherence-dependent water efflux found in literature, there is an adherence-independent topography-induced mechanism that plays a role in regulating cell size as well.

With a reduction of both cytoplasm and nucleus the karyoplasmic ratio remains constant. Several theories exists on the control of this nucleus/cytoplasm ratio, however, thorough understanding of the involved mechanisms remain to be elucidated. For example, during dedifferentiation of matured cell types into stem cells it is known that the karyoplasmic ratio also increases (stem cells have a relative small cytoplasm)[42]. In the current report, we did not present data on this ratio, however, extrapolation of the measured cell radii by flow cytometry revealed a 40% reduction in cell volume which approximates the 50% reduction of nucleus size. While the karyoplasmic ratio is described to be maintained in many occasion, like e.g. cell attachment[11] and micropillar-induced deformation[32], it is known that external stimuli can cause changes in this ratio[43]. Moreover, this regulation is known to be important, since disturbed karyoplasmic ratios are e.g. related to several types of cancer[44,45].

In many cell types, the lowest nucleus volume is found directly after cell division, after which the cells start growing and DNA is replicated once S phase of the cell cycle has been entered. Furthermore, the transcriptional activity of nuclei is correlated with larger nuclei[46]. Since many protein interactions are occurring in a stochastic manner, it is important to realise that nuclear deformation has an effect on local protein concentration. Here, the nuclear volume can thus be of great influence in terms of enabling interactions[47]. Also in deformed nuclei, genes can be differentially localized within the nucleus which can alter their availability for

the transcription machinery [48]. Furthermore, evidence is found that mechanotransduction – by using dynamic loading on cells, without any exogenous differentiation factors – can induce the condensation of chromatin via acto-myosin mediated cytoskeletal tension[49]. Spatial organization of DNA is increasingly appreciated as an important contributor to genomic functions, and using 4C-technology (chromosome conformation capture on-chip) it has been observed that different DNA loci are interconnected. Within regularly shaped nuclei, these intrachromosomal interactions can occur at "long-ranges" within the nucleus[50]. The genes which are in contact with each other share transcription factors, which can lead to so-called variegated expression[51]. Higher-order chromosome structure is known the be important in the growth and development of organisms[52], and in pluripotent stem cells e.g. it is known that there is a unique genome structure around pluripotency factor OCT4 and NANOG[53]. Especially in terms of chromosomal organization, topography-induced nuclear deformations may create great impact. Besides the large size reduction, the dramatic changes in nucleus morphology will strongly influence the spatial distribution of the chromosomes. Advanced techniques such as 4C might provide us with more insight in the altered transcriptional activity and affected downstream cellular processes.

The differential activity and functionality in smaller nuclei holds also true for smaller cells[54]. Here, little is known about the mechanisms that regulate homeostasis of mammalian cell size. In human cells Largen – a product of the PRR16-gene resulting in an increased cell size when overexpressed – was described by Yamamoto et al. to correlate with a higher mitochondrial activity[55]. In line with this, on our topographies we observed that smaller cells had a lower mitochondrial activity. Additionally – and also in line with our data on mitochondrial abundance – it is known that smaller cells contain fewer organelles[26]. Nonetheless, contradictory reports on this topic also exist, where transcriptomics analysis of cyclin-depended kinase 1 lacking cells revealed that an increase in cell size resulted in a decreased gene expression involved in mitochondrial function[56]. Without significantly altering hMSC size and shape, McNamara et al. observed changes in metabolic processes induced by surface structure. Here, ordered arrays of nanopits activate small RNAs which are in involved in repressing metabolic pathways, resulting in a longer maintenance of stemness[57].

The reduced proliferation rates observed in cell populations exposed to our topographies can be linked to multiple mechanobiological molecular mechanisms. For example, YAP is a well-known mechanosensitive protein[58], and strongly involved in tissue growth and proliferation[59]. YAP is part of the Hippo-pathway, which is named after its involvement in developmental growth of organs where inhibiting the pathway results in tissue overgrowth[60]. In active canonical Hippo signaling – for example by cell-cell contact (contact inhibition) – LATS phosphorylates YAP, which results in sequestering of YAP in the cytoplasm and subsequently degradation[61]. Un-phosphorylated YAP – as a result of inactive Hippo – is translocated into the nucleus where it acts as co-transcription factor for many gene expression programs, including proliferation programs[60]. However, upon mechanical activation, YAP becomes

nuclear active via numerous (mostly not elucidated yet) non-canonical Hippo signaling. Here, for example cytoskeletal reorganization can play an important role[62].

Besides YAP, Lee et al. found MAKP/ERK signaling to be activated in MSCs via mechanotransduction, by exposure to nanopit-substrates. Moreover, these MSC populations contained a larger fraction of cells in the G_0/G_1-phase. Here, the progression from the G_1-phase was hypothesized to be inhibited via a cdc2-dependent mechanism, and repression of the S-phase transition by p27kip1 activity[10]. Surface structure-induced shifts in cell cycle distribution were found to be similar to our data. Accompanying increases in cell size is the chromatin decondensation mediated increase in nucleus size which strongly correlates with DNA synthesis[63]. In terms of the reduced nucleus volumes as found on our topographies, it has been described that smooth muscle cells with deformed nuclei barely proliferate. This reduction in proliferation rate is hypothesized to come from the deformation of mature lamin structures which might be exposed to higher internal stress[64]. In our transcriptomics data we found multiple ribosomal protein encoding genes with reduced expression. It is known that the ribosomal proteins are involved in p53-depentent metabolic regulation of cell cycle and cell growth via protein synthesis. Compared to cells cultured on flat substrates – with a high mitochondrial metabolism – ribosomal protein expression is down-regulated on topographies. This reduction in ribosomal proteins causes less inhibition of the p53-inhibitor Mdm2, and thus results in stabilization of p53 and lower level of mitochondrial metabolism[65]. This seems to fit our hypothesis that cells *in vivo* have a lower energetic state compared to cells which are brought *in vitro* onto flat substrates, and which is undone when subsequently topographies are introduced and result in a lower metabolism. Furthermore, ribosomal proteins are found to activate p53-dependent cell cycle check points, and thus strongly involved in cell cycle regulation[66–68].

Mechanotransduction plays an important role in cancer biology, with e.g. often a higher tissue stiffness found in tumors and strong migratory phenotypes of metastatic cells. In most cancers, fascin – an F-actin-bundling protein – is significantly upregulated, which correlates with poor clinical prognosis[69]. Furthermore, cisplatin-induced hair cell death is dependent on functional mechanotransduction in the zebrafish lateral line[70]. Activation of YAP is often observed in carcinomas, and resistance of tumor cells to chemotherapeutics correlates to YAP activity. For example, is it known that YAP activation in breast cancer cells can promote survival treatment to paclitaxel, and protects cancer cells against the effects of the DNA-damaging agents as cisplatin[71]. In this work we used the anti-cancer drug paclitaxel as a compound which stabilizes the microtubules and by this causes a defect in the mitotic spindle function, resulting in apoptosis of those cells. There might be a role for the mechanosensitive protein YAP in the topographically-induced mechanotransduction-controlled resistance against paclitaxel as well. Having an *in vitro* cell culture system which is potent to control proliferation and metabolism might be a very interesting addition to experimental cancer research and toxicology. In this report we demonstrate that topographically enhanced substrates reduce the sensitivity of MSCs to anti-cancer drugs in terms of cell viability after

treatment. Therefore, using topographies can allow researchers to investigate mechanisms underlying the effects of anti-cancer drugs on cells in a chemically and genetically unchanged system.

As a result of a high metabolism and proliferation rate, metabolites and accompanying cellular stressors can accumulate within cells[72]. In this work, we describe how cells reduce their metabolism and proliferation rate when adapting towards a topographically enhanced cell culture substrate. This adapted phenotype might therefore lower the amount of metabolic stressors, and therewith lower the risk for developing malfunctioning cellular processes. Topographically enhanced substrates can thus serve as model system for the study of very basal cell function involved in cancer and ageing.

References

1. Dominici, M. *et al.* Minimal criteria for defining multipotent mesenchymal stromal cells. The International Society for Cellular Therapy position statement. *Cytotherapy* **8,** 315–317 (2006).

2. Alves, H. *et al.* A link between the accumulation of DNA damage and loss of multi-potency of human mesenchymal stromal cells. *J. Cell. Mol. Med.* **14,** 2729–2738 (2010).

3. Alves, H., Mentink, a, Le, B., van Blitterswijk, C. a & de Boer, J. Effect of antioxidant supplementation on the total yield, oxidative stress levels, and multipotency of bone marrow-derived human mesenchymal stromal cells. *Tissue Eng Part A* **19,** 928–937 (2013).

4. Jaiswal, N., Haynesworth, S. E., Caplan, A. I. & Bruder, S. P. Osteogenic Differentiation of Purified , Culture-Expanded Human Mesenchymal Stem Cells In Vitro. *J. Cell. Biochem.* **64,** 295–312 (1997).

5. Mosiewicz, K. A. *et al.* In situ cell manipulation through enzymatic hydrogel photopatterning. *Nat. Mater.* **12,** 1072–1078 (2013).

6. Mei, Y. *et al.* Combinatorial development of biomaterials for clonal growth of human pluripotent stem cells. *Nat. Mater.* **9,** 768–778 (2010).

7. Dalby, M. J. *et al.* The control of human mesenchymal cell differentiation using nanoscale symmetry and disorder. *Nat. Mater.* 997–1003 (2007). doi:10.1038/nmat2013

8. Unadkat, H. V *et al.* An algorithm-based topographical biomaterials library to instruct cell fate. *Proc. Natl. Acad. Sci.* **109,** 5905–5905 (2012).

9. Hulshof, F. F. B. *et al.* Mining for osteogenic surface topographies: In silico design to in vivo osseo-integration. *Biomaterials* **137,** 49–60 (2017).

10. Lee, L. C. Y. *et al.* Nanotopography controls cell cycle changes involved with skeletal stem cell self-renewal and multipotency. *Biomaterials* **116,** 10–20 (2017).

11. Guo, M. *et al.* Cell volume change through water efflux impacts cell stiffness and stem cell fate. *Proc. Natl. Acad. Sci.* **c,** 201705179 (2017).

12. Zhao, Y. *et al.* High-definition micropatterning method for hard, stiff and brittle polymers. *Mater. Sci. Eng. C* **71,** 558–564 (2017).

13. Schindelin, J. *et al.* Fiji: An open-source platform for biological-image analysis. *Nat. Methods* **9,** 676–682 (2012).

14. Carpenter, A. E. *et al.* CellProfiler: image analysis software for identifying and quantifying cell phenotypes. *Genome Biol.* **7,** R100 (2006).

15. R Core team. R. A Language and environment for statistical Computing. (2014).

16. Ritchie, M. *et al.* limma powers differential expression analyses for RNA-sequencing and microarray studies. *Nucleic Acids Res.* **43,** (2014).

17. Thomas, P. D. *et al.* PANTHER: A library of protein families and subfamilies indexed by function. *Genome Res.* **13,** 2129–2141 (2003).

18. Jorgensen, P. *et al.* The Size of the Nucleus Increases as Yeast Cells Grow. *Mol. Biol. Cell* **18,** 3523–3532 (2007).

19. Zhou, X., Thorgeirsson, S. S. & Popescu, N. C. Restoration of DLC-1 gene expression induces apoptosis and inhibits both cell growth and tumorigenicity in human hepatocellular carcinoma cells. *Oncogene* **23,** 1308–1313 (2004).

20. Liao, Y.-C. & Lo, S. H. Deleted in Liver Cancer-1 (DLC-1): a tumor suppressor not just for liver. *Int J*

Biochem Cell Biol. **49,** 1841–1850 (2009).

21. Kim, T. Y. *et al.* DLC-1, a GTPase-activating protein for Rho, is associated with cell proliferation, morphology, and migration in human hepatocellular carcinoma. *Biochem. Biophys. Res. Commun.* **355,** 72–77 (2007).

22. Denais, C. M. *et al.* Supplementary Materials for Nuclear envelope rupture and repair during cancer cell migration. *Science (80-.).* **352,** 353–358 (2016).

23. Gauthier, N. C., Masters, T. A. & Sheetz, M. P. Mechanical feedback between membrane tension and dynamics. *Trends Cell Biol.* **22,** 527–535 (2012).

24. Beijer, N. R. M. *et al.* TopoWellPlate : A Well-Plate-Based Screening Platform to Study Cell – Surface Topography Interactions. *Adv. Biosyst.* **1,** 1–8 (2017).

25. Echave, P., Conlon, I. J. & Lloyd, A. C. Cell size regulation in mammalian cells. *Cell Cycle* **6,** 218–224 (2007).

26. Schmoller, K. M. & Skotheim, J. M. The Biosynthetic Basis of Cell Size Control. *Trends Cell Biol.* **25,** 793–802 (2015).

27. Bacus, S. S. *et al.* Taxol-induced apoptosis depends on MAP kinase pathways (ERK and p38) and is independent of p53. *Oncogene* **20,** 147–155 (2001).

28. Bharadwaj, R. & Yu, H. The spindle checkpoint, aneuploidy, and cancer. *Oncogene* **23,** 2016–2027 (2004).

29. Curtis, A. S. G. The Mechanism of Adhesion of Cells to Glass: A Study by Interference Reflection Microscopy. *J. Cell Biol.* **20,** 199–215 (1964).

30. Pierres, A., Benoliel, A. M., Touchard, D. & Bongrand, P. How cells tiptoe on adhesive surfaces before sticking. *Biophys. J.* **94,** 4114–4122 (2008).

31. Ramirez-San Juan, G. R., Oakes, P. W. & Gardel, M. L. Contact guidance requires spatial control of leading-edge protrusion. *Mol. Biol. Cell* **28,** 1043–1053 (2017).

32. Sales, A., Holle, A. W. & Kemkemer, R. Initial contact guidance during cell spreading is contractility-independent. *Soft Matter* **13,** 5158–5167 (2017).

33. Davidson, P. M., Özçelik, H., Hasirci, V., Reiter, G. & Anselme, K. Microstructured surfaces cause severe but non-detrimental deformation of the cell nucleus. *Adv. Mater.* **21,** 3586–3590 (2009).

34. Hasturk, O. *et al.* Quantification of Type, Timing, and Extent of Cell Body and Nucleus Deformations Caused by the Dimensions and Hydrophilicity of Square Prism Micropillars. *Adv. Healthc. Mater.* **5,** 2972–2982 (2016).

35. Liu, X., Liu, R., Gu, Y. & Ding, J. Nonmonotonic Self-Deformation of Cell Nuclei on Topological Surfaces with Micropillar Array. *ACS Appl. Mater. Interfaces* **9,** 18521–18530 (2017).

36. Liu, X. *et al.* Subcellular cell geometry on micropillars regulates stem cell differentiation. *Biomaterials* **111,** 27–39 (2016).

37. Kim, D.-H. *et al.* Volume regulation and shape bifurcation in the cell nucleus. *J. Cell Sci.* **129,** 457–457 (2016).

38. Davidson, P. M. *et al.* Topographically induced self-deformation of the nuclei of cells: Dependence on cell type and proposed mechanisms. *J. Mater. Sci. Mater. Med.* **21,** 939–946 (2010).

39. Badique, F. *et al.* Directing nuclear deformation on micropillared surfaces by substrate geometry and cytoskeleton organization. *Biomaterials* **34,** 2991–3001 (2013).

40. Ermis, M., Akkaynak, D., Chen, P., Demirci, U. & Hasirci, V. A high throughput approach for analysis of cell nuclear deformability at single cell level. *Sci. Rep.* **6,** 36917 (2016).

41. Versaevel, M., Grevesse, T. & Gabriele, S. Spatial coordination between cell and nuclear shape within micropatterned endothelial cells. *Nat. Commun.* **3,** 1–11 (2012).

42. Cai, S., Fu, X. & Sheng, Z. Dedifferentiation: A New Approach in Stem Cell Research. *Bioscience* **57,** 655 (2007).

43. Swanson, J. A., Lee, M. & Knapp, P. E. Cellular dimensions affecting the nucleocytoplasmic volume ratio. *J. Cell Biol.* **115,** 941–948 (1991).

44. Slater, D. N. *et al.* Proposed Sheffield quantitative criteria in cervical cytology to assist the grading of squamous cell dyskaryosis , as the British Society for Clinical Cytology definitions require amendment. *Cytopathology* **16,** 179–192 (2005).

45. Johnston, D. G. Cytoplasmic nuclear ratios in the cytological diagnosis of cancer. *Cancer* **5,** 1–5 (1952).

46. Webster, M., Witkin, K. L. & Cohen-Fix, O. Sizing up the nucleus: nuclear shape, size and nuclear-envelope assembly. *J. Cell Sci.* **122,** 1477–1486 (2009).

47. Misteli, T. Nuclear order out of chaos. *Nature* **456,** 333–334 (2008).

48. Anselme, K., Wakhloo, N. T., Rougerie, P. & Pieuchot, L. Role of the Nucleus as a Sensor of Cell Environment Topography. *Adv. Healthc. Mater.* **1701154,** 1701154 (2017).

49. Heo, S. J. *et al.* Biophysical regulation of chromatin architecture instills a mechanical memory in mesenchymal stem cells. *Sci. Rep.* **5,** 1–14 (2015).

50. Simonis, M. *et al.* Nuclear organization of active and inactive chromatin domains uncovered by chromosome conformation capture-on-chip (4C). *Nat. Genet.* **38,** 1348–1354 (2006).

51. Noordermeer, D. *et al.* Variegated gene expression caused by cell-specific long-range DNA interactions. *Nat. Cell Biol.* **13,** 944–951 (2011).

52. De Laat, W. & Duboule, D. Topology of mammalian developmental enhancers and their regulatory landscapes. *Nature* **502,** 499–506 (2013).

53. De Wit, E. *et al.* The pluripotent genome in three dimensions is shaped around pluripotency factors. *Nature* **501,** 227–231 (2013).

54. Lloyd, A. C. The regulation of cell size. *Cell* **154,** 1194–1205 (2013).

55. Yamamoto, K. *et al.* Largen : A Molecular Regulator of Mammalian Cell Size Control. *Mol. Cell* **53,** 904–915 (2014).

56. Miettinen, T. P. *et al.* Identification of transcriptional and metabolic programs related to mammalian cell size. *Curr. Biol.* **24,** 598–608 (2014).

57. Mcmurray, R. J. *et al.* Nanoscale surfaces for the long-term maintenance of mesenchymal stem cell phenotype and multipotency. *Nat. Mater.* **10,** 637–644 (2011).

58. Dupont, S. *et al.* Role of YAP/TAZ in mechanotransduction. *Nature* **474,** 179–183 (2011).

59. Huang, J., Wu, S., Barrera, J., Matthews, K. & Pan, D. The Hippo signaling pathway coordinately regulates cell proliferation and apoptosis by inactivating Yorkie, the Drosophila homolog of YAP. *Cell* **122,** 421–434 (2005).

60. Hansen, C. G., Moroishi, T. & Guan, K. L. YAP and TAZ: A nexus for Hippo signaling and beyond. *Trends Cell Biol.* **25,** 499–513 (2015).

61. Zhao, B. *et al.* Inactivation of YAP oncoprotein by the Hippo pathway is involved in cell contact inhibition and tissue growth control. *Genes Dev.* **21,** 2747–2761 (2007).

62. Aragona, M. *et al.* A Mechanical Checkpoint Controls Multicellular Growth through YAP / TAZ Regulation by Actin-Processing Factors Mechanical Regulation of Cell Proliferation through. *Cell* **154,** 1047–1059 (2013).

63. Raimon Sunyer1, Vito Conte1, Jorge Escribano2, Alberto Elosegui-Artola1, Anna Labernadie1, Léo Valon1, Daniel Navajas1, 3, 4, José Manuel García-Aznar2, José J. Muñoz5, Pere Roca-Cusachs1, 3,*, Xavier Trepat1, 3, 6, 7,* Raimon Sunyer1, Vito Conte1, Jorge, 7. Re s ear ch | r e p o r t s. *Science (80-.).* **353,** 1157–1161 (2016).

64. Nagayama, K., Hamaji, Y., Sato, Y. & Matsumoto, T. Mechanical trapping of the nucleus on micropillared surfaces inhibits the proliferation of vascular smooth muscle cells but not cervical cancer HeLa cells. *J. Biomech.* **48,** 1796–1803 (2015).

65. Deisenroth, C. & Zhang, Y. The ribosomal protein-mdm2-p53 pathway and energy metabolism: Bridging the gap between feast and famine. *Genes and Cancer* **2,** 392–403 (2011).

66. Boulon, S., Westman, B. J., Hutten, S., Boisvert, F. M. & Lamond, A. I. The Nucleolus under Stress. *Mol. Cell* **40,** 216–227 (2010).

67. Bursac, S. *et al.* Mutual protection of ribosomal proteins L5 and L11 from degradation is essential for p53 activation upon ribosomal biogenesis stress. *Proc. Natl. Acad. Sci.* **109,** 20467–20472 (2012).

68. Kapoor, N. R., Ahuja, R., Shukla, S. K. & Kumar, V. The HBx protein of hepatitis B virus confers resistance against nucleolar stress and anti-cancer drug-induced p53 expression. *FEBS Lett.* **587,** 1287–1292 (2013).

69. Jayo, A. *et al.* Fascin Regulates Nuclear Movement and Deformation in Migrating Cells. *Dev. Cell* **38,** 371–383 (2016).

70. Thomas, A. J. *et al.* Functional mechanotransduction is required for cisplatin- induced hair cell death in the zebrafish lateral line. *J. Neurosci.* **3,** 4405–4414 (2013).

71. Zanconato, F., Battilana, G., Cordenonsi, M. & Piccolo, S. YAP/TAZ as therapeutic targets in cancer. *Curr. Opin. Pharmacol.* **29,** 26–33 (2016).

72. Chen, F., Evans, A., Pham, J. & Plosky, B. Cellular Stress Responses: A Balancing Act. *Mol. Cell* **40,** 175 (2010).

Supplementary figures

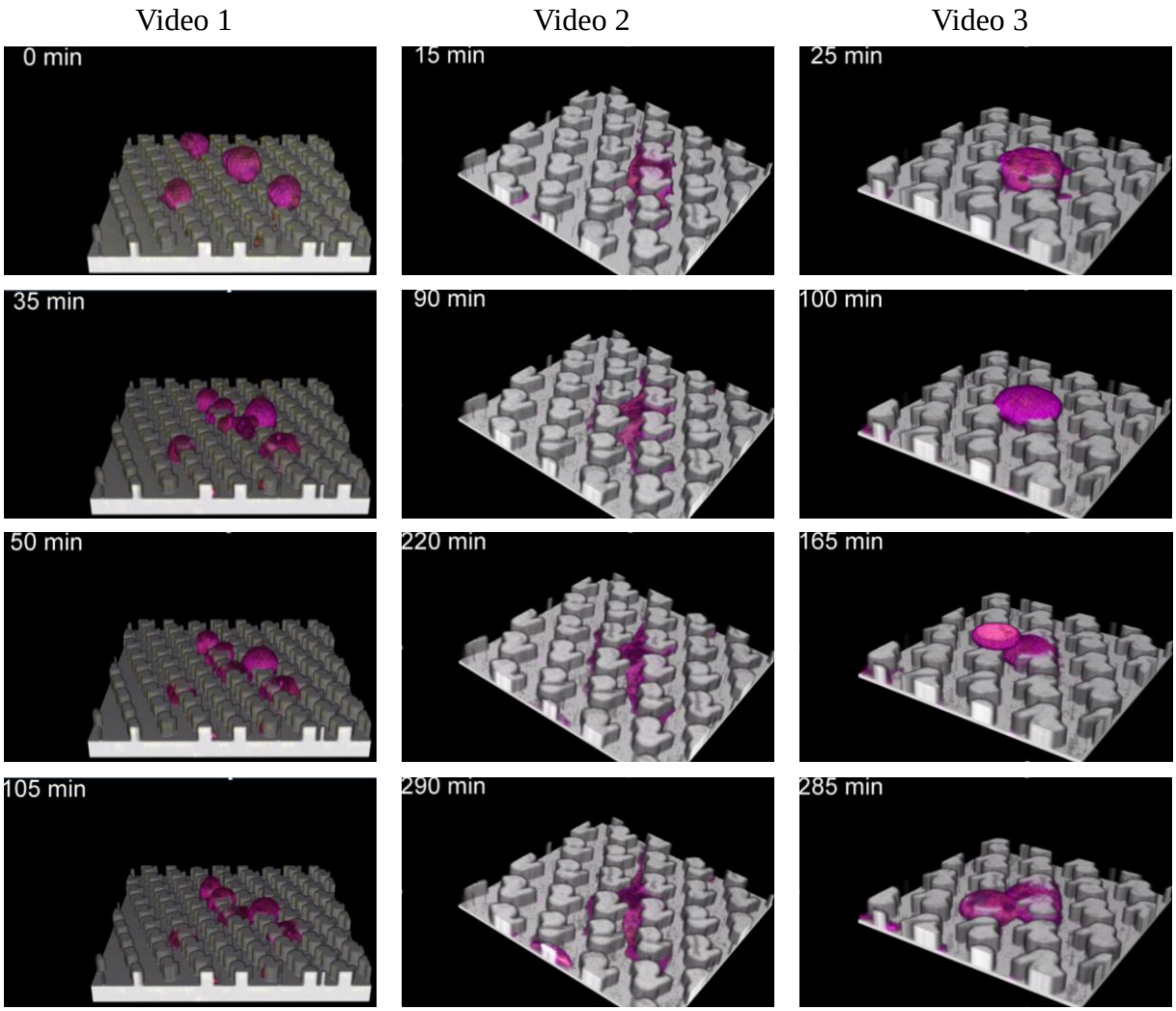

Supplementary figure 1. Cells adapting to surface topography. Selected frames of three-dimensional reconstructed confocal live cell image micrographs. Video 1 shows the attachment of fluorescently labeled U2OS cells to a topography M substrate. Video 2 shows the constant remodeling of protrusions. Video 3 shows the differences in cell-material contact during cell division. Full videos are available at www.jandeboerlab.com.

topographically enhanced cell culture systems t
pographically enhanced cell culture systems to
graphically enhanced cell culture systems to i
raphically enhanced cell culture systems to in
phically enhanced cell culture systems to indu
ically enhanced cell culture systems to induce
ally enhanced cell culture systems to induce an
lly enhanced cell culture systems to induce and
y enhanced cell culture systems to induce and m
enhanced cell culture systems to induce and mon
hanced cell culture systems to induce and monit
anced cell culture systems to induce and monito
ced cell culture systems to induce and monitor
d cell culture systems to induce and monitor me
cell culture systems to induce and monitor mech
ell culture systems to induce and monitor mecha
ll culture systems to induce and monitor mechano
culture systems to induce and monitor mechanobi
lture systems to induce and monitor mechanobiol
ture systems to induce and monitor mechanobiolo
re systems to induce and monitor mechanobiology

Chapter 5

TopoWellPlate:

A well-plate-based screening platform to study cell-surface topography interactions

Nick R.M. Beijer[1], Aliaksei S. Vasilevich[1], Bayram Pilavci[1], Roman K. Truckenmüller[2], Yiping Zhao[3], Shantanu Singh[4], Bernke J. Papenburg[3] & Jan de Boer[1]

Published in: Advanced Biosystems (2017)

[1] Department of Cell Biology Inspired Tissue Engineering, MERLN Institute for Technology-Inspired Regenerative Medicine, Maastricht University, the Netherlands. [2] Department of Complex Tissue Regeneration, MERLN Institute for Technology-Inspired Regenerative Medicine, Maastricht University, the Netherlands. [3] Materiomics BV, Maastricht, the Netherlands. [4] Imaging Platform, Broad institute of MIT and Harvard, Cambridge, MA, USA.

Abstract

The field of biomaterial engineering is increasingly using high-throughput approaches to investigate cell–material interactions. Because most material libraries are prepared as chips, immunofluorescence-based read-outs are used to uniquely image individual materials. This paper proposes to produce libraries of materials using a well-based strategy in which each material is physically separated, and thus compatible with standard biochemical assays. In this work, the TopoWellPlate, a novel system to study cell–surface topography interaction in high-throughput is presented. From a larger library of topographies, 87 uniquely defined bioactive surface topographies are identified, which induce a wide variety of cellular morphologies. Topographically enhanced polystyrene films are fabricated in a multistep cleanroom process and served as base for the TopoWellPlate. Thermal bonding of the films to bottomless 96-well plates results in a cell culture ready, topographically enhanced, 96-well plate. The overall metabolic activity of bone marrow-derived human mesenchymal stem cells is measured to show the functionality of the TopoWellPlate as a screening tool, which showed a 2.5-fold difference range in metabolic activity per cell. TopoWellPlates of this and other topographical designs can be used to analyze cells using the wealth of standardized molecular assays available and thus disclose the mechanisms of biomaterials-induced mechanotransduction.

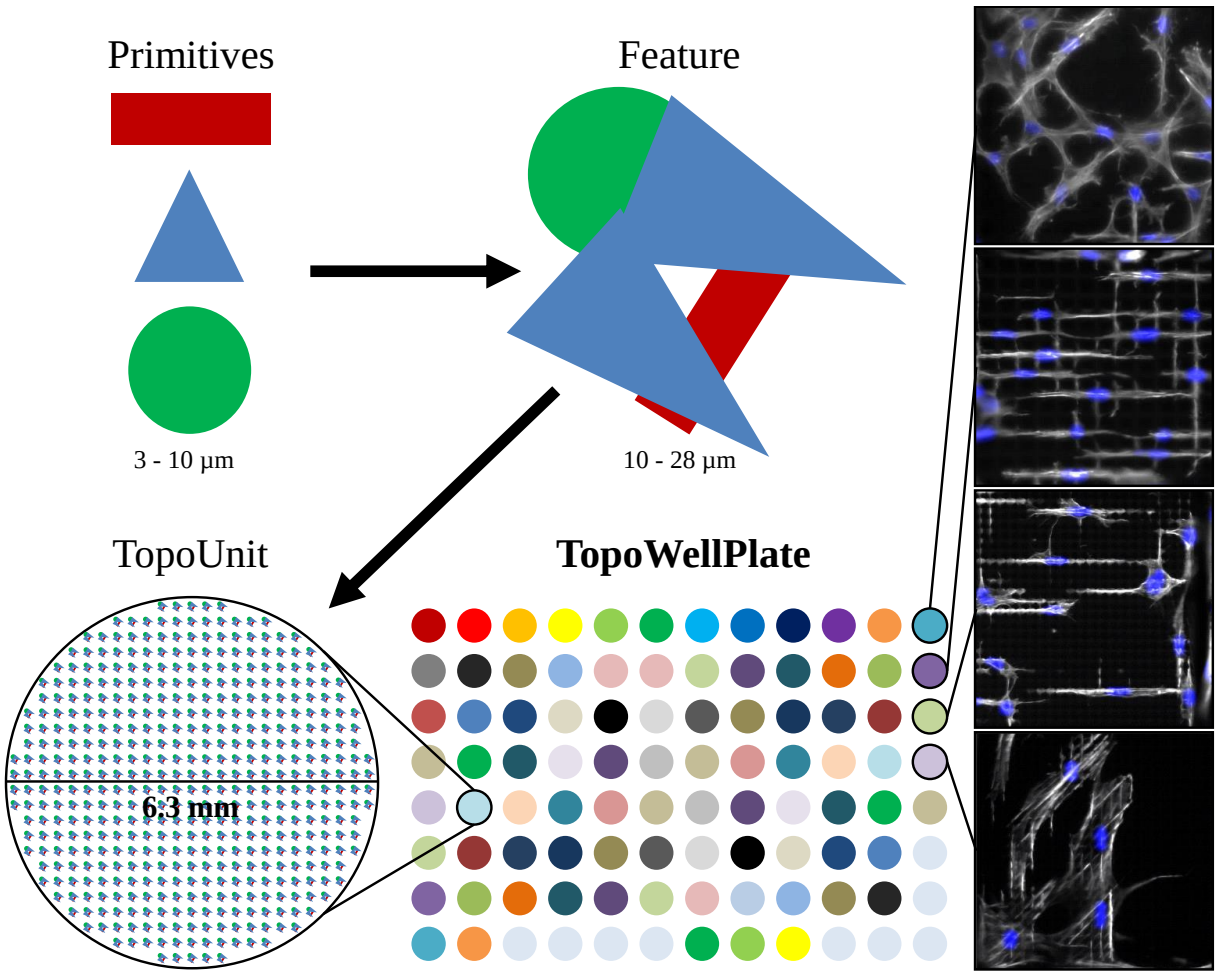

Introduction

Biomaterials can be engineered to alter cell behavior, often by impinging on mechanotransduction signaling pathways, resulting in phenotypic changes such as in cell morphology and alignment, migration, proliferation rates, and directed cell fate[1–3]. The influence of individual material parameters on cell behavior is widely studied, often by modifying one property of the biomaterial. For example, substrate surface chemistries can be varied, from synthetic polymers to biomolecules and bulk material properties such as degradability and elasticity can be modified[4,5]. Furthermore, microcontact printing is used to change the size and shape of cell adhesive islands. In a seminal paper, Chen et al. showed that apoptosis and proliferation of endothelial cells can be controlled by altering the size of the adhesive island on which the cell grows[6]. Using a similar approach, the same group demonstrated a role for Rho-mediated signaling in the control of adipogenic and osteogenic differentiation. Another relation between a biomaterial property and cellular response is reported by Swift et al. who demonstrated that extra cellular matrix stiffness correlates to lamin-A conformation and expression levels[7].

In these, and most other cases, only a very limited part of the full biomaterial design space is covered. Moreover, in most cases, a relation is found between material properties and a phenotypical read-out, but the complex molecular mechanisms linking this material property to the change in phenotype is largely unknown. To address this, state-of-the-art high-throughput platforms are used. These systems serve as excellent starting points to identify materials which are able to induce desirable cell behavior. Comparable to low-throughput work, high-throughput systems are used to explore material properties such as bulk material chemistry[8,9], surface chemistry[10], and surface structure. Here, primarily imaging-based read-outs are used to screen for one biomarker in the desired phenotype because the material libraries are spotted onto glass slides or produced as arrays on chemically non-separated sheets. For example, three different platforms are used nowadays to screen for bioactive surface topographies in high-throughput: multi-architecture chip (MARC, consisting of isotropic/anisotropic, nano- and micrometer scale, polydimethylsiloxane (PDMS) surface topographies)[11], biosurface structure array (BSSA, consisting of topographical features designed using a combinatorial approach of lateral and vertical dimensions)[12], and the TopoChip[13]. Using MARC, Moe et al. identified a surface structure able to enhance neural differentiation of primary murine neural progenitor cells[11]. Lovmand et al. used the BSSA to identify surface structures that enhanced mineralization as well as the expression of osteogenic markers of a pre-osteoblastic murine cell line[12].

On the TopoChip, defined surface structures are created by combining circles, squares, and rectangles (Figure 1A) into topographical features (Figure 1B) that vary in size, density, and roundness. These topographical features are placed in an arrayed order in 290 × 290 μm TopoUnits (Figure 1C). In total 2176 TopoUnits with unique surface topographies are placed in duplicate on a 2 × 2 cm polymer cell culture tool, designated the TopoChip (Figure 1D).

We observed dramatic changes in cell and nuclear morphologies correlating to the topographical feature design parameters[14]. In present — more application driven — work, we identified a bioactive surface that can be used to improve the lifespan of orthopedic implants. Here, surface topographies are selected that induced osteogenesis *in vitro* and increased bone bonding *in vivo*[15]. Furthermore, a set of specific topographical features is identified which maintained the expression levels of the pluripotency markers OCT4 and SOX2, and thus overcomes difficulties in *xeno*-free induced pluripotent stem cell (IPSC) culture[16].

As most other high-throughput screening systems, the TopoChip relies on imaging-based read-outs as it is difficult to address individual TopoUnits differently. However, the study of topography-induced cellular responses could greatly benefit from the realm of molecular biology techniques available, such as RNA sequencing, enzyme-linked immunosorbent assays (ELISA), mass spectrometry, or other biochemical assays. To be able to do so, the cell cultures should meet two criteria; the populations exposed to a unique surface topography should be isolated, and should be large enough to retrieve sufficient amounts of biological material. In order to validate screening results, selected hit topographies are further assessed in low throughput on larger, isolated replicates. So far, this led to valuable insights in cell–surface topography interaction such as the regulation of chondrogenic differentiation marker genes in ATDC5 cells[17] and M1/M2 differentiation of macrophages observed during different phases. (Manuscript submitted)

Upscaling of topographically enhanced materials is a costly and time consuming process, which raises the urge for a system to study a wide range of surface topographies, and which has compatibility with standard well plate technologies. A few platforms are available for screening cell–material interactions in a well plate format. Zant and Grijpma designed a method to screen hydrogel properties for their influence on cell attachment and proliferation. Synthesizing 255 different hydrogels in 96-well plates allowed them to quickly assess the individual populations by collecting culture medium and cell lysates[9]. A second example is described by Yang et al. who studied the influence of inorganic additives in calcium phosphates on behavior of osteoblasts and osteoclasts in a screening manner[18]. Hu et al. introduced a PDMS-based platform to test the influence of multiple grid and grating conformations in combinations with drugs on T cell activity. Using this combinatorial approach, they were able to identify both IL-2 secretion enhancing and suppressing cell microenvironments[19].

In this work, we present the TopoWellPlate, a screening tool for bioactive surface topographies which allows in-depth analysis of the involved molecular mechanisms. The TopoWellPlate consists of 87 isolated TopoUnits displayed over larger areas of surface in the well base (Figure 1E and F). Furthermore, the supervised machine learning approach to select the surface topographies as well as the multistep cleanroom process are described in detail. To show the functionality of the TopoWellPlate, we measured the metabolized cell culture

medium of the individual cell populations and observed a wide range of cellular reactions to the surface topographies.

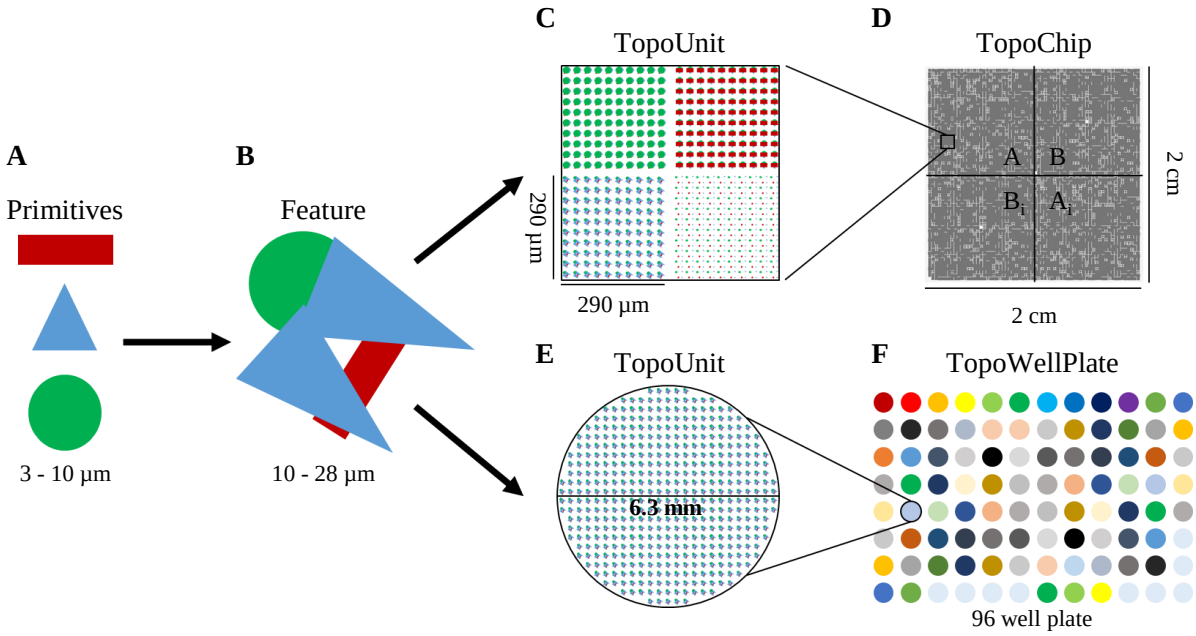

Figure 1. TopoWellPlate as a new member of the TopoChip platform. A) Primitive shapes (namely, circles, triangles, and rectangles) are used to design (B) topographical features. Arrays of a unique topographical feature build (C) a 290 × 290 µm square TopoUnit for (D) the TopoChip and (E) an isolated circular TopoUnit of 6.3 mm in diameter for (F) the TopoWellPlate. The TopoChip contains 2176 unique surface topographies in duplicate and 4 unpatterned units, whereas the TopoWellPlate contains 87 unique surface topographies and 9 unpatterned wells.

Materials and methods

Topography selection

Bone marrow derived hMSCs cultured for 5 d under basic conditions on eight titanium coated poly-lactic-acid TopoChips were fluorescently stained for DNA (DAPI, Life Technologies), actin cytoskeleton (phalloidin, Life Technologies), and osteogenic differentiation related protein alkaline phosphatase (ALP, sc137213, Santa Cruz Biotech). High-content imaging of the cells on the TopoChips was performed using the BD pathway. The 2176 unique surface topographies (duplicates per chip) and the unpatterned TopoUnits (four replicas per chip) were captured in individual images of all eight TopoChips. Prior to image analysis, a variety of image correction steps were performed which included: region of interest (ROI) cropping, alignment, and background signal removal.

Image analysis was performed using CellProfiler[20]. After segmentation of individual cells in the ROI, a 1000 node cluster analysis was performed. With this datasets on most morphological parameters were obtained that are available in the CellProfiler software.

Subsequently, CellProfiler analyst 2.0[21], a tool for supervised machine learning analysis relying on a gently boosting algorithm, was used to explore the variety of cell morphologies in the TopoChip data. To initiate this algorithm, five eye catching cell morphologies were selected from the image database. Subsequently, CellProfiler analyst was used to create the five corresponding binary classifiers. Here, at least 100 cells per morphological cluster were presented to the program in order to create a classification accuracy of 70%. The obtained binary classifiers (features used in these classifiers are shown in Table 1) were then used to assess the complete dataset, where all images (corresponding to one TopoUnit) were scored based on the percentage of cells that belong to one of the defined classifiers. The most frequent TopoUnits in the 1000 highest scored images were selected as surface topography inducing one of the five classified cell morphologies in a robust and reproducible way.

Table 1. Binary classifier parameters for five cellular morphologies. CellProfiler analyst supervised machine learning on five distinct cell morphologies led to the description of corresponding binary classifiers. The rules for classification are based on few morphological parameters all with a different weight in the classification process. Here, orange shading represents morphological parameters important in the binary classifying process with an accuracy of 70%, green parameters of medium importance, and blue of low importance.

Class 1	Class 2	Class 3	Class 4	Class 5
Eccentricity	Area	Solidity	Eccentricity	Area
Compactness	Minor axis	Eccentricity	Area	Compactness
Neighbors	Solidity	Area	Solidity	
Minor axis	Extent			

Topography enhanced polystyrene film fabrication process

Patterns of the selected surface topographies were placed in a 96-well plate format as the lay-out of the chromium masks for photolithography. The micrometer-scale patterns were etched from the silicon wafer by directional reactive ion etching (DRIE), generating a silicon master mould. Due to wafer size limitations, two moulds were needed to create a lay-out with the size of a 96-well plate. These silicon master moulds contained the inverse topography patterns. A three-replication process was used to fabricate the surface topography enhanced polystyrene films[22]. In these three replications, silicon moulds, PDMS moulds, and Ormostamp moulds were subsequently used.

Silicon master mould fabrication

Si [100] wafers were prepared with positive photoresist (907-16, Olin) by spin-coating at 4000 rpm for 30 min. The prepared substrates were patterned using the designed masks in conventional UV lithography (EVG 620). After development (OPD 4262) and hard baking on a hotplate at 120 °C for 30 min, the wafers were etched by DRIE (Adixen AMS 100 SE) using a Bosch process of SF6/C4F8 flow of 250/200 sccm (3/1 s), ICP of 1500 W, CCP of 80 W, and a substrate temperature of 80 °C for 3 min and 18 s. By this, a feature depth of 10 μm was obtained. The photoresist was then stripped in O_2 plasma.

PDMS mould fabrication

The silicon master moulds (Figure 2A) were first cleaned in Piranha solution (H_2SO_4: H_2O_2 = 3:1 v/v) for 30 min at 95 °C, rinsed with deionized water, spun dried with N_2, and coated with a monolayer of trichloro(1H, 1H, 2H, 2H-perfluorooctyl)silane (FOTS, Sigma-Aldrich) in the gas phase under vacuum in a desiccator. Degassed PDMS (curing agent: base = 1:10 w/w, Sylgard 184 silicone elastomer kit, Dow Corning Corporation) was casted (Figure 2B) on the full 100 mm silicon master mould to create a 1–2 mm thick PDMS mould, and cured on a leveled hotplate at 80 °C for at least 8 hours (Figure 2C). After curing, the PDMS film was peeled from the silicon mould (Figure 2D), and ready to be used for the next replication cycle.

Ormostamp mould fabrication

Due to thermal expansion and mechanical properties of PDMS, the obtained PDMS mould could not be used as a proper template for hot embossing. Therefore, a second replication step was needed using a much harder polymer. For this, Ormostamp (OrmoStamp, Micro Resist Technology GmbH, Germany), a UV-curable inorganic-organic hybrid polymer was used. A layer of Ormoprime (OrmoPrime08, Micro Resist Technology GmbH, Germany) was applied on a clean support Borofloat wafer (Borofloat 33 of 100 mm diameter and 500 μm thickness from Schott) via spin-coating for 30 seconds at 4000 rpm followed by 5 min on a hot plate at 150 °C. This layer promoted adhesion of the Ormostamp and was prepared immediately before application. 1.5 mL Ormostamp was slowly dispensed in the middle of the PDMS mould (Figure 2E) and carefully brought into contact with the Borofloat wafer with the Ormoprime coating. The gap between the two substrates was completely filled by capillary force after 30 min (Figure 2F). The PDMS/Ormostamp/Borofloat sandwich was exposed to 365 nm UV light for 300 seconds with a light intensity of 12 W/cm^2 (EVG 620 i-line exposure system) (Figure 2G), after which the PDMS mould was peeled from the Ormostamp mould (Figure 2H). UV curing was followed by a hard bake process on a hot plate at 130 °C for 30 min (ramping up from room temperature at a ramping speed of 5 °C/min) to finalize this replication cycle.

Polystyrene hot embossing

Before the third replication step, the Ormostamp mould was treated with a gentle O_2 plasma (reactive ion etching (home-build) at 10 °C, 50 sccm oxygen flow, 75 mTorr pressure, and 50 W CCP power for 30 s) and FOTS coated as described earlier (Figure 2I). Commercially available biaxially oriented 190 µm thick polystyrene films (Goodfellow, United Kingdom) were used as substrate material (Figure 2J) for hot embossing (Obducat Eitre6 Nano Imprint Lithography system, Obducat, Sweden) the inverse ORMO stamp template at 140 °C and 10 bars for 5 min (Figure 2K). The replication process was finalized by separating the Ormostamp template from the 10 µm high topographical features enhanced polystyrene films at 95 °C (Figure 2L). To improve cell adhesion in the later stages of the project, a gentle O_2-plasma treatment was applied as described above.

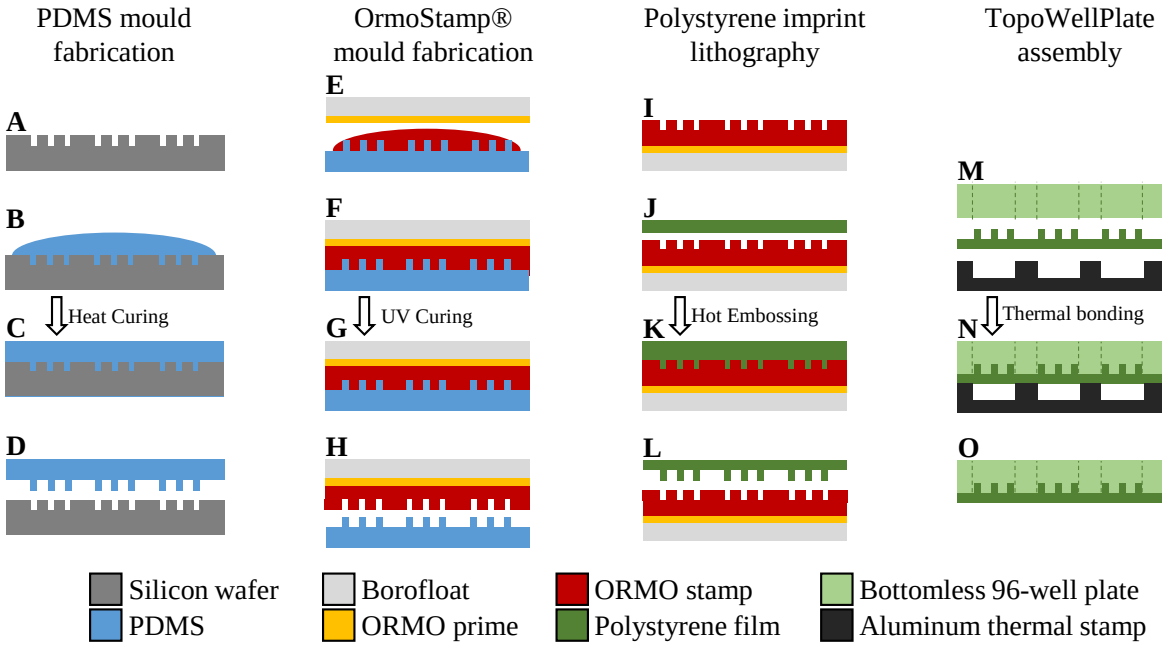

Figure 2. Fabrication scheme of PDMS and Ormostamp moulds and hot embossing of topography enhanced polystyrene films. The process of creating the topography enhanced polystyrene films for the TopoWellPlate consists of the following steps (see the Experimental Section for a more in depth description): A) Silicon master mould containing the inverse structures of the selected topographies used to (B) cast a layer of PDMS followed by (C) the curing of the PDMS layer and (D) peeling it off the silicon master. E) OrmoPrime08 is applied to a Borofloat wafer and application of Ormostamp on the PDMS copy, (F) spreading by capillary forces, (G) UV curing, and (H) peeling off the Ormostamp mould. The hot embossing process starts with (I) the inverse Ormostamp mould, (J) aligning the polystyrene film and the mould, (K) hot embossing, and finally (L) gently peeling it off the topographically enhanced film used as bottom for the TopoWellPlate. Assembling the TopoWellPlate starts by (M) aligning the bottomless 96-well plate, topographically enhanced polystyrene film and aluminum thermal stamp, followed by (N) thermal bonding at 108 °C and 6.4 MPa for 45 s, resulting in (O) a leakage-free well plate containing high-quality defined surface structures.

TopoWellPlate assembly

Size adjustment of both produced films was needed before substrate alignment for thermal bonding. Here, the topographically enhanced areas of the polystyrene films were exactly aligned (Figure 2M) with the chimneys of a bottomless 96-well plate (Greiner Bio-One) and an in-house developed aluminum controlled heat transmitting stamp. The stack was placed in a temperature controlled press where the temperature of the well plate was increased to 50 °C and the aluminum stamp to 108 °C for 4 min, followed by 45 seconds at a compression pressure of 6.4 MPa (Figure 2N) and demolding immediately afterward (Figure 2O). This resulted in a polystyrene 96-well plate with 87 wells that were enhanced with a surface topography and 9 wells that remained unpatterned.

Cell culture

A bone marrow aspirate was obtained from a donor (D210, female/74 years old) who was undergoing a total hip replacement surgery and had given informed consent. In the aspirate, the nucleated cells were counted and plated at a density of 500 000 cells/cm^2 in hMSC proliferation medium which consists of basic medium (a-minimal essential medium (a-MEM, Life Technologies), 10% fetal bovine serum (Sigma), 0.2×10^{-3} M ascorbic acid (Sigma), 2×10^{-3} M l-glutamine (Fisher Scientific) and 100 units/mL penicillin with 100 mg/mL streptomycin (Fisher Scientific)) with an additional 1 ng/mL basic fibroblast growth factor (Neuromics). Cells were grown at 37 °C, 5% CO_2, and a humidified atmosphere. The hMSCs obtained after the first trypsinization (Trypsin-EDTA (0.05%), Fisher Scientific) were plated at 5000 cells/cm^2 and considered as passage 1. Basic medium was replaced twice a week and hMSCs were used for expansion, cryopreservation or experiments once 80% confluency was reached. All experiments were performed with passage 5 hMSCs.

Metabolic activity

The metabolic activity of isolated cell populations exposed to unique surface topographies was measured using the Presto Blue assay (Invitrogen) according to the manufacturer's protocol. In brief, after 3 days basic hMSC culture medium was replaced by Presto Blue medium (1× concentrated in basic hMSC medium), which was incubated with the cell cultures for 1 hour at 37 °C in a humid environment. Equal amounts of supernatant were subsequently transferred to a black/black bottom 96-well plate and followed by the quantification of the fluorescent signal measured at 590 nm using a plate reader (Perkin Elmar Victor 3).

Fluorescent staining and microscopy

Cells were fixated in freshly prepared 3.7% paraformaldehyde for 10 min at room temperature, permeabilized by 1% Triton-x (Sigma) in phosphate buffered saline (PBS) for 10 min and blocked for a specific binding by 1% bovine serum albumin (Sigma-Aldrich) in PBS for 30 min. The actin cytoskeleton was labeled with phalloidin 488 (1:80, Biotium inc.) for 40 min and the DNA with 4′,6-diamidino-2-phenylindole (DAPI, 14.3×10^{-6} m, Life technologies) for 5 min both in dark and at room temperature. The staining protocol was finalized after multiple washing steps and the samples were kept humid in PBS. Fluorescence images were obtained using the BD pathway.

Results

To study cell–material interactions by systematic screening using techniques other than immunocytochemistry, we developed the TopoWellPlate. Clearly, the TopoWellPlate had to resemble a normal tissue culture 96-well plate, as a leakage-free system without cytotoxic chemical contamination of the cell culture environment. A supervised machine learning algorithm was used to select 87 defined surface topographies in order to create a large diversity in cell morphologies on the TopoWellPlate. From the original image database of human mesenchymal stromal cells (hMSCs) on a titanium-coated TopoChip[15] we selected five distinct cell morphologies. These particular morphologies were eye-catching during unautomated image analysis and intuitively labeled as “pancakes,” “stretched pancakes,” “sticks,” “multipolar,” and “branched” (Figure 3A). Images corresponding to the defined cell morphologies were then introduced (supervised) to an algorithm to create binary classifiers for each morphological group (Figure 3B). Assessing the complete library of images using the obtained binary classifiers allowed us to select multiple unique surface topographies which induced similar cell morphologies. The percentage of cells classified as the desired morphology per image was a measure for the robustness with which the surface topography induced this particular cell morphology. The surface topographies included in the TopoWellPlate were all selected based on this robustness (data not shown). Additionally, we included topographies inducing three different classes of nuclear morphologies as well as three classes of extreme cell morphologies that were rarely—however robustly—observed. We confirmed a great resemblance of cell morphologies when comparing the original images from the TopoChip database with the cells cultured in the TopoWellPlate (Figure 3C). With this, we created the TopoWellPlate consisting of 87 wells with unique surface topographies, which will induce 11 distinct classes of cellular and nuclear morphologies in a very reproducible manner, and 9 wells which remain without any surface topography.

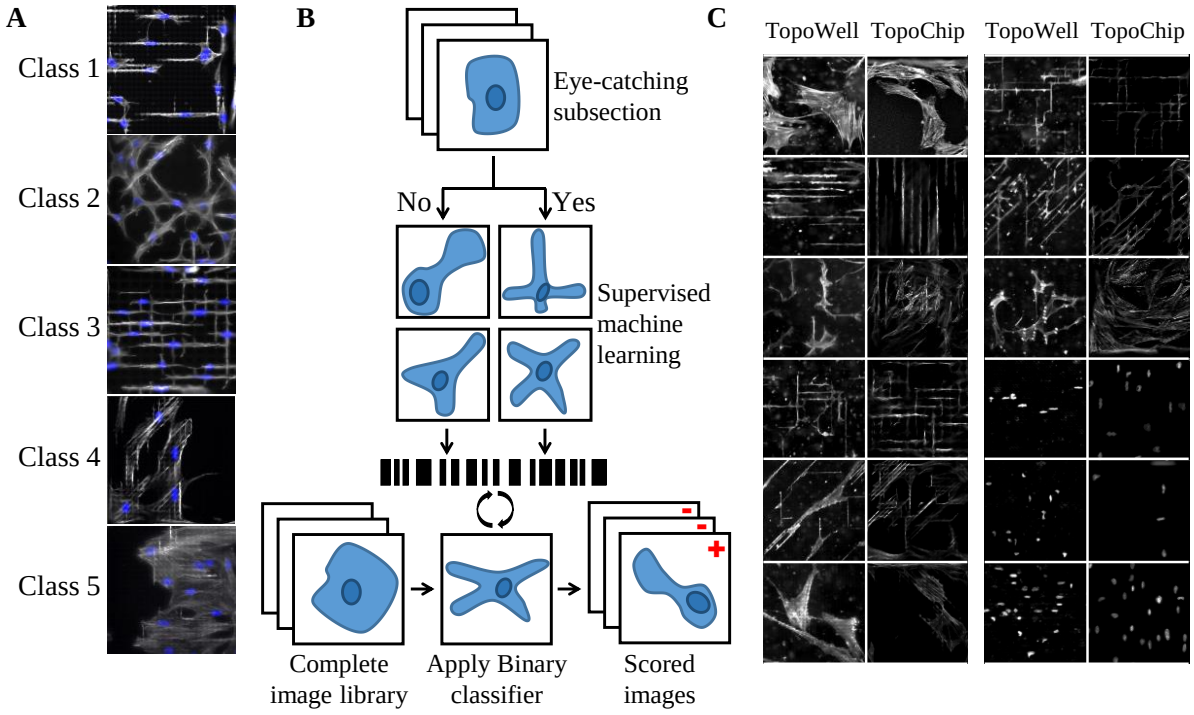

Figure 3. Robust clustering of cellular morphologies. A) Fluorescence images, obtained in a high-throughput TopoChip screen, were used to identify five distinct cell morphologies to perform binary classification. B) The classifiers obtained by supervised machine learning in CellProfiler Analyst were able to classify cells based on morphology with at least 70% accuracy. C) Testing the complete library of images with the binary classifiers let to the identification of multiple surface topographies able to induce the desired described cell morphologies, and in addition extreme morphologies (both cellular and nuclear) found to occur on fewer occasions. All described classes were scattered on the design of the TopoWellPlate.

The fabricated polystyrene films with the selected topographies distributed to cover the surface areas under the chimneys of a bottomless 96-well plate, were cropped to exactly fit the bottom region of the well plates. Prior to thermal bonding, the bottomless well plates and the two topography enhanced films were aligned. Applying 108 °C and 6.4 MPa for 45 seconds resulted in tightly sealed wells, and by this, a ready-to-use cell culture system (Figure 4). Here, neither the polystyrene base material nor the thermal bonding process caused changes in cell viability when compared to standard cell culture plates. And visual inspection of the topographical features showed high-quality defined surface structure over the entire area of the wells before, during and after cell culture (data not shown).

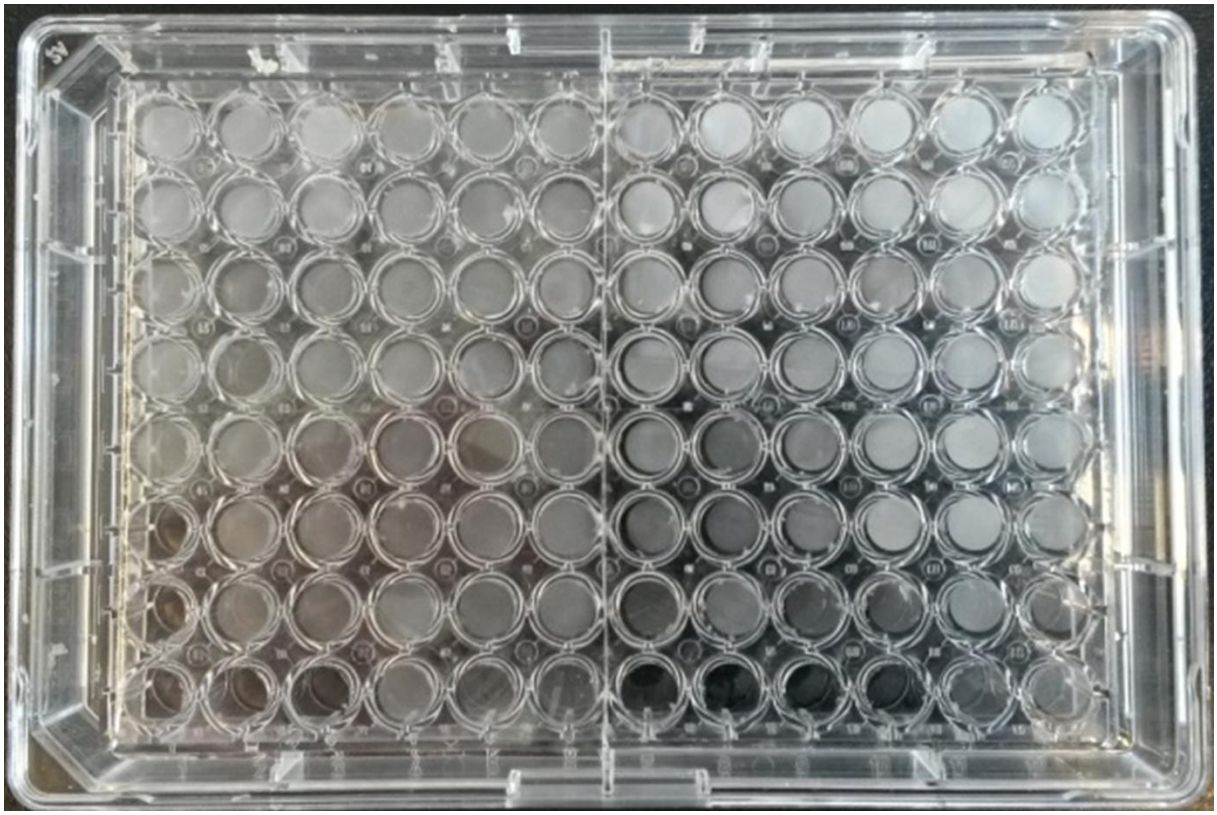

Figure 4. The TopoWellPlate. The thermal bonding of the topographically enhanced polystyrene film and the bottomless 96-well plate, results in a leakage free well plate containing high-quality defined surface structures.

The TopoWellPlate is envisioned to be used as high-throughput system to study the influence of surface topography on cell behavior with non-imaging-based techniques. To show this potential, we performed a biochemical assay on the culture medium of all individual TopoUnits. Here, we measured the overall metabolic activity of hMSC populations exposed to the 87 defined surface topographies and the populations on the unpatterned references. The Presto Blue assay used measures the conversion of the non-fluorescent resazurin into the highly fluorescent resorufin. This conversion takes mainly place in the reducing environment of mitochondria where NADPH/NADH (nicotinamide adenine dinucleotide phosphate/nicotinamide adenine dinucleotide) dehydrogenase creates the reductant NADPH/NADH. Fluorescence intensities measured in the Presto Blue assay thus represent the mitochondrial metabolic activity. Figure 5 shows the distribution of resazurin conversions in cell populations exposed to unique surface topographies. We observed a clear 2.5 times difference between the lowest and highest scoring populations, and remarkably, cell populations grown in unpatterned wells were all among the highest scoring populations. This demonstrated the diversity in physical stimuli on the TopoWellPlate and its influence on cell behavior.

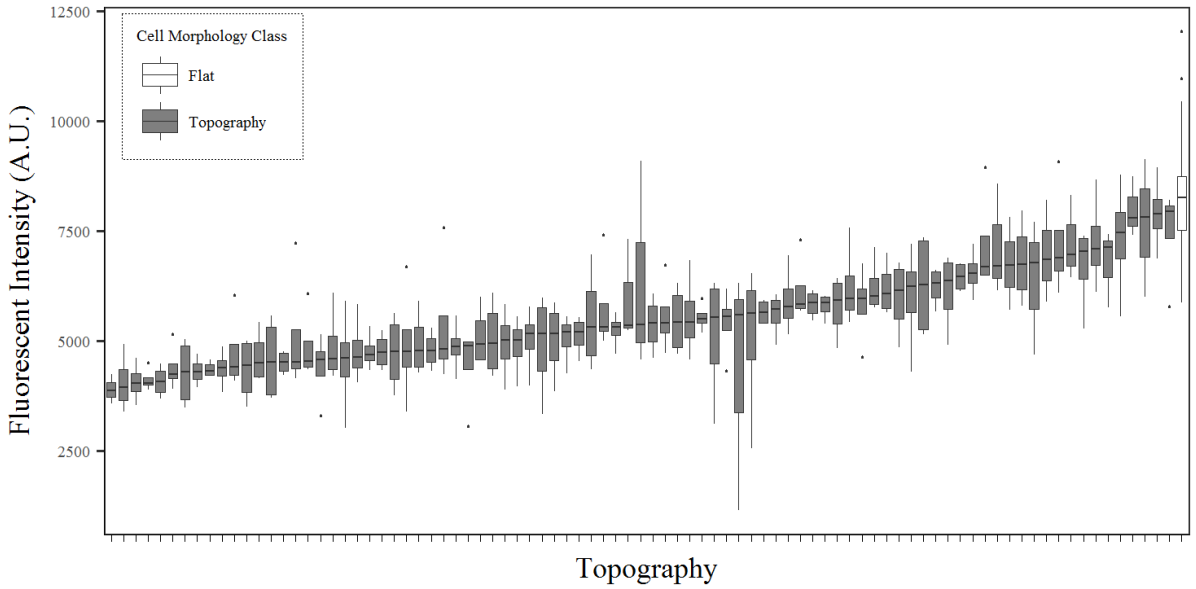

Figure 5. Topography induced changes in metabolic activity of cells cultured on different topographies in the TopoWellPlate. Metabolic activity of hMSC populations in the TopoWellPlate exposed to 87 unique surface topographies and 9 unpatterned surfaces for 3 days measured using Presto Blue. Box plots represents the median metabolic activity for a cell population cultured on a single unique surface topography (flat N=36, topography N=4) extended towards the first and third quartile. The whiskers represent the highest and lowest values, and the dots were considered outliers. All topographies are ranked from low to high.

Discussion

In this work, we have introduced the TopoWellPlate as a valuable tool to study cell–material interaction in a high-throughput manner. We established the TopoWellPlate production flow and set-up cell culture protocols that resemble the standard well plate cell culture systems. Our growing database on the bioactivity of surface topographies from the TopoChip platform in combination with the used fabrication pipeline has great potential for further development. First, the surface topographies included in the current design of the TopoWellPlate can be replaced by any other topography available in our *in silico* library. Besides the selection of topographies on the current TopoWellPlate, which is known to induce a wide variety of cell morphologies, one could, for example, include a selection of topographies that cover the full spectrum of a single design parameter for the topographical features. Second, the current 96-well plate design can be transformed into 384 and even 1536-well formats to cover the range of topographical features even more comprehensively. Third, recent data showed the ability to scale topographical feature sizes down from micrometer to nanometer scale while maintaining the high-topographical feature structures quality and reproducibility[23]. Furthermore, it is shown that the effect of surface topography on cell behavior is strongly influenced by bulk material chemistry[24]. One specific combination of surface topography, material chemistry, and cell type will give a unique result, and therefore, we foresee the use of the TopoWellPlate

of various materials to study many more mechanobiologically relevant models. To add another layer of complexity, well-plate-based system can be developed in which a defined 3D cell culture is created. Multiple platforms are used to study the influence of an engineered 3D microenvironment on cell behavior. For example, Ma et al. used a bioprinting approach to create arrays of 3D cell laden hydrogels with gradients of extra cellular matrix components able to alter cell behavior of periodontal ligament stem cells[25]. Using rapid prototyping, Higuera et al. created defined 3D structures of biomaterials in wells which allowed them to study the influence of the construct in higher throughput both *in vitro* and *in vivo*[26].

The proof of principle described in this work shows the diversity in cellular responses to surface topography as measured by the cells their mitochondrial metabolic activity. With mitochondria as the main energy producing cell organelles, one can hypothesize that changes in mitochondrial abundance occur induced by surface topography. The dramatic changes in cell morphology—observed on the TopoWellPlate–are accompanied by changes in cell size. With this, a proportionate decrease in cell organelles as mitochondria in smaller cells is possible[27]. Furthermore, the cell metabolism can be divided in multiple pathways, and the TopoWellPlate allows us to investigate the effect of surface topography on these pathways in depth.

The use of different omics approaches on the TopoWellPlate is in line with our current high-throughput approach. In particular, transcriptomic profiling using the L1000 technology allows us to create a gene expression dataset on cell-material interaction which is unique to our knowledge[28]. Besides standard gene expression data analysis techniques focusing on differentially expressed genes and their functions, other types of analysis offer interesting opportunities for further research. For example, our transcriptomic data could be used for analysis in the Connectivity Map which allows for a comparison of the biomaterial-induced gene expression profile with small molecule-induced profiles[29]. In addition, our data can be placed in the compendium for biomaterial transcriptomics (cBiT), which accumulates biomaterial-based transcriptomics studies along with a detailed characterization of the biomaterial properties, making comparisons with similar materials possible (https://cbit.maastrichtuniversity.nl)[30]. However, besides transcriptomics, many other techniques can be used to obtain valuable information. The TopoWellPlate allows us to study surface topography induced cytokine secretion by the multiplex ELISA, and to create proteomic and metabolomics profiles using mass spectrometry.

Recently, the number of mechanobiologically relevant cell systems has been growing and future applications of defined bioactive surface topographies can be introduced here. We aim to target a wide variety of biological models in which mechanical stimuli might play an important role. For example, corneal endothelium regeneration[31], macrophage stimulation[32], activation of the immune responses in mesenchymal stromal cells[33], and tailoring the epigenetic state of cells[34]. We also aim to improve standard cell culture protocols by developing culture plates that overcome current limiting factors. For example, IPSC

maintenance[5] and differentiation[35], the loss of stemness in stem cell cultures, increase proliferation rates for slow growing cell types, disrupting colony formation, and stimulating monolayer formation. We recently identified a surface topography able to maintain primary hepatocytes viable during prolonged periods of *in vitro* cell culture[36]. Including only this specific topography in a TopoWellPlate system allows us to screen libraries of small molecules for drugs discovery in this engineered biological model.

To conclude, the TopoWellPlate allows us to compile large datasets on various levels of cell behavior that can be used to uncover the "big black box" of signaling cascades in mechanobiology. This knowledge will help us to elucidate the full underlying mechanism of mechanotransduction in mechanobiologically relevant models.

References

1. Chaudhuri, O. *et al.* Hydrogels with tunable stress relaxation regulate stem cell fate and activity. *Nat. Mater.* **15,** 326–333 (2015).

2. Khetan, S. *et al.* Degradation-mediated cellular traction directs stem cell fate in covalently crosslinked three-dimensional hydrogels. *Nat. Mater.* **12,** 458–465 (2013).

3. Dupont, S. *et al.* Role of YAP/TAZ in mechanotransduction. *Nature* **474,** 179–183 (2011).

4. Lutolf, M. P. *et al.* Synthetic matrix metalloproteinase-sensitive hydrogels for the conduction of tissue regeneration: engineering cell-invasion characteristics. *Proc. Natl. Acad. Sci. U. S. A.* **100,** 5413–8 (2003).

5. Saha, K. *et al.* Surface-engineered substrates for improved human pluripotent stem cell culture under fully de fi ned conditions. *Proc. Natl. Acad. Sci. U.S.A.* **108,** 18714–18719 (2011).

6. Chen, C. S. *et al.* Geometric Control of Cell Life and Death. *Science (80-.).* **276,** 1425–1428 (1997).

7. Swift, J. *et al.* Nuclear lamin-A scales with tissue stiffness and enhances matrix-directed differentiation. *Science* **341,** 1240104 (2013).

8. Mei, Y. *et al.* Combinatorial development of biomaterials for clonal growth of human pluripotent stem cells. *Nat. Mater.* **9,** 768–778 (2010).

9. Zant, E. & Grijpma, D. W. Synthetic Biodegradable Hydrogels with Excellent Mechanical Properties and Good Cell Adhesion Characteristics Obtained by the Combinatorial Synthesis of Photo-Cross-Linked Networks. *Biomacromolecules* acs.biomac.5b01721 (2016). doi:10.1021/acs.biomac.5b01721

10. Amin, Y. Y. I. *et al.* Combinatorial Biomolecular Nanopatterning for High-Throughput Screening of Stem-Cell Behavior. *Adv. Mater.* 1472–1476 (2015). doi:10.1002/adma.201504995

11. Moe, A. A. K. *et al.* Microarray with micro- and nano-topographies enables identification of the optimal topography for directing the differentiation of primary murine neural progenitor cells. *Small* **8,** 3050–3061 (2012).

12. Lovmand, J. *et al.* The use of combinatorial topographical libraries for the screening of enhanced osteogenic expression and mineralization. *Biomaterials* **30,** 2015–2022 (2009).

13. Unadkat, H. V *et al.* An algorithm-based topographical biomaterials library to instruct cell fate. *Proc. Natl. Acad. Sci.* **109,** 5905–5905 (2012).

14. Hulsman, M. *et al.* Acta Biomaterialia Analysis of high-throughput screening reveals the effect of surface topographies on cellular morphology. *Acta Biomater.* **15,** 29–38 (2015).

15. Hulshof, F. F. B. *et al.* Mining for osteogenic surface topographies: In silico design to in vivo osseo-integration. *Biomaterials* **137,** 49–60 (2017).

16. Reimer, A. *et al.* Scalable topographies to support proliferation and Oct4 expression by human induced pluripotent stem cells. *Sci. Rep.* **6,** 18948 (2016).

17. Le, B. Q. *et al.* Micro-Topographies Promote Late Chondrogenic Differentiation Markers in the ATDC5 Cell Line. *Tissue Eng Part A* **23,** 458–469 (2017).

18. Yang, L. *et al.* The effects of inorganic additives to calcium phosphate on in vitro behavior of osteoblasts and osteoclasts. *Biomaterials* **31,** 2976–2989 (2010).

19. Hu, J. *et al.* High-Throughput Mechanobiology Screening Platform Using Micro- and Nanotopography. *Nano Lett.* **16,** 2198–2204 (2016).

20. Carpenter, A. E. *et al.* CellProfiler: image analysis software for identifying and quantifying cell

phenotypes. *Genome Biol.* **7,** R100 (2006).

21. Jones, T. R. *et al.* CellProfiler Analyst: data exploration and analysis software for complex image-based screens. *BMC Bioinformatics* **9,** 482 (2008).

22. Zhao, Y. *et al.* High-definition micropatterning method for hard, stiff and brittle polymers. *Mater. Sci. Eng. C* **71,** 558–564 (2017).

23. Hulshof, F. F. B. *et al.* NanoTopoChip: High-throughput Nanotopographical Cell Instruction. *Acta Biomater.* (2017). doi:10.1016/j.actbio.2017.08.023

24. Hulshof, F., de Boer, J. & Stamatialis, D. F. TopoChip: technology for instructing cell fate and morphology via designed surface topography. (2016).

25. Ma, Y. *et al.* Bioprinting 3D cell-laden hydrogel microarray for screening human periodontal ligament stem cell response to extracellular matrix. *Biofabrication* **7,** 44105 (2015).

26. Higuera, G. A. *et al.* In vivo screening of extracellular matrix components produced under multiple experimental conditions implanted in one animal. *Integr. Biol.* **5,** 889–898 (2013).

27. Schmoller, K. M. & Skotheim, J. M. The Biosynthetic Basis of Cell Size Control. *Trends Cell Biol.* **25,** 793–802 (2015).

28. Senkowski, W. *et al.* Large-Scale Gene Expression Profiling Platform for Identification of Context-Dependent Drug Responses in Multicellular Tumor Spheroids. *Cell Chem. Biol.* **23,** 1428–1438 (2016).

29. Lamb, J. *et al.* The Connectivity Map : Using Gene-Expression Signatures to Connect Small Molecules, Genes, and Disease. *Science (80-.).* **313,** 1929–1936 (2006).

30. Hebels, D. G. A. J., Carlier, A., Coonen, M. L. J., Theunissen, D. H. & de Boer, J. cBiT: A transcriptomics database for innovative biomaterial engineering. *Biomaterials* **149,** (2017).

31. Muhammad, R. *et al.* Micro- and nano-topography to enhance proliferation and sustain functional markers of donor-derived primary human corneal endothelial cells. *Acta Biomater.* **19,** 138–148 (2015).

32. Hotchkiss, K. M. *et al.* Titanium surface characteristics, including topography and wettability, alter macrophage activation. *Acta Biomater.* **31,** 425–434 (2015).

33. Yagi, H. *et al.* Mesenchymal Stem Cells: Mechanisms of Immunomodulation and Homing. *Cell Transplant.* **19,** 667–679 (2010).

34. Downing, T. L. *et al.* Biophysical regulation of epigenetic state and cell reprogramming. *Nat. Mater.* **12,** 1154–1162 (2013).

35. Pan, F. *et al.* Topographic effect on human induced pluripotent stem cells differentiation towards neuronal lineage. *Biomaterials* **34,** 8131–8139 (2013).

36. Materiomics. Designed Topographies Enable Long-term In Vitro Hepatocyte Culture Model. 1–5 (2015).

⠠⠞⠓⠑ ⠠⠟⠥⠊⠉⠅ ⠃⠗⠕⠺⠝ ⠋⠭ ⠚⠥⠍⠏⠎ ⠕⠧⠑⠗ ⠞⠓⠑ ⠇⠁⠵⠽ ⠙⠕⠛

Chapter 6

The cytokine secretion profile of mesenchymal stromal cells is determined by surface structure of the microenvironment

Daniëlle G. Leuning[1 ǂ], **Nick R.M. Beijer**[2 ǂ], Nadia A. du Fossé[1], Steven Vermeulen[2], Ellen Lievers[1], Cees van Kooten[1], Ton J. Rabelink[1] & Jan de Boer[2]

Under review for publication in: Scientific Reports

‡ DL and NB contributed equally to the work. [1] Department of Nephrology, Leiden University Medical Centre, Leiden, the Netherlands. [2] Department of Cell Biology Inspired Tissue Engineering, MERLN Institute for Technology-Inspired Regenerative Medicine, Maastricht University, Maastricht, the Netherlands.

Abstract

Mesenchymal stromal cells (MSC) secrete factors that contribute to organ homeostasis and repair in a tissue specific manner. For instance, kidney perivascular mesenchymal stromal cells (kPSCs) can facilitate renal epithelial repair through secretion of hepatocyte growth factor (HGF) while the secretome of bone marrow MSCs gives rise to immunosuppression. Stromal cells function in a complex 3-dimensional (3D) connective tissue architecture that induces conformational adaptation. Here we tested the hypothesis that surface topography and associated cell adaptations dictate stromal cell function through tuning of the cytokines released. To this end, we cultured human bone marrow and kidney perivascular stromal cells in the TopoWellPlate, a custom-fabricated multi-well plate containing 76 unique bioactive surface topographies. Using fluorescent imaging, we observed profound changes in cell shape, accompanied by major quantitative changes in the secretory capacity of the MSCs. The cytokine secretion profile was closely related to cell morphology and was stromal cell type specific. Our data demonstrate that stromal cell function is determined by microenvironment structure and can be manipulated in an engineered setting. Our data also have implications for the clinical manufacturing of mesenchymal stromal cell therapy, where surface topography during bioreactor expansion should be taken into account to preserve therapeutic properties.

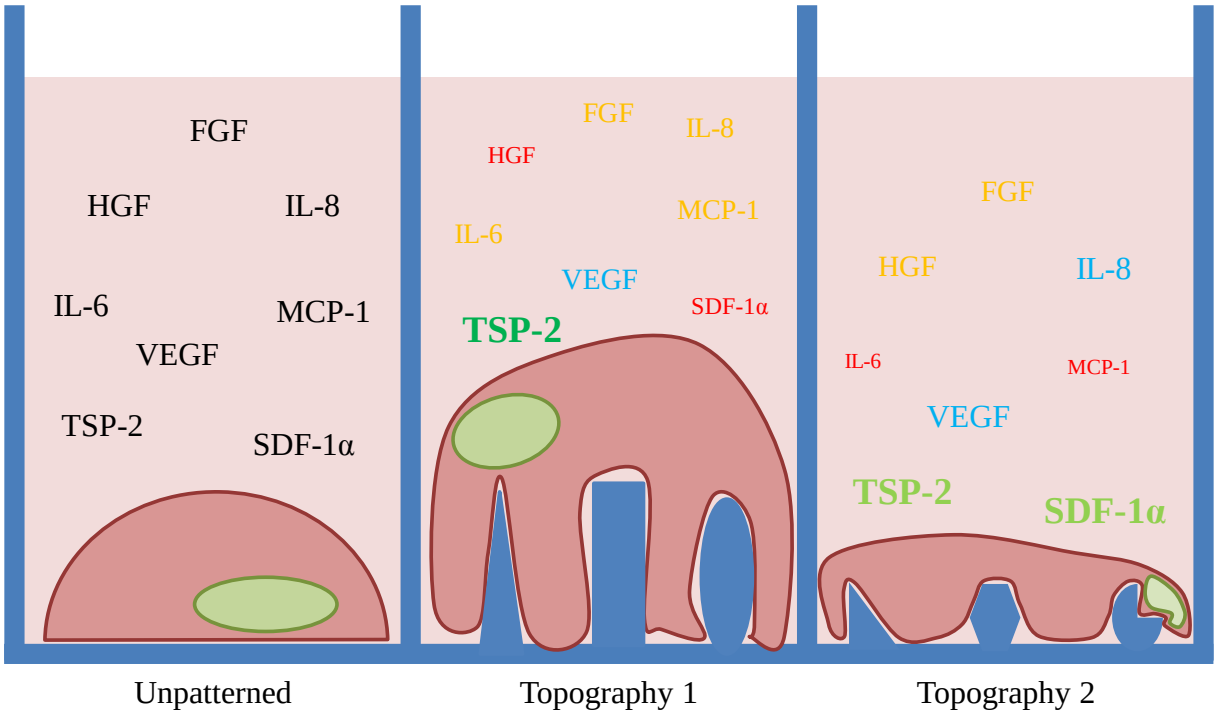

Introduction

Mesenchymal stromal cells are immunomodulatory and regenerative cells originally isolated from the bone marrow (bmMSCs). The functionality of MSCs largely depends on the secretion of soluble factors such as growth factors and cytokines. For the immunomodulatory potential of MSCs, for example, indoleamine 2,3-dioxygenase (IDO), prostaglandin E2, macrophage colony-stimulating factor (M-CSF) and interleukin (IL)-6 are of major importance[1,2], while for vascular stabilization the secretion of VEGF and angiopoietin-1 is essential[3,4]. Due to these characteristics, bmMSCs are an interesting cell source for cellular therapy for, amongst others, graft versus host disease (GvHD) and kidney transplantation and currently several trials are being performed with these cells[2,5,6].

Mesenchymal stromal cells are a diverse cell population with different functionalities throughout the body[7-9]. We showed, for example, that kidney derived perivascular stromal cells (kPSCs) display a distinct organotypic gene expression profile as well as different functionality compared to bmMSCs[9]. kPSCs were, in contrast to bmMSCs, able to support kidney epithelial wound healing, which could be attributed to the specific production of hepatocyte growth factor (HGF) by kPSCs[9]. It is of relevance to know whether such organotypic features can be preserved during MSC culture for clinical purposes.

The current standard clinical grade cell culture method of bmMSCs and kPSCs consists of culture on cell culture plastic in flasks or in cell factories. However, this method is time consuming and, due to the need of clean room facilities, costly. Therefore, there is a growing interest in closed-system bioreactor culture systems. In these systems, cells are usually grown on microcarriers[10,11]. These microcarriers can be different in material and culture surface compared to standard cell culture plastic. However, little is known about how these differences in microenvironment influence the functionality of stromal cells.

In order to study the effects of both the chemistry and surface structure of the microenvironment on cell behavior, we previously developed the TopoChip. The TopoChip is a high-throughput screening tool for bioactive algorithm-generated surface topographies, allowing to screen biomarker expression in cells exposed to over 2000 unique surface topographies on application-specific materials of interest[12]. On the TopoChip, we identified surfaces able to induce osteogenic differentiation of bmMSCs *in vitro* and bone bonding in *vivo*. Similarly, we were able to optimize clonogenic growth of IPSCs, growth of human hepatocytes and bmMSC proliferation where we observed a correlation between cell shape and cell physiology, based on high content imaging of single biomarkers[12-14].

This system does, however, not allow the assessment of the secretome of the cells studied. To allow analysis of multiple genes or secreted proteins we therefore subsequently developed the TopoWellPlate (TWP), comprising a 96-well plate with unique topographies selected based on cell shape diversity from the earlier TopoChip experiments[15].

Here, using the TWP technology, the effect of surface topographies on major growth factors and cytokines released by two different organotypic sources of MSCs, bmMSCs and kPSCs, was analyzed.

Materials and methods

TopoWellPlate production

As described previously, the topography enhanced well plates (TWP) are produced using a multiple step cleanroom process[15,27]. In short, a supervised machine learning approach was used to identify multiple defined surface topographies which are able to induce 11 morphology classes including specific cell (8) and nuclear (3) morphologies in a robust and reproducible manner. Topography numbers used in this manuscript are derived from the second generation TopoChip[12] produced in polystyrene. Instead of the full topography identifier, we use a short notation throughout this manuscript. For example, T2_PS_0365 will be referred to as 0365. The short 4 digit annotations are built-up as followed: the first two digits represent the row number counted from the top, and the second two digits represent the column number. These surface topographies were included in a 96-well plate lay-out as design for a chromium mask for photolithography of a silicon wafer. Using a polydimethylsiloxane (PDMS, curing agent: base = 1:10 w/w, Sylgard 184 silicone elastomer kit, Dow Corning Corporation) and Ormostamp (Micro Resist Technology GmbH, Germany) intermediate mould, we created topographically enhanced polystyrene films (Goodfellow, United Kingdom) by hot embossing. Subsequently the topographically enhanced polystyrene films were fused to bottomless 96-well plates (Greiner Bio-One) using thermal bonding, giving rise to leakage and chemical contaminant free TopoWellPlates. Prior to cell culture, TopoWellPlates were sterilized with 70% ethanol and washed thoroughly with phosphate buffered saline.

Isolation and expansion of clinical-grade human kidney-derived perivascular stromal cells

Kidney perivascular stromal cells were isolated and cultured as described in detail previously[9]. In short, cells were isolated from a human transplant-grade kidney discarded for surgical reasons. Specific research consent was given for all kidneys by either the donor, confirmed by the next of kin or by the next of kin directly according to Dutch legislation. None of the transplant donors were from a vulnerable population. The study was approved by the local medical ethical committee of the Leiden University Medical Centre (p13.054) and the ethical advisory board of the European Union consortium STELLAR. All methods were performed in accordance with the relevant guidelines and regulations. The kidney was

perfused via the renal artery with collagenase (2500 units, NB1, Serva) and DNAse (2,5 ml Pulmozyme, Genetech) at 37 °C with a flow of 100ml/min. After approximately 30 minutes, the tissue was digested and the resulting cell suspension was washed and collected. Cells were either directly cultured at 37 °C, 5% carbon dioxide or frozen in liquid nitrogen. Kidney cell suspensions were cultured in alphaMEM (Lonza) containing 5% platelet lysates, glutamine (Lonza) and penicillin/streptomycin (Lonza). At passage 1 NG2 cell enrichment was performed using MACS according to manufacturer's protocol (Miltenyi Biotech, Gladbach, Germany) and afterwards cells were cultured in α-MEM containing 5% platelet lysates in a density of $4x10^3$ cells per cm^2 [9]. Experiments were performed with kPSCs from one donor at passage 7.

Isolation and expansion of human bone marrow-derived mesenchymal stromal cells

Ethical committee approval from the ethical advisory board of the Leiden University Medical Centre was given and written consent from the donors was obtained for the aspiration of human bone marrow. Heparinized bone marrow was aspirated under local or general anaesthesia. The mononuclear cell fraction was isolated by Ficoll density gradient separation and plated in tissue culture flasks at a density of $160x10^3$ mononuclear cells per cm^2 in α-MEM (Lonza), supplemented with penicillin/streptomycin (Lonza) and 5% platelet lysate. The cultures were maintained at 37°C, 5% carbon dioxide. Half of the medium was refreshed twice a week. When the MSC colonies or cultures reached confluence, the cells were collected using trypsin (Lonza) and replated at $4x10^3$ cells per cm^2. Experiments were performed with bmMSCs from one donor at passage 7.

Cytokine secretion profiling

kPSCs and bmMSCs were seeded on 3 TopoWellPlates per cell type in a density of 6700 cells/well. Cells were cultured for 48 hours in 200 µl 5% α-MEM platelet lysates/well before the culture medium was collected. Subsequently, growth factors and cytokines were measured of the 3 plates per cell type with a custom-made Luminex® multiplex ELISA following manufacturer's protocols (R&D Systems, Minneapolis, MN).

Imaging for data normalization

After removal of the supernatant, cells were fixed with 4% PFA for 10 minutes, washed twice with PBS and stained for phalloidin and Hoechst (Thermo Fisher Scientific, Landsmeer, the Netherlands). Cells were imaged at 5x magnification (Leica AF6000, Leica Biosystems) and

nuclei/field of view were determined for 1 field per view for all wells with Image J software. Wells with less than respectively 200 cells per field of view (kPSC) or 150 cells per field of view (bmMSCs) were excluded from further analysis to prevent biased results based on cell numbers.

Data analysis

To assess the quality of the data, we calculated the coefficient of variation (CV) of each triplicate measurement by dividing their respective standard deviation with the mean of the measurements and is represented as a percentage.

The averaged concentrations of secreted growth factors and cytokines from the individual cell culture supernatants (separated analyses per cell type in triplicate) were used to create a scaled heatmap. To create a heatmap in which the different factors could be compared, we standardized the data according to z-scores. Dissimilarities between secreted factors as well as the topography specific secretion fingerprints were calculated using Euclidean distances and visualized in dendrograms via Ward's clustering (analysis in R ver.3.3.2[28], using packages: "cluster" ver. 2.0.6.[29], and "ggplot2" ver. 2.2.1[30]). For the clustering of surface topography induced secretion fingerprints, we calculated the ideal number of clusters to divide the topographical responses in cytokine secretion profile in comparable groups per cell types. Subsequently, the cell morphologies – as classified before – were assigned to each topography-induced secretion profile to visualize the effect of cell morphology on secretion profiles.

Statistical analysis

Statistical analysis was performed with Graph Pad Prism (Graph Pad Prism Software Incl. San Diego, USA). Differences between kPSCs and bmMSCs were analysed using a two-way ANOVA with Bonferroni's posthoc comparison analysis.

Results

Stromal cells show an organotypic cytokine secretion profile

When looking at the reference unpatterned wells most of the factors (FGF, VEGF, MCP-1, IL-8, IL-1ra, and Thrombospondin-2) are secreted in similar amounts comparing kPSCs and bmMSCs. GM-CSF, IFN-y and TNF-α were below detection limit in all conditions. Interestingly, HGF and SDF-1α showed significant differences in secretion. HGF, important

for kidney epithelial wound repair, was not detectable in bmMSC-conditioned medium and high in kPSCs (890 pg/ml) and SDF-1α was secreted in a more then 100-fold higher concentration by kPSCs compared to bmMSCs (respectively 1579 and 10 pg/ml) (Figure 1A). SDF-1α is, as HGF, an important factor for kidney regeneration.[16]

Both kPSCs and bmMSCs showed a marker expression typical for MSCs, as these cells were positive for the pericyte markers NG2, PDGFR-β and CD146 and the MSC markers CD73, CD90 and CD105 while being negative for CD31, CD34, CD45, CD56 (Supplementary Figure 1 and 2).

Stromal cells cultured on different topographies show pronounced differences in cell and nuclear morphology

The TWP consists of 76 unique bioactive algorithm-generated surface topographies (Figure 1B). We previously observed that surface topography can greatly influence the phenotype of mesenchymal stromal cells[12,15]. To evaluate cell- and nuclear morphology of bmMSCs and kPSCs cultured on the different topographies on the TWP, we stained the actin cytoskeleton and nucleus of the cells and we observed pronounced differences in cell and nuclear morphology both in bmMSCs and kPSCs (Figure 1B, Supplementary Figure 3). In figure 1C, an example of a surface topography on the TWP is shown, with the corresponding cell morphology of kPSCs and bmMSCs cultured on this specific topography (Figure 1D). Nuclear counting displayed little effect of different topographies on cell numbers (Figure 1E and F). However, in few cases viable cell numbers were below the lower threshold (dashed line Figure 1E and F) and to exclude an effect on cytokine and growth factor secretion caused by cell density, these wells were excluded.

Figure 1. Cell behavior on the TopoWellPlate. A) Cytokine and growth factor secretion of bmMSCs and kPSCs cultured on unpatterned "flat" culture surfaces. B) Development of the TopoWellPlate. Cells were cultured on 76 unique algorithm generated topographies in a 96 wells plate resulting in different cell (8) and nuclear (3) morphologies. C) Example of a surface topography on the TWP (#1901). D) kPSC and bmMSC cell morphology when cultured on topography 1901. E) Cell numbers of kPSCs and F) bmMSCs cultured for 48 hours on different topographies were stable. Below dashed line: excluded values based on cell number. ***p<0.001, Abbreviations: kPSC: kidney-derived perivascular stromal cell; bmMSC: bone marrow-derived mesenchymal stromal cell; FGF: fibroblast growth factor; HGF: hepatocyte growth factor; VEGF: vascular endothelial growth factor; MCP-1: monocyte chemotactic protein-1; IL: interleukin; GM-CSF: granulocyte macrophage colony-stimulation factor; IFN-y: interferon gamma; TNF-α: tumor necrosis factor alpha; SDF-1 α: stromal cell-derived factor 1 alpha; TSP2: thrombospondin-2; DIC: differential interference contrast; Br: branched; BN: bizar nuclei; EN: eccentric nuclei; IS: interesting shapes; MP: multipolar; NCM: normal cell morphology; ON: oval nuclei; P: pancake; S: stick; SB: small and branched; SP: stretched pancake. Scalebar C: 25 μm, scalebar D: 200 μm.

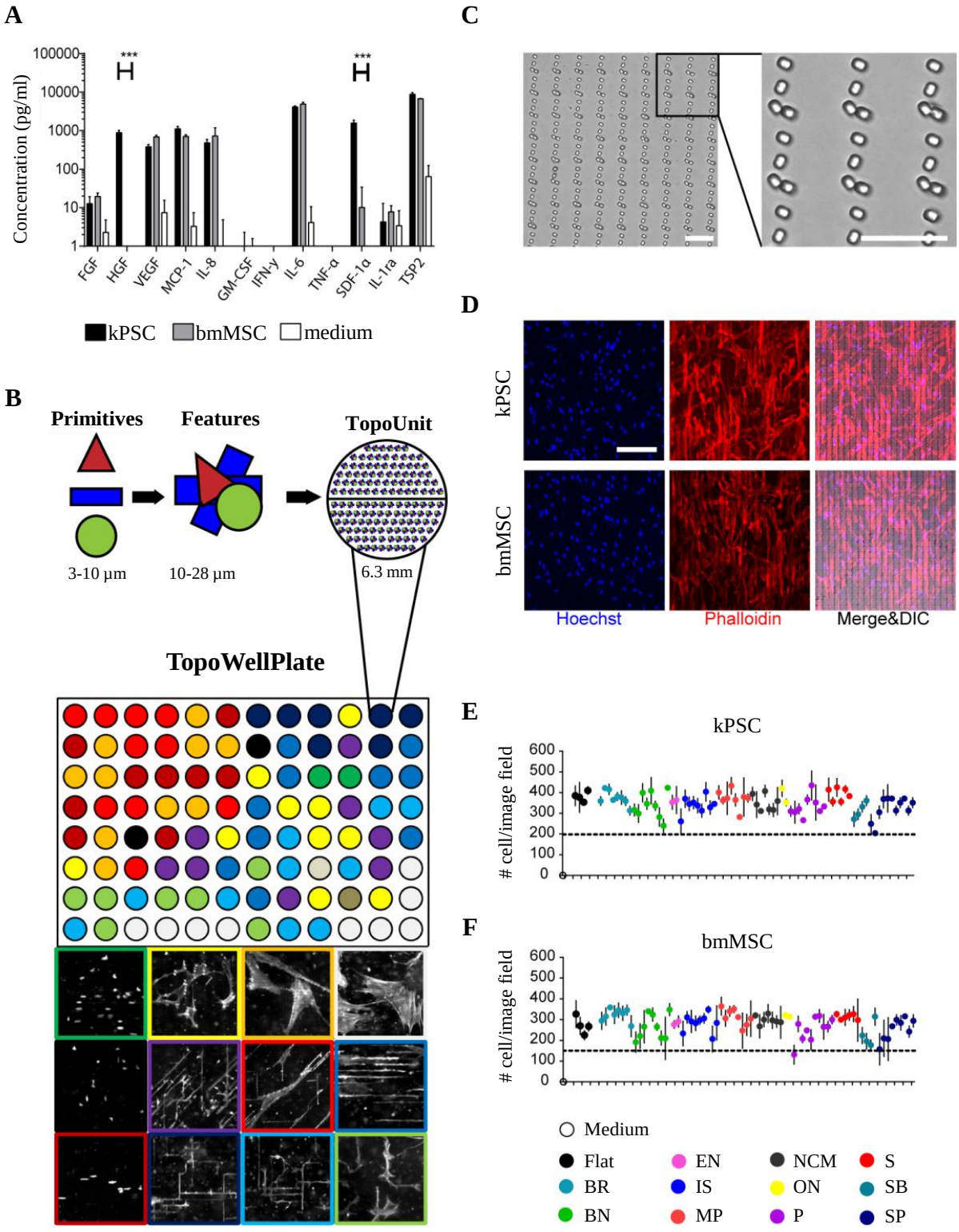

Figure 1: see description on previous page.

Cell type specific effects of topography on cytokine and growth factor secretion

When comparing the 76 different surface topographies in growth factor and cytokine expression profile, major differences can be observed between secretion levels between topographies of several growth factor and cytokine levels, such as HGF, SDF-1α and trombospondin-I while others showed a more stable secretion such as VEGF (figure 2). Importantly, the variation between the triplicates for most cytokines is low as shown by the coefficient of variation (CV) of each triplicate measurement (Figure 2). There were, however, two exceptions, FGF secreted by the kPSCs is highly variable which is due to the low secretion resulting in higher relative variability. Furthermore, we noticed a higher variability for IL-8 secreted by the bmMSCs, which can most likely be attributed to technical variation.

Figure 2: Cytokine and growth factor secretion on different culture surfaces. A) Concordance of replicas of bmMSCs as shown by the coefficient of variation (CV) of each triplicate. B) Cytokine and growth factor secretion of bmMSCs cultured on different classes of surface topographies. C) Coefficient of variation of cytokines and growth factors secreted by kPSCs. D) Cytokine and growth factor secretion of bmMSCs cultured on different classes of surface topographies. Abbreviations: kPSC: kidney-derived perivascular stromal cell; bmMSC: bone marrow-derived mesenchymal stromal cell; FGF: fibroblast growth factor; HGF: hepatocyte growth factor; VEGF: vascular endothelial growth factor; MCP-1: monocyte chemotactic protein-1; IL: interleukin; GM-CSF: granulocyte macrophage colony-stimulation factor; IFN-y: interferon gamma; TNF-α: tumor necrosis factor alpha; SDF-1 α: stromal cell-derived factor 1 alpha; TSP2: thrombospondin-2; DIC: differential interference contrast; Br: branched; BN: bizar nuclei; EN: eccentric nuclei; IS: interesting shapes; MP: multipolar; NCM: normal cell morphology; ON: oval nuclei; P: pancake; S: stick; SB: small and branched; SP: stretched pancake; CV: coefficient of variation.

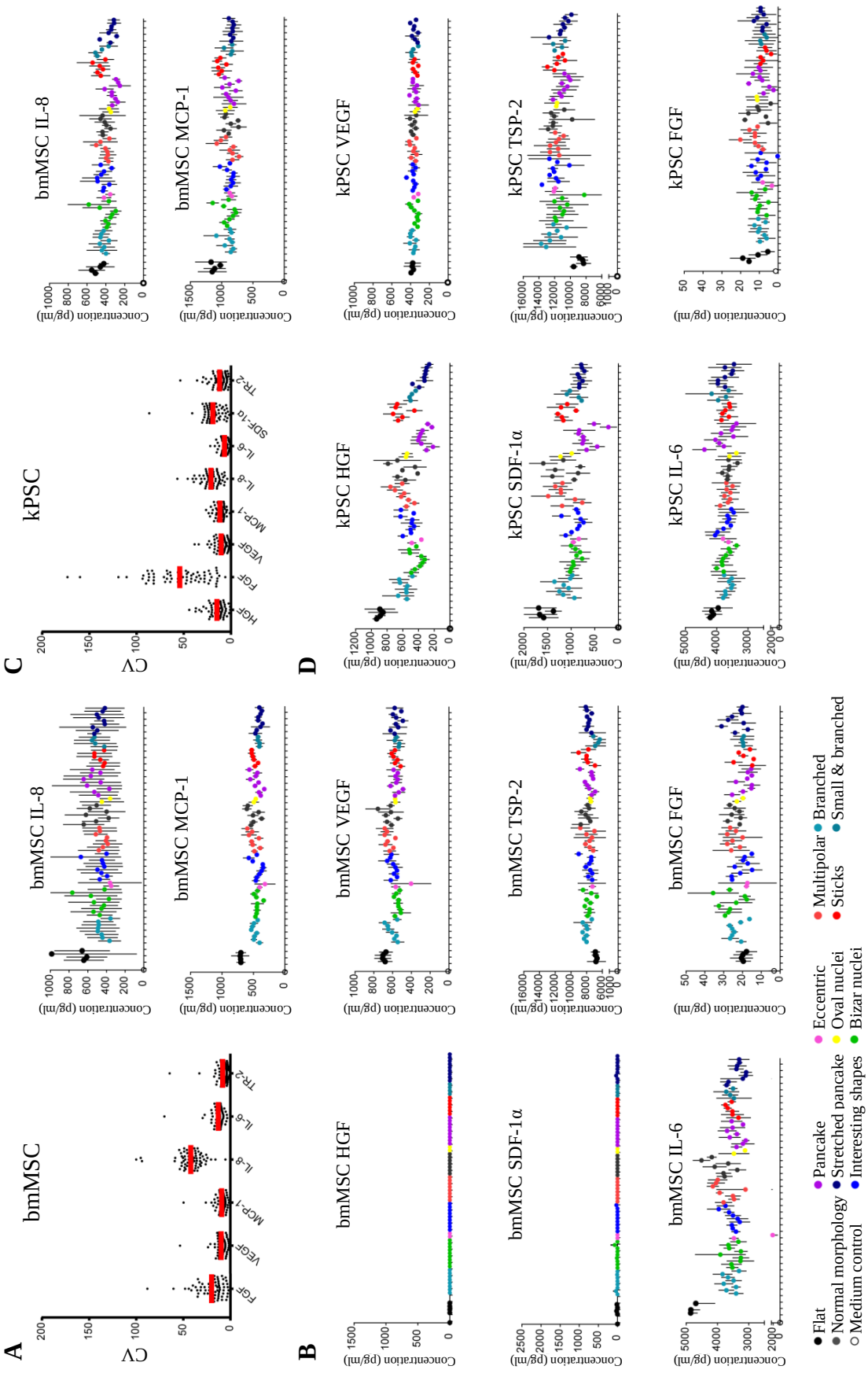

Figure 2: see description on previous page.

Similar results were obtained when secretion levels were adjusted for cell numbers (Supplementary Figure 4). Moreover, each topography resulted in a unique kPSC and bmMSC cytokine secretion profile as depicted in Figure 3A and 3B respectively. Some cytokines are secreted similarly when comparing kPSCs to bmMSCs during culture on the various topographies, but some noticeable differences were observed as well. bmMSCs cultured on topography 0365, for example, showed a 2.3 and 2.2-fold decrease in secretion of IL-6 and MCP-1 respectively compared to flat reference wells while IL-6 and MCP-1 secretion by kPSCs stayed rather stable (respectively 1.08 and 1.27). In the principal component analysis (PCA) plots, disparate secretory responses to the same defined topographies can be observed between the two organotypic stromal cell populations. Moreover, the topography induced variability in function exceeds the variability observed when such topography is compared to a flat surface as reference, underscoring the strong influence of surface structure on adaptive cell function (Supplementary Figure 5).

Stromal cell cytokine secretion is closely related to cell morphology

We analyzed whether the cytokine profiles correlated to classes of predefined adaptive cell morphology to the various topographies[15]. kPSCs with similar cell shape are enriched in cytokine profile classes (Figure 3A). For instance, when looking at the 9 different clusters, the first 2 clusters contained 15 topographies and all cells in these clusters show a similar broad and flat morphology indicated as “pancakes” or “stretched pancakes”.

Similar results were obtained with bmMSCs. When clustered based on secretion profile, 8 different clusters were defined which clustered according to specific cell shape adaptations (Figure 3B). For example, bmMSCs cultured on the 16 topographies that constitute the last two clusters, characterized by a relatively high cytokine secretion profile, have a predominance of multipolar and branched cell morphology (Figure 3B). Together, this indicates that the cytokine secretion profile of both kPSCs and bmMSCs is correlated to the morphology of the cells.

Figure 3. Unique secretome fingerprint of kPSCs and bmMSCs cultured on different topographies related to cell shape. A) Heatmap of the secretome of kPSCs cultured on the 76 different topographies and 4 references unpatterned “flat” culture surfaces, including a dendrogram of the secretome of kPSCs showing clustering into 9 different classes. This clustering according to secretome is closely related to clustering according to cell morphology. B) Heatmap of the secretome of bmMSCs, including a dendrogram of the secretome of bmMSCs showing clustering into 8 different classes which is again closely related to cell morphology. Abbreviations: kPSC: kidney-derived perivascular stromal cell; bmMSC: bone marrow-derived mesenchymal stromal cell; FGF: fibroblast growth factor; HGF: hepatocyte growth factor; VEGF: vascular endothelial growth factor; MCP-1: monocyte chemotactic protein 1; IL: interleukin; GM-CSF: granulocyte macrophage colony-stimulation factor; IFN-y: interferon gamma; TNF-α: tumor necrosis factor alpha; SDF-1 α: stromal cell-derived factor 1 alpha; TSP2: thrombospondin-2.

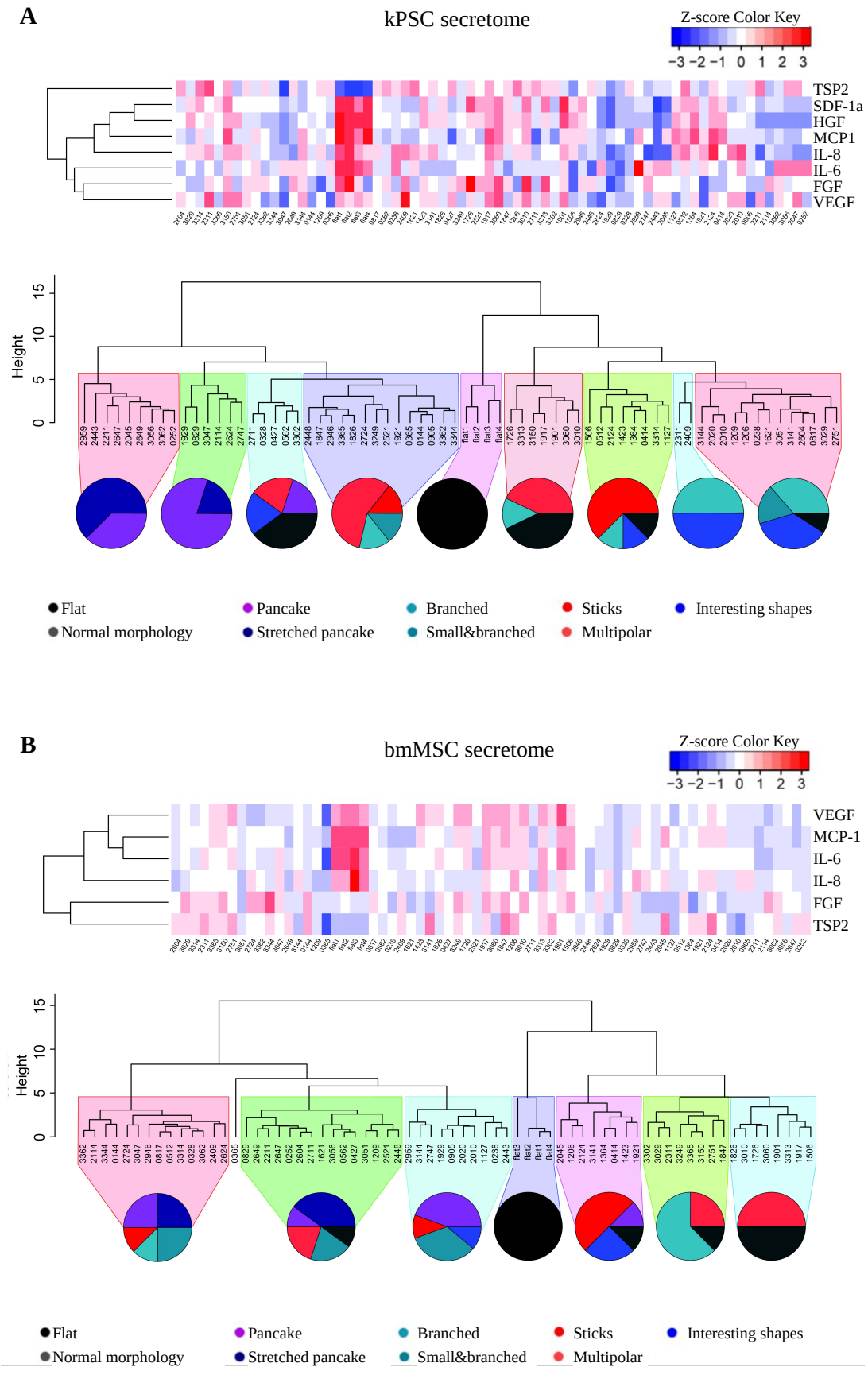

Figure 3: see description on previous page

Surface topography influences the secretion of functional important factors IL-6, SDF-1α and HGF

From a clinical perspective it is of interest to identify surface structures and cellular responses of MSCs that preserve the secretion of cytokines involved in tissue homeostasis. This is of particular relevance to the use of microcarriers in bioreactor systems for expansion of MSCs as noticeable differences could be observed in the secretion of these factors on the different topographies. This is depicted in box plots of the fold change of cytokine and growth factor secretion of both bmMSCs and kPSCs compared to controls (Figure 4A and B). For example, when bmMSCs are cultures on surface 0365 they will respond with a very elongated morphology with eccentric nuclei (Figure 4C) and a 2.3-fold decrease in IL-6 secretion, one of the effector cytokines in immune regulation by bmMSCs (Figure 4D). Similarly, specific topographies could be identified that foster the combined secretion of HGF and SDF-1α by kPSCs, two cytokines that have been implicated in kidney regeneration[9,16-18]. HGF and SDF-1α showed a strong correlation in secretion levels (Figure 4E) with a Pearson's correlation of 0.81 ($p<0.0001$). Moreover, this was also highly associated with cell shape as surface structures that resulted in a normal cell shape, long elongated small cells ("sticks") or cells with a multipolar morphology showed the highest levels of HGF and SDF1 secretion (respectively 40, 20 and 30% in the top 10 highest secretion of HGF and SDF-1 α), while broad spreading cells on top of the topographies resulted in the lowest levels ("pancakes" and "stretched pancakes", both 50% in the top 10 lowest secretion of HGF and SDF-1α) (Figure 4F).

Another noticeable difference was observed with respect to thrombospondin-2, which is expressed higher in both kPSCs and bmMSCs on most surfaces compared to flat reference surfaces. As thrombospondin-2 is a matricellular protein involved in cellular adaptation[19], this points to the active stromal cell adaptation induced by the cell surface changes.

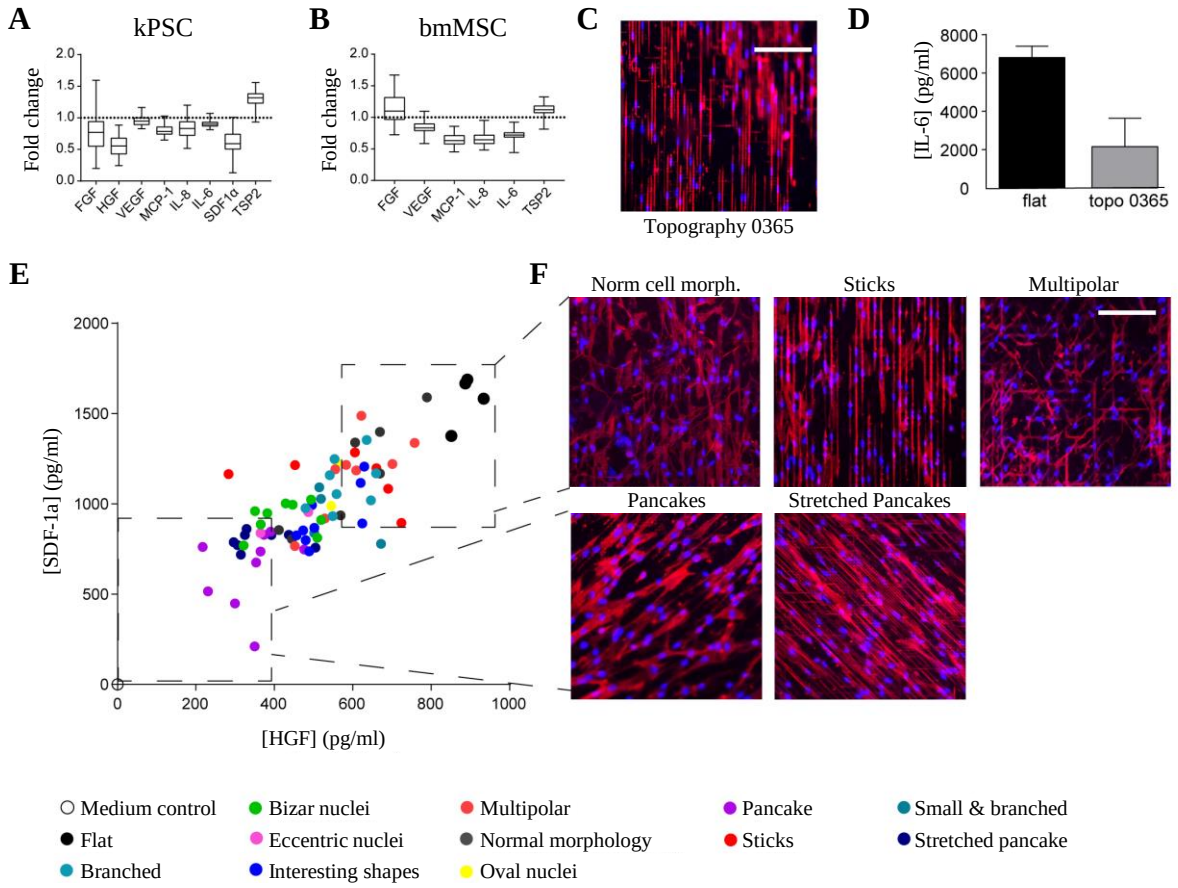

Figure 4. Surface topographies influence secretion of functional important factors. A) There is a large variation in trophic factor secretion of kPSCs on different topographies as depicted as fold change compared to reference "flat" culture surface and shown in boxplots. B) Similar variation was observed with bmMSCs C) Cell morphology of bmMSCs cultures on the topography with the largest difference in cytokine secretion D) The largest difference in secretion of trophic factors of bmMSCs was observed for IL-6. E) Correlation between HGF and SDF-1α secretion. F) Characteristic cell shapes of kPSCs on topographies with the highest and lowest secretion of HGF and SDF-1α. Scale bar 40µm. Abbreviations: kPSC: kidney-derived perivascular stromal cell; bmMSC: bone marrow-derived mesenchymal stromal cell; FGF: fibroblast growth factor; HGF: hepatocyte growth factor; VEGF: vascular endothelial growth factor; MCP-1: monocyte chemotactic protein 1; IL: interleukin; GM-CSF: granulocyte macrophage colony-stimulation factor; IFN-y: interferon gamma; TNF-α: tumor necrosis factor alpha; SDF-1 α: stromal cell-derived factor 1 alpha; TSP2: thrombospondin-2.

Discussion

In contrast to 2D *in vitro* cell culture, stromal cells normally function *in vivo* in a 3D connective tissue environment where they stretch between the different cell types and communicate via paracrine signaling[5]. While stromal cells are a diverse cell population important for tissue structure, organization and homeostasis, little is known about how changes in the microenvironmental structure influence stromal cell function in reverse. Here we show for the first time, using a novel high throughput screening platform, that changing

the microenvironment *in vitro,* specifically via surface topographies, is able to change the shape of stromal cells and influence quantitatively the cytokine secretion profile of stromal cells. Qualitative, however, organotypic, stromal cell secretory characteristics are preserved irrespective of microenvironmental surface factors. This points to a deeper imprinting of MSC function depending on the tissue, or site, of origin.

Only little data is available on the role of the microenvironment on MSC function. We and others previously demonstrated that *in vitro* culture conditions can greatly influence the cytokine expression profiles and thus their therapeutic efficacy. Treatment of bmMSCs with the small molecule dibutyryl-cAMP induced the expression of a panel of pro-osteogenic cytokines among which BMP2 and IGF1 resulting in a profound increase in *in vivo* bone formation[20,21]. Substrate stiffness can also greatly influence cell function as several cell types, including bmMSCs, showed not only different cell morphology but also different secretory profiles based on substrate elasticity[22-26]. Our current data extend these observations in that not only stiffness but also the cell shape adaptations enforced by surface morphology is an important determinant of the secretory profile of MSCs. In particular, the quantitative capacity to secrete cytokines and chemokines seemed to be directly related to these cell shape adaptations.

In line with the observation that stromal cells derived from different parts of the body show different functionality[7-9], we found cell type specific differences in cytokine and growth factor secretions between kPSCs and bmMSCs which were qualitatively preserved independent of the surface topography. Moreover, while bmMSCs cultured on specific topographies resulted in changes of cytokine secretion, no differences were observed for kPSCs cultured on these same topographies, and vice versa. These observations point to a deeper organotypic programming of MSCs that is independent of its microenvironment.

As the concentration of important factors for the homeostatic function of stromal cells, including HGF and IL-6, varied directly with topographies, our findings are of importance for the development of bioreactor culture systems. The culture surface of the carriers in these bioreactors should be designed in such a way that there is preservation of important characteristics of these cells, taking into account the cellular adaptations to the ultrastructure of the surface on which they grow.

References

1 Reinders, M. E., Leuning, D. G., de Fijter, J. W., Hoogduijn, M. J. & Rabelink, T. J. Mesenchymal Stromal Cell Therapy for Cardio Renal Disorders. *Curr Pharm Des* (2013).

2 Schepers, K. & Fibbe, W. E. Unraveling mechanisms of mesenchymal stromal cell-mediated immunomodulation through patient monitoring and product characterization. *Ann N Y Acad Sci* **1370**, 15-23, doi:10.1111/nyas.12984 (2016).

3 Carmeliet, P. & Jain, R. K. Molecular mechanisms and clinical applications of angiogenesis. *Nature* **473**, 298-307, doi:10.1038/nature10144 (2011).

4 Carrion, B., Kong, Y. P., Kaigler, D. & Putnam, A. J. Bone marrow-derived mesenchymal stem cells enhance angiogenesis via their alpha6beta1 integrin receptor. *Exp Cell Res* **319**, 2964-2976, doi:10.1016/j.yexcr.2013.09.007 (2013).

5 Leuning, D. G., Reinders, M. E., de Fijter, J. W. & Rabelink, T. J. Clinical translation of multipotent mesenchymal stromal cells in transplantation. *Semin Nephrol* **34**, 351-364, doi:10.1016/j.semnephrol.2014.06.002 (2014).

6 Doorn, J., Moll, G., Le Blanc, K., van Blitterswijk, C. & de Boer, J. Therapeutic applications of mesenchymal stromal cells: paracrine effects and potential improvements. *Tissue Eng Part B Rev* **18**, 101-115, doi:10.1089/ten.TEB.2011.0488 (2012).

7 Chen, W. C. *et al.* Human myocardial pericytes: multipotent mesodermal precursors exhibiting cardiac specificity. *Stem Cells* **33**, 557-573, doi:10.1002/stem.1868 (2015).

8 Naftali-Shani, N. *et al.* The origin of human mesenchymal stromal cells dictates their reparative properties. *J Am Heart Assoc* **2**, e000253, doi:10.1161/JAHA.113.000253 (2013).

9 Leuning, D. G. *et al.* Clinical-Grade Isolated Human Kidney Perivascular Stromal Cells as an Organotypic Cell Source for Kidney Regenerative Medicine. *Stem Cells Transl Med*, doi:10.5966/sctm.2016-0053 (2016).

10 Fernandes-Platzgummer, A., Carmelo, J. G., da Silva, C. L. & Cabral, J. M. Clinical-Grade Manufacturing of Therapeutic Human Mesenchymal Stem/Stromal Cells in Microcarrier-Based Culture Systems. *Methods Mol Biol* **1416**, 375-388, doi:10.1007/978-1-4939-3584-0_22 (2016).

11 Lam, A. T. *et al.* Biodegradable poly-epsilon-caprolactone microcarriers for efficient production of human mesenchymal stromal cells and secreted cytokines in batch and fed-batch bioreactors. *Cytotherapy* **19**, 419-432, doi:10.1016/j.jcyt.2016.11.009 (2017).

12 Unadkat, H. V. *et al.* An algorithm-based topographical biomaterials library to instruct cell fate. *Proc Natl Acad Sci U S A* **108**, 16565-16570, doi:10.1073/pnas.1109861108 (2011).

13 Hulshof, F. F. B. *et al.* Mining for osteogenic surface topographies: In silico design to in vivo osseo-integration. *Biomaterials* **137**, 49-60, doi:10.1016/j.biomaterials.2017.05.020 (2017).

14 Reimer, A. *et al.* Scalable topographies to support proliferation and Oct4 expression by human induced pluripotent stem cells. *Sci Rep* **6**, 18948, doi:10.1038/srep18948 (2016).

15 Beijer N.R.M, V. A. S. V., Pilavci B., Truckenmüller R.K., Zhao Y., Singh S. , Papenburg B., de Boer J. TopoWellPlate: A Well-Plate-Based Screening Platform to Study Cell–Surface Topography Interactions. *Advanced biosystems*, doi:10.1002/adbi.201700002 (2017).

16 Togel, F., Isaac, J., Hu, Z., Weiss, K. & Westenfelder, C. Renal SDF-1 signals mobilization and homing of CXCR4-positive cells to the kidney after ischemic injury. *Kidney Int* **67**, 1772-1784, doi:10.1111/j.1523-1755.2005.00275.x (2005).

17 Liu, Y. Hepatocyte growth factor in kidney fibrosis: therapeutic potential and mechanisms of action. *Am J Physiol Renal Physiol* **287**, F7-16, doi:10.1152/ajprenal.00451.2003 (2004).

18 Kellenberger, T., Marcussen, N., Nyengaard, J. R., Wogensen, L. & Jespersen, B. Expression of hypoxia-inducible factor-1alpha and hepatocyte growth factor in development of fibrosis in the transplanted kidney. *Transpl Int* **28**, 180-190, doi:10.1111/tri.12475 (2015).

19 Bornstein, P., Armstrong, L. C., Hankenson, K. D., Kyriakides, T. R. & Yang, Z. Thrombospondin 2, a matricellular protein with diverse functions. *Matrix Biol* **19**, 557-568 (2000).

20 Siddappa, R. *et al.* cAMP/PKA pathway activation in human mesenchymal stem cells in vitro results in robust bone formation in vivo. *Proc Natl Acad Sci U S A* **105**, 7281-7286, doi:10.1073/pnas.0711190105 (2008).

21 Doorn, J. *et al.* Pro-osteogenic trophic effects by PKA activation in human mesenchymal stromal cells. *Biomaterials* **32**, 6089-6098, doi:10.1016/j.biomaterials.2011.05.010 (2011).

22 Seib, F. P., Prewitz, M., Werner, C. & Bornhauser, M. Matrix elasticity regulates the secretory profile of human bone marrow-derived multipotent mesenchymal stromal cells (MSCs). *Biochem Biophys Res Commun* **389**, 663-667, doi:10.1016/j.bbrc.2009.09.051 (2009).

23 Zhou, S. B., Wang, J., Chiang, C. A., Sheng, L. L. & Li, Q. F. Mechanical stretch upregulates SDF-1alpha in skin tissue and induces migration of circulating bone marrow-derived stem cells into the expanded skin. *Stem Cells* **31**, 2703-2713, doi:10.1002/stem.1479 (2013).

24 Wang, D. L. *et al.* Mechanical strain induces monocyte chemotactic protein-1 gene expression in endothelial cells. Effects of mechanical strain on monocyte adhesion to endothelial cells. *Circ Res* **77**, 294-302 (1995).

25 Quinn, T. P., Schlueter, M., Soifer, S. J. & Gutierrez, J. A. Cyclic mechanical stretch induces VEGF and FGF-2 expression in pulmonary vascular smooth muscle cells. *Am J Physiol Lung Cell Mol Physiol* **282**, L897-903, doi:10.1152/ajplung.00044.2001 (2002).

26 Mammoto, A. *et al.* A mechanosensitive transcriptional mechanism that controls angiogenesis. *Nature* **457**, 1103-1108, doi:10.1038/nature07765 (2009).

27 Zhao, Y. *et al.* High-definition micropatterning method for hard, stiff and brittle polymers. *Mater Sci Eng C Mater Biol Appl* **71**, 558-564, doi:10.1016/j.msec.2016.11.004 (2017).

28 Core-team, R. A Language and environment for statistical Computing. *R Foundation for Statistical Computing* (2014).

29 Maechler, M. R., P.; Struyf A., Huberts, M. Hornik, K. . Cluster: Cluster Analysis Basics and Extensions. (2017).

30 Wickham, H. ggplot2: Elegant Graphics for Data Analysis. *Springer-Verslag* (2009).

Supplementary data

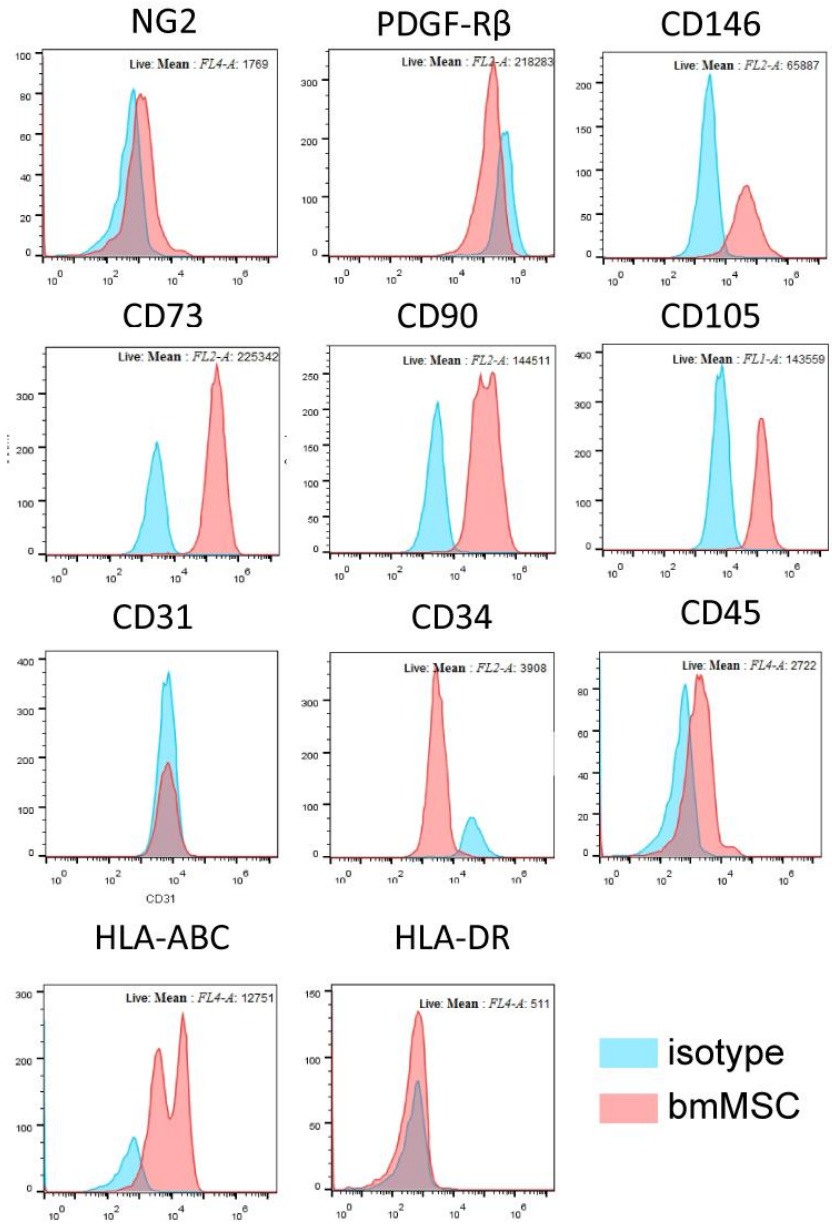

Supplementary Figure 1. Marker expression of bmMSCs as analysed by flow cytometry. These cells are positive for the pericytic markers NG2, PDGFR-β and CD146 and the MSC markers CD73, CD90 and CD105 while being negative for CD31, CD34, CD45. Cells expressed type I HLA (HLA-ABC) and are negative for type II HLA (HLA-DR). Blue: isotype control, orange: bmMSC.

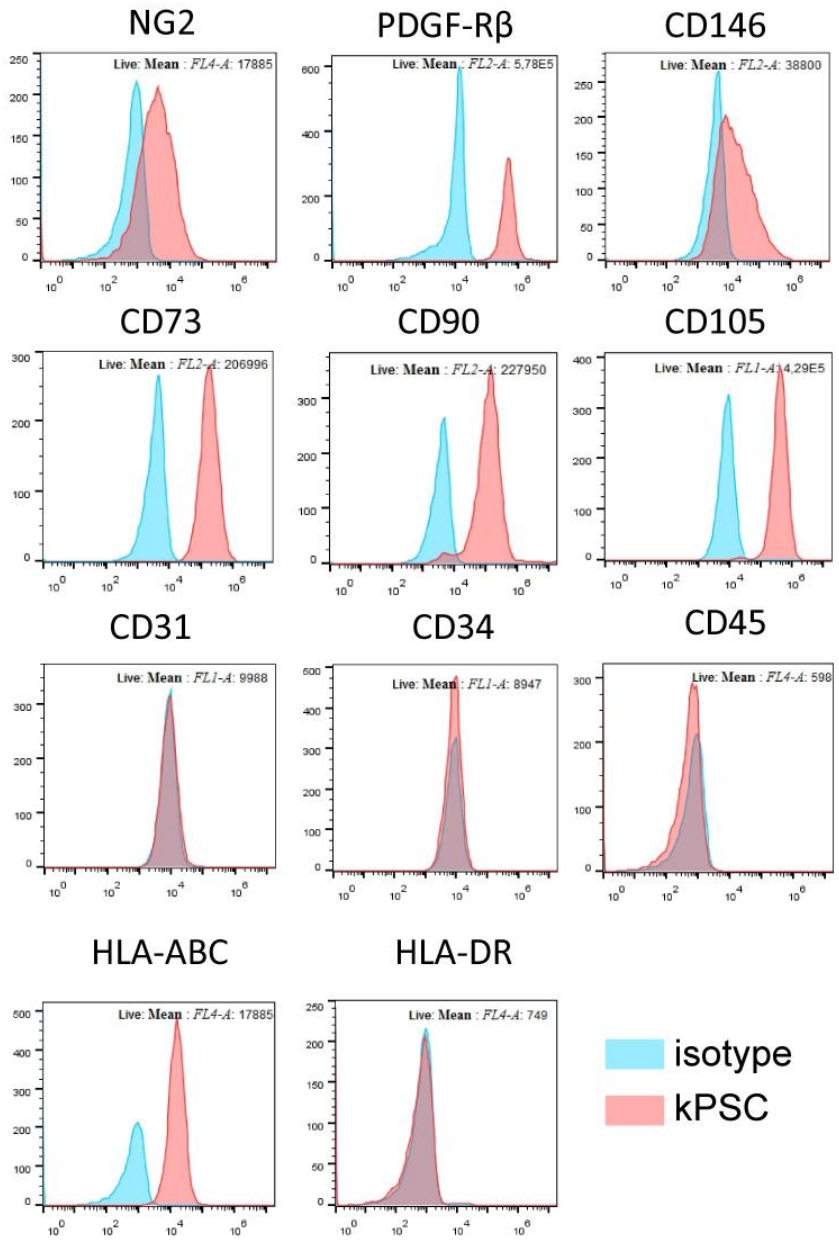

Supplementary Figure 2. Marker expression of kPSCs as analysed by flow cytometry. These cells are positive for the pericytic markers NG2, PDGFR-β and CD146 and the MSC markers CD73, CD90 and CD105 while being negative for CD31, CD34, CD45. hkPSCs express type I HLA (HLA-ABC) and are negative for type II HLA (HLA-DR). Blue: isotype control, orange: kPSC.

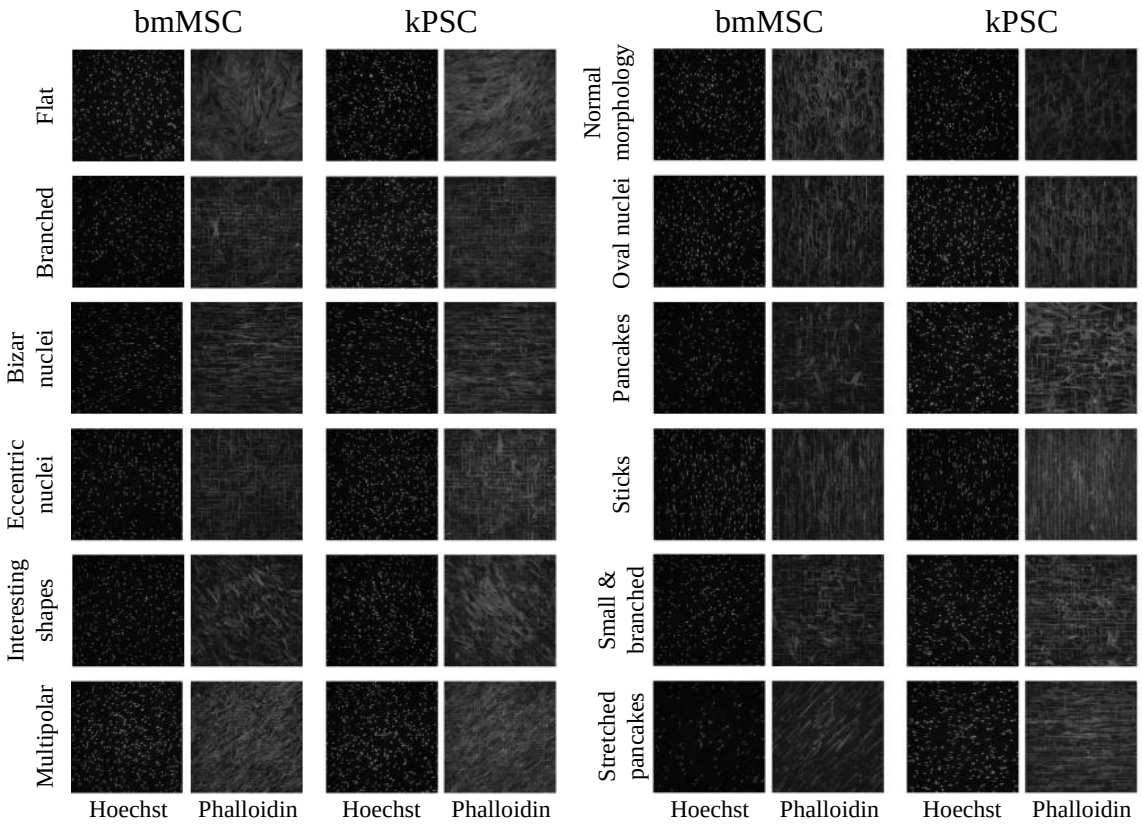

Supplementary Figure 3. Cell and nuclear morphology of both bmMSCs (left panels) and kPSCs (right panels) cultured on different classed of surface topographies.

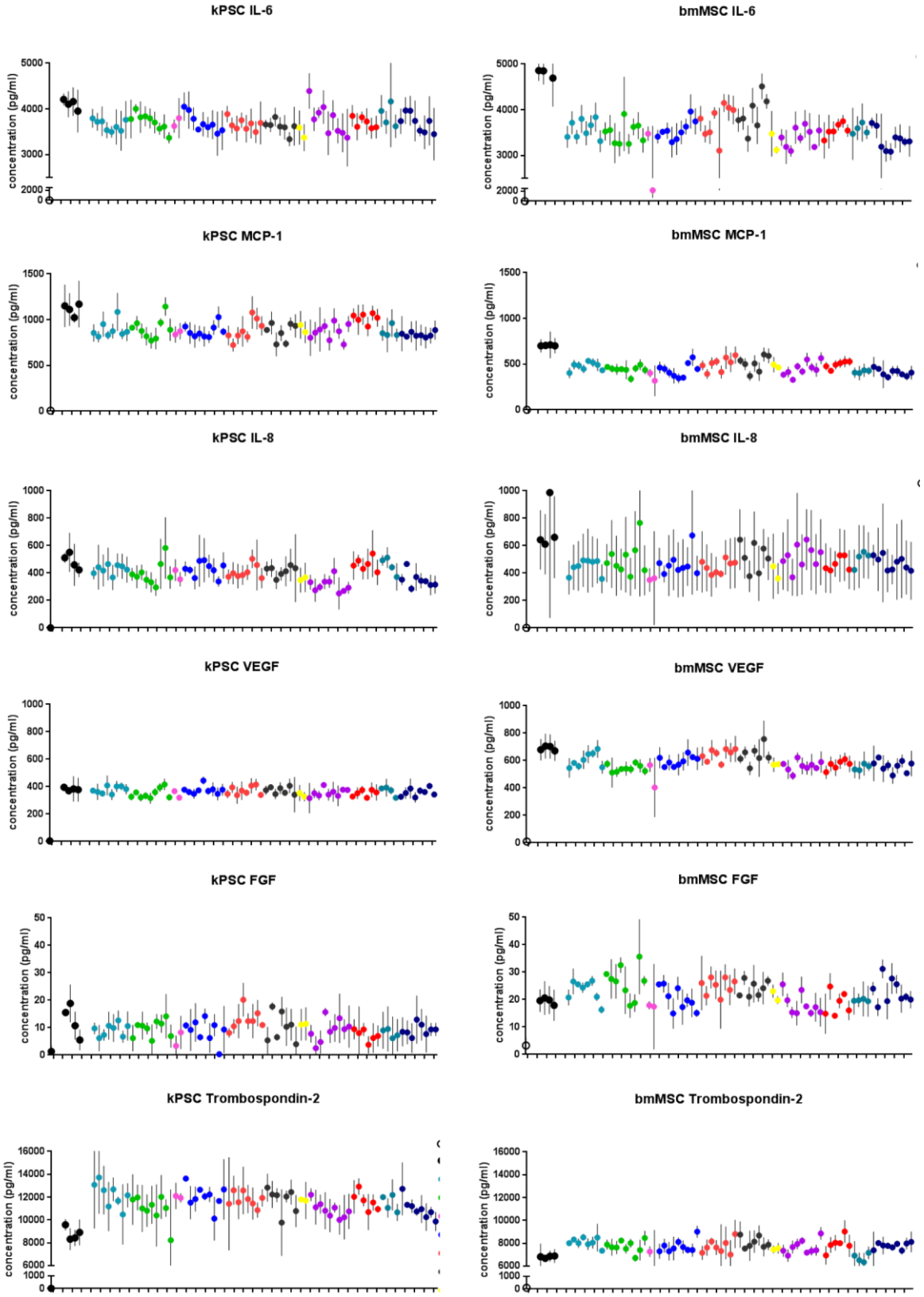

Supplementary Figure 4. Cytokine and growth factor secretion of bmMSCs and kPSCs cultured on different classes of surface topographies adjusted for cell numbers.

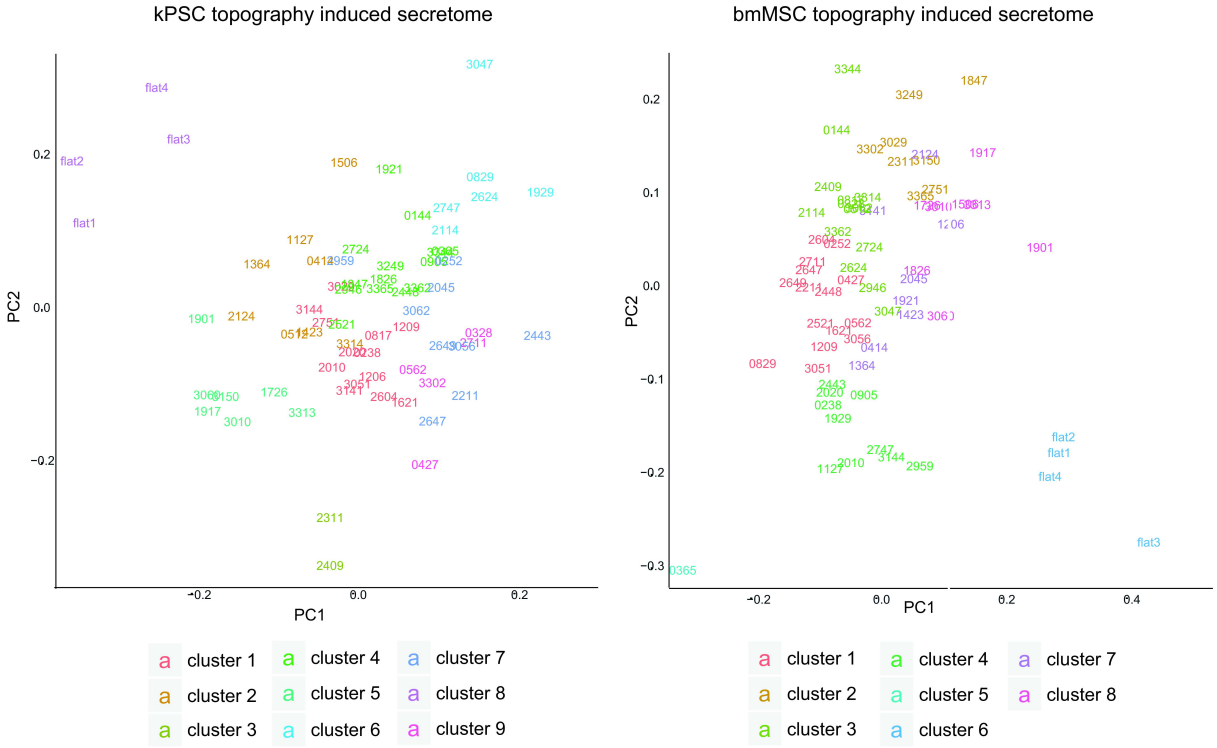

Supplementary Figure 5. Principal Component Analysis (PCA) of kPSCs and bmMSCs cultured on 76 unique surface topographies. Colors respresent the clustering of secretome fingerprints as stated in figure 3.

⠠⠞⠓⠑ ⠠⠟⠥⠊⠉⠅ ⠃⠗⠕⠺⠝ ⠋⠭ ⠚⠥⠍⠏⠎ ⠕⠧⠑⠗ ⠞⠓⠑ ⠇⠁⠵⠽ ⠙⠕⠛

Chapter 7

The NanoTopoChip:
high-throughput nanotopographical cell instruction

Frits F.B. Hulshof[1,2], Yiping Zhao[3], Aliaksei S. Vasilevich[2], **Nick R.M. Beijer**[2], Meint de Boer[4], Bernke J. Papenburg[3], Clemens van Blitterswijk[5], Dimitrios Stamatialis[1] & Jan de Boer[2]

Published in: Acta Biomaterialia (2017)

[1] (Bio)artificial Organs, Department of Biomaterials Science and Technology, MIRA Institute for Biomedical Technology and Technical Medicine, University of Twente, Enschede, the Netherlands. [2] Department of Cell Biology Inspired Tissue Engineering, MERLN Institute for Technology-Inspired Regenerative Medicine, Maastricht University, the Netherlands. [3] Materiomics BV, Maastricht, the Netherlands. [4] MESA+ Institute for Nanotechnology, University of Twente, Enschede, the Netherlands. [5] Department of Complex Tissue Regeneration, MERLN Institute for Technology-Inspired Regenerative Medicine, Maastricht University, the Netherlands.

Abstract

Surface topography is able to influence cell phenotype in numerous ways and offers opportunities to manipulate cells and tissues. In this work, we develop the NanoTopoChip and study the cell instructive effects of nanoscale topographies. A combination of deep UV projection lithography and conventional lithography was used to fabricate a library of more than 1200 different defined nanotopographies. To illustrate the cell instructive effects of nanotopography, actin-RFP labeled U2OS osteosarcoma cells were cultured and imaged on the NanoTopoChip. Automated image analysis shows that of many cell morphological parameters, cell spreading, cell orientation and actin morphology are mostly affected by the nanotopographies. Additionally, by using modeling, the changes of cell morphological parameters could by predicted by several feature shape parameters such as lateral size and spacing. This work overcomes the technological challenges of fabricating high quality defined nanoscale features on unprecedented large surface areas of a material relevant for tissue culture such as polystyrene and the screening system is able to infer nanotopography – cell morphological parameter relationships. Our screening platform provides opportunities to identify and study the effect of nanotopography with beneficial properties for the culture of various cell types.

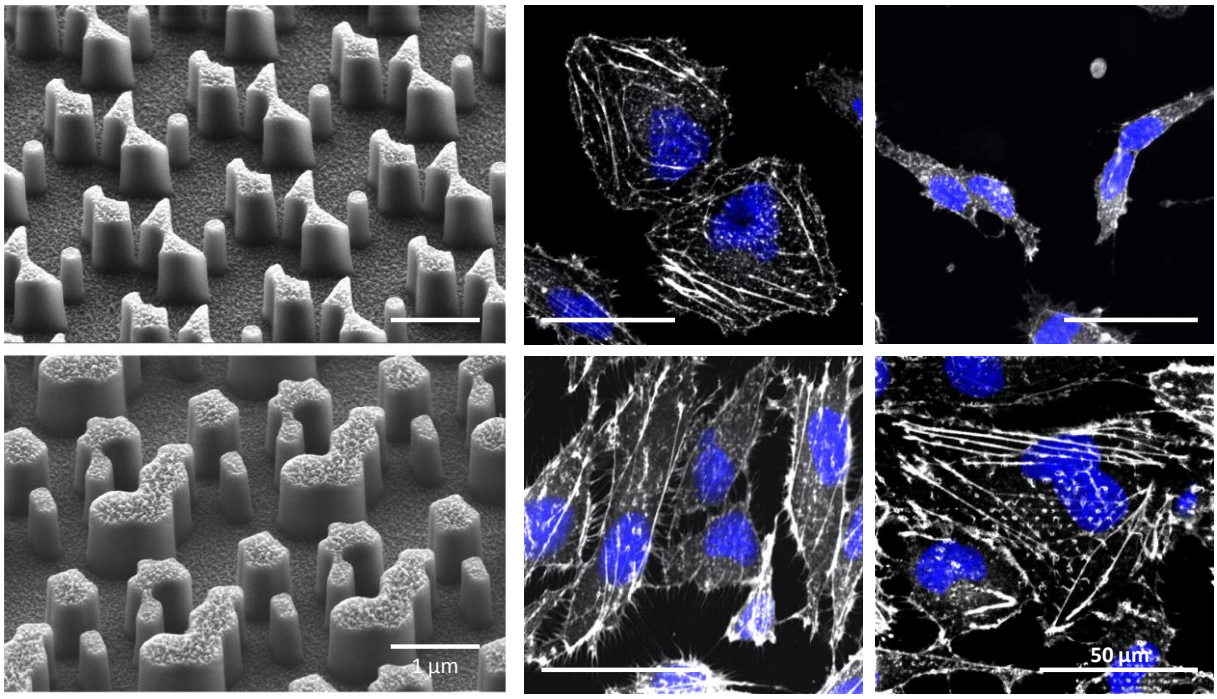

Introduction

Cells are known to respond to topographical cues of the substrate they come into contact with. Therefore, design of surface topography can be a strategy to influence the response of cells and tissues to biomaterials. Understanding the underlying mechanisms of cell-topography interactions and applying them for biomaterial design is valuable not only to improve in vitro culture systems[1], but also to improve the interaction of biomedical devices with the human body[2]. Micrometer scale topography can strongly affect cellular and nuclear morphology. It can have a strong effect on cell adhesion, the organization of the (nucleo)cytoskeletal system and on fundamental aspects of cell physiology such as differentiation, proliferation, pluripotency and motility[3]. Nanoscale topographies are in the size range of filopodia, focal adhesions, lipid rafts, endocytic vesicles and extracellular matrix fibers and may thus affect very different molecular mechanisms than microscale topographies. Molecular events affected are the spacing and clustering of transmembrane adhesion proteins such as integrins that are part of focal adhesion signaling complexe[4,5]. This is also supported by the fact that nanotopography affects downstream signaling events such as activation of the integrin-linked kinase/β-catenin pathway[6]. Cells are aligned through the spacing and alignment of focal adhesions by nanoscale wrinkled surfaces[7]. Further downstream, nanotopographies affect cell migration[8], proliferation[9], and differentiation[10,11]. Additionally, nanotopography can enhance extracellular matrix (ECM) production and may also affect the ECM architecture[12]. Furthermore, there are strong indications that nanotopography plays a role in vivo, for example: the surface structure of the basement membrane that interacts with epithelial cell layers[13].

The ability of exact shape design offered by lithographic techniques provides a more precise control over the dimensions of microscale topographies in comparison to non-lithographic techniques such as sand blasting, acid etching[14], and polymer phase separation[15]. Although this exact control over the dimensions of the surface topography improved the manipulation of aspects of cell morphology, the correlation between cell shape and cell phenotype is largely unknown. Therefore we and others have employed screening approaches to learn about the relationship between topographical design and cellular response[16,17]. We previously created the TopoChip high throughput screening platform[18], which allows simultaneous screening of thousands of randomly generated microtopographies. This “micro-TopoChip” contains topographies with height of 10 µm and lateral dimensions that range between 5 µm and 30 µm. We have shown that these topographies have significant effects on hMSC differentiation[18] and can maintain pluripotency of induced pluripotent stem cells.[1] Additionally the screening systems can be used to infer topography design – cell morphology/differentiation relationships[19].

In this work we aim to expand the high-throughput screening system with designed nanoscale topographies, which allows investigation of a library of nanoscale topographies and to tap into a new array of cellular mechanisms to influence cell fate. Systematic investigation of cell

response requires larger substrate areas to be able to measure enough cells to perform statistical analyzes on subtle changes. To fabricate such nanotopographies for biological studies, high resolution beam writing techniques such as e-beam or ion-beam lithography are often used, because standard photolithography cannot reach the required resolutions. However, compared to lithography, beam writing has long writing times covering large areas of multiple squared centimeters, which lowers the throughput. This severely limits the realistic area size, which can be patterned by these techniques. Advanced lithographic techniques such as Deep UV (DUV) and extreme UV (EUV) lithography are more suitable for the nanopatterning of large areas. While these techniques are being employed in the semi-conductor industry, they are usually not easily accessible by academic institutions due to their complexity and resulting high cost[20]. Here, to create the NanoTopoChip, we use conventional UV lithography and DUV lithography in combination with a custom designed DRIE process to fabricate moulds for nano imprint lithography (NIL). Its design is made by computational pattern generation similar to the micro-TopoChip generation algorithm[18]. After successful production of the NanoTopoChip, we first compare the effects of micro and nanotopography on U2OS osteosarcoma cells. Subsequently, we use bioinformatics tools to identify which cell morphological parameters are affected by the nanotopographies. Finally, the links between surface topography design and cell morphological parameters are investigated by predictive modeling to understand how feature dimensions affect cell morphology.

Materials and methods

NanoTopoChip design

Similar to the design of the micro-TopoChip[18], a custom C++ script is used to randomly select 1246 unique topographies from an in silico library of with a theoretical design space of millions of topographies that was generated by combining the primitive shapes triangle, rectangle and circle. A feature was generated by first randomly selecting parameter values for its size, the number of primitives to be used and the distribution over the different primitive types, the size of the primitives, and the degree to which the primitives were to be aligned. The parameter values were selected within the ranges that are shown in the Supplementary Table 1. Next, each primitive was placed at a random position inside the feature. Overlapping of primitives was also allowed. This random combination of the geometrical characteristics of the primitive shapes, such as sharp corners from triangles and rounded edges from circles, theoretically allows the generation of any shape. The script creates a Clewin image file, which was applied on a photomask. The resulting NanoTopoChip contains a surface of 20 × 20 mm with 1246 unique topography designs in duplicate in individual test surfaces of 390 × 390 µm called TopoUnits, each separated by 30 µm high, 10 µm wide walls in a 50 × 50 µm grid. The nano features within each TopoUnit are comprised of primitives of lines, circles and triangles

have minimum and maximum lateral dimensions of 200 nm and 700 nm. Nano features with random shapes are generated with lateral dimensions ranging from 200 nm to 1000 nm.

NanoTopoChip silicon master-mould fabrication

Supplementary Figure 1 illustrates the Silicon NanoTopoChip fabrication process. Due to the difference of wafer size compatibility between different lithography instruments, the 76 mm diameter Si wafers were attached to the 100 mm diameter Si wafers using Fomblin oil during plasma etching processes. Double side polished, [100] oriented, 76 mm diameter Si wafers were used as obtained (Supplementary Figure 1A). A bottom anti reflective coating (BARC) layer of 38 nm, a DUV resist layer of 225 nm, and a top anti reflective coating (TARC) layer of 90 nm were subsequently spin-coated and baked on the Si wafers (Supplementary Figure 1B). The exposure was performed by an ASML PAS5500/1100B 100 nm ArF scanner using the conventional exposure mode. After exposure, the resist layer was developed and the TARC layer was removed during development. Detailed information about lithography materials, wafer preparation and exposure settings are proprietary information of ASML (Supplementary Figure 1C). Next, the BARC layer was etched using mixed directional ion etching (DRIE, Alcatel AMS100SE Deep RIE system) by CHF3 and Ar flow of 50 sccm respectively, automatic pressure control (APC) of 100%, inductively coupled plasma (ICP) power of 700 W, capacitively coupled plasma (CCP) power of 20 W with pulsed low frequency of 80/20 (on/off) milliseconds and electrode temperature of -20 °C. The etch rate of BARC was approximately 60 nm/min, and therefore the 38 nm BARC was removed in 45 seconds (Supplementary Figure 1D). Si etching was performed using a nano Bosch DRIE (Alcatel AMS100SE Deep RIE system) by SF6 (etching) and C_4F_8 (passivation) flow of 50 sccm respectively and cycle times of 1.5 s and 0.5 seconds respectively. Other settings were kept the same for both gases: APC of 100% ICP power of 1000 W, CCP power of 30 W with pulsed low frequency of 10/90 (on/off) milliseconds and electrode temperature of -40 °C. The etch rates of silicon and resist are approximately 200 nm/min and 50 nm/min respectively (Supplementary Figure 1E). Resist and BARC layers are stripped in O_2 plasma (Tepla 300), followed by Piranha cleaning for 15 min (H_2SO_4:H_2O_2 = 3:1, v/v, 96 °C). A fluorocarbon (CF) removal step was performed by first dry oxidizing the wafers at 800°C for 30 min followed by oxide removal in 50% HF for 1 min (Supplementary Figure 1F). After standard cleaning (fumic HNO_3) for 10 min, and 69% HNO_3 at 96 °C for 10 min and native oxide removal 1% HF for 1 min, the wafers were prepared with 600 nm low pressure chemical vapor deposition (LPCVD) TEOS (silicon oxide formed by decomposing Tetra-Ethyl-Ortho-Silicate) followed by annealing at 1150 °C in nitrogen environment for 3 hours (Supplementary Figure 1G). Adhesion promoter Hexamethyldisilane (HMDS) (Merck) and positive photo resist Olin 908-12 (Arch Chemicals) was spin-coated on the wafers (Supplementary Figure 1H). A chromium mask, created by laser beam pattern generation with a Heidelberg DWL 200, containing 400 µm × 400 µm grids of 10 µm wide was used and the

exposure was performed using conventional UV lithography (EVG 620) (Supplementary Figure 1I). Pattern transfer from photoresist to annealed TEOS layer was performed by mixed DRIE (Alcatel AMS100DE Deep RIE system) using C_4F_8, He and CH_4 flow of 20 sccm, 150 sccm and 15 sccm respectively, pressure of 8.5 mbar, ICP power of 2800 W, CCP power of 350 W and electrode temperature of -10 °C. The etch rates of the annealed TEOS and photoresist were approximately 500 nm/min and 50 nm/min respectively (Supplementary Figure 1J). After photoresist removal using O_2 plasma and Piranha cleaning (as described in step 6), silicon grids were etched using Alcatel AMS100 SE Deep RIE system by SF6 and O_2 flow of 100 sccm and 40 sccm respectively, ICP power of 1000 W, CCP of 20 W with pulsed low frequency of 20/80 (on/off) milliseconds and electrode temperature of -110 °C (Supplementary Figure 1K). The etch rates of Si was approximately 4.5 µm/min. In the final step, the annealed TEOS layer was removed by etching in 50% HF for 1 min (Supplementary Figure 1L).

Ormostamp® mould fabrication

Supplementary Figure 2 depicts the method to fabricate the OrmoStamp® mould. The silicon master mould was replicated into Ormostamp moulds in two replication steps. OrmoStamp® (Micro Resist Technology GmbH, Germany) is a UV curable inorganic-organic hybrid polymer and OrmoPrime®08 (Micro Resist Technology GmbH, Germany) is the adhesion promoter for OrmoStamp®. Detailed information about these two polymers can be found in the manufacturer's processing protocols. Borofloat wafers (Borofloat® 33 from Schott) of 100 mm diameter and 500 µm thickness were used. After Piranha cleaning and dehydration baking on a hot plate at 120 °C for a minimum of 10 min, OrmoPrime®08 was spin-coated on the Borofloat wafer at 4000 rpm for 30 seconds and then baked on a hot plate at 150 °C for 5 min. In our experiments, a Borofloat wafer with OrmoPrime®08 was prepared right before the application of OrmoStamp® (Supplementary Figure 2A). A droplet of 1.5 mL OrmoStamp® was slowly dispensed on the Si master mould and was slowly brought into contact with the Borofloat wafer with OrmoPrime®08 coating. Slow spreading of the droplet between the Borofloat wafer and Si mould was required to avoid air bubbles getting trapped (Supplementary Figure 2B). The gap between the two substrates was completely filled by capillary force, which takes about 15–30 min (Supplementary Figure 2C). The Si and Borofloat wafer stack was exposed to 350–450 nm UV light for 90 seconds with the light intensity set at 12 W/cm^2 (EVG 620 i-line exposure system) (Supplementary Figure 2D). The Si mould could easily be peeled off from the OrmoStamp® mould, after which the OrmoStamp® mould immediately followed a hard bake process at 130 °C on a hot plate (ramping up from 20 °C to 130 °C with a ramping speed of 5 °C/min). After hard baking for 30 min at 130 °C, this negative OrmoStamp® mould was cooled down together with the hot plate to room temperature (Supplementary Figure 2E). Before the second replication step, the OrmoStamp® mould received a gentle O_2-plasma treatment by reactive ion etching (RIE,

home-build) at 10 °C, 50 sccm O2 flow, 75 mTorr pressure, and 50W CCP power for 30 seconds. After this a monolayer of fluoroctatrichlorosilane (FOTS) was deposited from gas phase under vacuum condition in a desiccator. For the second replication step another borofloat wafer was coated with OrmoPrime®08 (Supplementary Figure 2F). As before, a droplet of 1.5 mL OrmoStamp® was slowly dispensed on the negative OrmoStamp® mould and is slowly brought into contact with the Borofloat wafer with OrmoPrime®08 coating (Supplementary Figure 2G). Again, the gap between the two substrates was filled by capillary force (Supplementary Figure 2H). The wafer stack was exposed to UV light (Supplementary Figure 2I) after which the negative OrmoStamp® mould could easily be peeled off from the positive OrmoStamp® mould, after hardbaking (Supplementary Figure 2J).

Polymer NanoTopoChip fabrication

To prepare the OrmoStamp® mould for hot embossing, a gentle O_2-plasma treatment was performed using reactive ion etching (RIE, home-build) at 10 °C, 50 sccm O2 flow, 75 mTorr pressure, and 50W CCP power for 30 seconds. A monolayer of FOTS was deposited from gas phase under vacuum condition in a desiccator (Supplementary Figure 2K). Commercially available bi-axially oriented polystyrene (PS) films of 190 µm (Goodfellow, United Kingdom) were used for hot embossing. PS hot embossing process was performed using the Obducat Eitre®6 Nano Imprint Lithography system (Obducat, Sweden). The PS film and OrmoStamp® mould were brought into contact (Supplementary Figure 2L) and the hot embossing was performed at a temperature of 140 °C and a pressure of 10 bar for 5 min (Supplementary Figure 2M). Finally, the PS film was separated from the OrmoStamp® mould at 90 °C (Supplementary Figure 2N). The NanoTopoChips were treated with a mild oxygen plasma before cell culture (the SEM images of the NanoTopoChip were made after this treatment to make sure the nanotopographies were still intact). The Ormostamp moulds® could be used 3 times for hot embossing after which a deterioration of feature and wall quality was observed.

SEM imaging

The moulds and NanoTopoChips were imaged with a Zeiss Merlin HR-SEM. Because the images where taken at an angle of 45° and some of the features are circles, the height (vertical dimensions) of the pillars was inferred with a correction factor, instead of being measured from cross sections. The correction factor was calculated by dividing the number of pixels comprising the × dimension of a circular feature by number of pixels comprising the y dimension of a circular feature. The true height of the features could be calculated by multiplying the measured height (under an angle of 45°) by the correction factor (1.33) (Supplementary Figure 3).

Cell culture and imaging

U2OS cells, stably expressing Lamin B1 BFP, αTubulin GFP and Actin RFP (U2OS LMNB1-TUBA1B-ACTB, Sigma-Alldrich) were cultured in McCoys medium (Sigma-Alldrich) with 10% FBS (Sigma-Alldrich), 100 U/ml penicillin and 100 g/ml streptomycin (Gibco). The cells were passaged according to manufacturer's protocol. In all experiments, medium was refreshed every two days. For the screening experiment, the cells were seeded at a density of 5000 cells/cm^2 on 6 NanoTopoChips with a custom built seeding device. The device consists of a culture chamber that fits two NanoTopoChips and creates a small space (500 µm height) on top of the TopoChips. The limited space immobilizes the cell suspension by capillary force to achieve homogenous cell seeding for 4 hours after which the lid is removed to allow culture in a conventional volume of medium for adequate nutrient supply and gas exchange. After 3 days of culture, the cells were washed in phosphate buffered (PBS, Sigma Aldrich) and fixated with 1% paraformaldehyde for 10 mins at 0 °C, followed by quenching with 50 mM ammonium chloride (Sigma Aldrich). Next, the cells were washed with PBS and incubated with 1: 10000 4′,6-Diamidino-2-phenylindole (Dapi, Life technologies) for 30 min. Finally the NanoTopoChips were mounted on coverslips with Mowiol 4-88 (Sigma Aldrich) after washing with PBS twice. After sample drying the chips were imaged using a Hamamatsu Nanozoomer. A complete image was generated from every NanoTopoChip, which were subsequently cut into smaller images from individual TopoUnits for each separate channel.

Data analysis

Prior to image analysis, flat-field correction and image normalization were performed as described previously[19]. Open source software Cell Profiler (CP) was used for the image analysis[21]. In order to perform the automated image analysis in CP, a robust pipeline able to recognize the different cell features was built. The Data analysis was performed using R, a programming language and software environment for statistical computing and graphics[22]. The potential mis-segmentation of cells was detected based on cell area and intensity of the nucleus. The cells were gated based on cell area and perimeter, after which the cells in the upper right quadrant were excluded from further analysis (Supplementary Figure 4). To exclude imaging artifacts that could be mistakenly recognized as nuclei, the cells were gated based on nuclei mean and integrated intensity, after which the cells in the lower left quadrant were excluded from further analysis (Supplementary Figure 5).

The cell features with the highest variation within the whole dataset where identified with a Kruskall-Wallis test. The Kruskall-Wallis test is a non-parametric rank based-based test, analogues to analysis of variance (ANOVA) (Figure 4A). For cell profiler features we took the distance weighted median[23] across all cells in TopoUnit. For the selected descriptors a rank of surfaces was created based on the distance-weighted median calculated from the

replicas. For the classification analysis, the top and bottom 100 surfaces were selected. Before training the model we used a recursive feature elimination step to identify features that were important to discriminate these two classes. To create the models we used 75% of the TopoUnits and the accuracy of the model was accessed on the remaining 25%. The models were trained with a 10-fold cross validation in the "caret" package[24]. The performance of the model was assessed by accuracy which is the match between predicted class and actual class and ROC curve.

Results

Fabrication of the NanoTopoChip

The NanoTopoChip design was created by computational pattern generation. It has an area of 20 × 20 mm and contains 2500 TopoUnits of 390 × 390 μm each, separated by 10 μm thick walls. The nanotopographies were defined using an ASML PAS5500/1100B of 100 nm ArF scanner while the wall features were defined by conventional UV lithography. Therefore, a reticle for DUV exposure and a mask for conventional UV lithography were designed. The nanotopographies within the TopoUnits are comprised of primitives of squares, triangles and circles. Considering the maximum resolution of the ASML PAS5500/1100B ArF scanner of 100 nm, the lateral dimension of the nanotopographies range from 200 nm to 1 μm. Four NanoTopoChips with a row and column spacing of 2.4 mm and 2.6 mm, respectively, were scanned on the wafer during DUV exposure. Accordingly, for the walls, grids of 20 × 20 mm area in the mask for conventional UV lithography were designed sharing the same row and column spacing. Wafers with testing features were first fabricated to test the DRIE BARC and DRIE processes. High-resolution scanning electron microscopy (SEM) images of BARC layer before and after etching are shown in Figure 1A and B.

The optimized etching processes (described in methods) were used to fabricate the Si mould which is the negative of the NanoTopoChip. The mould contains the 30 μm deep trenches (Figure 1C) to form the walls that will separate the TopoUnits and the nano-sized cavities (Figure 1D) that will form the nanotopographies. The clearly defined feature shapes are recognizable in the cavities. The silicon moulds were replicated into OrmoStamp® moulds with a two-step process described in the methods section. In summary the silicon mould is first replicated in first (positive) OrmoStamp® (Figure 1E) which is subsequently replicated into a second (negative) Ormostamp (Figure 1F). OrmoStamp® moulds enable hot-embossing of PS films to create PS NanoTopoChips. To demonstrate differences in dimensions between the features on the micro-TopoChip and the NanoTopoChip an image of the micro-TopoChip (Figure 1G) is shown below the image of the first NanoTopoChip Ormostamp® mould (Figure 1E) of the same magnification.

The second Ormostamp® mould was used to fabricate PS NanoTopoChips by hot-embossing. SEM was used for quality inspection of several topographical features of the NanoTopoChip (Figure 2). The smallest pillars have lateral dimensions of 230 nm. The large features have lateral dimensions of up to 2 µm. The features have an average height of 750 nm (standard deviation of 68 nm). Due to the hot embossing process, the relatively smaller features are usually shorter (between 650 nm and 750 nm) while the relatively large features are taller (between 750 nm and 900 nm). We did not measure any significant differences in height of features within a TopoUnit (Supplementary Figure 6). Despite the high aspect ratio of features, for example the small pillars (Figure 2A and C), the features are stable and the replication is very good without having bending or breakage due to demoulding. Sharp angles of the features (Figure 2B and D) are maintained through the replication process. The top of the features has nano-roughness similar to the non-patterned areas; this roughness is probably created by the mild oxygen plasma treatment of the NanoTopoChips that is required for adequate cell adhesion to PS. In fact, complex defined shapes are produced with high quality and reproducibility at varying densities on relatively large surface areas. Therefore, we think that the NanoTopoChip can set a new benchmark for resolution of topographies on a large biomaterial surface area, in comparison to state of the art topographies used for biomedical studies[17,25–27].

The NanoTopoChip generates distinct U2OS cell morphologies in comparison to the micro-TopoChip

To compare the effect of the topographies on cell morphology between the micro- and NanoTopoChip, we first performed an experiment with the transgenic U2OS cell line, which stably expresses Actin-RFP, cultured on the micro-TopoChip (Figure 3A). Similar to earlier observations using bone marrow-derived human mesenchymal stem cells[18], U2OS cells show a large variety of morphologies on the micro-TopoChip. The topographies mould the cells in various shapes and in some cases, align the cells into grids (Figure 3A, image 2). In many cases the actin fibers are combined into thick bundles with a clear orientation directed by the topography (Figure 3A, images 1, 2, and 3). Noteworthy are the extreme nuclear morphologies (Figure 3A, images 4 and 5) that are induced micro topographies. On the microtopographies a classic oval nuclear shape, common on standard culture plastics, is rarely encountered. In fact, the microtopographies induce strong bends in the nuclear membrane and in some cases the nucleus is forced around the features in thin curves shapes (Figure 3A, image 4).

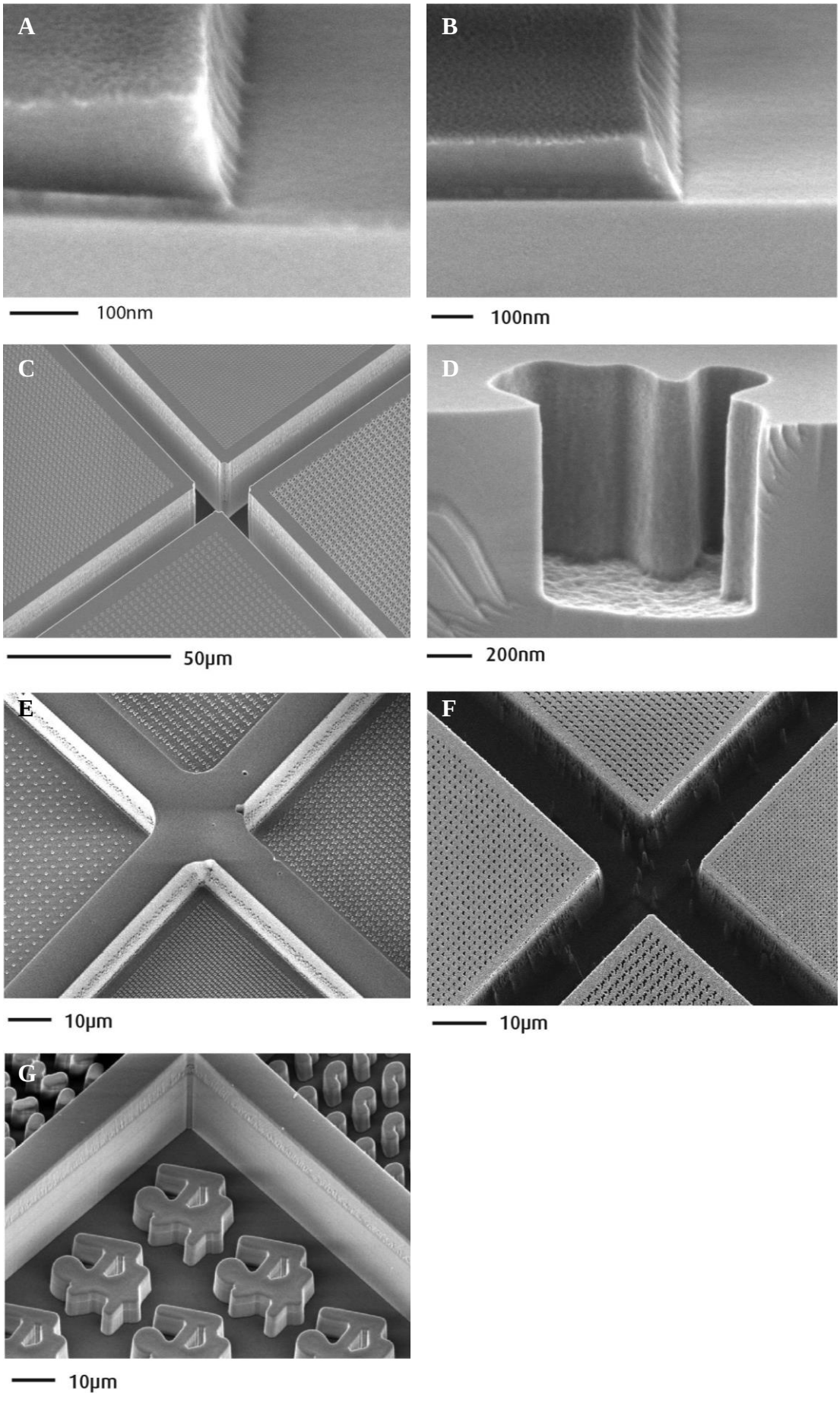
A
100nm
B
100nm
C
50µm
D
200nm
E
10µm
F
10µm
G
10µm

Figure 1. Quality control of NanoTopoChip mould fabrication steps. A) SEM images of BARC layer before etching. B) SEM images of BARC layer after etching. SEM images of NanoTopoChip fabrication result, with (C) A zoom-out image of nano features separated by 30 μm grid trenches, (D) zoom-in image of a nano feature with random contour and smooth bottom and sidewall profile, (E) S the first (positive) Ormostamp mould, (F) the second (negative) Ormostamp mould used for hot-embossing of PS to create the NanoTopoChips, and (G) a Titanium coated micro-TopoChip for size comparison to the first (positive) Ormostamp® mould with the same magnification.

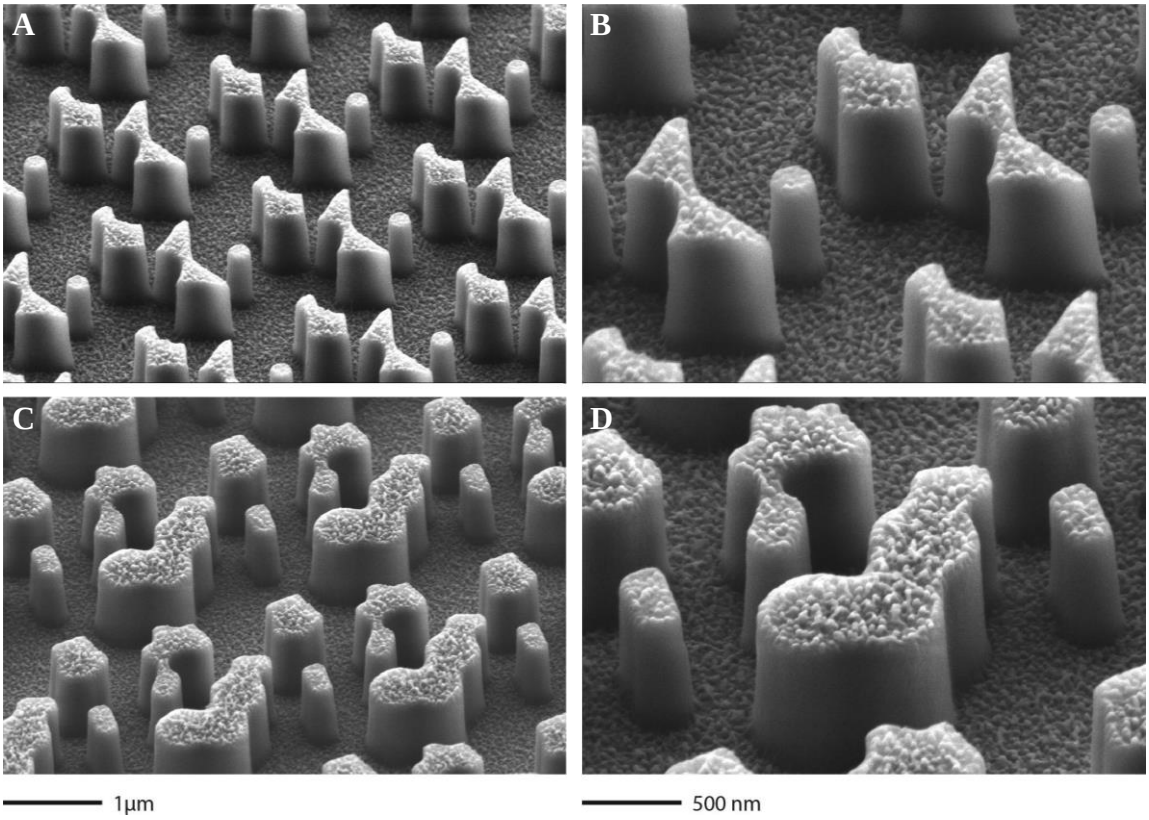

Figure 2. Quality control of PS NanoTopoChip. Two topographical features (A and B vs. C and D) were selected to demonstrate the fabrication quality of nanostructures that have various shapes and densities. (B) and (D), are higher magnification images of topographies shown in (A) and (C) respectively.

Next, to investigate the effect of nanotopography on cell morphology, U2OS cells were cultured on 6 NanoTopoChips for three days. Visual inspection of the images shows that the nanotopographies also affect U2OS morphology in various ways and that those are distinctly different from the micro-TopoChip (Figure 3B). On the NanoTopoChip, we do not observe gross differences in cellular shapes but the nanotopographies seem to affect the extent of cell spreading and the organization of the actin localization. On the nano features, the actin fibers align in various different orientations and patterns (Figure 3B, images 1, 2, and 3). Interestingly, some features induce the formation of a greater number and larger size filopodia (Figure 3B, images 4 and 5), while other nano features create very fine actin distinctly spaced actin fibers (Figure 3B, images 3 and 6). The more spread cells have very distinct punctate

patterns of actin fibers (Figure 3B, image 7), while the less spread cells tend to have more cortical actin (Figure 3B, image 4). In this initial observation, the morphology of U2OS nuclei does not seem to deviate much from the common 'classic' oval shape (Figure 3c).

To quantify the morphological effects of the nanotopographies, we analyzed the images from the 6 NanoTopoChips using a combination of bioinformatics tools. First, images in the dataset were filtered for outliers caused by events such as focus artifacts and dust particles by using a power log-log slope method (see methods), which might otherwise cause extreme mis-segmentation artifacts. The amount of cells per unit followed a normal distribution (Supplementary Figure 9) and a median of 24 cells were measured in every TopoUnit in the filtered dataset. Because a total of 6 NanoTopoChips (which each contain the topographies in duplicate) were used in the screening experiment, this resulted in more than 200 measured cells for every topography. Next, the images were segmented and parameters (Supplementary Table 2) such as cell solidity, alignment, number, size and extent were measured by CellProfiler, resulting in a dataset for analysis containing 288 (including Metadata) features for each cell. In this experiment, more than 470 thousand cells were measured on a total of 15000 TopoUnits.

The NanoTopoChip is to infer nanotopography – cell morphology relationships

To identify the cell features with the highest variation within the whole dataset, a Kruskall-Wallis test was performed on the cell morphology parameters (Figure 4A). In line with the visual observations the highest variation within the dataset is on parameters that determine cell area (Perimeter, Area, Axis Lengths, Diameter) and orientation (Orientation). When we performed the same test on nuclear morphology parameters, we noticed that only the orientation is affected by the topographies (Figure 4B), whereas there is little effect on the nuclear morphology parameters such as shape and area. This is in line with our visual inspection, which showed that the nuclear morphology not affected by the nanotopographies, especially so when compared to the effect of microtopographies.

To confirm that we can screen for biologically meaningful parameters such as cell spreading, we also quantified the median cell area for every TopoUnit (Figure 5A). The S-shaped curve shows that the cell area has a normal distribution with a minimum median size of 2460 μm^2 (17500 pixels) and a maximum median size of 4570 μm^2 (32500) pixels. The cells on the non-patterned TopoUnits (indicated by the blue dot) have a median size of 3234 μm^2 (23000 pixels), which is right in the middle of the distribution, showing that a non-patterned surface, on average, leads to a medium cell size. Representative images of small area cells and large area cells as quantified by Cell profiler is shown in Figure 5B. The actin organization is very different between the large area and small area cells. The small area cells have a large amount densely aligned thin fibers, while the large cells have shorter, thicker fibers with isotropic orientations.

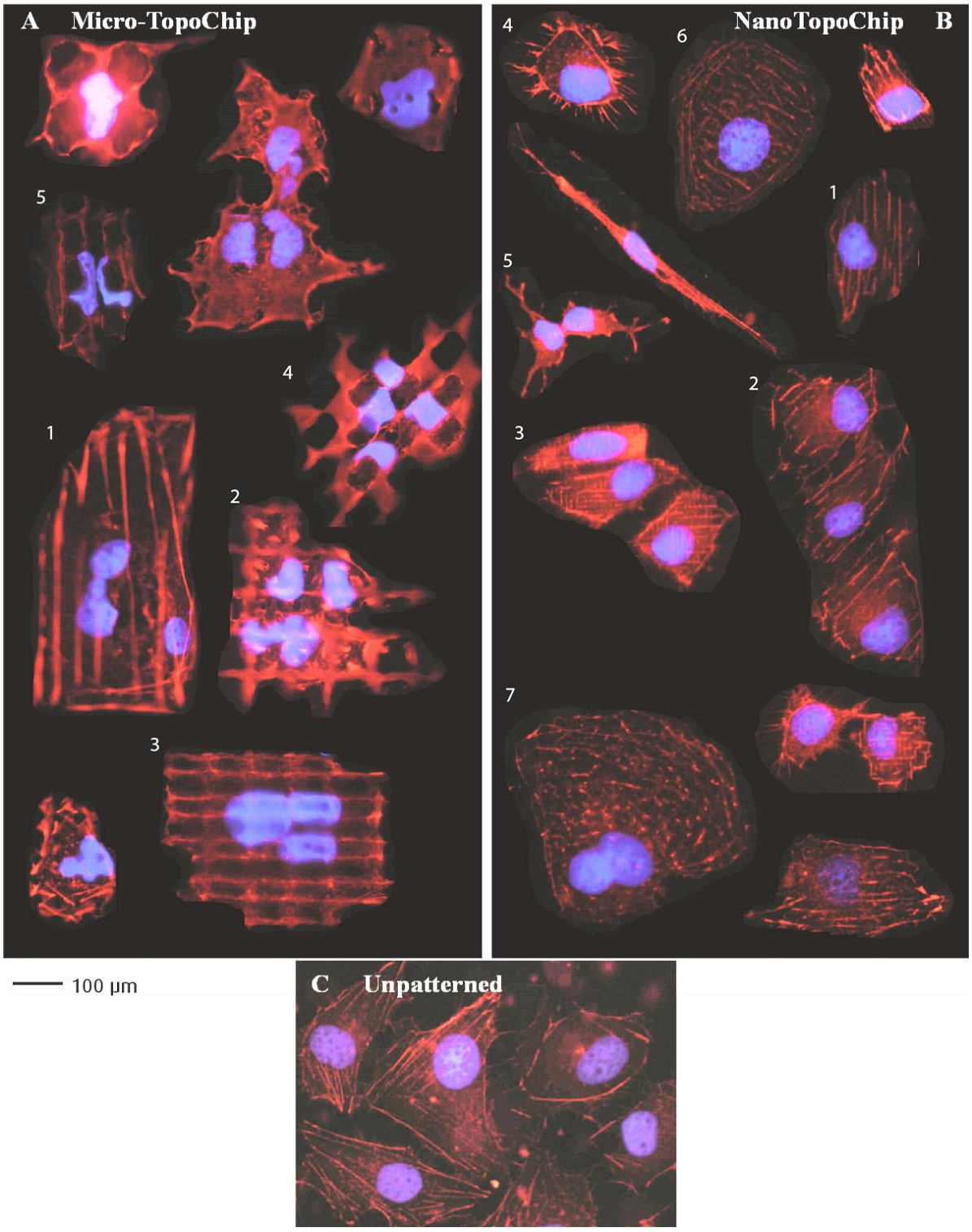

Figure 3. U2OS Cell morphology on micro- and NanoTopoChip. A) Collage of U2OS cultured on the micro-TopoChip. B) Collage of U2OS cultured on the NanoTopoChip. C) Micrograph of U2OS cultured on non-patterned surface. Actin cytoskeleton in red, nucleus in blue. Zoom-in images of these collages are shown in the Supplementary Figures 7 and 8.

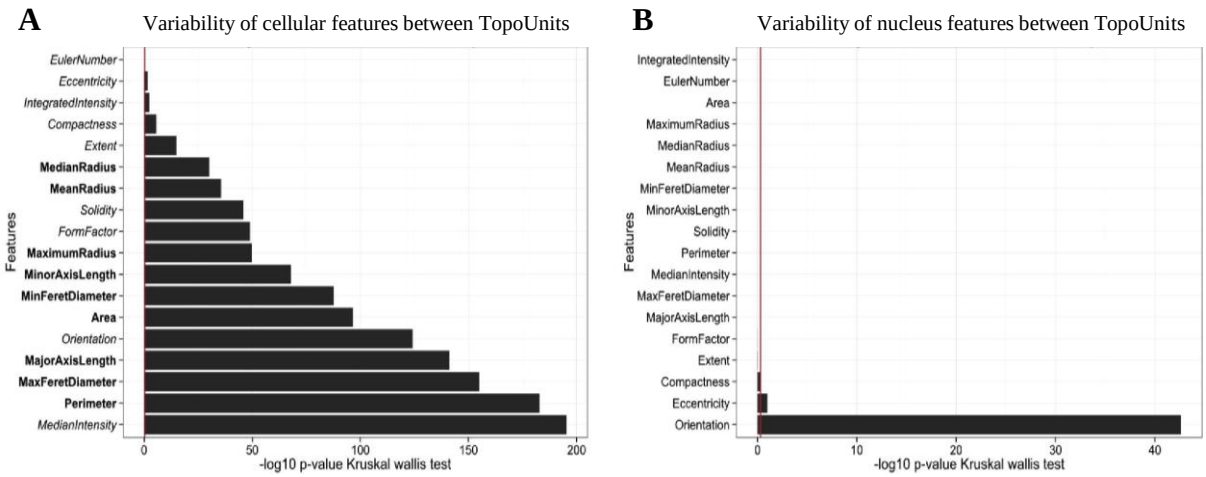

Figure 4. Nanotopographies influence many cell morphological parameters. A) Kruskall-wallis test to identify cell morphological parameters which show the most reproducible variation within the dataset. B) Kruskall-wallis test to identify nuclear morphological parameters which show the most reproducible variation within the dataset.

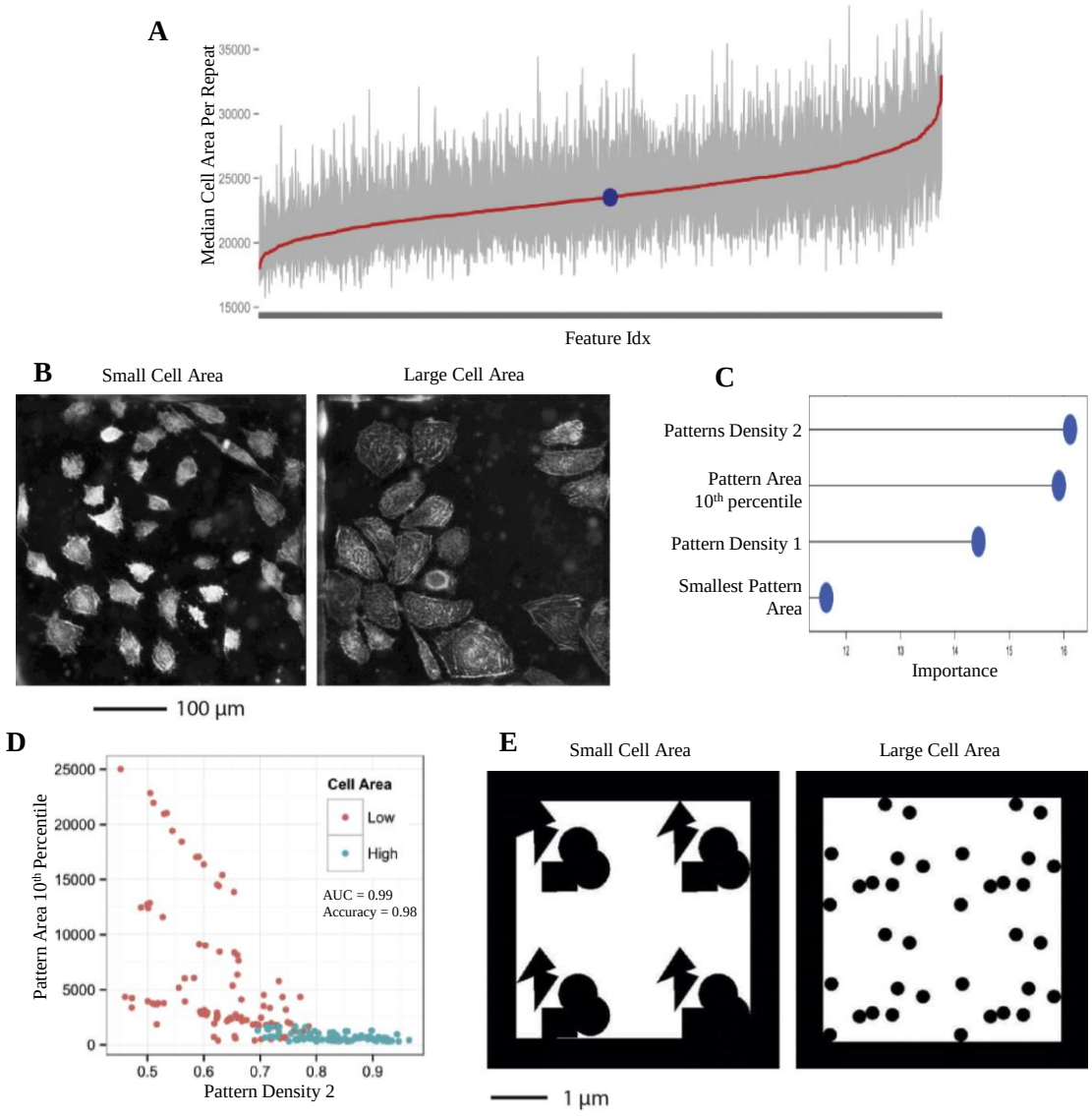

Figure 5. Nanotopographies affect cell area. A) S-curve of cell area measurement distribution among all topographies. B) Representative micrographs from the screening experiment which show U2OS with small and large cell areas. C) The importance of the measurements of feature design parameters which influence cell area, as revealed by the random forest algorithm. An explanation of the Cell profiler features is presented in the Supplementary Table S2. D) Scatterplot of cells with low and high cell area by the '10th percentile area' parameter and the 'pattern density' parameter. E) Representative images of features which influence cell area.

To assess if we can accurately predict cell size with surface design parameters, we selected top and bottom ranked surfaces based on cell area as was discussed before. We found that random forest was able to predict cell area most accurately (Figure 5C). The area of the smallest individual structure, the 10th percentile of pillars size within the topography and the ratio between area covered by topographical features and the area not covered by topographical features (pattern density) calculated by 2 methods were the most predictive parameters. These surface design parameters were able to predict cell size with 98% accuracy (Figure 5D). Visual inspection of the topography designs confirms the model predictions (Figure 5E). The topographies that induce small, more rounded cells, consist of relatively large topographies with large spacing between the topographies. The topographies which induce more spreading of the cells consist of smaller features which also cover a relatively small area. Other parameters such as cell number (Figure 6A), actin localization (Figure 6B) and fiber actin alignment (Figure 6C) could also be predicted by feature design parameters, using the same methods.

Discussion

This work shows, for the first time, the fabrication of high quality designed nanometer scale features on a large area such as a 4 cm^2 on the NanoTopoChip, using deep UV projection lithography in combination with conventional lithography[20]. Since large surface areas are required to accurately measure events in populations of cells the NanoTopoChip is an important step towards development of a platform for HTS of events at this scale. In this work we fabricated the NanoTopoChip in PS as it is the golden standard in tissue culture and provides excellent optical properties, which facilitate high-throughput image-based screening experiments. However, one of the major advantages of our fabrication method is that it can be produced in many other different (biomedical) polymers. Surface chemistry strongly dictates cell response[28–30] and may play a critical role in how cells respond to topography. A limitation of the fabrication method which relies on several hot-embossing steps is the introduction of variance in feature height between the small and large features. This is probably caused by imperfect filling of the cavities in the moulds which was unfortunately necessary to enable successful demoulding of a hard and brittle material such as PS. It is possible to achieve a more uniform feature height by using softer biomaterial substrates.

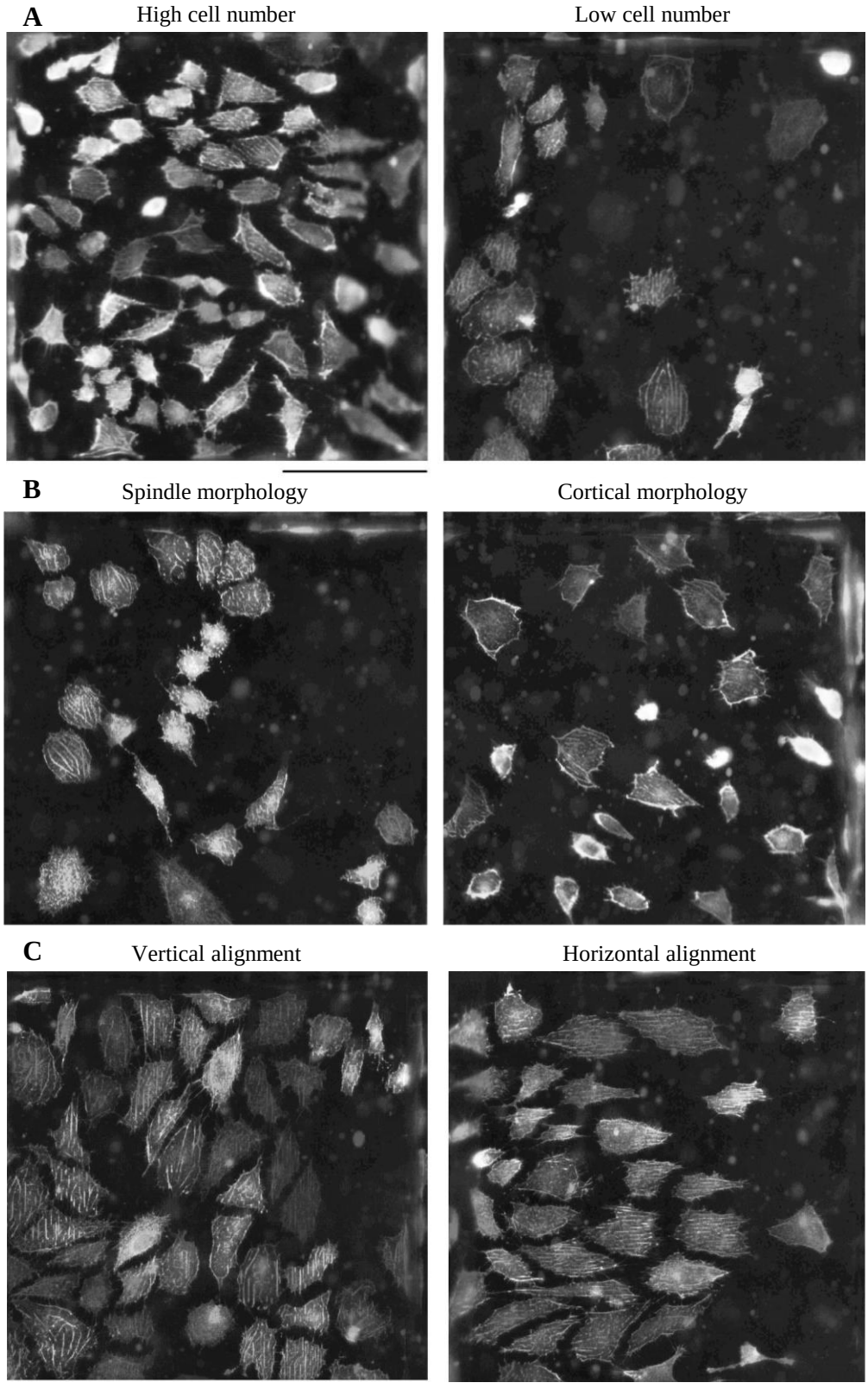

Figure 6. Cell parameters which are affected by nanotopography. A) Representative images from the screen of TopoUnits with low and high cell number. B) Representative images from the screen of cells cortical actin localization and actin spindle morphology. C) Representative images from the screen of cells with vertical and horizontal actin fiber orientation. The scale bar has a length of 100 µm. The designs of the underlying topographies are shown in Supplementary Figure 10.

Comparison of the influence of micro- and nanotopography on cell morphology yielded multiple important observations. The nanotopographies have a limited effect on nuclear morphology which can be extremely affected by micro topographies. The nanotopographies are not able to limit cell volume and shape by moulding the cells between the features such as is often the case with micro topographies. However, they are able to influence cell spreading and actin morphology. In stem cells subtle changes in actin morphology can be correlated to lineage fates[31]. By controlling actin morphology we might be able to steer stem cell differentiation.

The machine learning methods used to analyze the large dataset generated in a NanoTopoChip screening experiment allow us understand the relationship between nanotopography dimensions and shapes with the cell response. Many cell morphological parameters can be accurately predicted based on a few feature design parameters. With these methods we showed that size and spacing of the nanotopographies have a significant and reproducible effect on cell spreading. The nanotopographies cannot restrict the shape of the cells in contrast to the micro-scale topographies. This suggests that the nanotopographies must affect the availability and localization of cell attachment sites. Initially we hypothesized that this most likely occurs in an indirect manner, because unlike other studies that are able to restrict integrin binding domain availability by creating binding sites on a non-adhesive substrate, cells on the NanoTopoChip are expected to able to bind on the non-patterned areas. The cell attachment there might be somewhat restricted because of the relatively high aspect ratio on small topographies with little spacing (200 nm width, 800 nm height), but otherwise the non-patterned areas have the same surface chemistry as the topographical features. Cells bind to serum ECM proteins, such a fibronectin, that adhere to the substrate material[32]. It is plausible that the nanotopographies influence the alignment of ECM proteins and perhaps the presentation of binding motifs such as RGD sequences. In this way, the nanotopographies may indirectly affect binding to cell adhesion molecules such as integrins which are transmembrane proteins that play a key role in cell-ECM interactions[33]. Clusters of integrins form the focal adhesion complexes that on the one side attach the cell to matrix proteins while on the other side anchor to the cytoskeleton through adaptor proteins such as talin, paxillin and focal adhesion kinase[34]. Even the smallest features are large enough to provide the surface area required for the formation of a small integrin cluster required for focal adhesions[4,35]. Nevertheless, the smallest nano features might limit the size of the integrin clusters. It is suggested that fewer, large integrin clusters result in less cell spreading and thick actin bundles while more, smaller integrin clusters with small spacing leads to more spread cells with smaller focal adhesion sites[36]. If the cells in our experiments preferably attach to the top of the topographical features, this would be consistent with our findings which show that fewer large features lead to adhered cells with rounded morphology whereas many small topographical features lead to spread cells.

From our data we can conclude that the cell spreading is affected by the ratio of patterned versus non-patterned area. Although topographies with spread cells tend to have fewer cells

this was not due to space limitation because the cell density in all images was confirmed to be sub confluent. It appears that the fully spread cells have a lower proliferation rate. The integrins in the focal adhesion complexes are mechanically connected to the nucleus through the actin cytoskeleton, and in this way can affect nuclear processes such as transcription and the cell cycle progression[37]. This data is quite preliminary. To verify possible effect of cell spreading on proliferation, one would need to perform more studies with lower initial cell seeding density and longer culture time.

In conclusion, this work showed the fabrication of the NanoTopoChip, which contains a vast library of accurately defined, reproducible nanotopographies on biologically relevant surface areas. The flexibility of substrate material choice allows the identification of bioactive nanotopographies for many applications. Furthermore, a proof of principle screening experiment with U2OS cells demonstrated the NanoTopoChip high-throughput screening platform as an excellent tool to investigate nanotopography – cell morphological parameter relationships. In future experiments the NanoTopoChip can be used to identify specific nanotopographical designs, which influence functional cell phenotypes such as stem cell differentiation states.

References

1. Reimer, A. *et al.* Scalable topographies to support proliferation and Oct4 expression by human induced pluripotent stem cells. *Sci. Rep.* **6,** 18948 (2016).

2. Arlin, M. L. Survival and success of sandblasted, large-grit, acid-etched and titanium plasma-sprayed implants: A retrospective study. *J. Can. Dent. Assoc. (Tor).* **73,** 821 (2007).

3. Makhija, E., Jokhun, D. S. & Shivashankar, G. V. Nuclear deformability and telomere dynamics are regulated by cell geometric constraints. *Proc. Natl. Acad. Sci. U. S. A.* **113,** E32-40 (2015).

4. Schvartzman, M. *et al.* Nanolithographic control of the spatial organization of cellular adhesion receptors at the single-molecule level. *Nano Lett.* **11,** 1306–1312 (2011).

5. Cavalcanti-Adam, E. A. *et al.* Cell spreading and focal adhesion dynamics are regulated by spacing of integrin ligands. *Biophys. J.* **92,** 2964–2974 (2007).

6. Wang, W. *et al.* The role of integrin-linked kinase/b-catenin pathway in the enhanced MG63 differentiation by micro/nano-textured topography. *Biomaterials* **34,** 631–640 (2013).

7. Zhou, Q. *et al.* Directional nanotopographic gradients: A high-throughput screening platform for cell contact guidance. *Sci. Rep.* **5,** 1–12 (2015).

8. Diehl, K. A., Foley, J. D., Nealey, P. F. & Murphy, C. J. Nanoscale topography modulates corneal epithelial cell migration. *J. Biomed. Mater. Res. - Part A* **75,** 603–611 (2005).

9. Park, J. *et al.* TiO2 nanotube surfaces: 15 nm - an optimal length scale of surface topography for cell adhesion and differentiation. *Small* **5,** 666–671 (2009).

10. de Peppo, G. M. *et al.* Osteogenic response of human mesenchymal stem cells to well defined nanoscale topography in vitro. *Int. J. Nanomedicine* **9,** 2499–2515 (2014).

11. Dalby, M. J. *et al.* The control of human mesenchymal cell differentiation using nanoscale symmetry and disorder. *Nat. Mater.* 997–1003 (2007). doi:10.1038/nmat2013

12. Yamada, M., Kato, E., Yamamoto, A. & Sakurai, K. A titanium surface with nano-ordered spikes and pores enhances human dermal fibroblastic extracellular matrix production and integration of collagen fibers. *Biomed. Mater.* **11,** (2016).

13. Garland, S. P. *et al.* A cell culture substrate with biologically relevant size-scale topography and compliance of the basement membrane. *Langmuir* **30,** 2101–2108 (2014).

14. Zhao, G. *et al.* High surface energy enhances cell response to titanium substrate microstructure. *J. Biomed. Mater. Res. - Part A* **74,** 49–58 (2005).

15. MacLaine, S. E. *et al.* Optimizing the osteogenicity of nanotopography using block co-polymer phase separation fabrication techniques. *J. Orthop. Res.* **30,** 1190–1197 (2012).

16. Kolind, K. *et al.* A combinatorial screening of human fibroblast responses on micro-structured surfaces. *Biomaterials* **31,** 9182–9191 (2010).

17. Moe, A. A. K. *et al.* Microarray with micro- and nano-topographies enables identification of the optimal topography for directing the differentiation of primary murine neural progenitor cells. *Small* **8,** 3050–3061 (2012).

18. Unadkat, H. V *et al.* An algorithm-based topographical biomaterials library to instruct cell fate. *Proc. Natl. Acad. Sci.* **109,** 5905–5905 (2012).

19. Hulsman, M. *et al.* Analysis of high-throughput screening reveals the effect of surface topographies on cellular morphology. *Acta Biomater.* **15,** 29–38 (2015).

20. Chen, W., Shao, Y., Li, X., Zhao, G. & Fu, J. Nanotopographical surfaces for stem cell fate control: Engineering mechanobiology from the bottom. *Nano Today* **9,** 759–784 (2014).

21. Carpenter, A. E. *et al.* CellProfiler: image analysis software for identifying and quantifying cell phenotypes. *Genome Biol.* **7,** R100 (2006).

22. R Core team. R. A Language and environment for statistical Computing. (2014).

23. Dodonov, Y. *Distance-weighted statistics: robust estimation of location, spread and association between variables*. (2013).

24. Kuhn, M. Building Predictive Models in R Using the caret Package. *J. Stat. Softw.* **28,** 1–26 (2008).

25. Eichhorn, M., Stannard, C., Anselme, K. & R??he, J. Nucleus deformation of SaOs-2 cells on rhombic micro-pillars. *J. Mater. Sci. Mater. Med.* **26,** 108 (2015).

26. Li, W. *et al.* Large-scale topographical screen for investigation of physical neural-guidance cues. *Sci. Rep.* **5,** 1–8 (2015).

27. Muhammad, R. *et al.* Micro- and nano-topography to enhance proliferation and sustain functional markers of donor-derived primary human corneal endothelial cells. *Acta Biomater.* **19,** 138–148 (2015).

28. Brodbeck, W. G. *et al.* Biomaterial surface chemistry dictates adherent monocyte/macrophage cytokine expression in vitro. *Cytokine* **18,** 311–319 (2002).

29. Shadanbaz, S. & Dias, G. J. Calcium phosphate coatings on magnesium alloys for biomedical applications: A review. *Acta Biomater.* **8,** 20–30 (2012).

30. Mei, Y. *et al.* Combinatorial development of biomaterials for clonal growth of human pluripotent stem cells. *Nat. Mater.* **9,** 768–778 (2010).

31. Treiser, M. D. *et al.* Cytoskeleton-based forecasting of stem cell lineage fates. *Proc. Natl. Acad. Sci.* **107,** 610–615 (2010).

32. Sethuraman, A., Han, M., Kane, R. S. & Belfort, G. Effect of surface wettability on the adhesion of proteins. *Langmuir* **20,** 7779–7788 (2004).

33. Schwartz, M. A. & Ginsberg, M. H. Networks and crosstalk: Integrin signalling spreads. *Nat. Cell Biol.* **4,** 65–68 (2002).

34. Geiger, B., Spatz, J. P. & Bershadsky, A. D. Environmental sensing through focal adhesions. *Nat. Rev. Mol. Cell Biol.* **10,** 21–33 (2009).

35. Koo, L. Y., Irvine, D. J., Mayes, A. M., Lauffenburger, D. a & Griffith, L. G. Co-regulation of cell adhesion by nanoscale RGD organization and mechanical stimulus. *J. Cell Sci.* **115,** 1423–1433 (2002).

36. Huang, J. *et al.* Impact of order and disorder in RGD nanopatterns on cell adhesion. *Nano Lett.* **9,** 1111–1116 (2009).

37. Maniotis, A. J., Chen, C. S. & Ingber, D. E. Demonstration of mechanical connections between integrins, cytoskeletal filaments, and nucleoplasm that stabilize nuclear structure. *Proc. Natl. Acad. Sci. U. S. A.* **94,** 849–54 (1997).

38. CellProfiler. Module: MeasureObjectSizeShape. Available at: http://d1zymp9ayga15t.cloudfront.net/CPmanual/MeasureObjectSizeShape.html.

Supplementary data

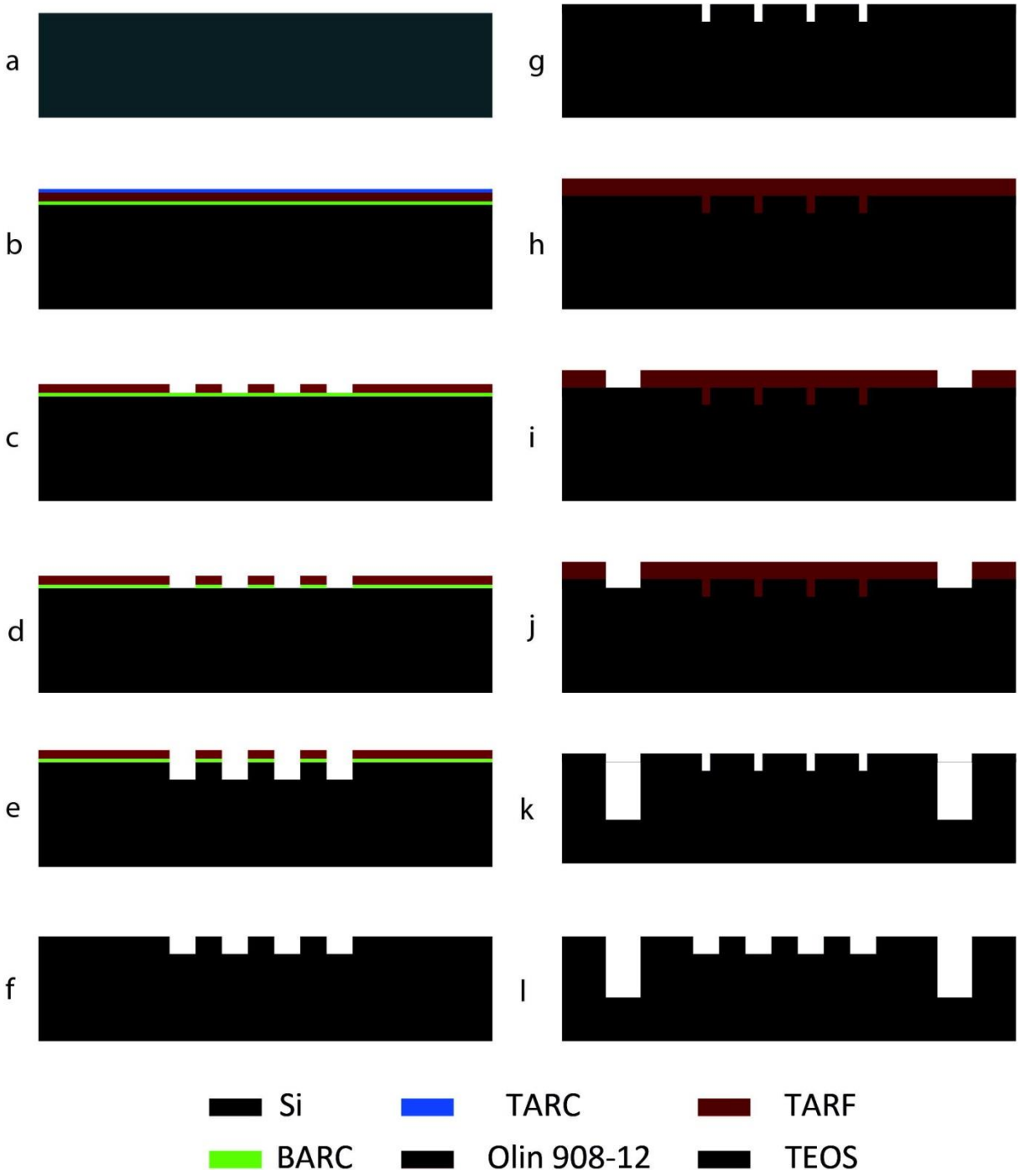

Supplementary Figure 1. Fabrication scheme for lithography and etching of Si NanoTopoChip mould. The process consists of the following steps (explained in detail in the methods section): Starting Double side polished, [100] oriented, 76 mm diameter Si wafer (A); spin coating of resists (B); DUV lithography (C); removal of BARC layer (D); Si DRIE (E); resist removal (F); TEOS layer application (G); spin-coating of photoresist (H); photolithography (I); TEOS DRIE (J); resist removal (K); TEOS layer removal (L).

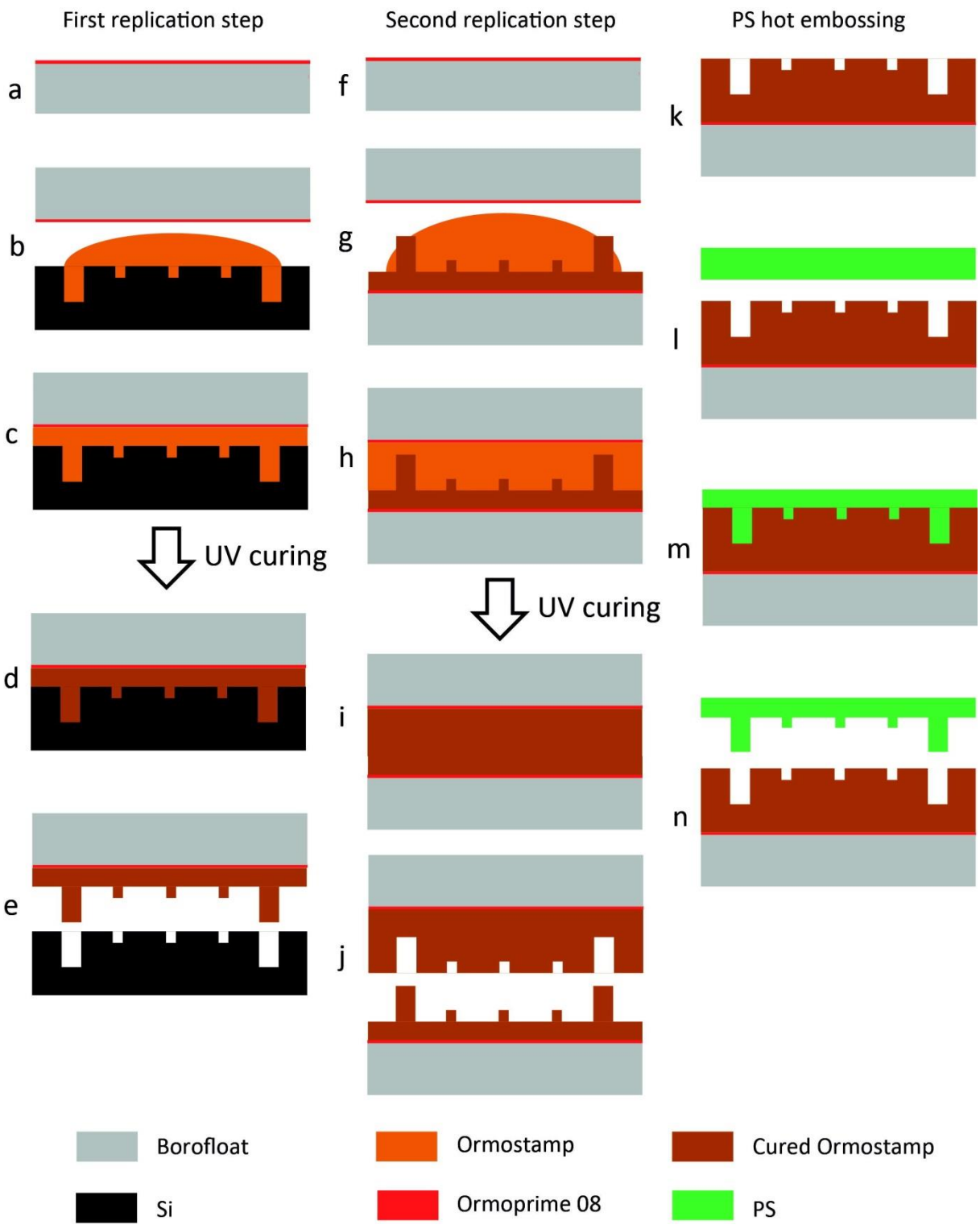

Supplementary Figure 2. Fabrication scheme for Ormostamp® mould fabrication and hot-embossing of PS NanoTopochips. The process to create the first (positive) OrmoStamp® mould consisted of the following steps (explained in detail in the methods section): OrmoPrime®08 is applied to a Borofloat® 33 (A); application of OrmoStamp® on Si wafer (B); filling by capillary forces (C); UV curing (D); peeling of OrmoStamp® mould (E). The second (negative) OrmoStamp® mould was created in the following steps (explained in detail in the methods section): OrmoPrime®08 is applied to a Borofloat® 33 (F); application of OrmoStamp® on first (positive) OrmoStamp® mould (G); filling by capillary forces (H); UV curing (I); peeling of the second OrmoStamp® mould (J). The

following steps were performed for the hot-embossing process to fabricate the PS NanoTopoChip: starting (negative) OrmoStamp® mould (explained in detail in the methods section) (K); application of PS film on the mould (L); hot-embossing (M); peeling of NanoTopoChip (N).

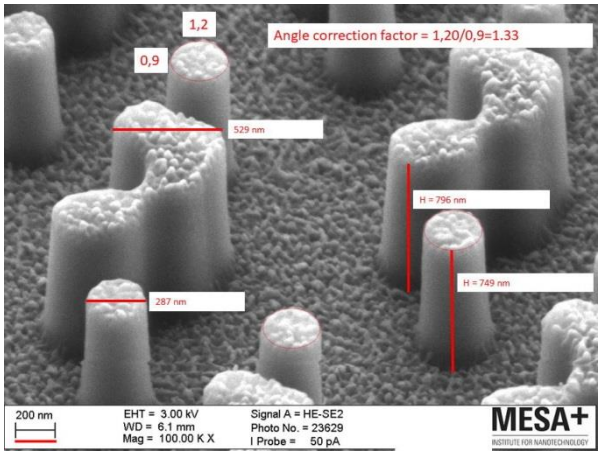

Supplementary Figure 3. Measurement method of nanotopographies. Since the images where taken at an angle of 45° and some of the features are circles, the height of the pillars could be inferred by calculating a correction factor from the vertical and horizontal dimensions of the ellipses on top of the circular features in the SEM image.

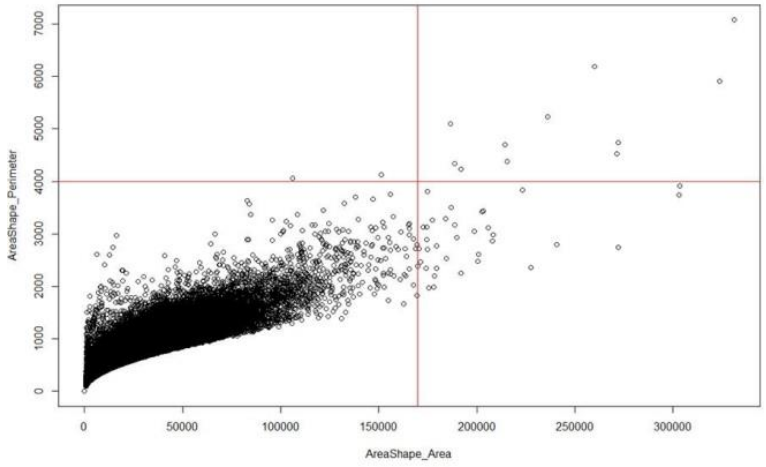

Supplementary Figure 4. Outlier removal caused by mis-segmentation. The cells were gated based on cell area and perimeter, and the cells in upper right quadrant were excluded from further analysis.

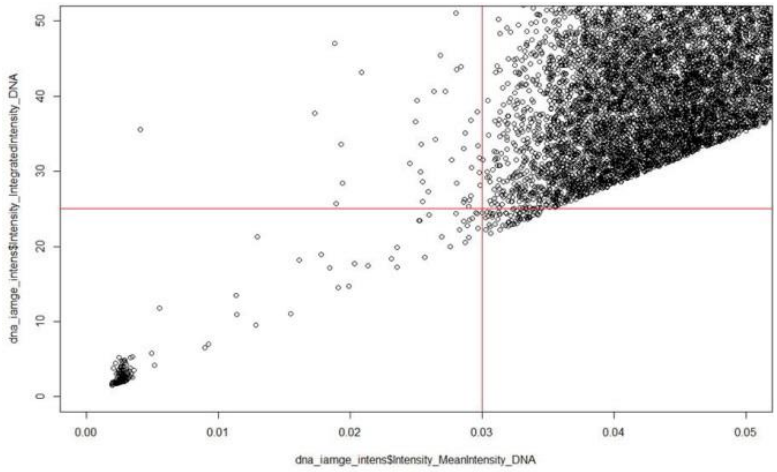

Supplementary Figure 5. Outlier removal caused by imaging artefacts. The cells were gated based on nuclei mean and integrated intensity and the cells in lower left quadrant were excluded from further analysis.

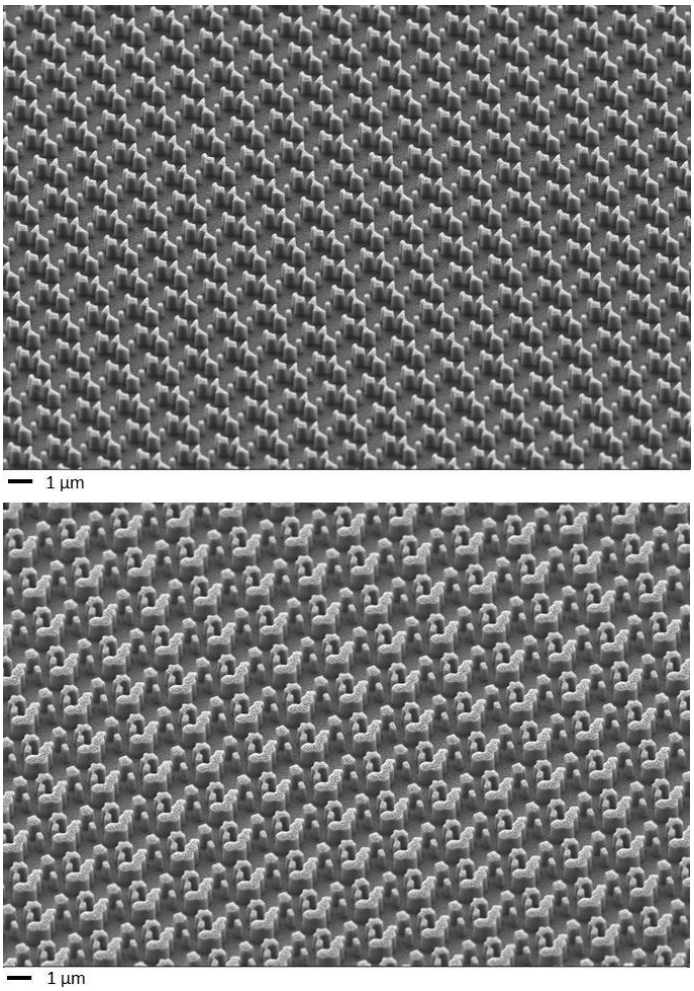

Supplementary Figure 6. Low magnification SEM images of 2 nanotopographies.

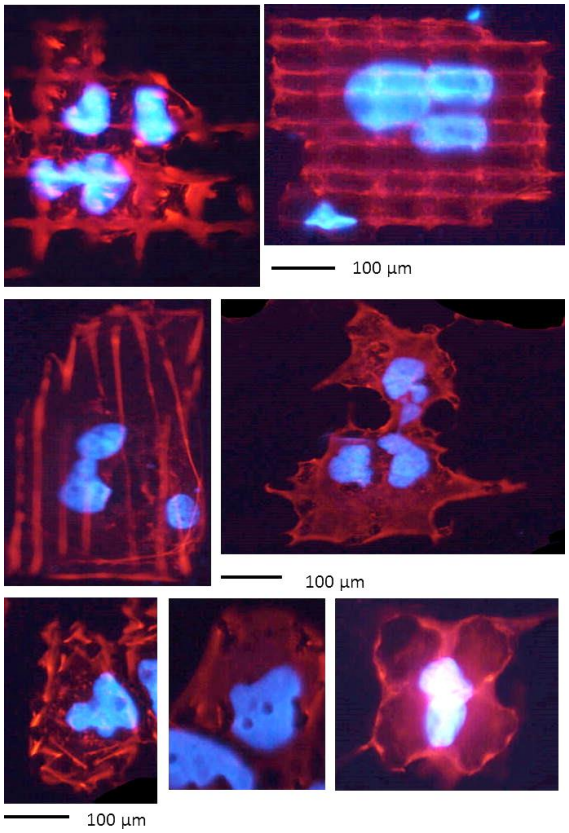

Supplementary Figure 7a. Zoom in images of cell morphologies visible on the micro-TopoChip shown in Figure 3.

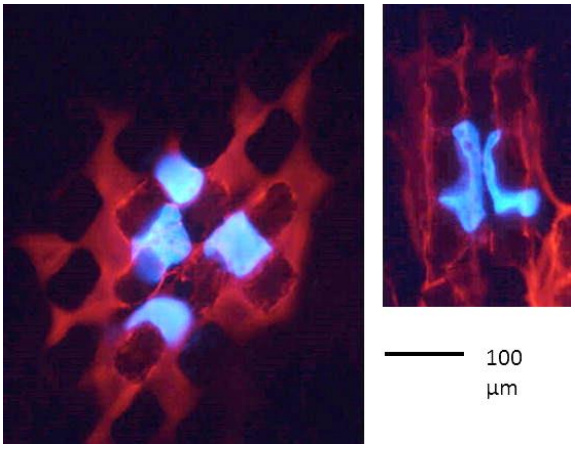

Supplementary Figure 7b. Zoom in images of cell morphologies visible on the micro-TopoChip shown in Figure 3.

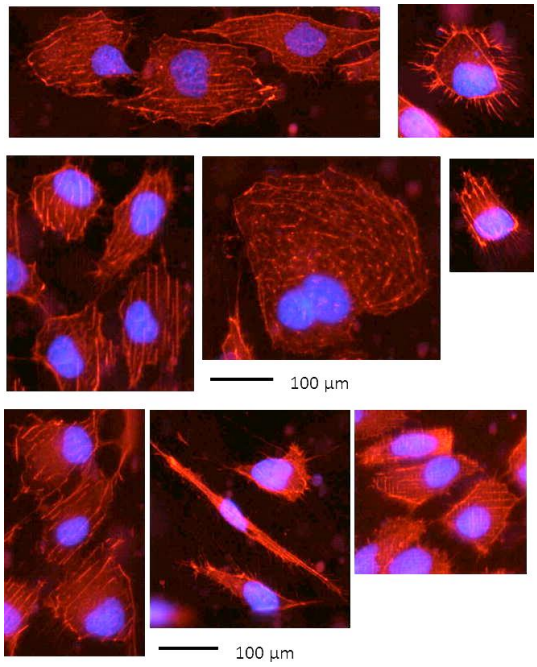

Supplementary Figure 8a. Zoom in images of cell morphologies visible on the NanoTopoChip shown in Figure 3.

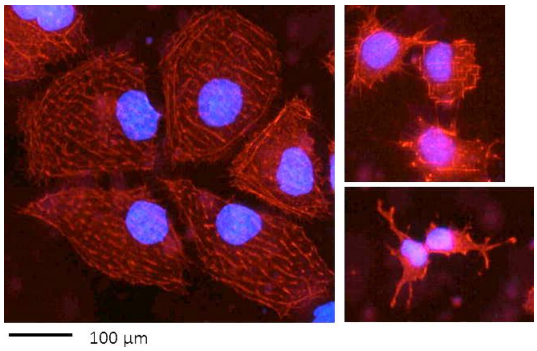

Supplementary Figure 8b. Zoom in images of cell morphologies visible on the NanoTopoChip shown in Figure 3.

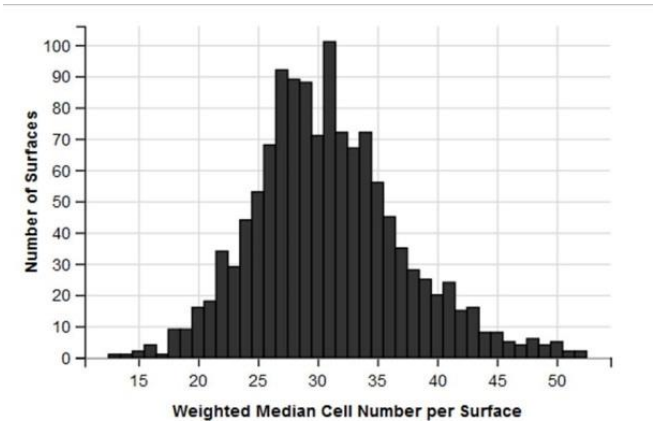

Supplementary Figure 9. Distribution of cells per unit on all NanoTopoChips within the screening experiment (filtered data).

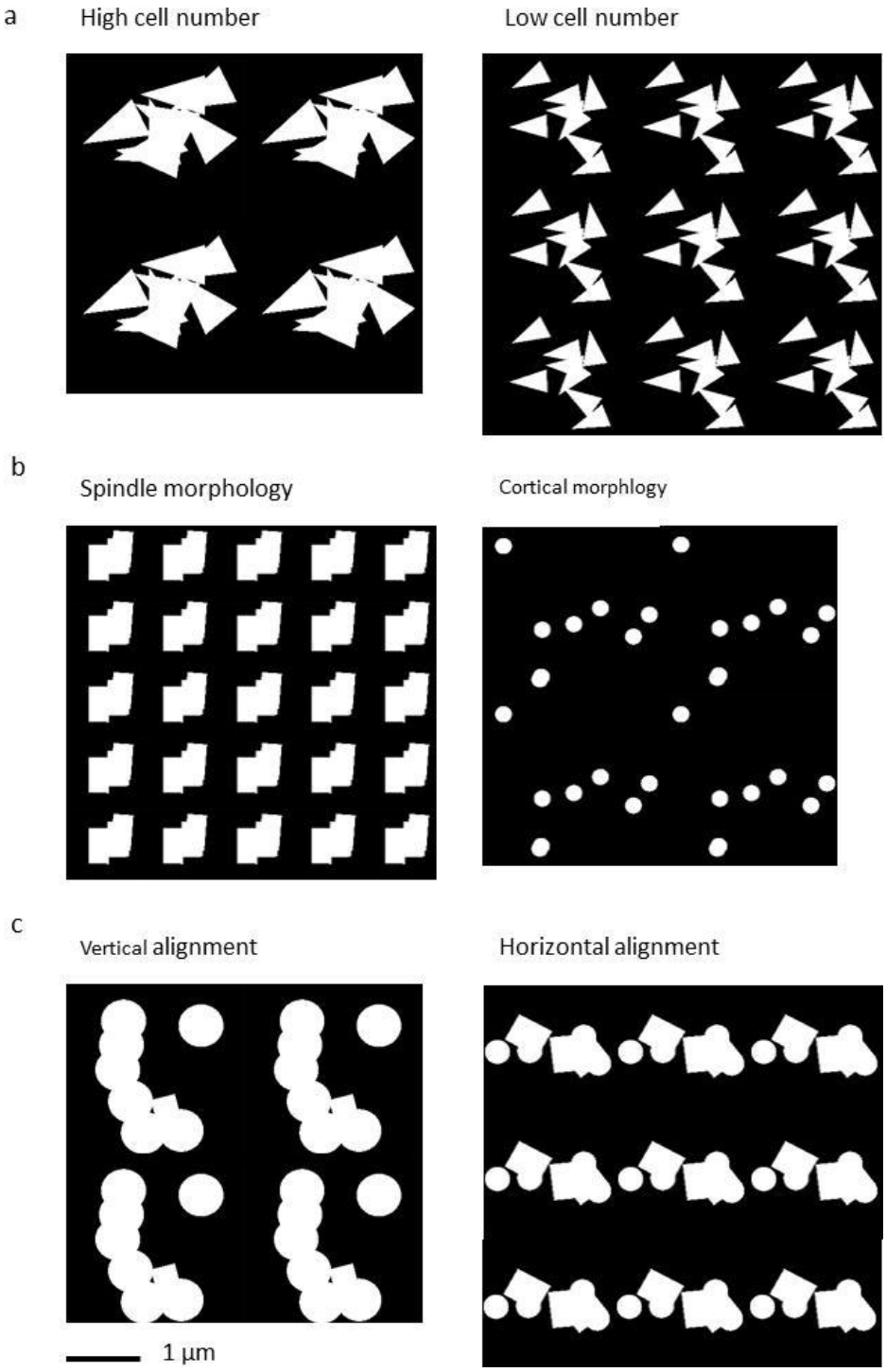

Supplementary Figure 10. Topography designs of the nanotopographies that cause the cell morphologies shown in Fig. 6. A) Topography designs from the screen of TopoUnits with low and high cell number. B) Topography designs from the screen which causes cortical actin localization and actin spindle morphology. C) Topography designs from the screen which causes vertical and horizontal actin fiber orientation.

Supplementary Table 1. Overview of parameter values and ranges used to construct features of the NanoTopoChip.

Parameter	Value or range
Feature space side length 10 μm, 20 μm, or 28 μm	1 μm, 1.8 μm, 2.4 μm
No. of primitives used (1 μm)	3 - 4
No. of primitives used (1.8 μm)	3 - 8
No. of primitives used (2.4 μm)	3 - 12
Diameter of a circle primitive (1 μm)	200 - 300 nm
Diameter of a circle primitive (1.8 μm)	200 - 500 nm
Diameter of a circle primitive (2.4 μm)	200 - 700 nm
Shortest side length of a triangle primitive	200 - 300 nm
Shortest side length of a triangle primitive	200 - 500 nm
Shortest side length of a triangle primitive	200 - 700 nm
Top angle of a triangle primitive	36°
Length of a line primitive	200 - 300 nm
Length of a line primitive	200 - 500 nm
Length of a line primitive	200 - 700 nm
Thickness of a line primitive	200 nm
Standard deviation for the rotation of a primitive	0.0°–180.0°

Supplementary Table 2. CellProfiler feature descriptions. (from [38])

Feature	Description
Compactness	The variance of the radial distance of the object's pixels from the centroid divided by the area.
EulerNumber	The number of objects in the region minus the number of holes in those objects, assuming 8-connectivity.
Extent	The proportion of the pixels in the bounding box that are also in the region. Computed as the Area divided by the area of the bounding box.
Major Axis Length	The length (in pixels) of the major axis of the ellipse that has the same normalized second central moments as the region.
Minor Axis Length	The length (in pixels) of the minor axis of the ellipse that has the same normalized second central moments as the region.
Solidity	The proportion of the pixels in the convex hull that are also in the object, i.e. Object Area / Convex Hull Area. Equals 1 for a solid object (i.e., one with no holes or has a concave boundary), or <1 for an object with holes or possessing a convex/irregular boundary.
Zernike	Measure shape by describing a binary object (or more precisely, a patch with background and an object in the center) in a basis of Zernike polynomials, using the coefficients as features (Boland et al., 1998). Currently, Zernike polynomials from order 0 to order 9 are calculated, giving in total 30 measurements. While there is no limit to the order which can be calculated (and indeed users could add more by adjusting the code), the higher order polynomials carry less information.
Eccentricity	The eccentricity of the ellipse that has the same second-moments as the region. The eccentricity is the ratio of the distance between the foci of the ellipse and its major axis length. The value is between 0 and 1. (0 and 1 are degenerate cases; an ellipse whose eccentricity is 0 is actually a circle, while an ellipse whose eccentricity is 1 is a line segment.)
Integrated intensity	The sum of the pixel intensities within an object.
Median Radius	The median distance of any pixel in the object to the closest pixel outside of the object.
Mean Radius	The mean distance of any pixel in the object to the closest pixel outside of the object.
Form Factor	Calculated as 4*π*Area/Perimeter2. Equals 1 for a perfectly circular object.
Maximum Radius	The maximum distance of any pixel in the object to the closest pixel outside of the object. For skinny objects, this is 1/2 of the maximum width of the object.
Min and Max Feret Diameter	The Feret diameter is the distance between two parallel lines tangent on either side of the object (imagine taking a caliper and measuring the object at various angles). The minimum and maximum Feret diameters are the smallest and largest possible diameters, rotating the calipers along all possible angles.
Area	The actual number of pixels in the region
Orientation	The angle (in degrees ranging from -90 to 90 degrees) between the x-axis and the major axis of the ellipse that has the same second-moments as the region.
Perimeter	The total number of pixels around the boundary of each region in the image
Median Intensity	The median intensity value within the object

⠠⠞⠓⠑ ⠠⠟⠥⠊⠉⠅ ⠃⠗⠕⠺⠝ ⠋⠭ ⠚⠥⠍⠏⠎ ⠕⠧⠑⠗ ⠞⠓⠑ ⠇⠁⠵⠽ ⠙⠕⠛

Chapter 8

General discussion

Development of biomaterials systems and analytic tools for biomaterial research

The project defined in September 2013 contained three key elements to be implemented in the research compiled in this thesis: surface topography, mesenchymal stromal cells (MSCs), and STELLAR kidney regeneration. Inevitably in scientific research, we needed to adjust scopes and goals along the way, and encountered the need for technological development of the research platform. As an example, the kidney derived MSC-like population – envisioned to study topography-induced differentiation into proximal tubule cells – turned out not to have this potency. Instead, we redirected our research focus to the paracrine activity of these kidney-derived cells in tissue homeostasis[1]. Due to the current TopoChip design, it was not possible to measure secreted factors coming from individual TopoUnits[2]. This created the need to develop a new tool, introduced in chapter 5 as the TopoWellPlate.

My multidisciplinary background allowed me to execute almost all steps needed for my research: from the cleanroom production of the topographically enhanced substrates, via cell culture and assay development, all the way towards data analysis. During my PhD, on many occasions, the experimental work led to interesting observations which turned out to be a great food for thoughts to further develop cell-surface topography research. In this chapter, the use of surface topography in the field of mechanobiology will be discussed, together with the development of biomaterials and analytical tools.

Biomaterial-induced changes in cellular phenotypes

The current healthcare system aims more-and-more for regenerative medicine approaches for a wide variety of diseases. In regenerative medicine, the aim is to restore the function of the damaged tissue using the power of the patients' own body[3]. To achieve this, there is the need for functional biomaterials which support the cells' desired behavior. Evolution of such biomaterials is driven by the technological developments which allow researchers to gain more control over the specific material properties[4–6]. As a result, the microenvironment to which cells are exposed can be tweaked in terms of chemical and physical appearance, such as material stiffness and surface topography. Additionally to such static systems with defined material properties, a growing number of biomaterials are currently introduced which have properties that can be dynamically changed. Such dynamic biomaterials are designed to be manipulated by e.g. light and temperature, stimuli which can be controlled during cell culture. For example, a material with a certain surface topographies and material stiffness becomes stiffer upon excitation by light, resulting in a change in the surface topography the cells sense[7].

A growing body of literature describes the response of multipotent cells to alterations in several distinct material properties. Here, the majority of biological read-outs focused on

differentiation-related processes, by quantification of differentiation marker expression at various levels[8–10]. For example: quantification of mRNA levels is used to describe material-induced differences in gene expression, measurements of fluorescently labeled antibody-constructs that bind an epitope of the protein of interest to assess protein expression, and metabolic products correlated to basic cellular physiology. As a result, we gather descriptions of changes in phenotypes of multipotent cells *in vitro* as a reaction to a biomaterial in terms of differentiation towards a desired cell typed for the application of interest. However, the underlying molecular mechanisms of cell-material interaction remain to be elucidated, even though this understanding is essential to being able to further improve biomaterial function specifically and rationally.

The physical parameters of substrates can manipulate cells via mechanotransduction. This means that an extracellular physical force is transferred into a cell where it is converted into a chemical signal. The opening of mechanosensitive channels which causes a difference in ion-distribution, or focal adhesion complex clustering that initiates cytoskeletal build-up, are two examples[11,12]. Some of these molecular mechanisms have been explored already, however, there is a need for additional steps in technological development and usage of analytic tools to be able to map the full canonical pathway of mechanotransduction.

In this thesis we performed experiments that could bring us one step further in unravelling the mechanisms of mechanotransduction. We started by building on previous work from our group in which we used the TopoChip high-throughput screening platform to identify and validate an osteogenic surface topography[13]. In chapter 3 for example, we aimed to elaborate on the underlying mechanisms of action initiated by this surface topography. For this, a genomics approach was used to generate hypotheses on possibly involved signaling pathways. But what is the context we are measuring these differences in, and can we even compare the cells that are exposed to flat or topographically enhanced substrates as these cells are executing basic cellular functions significantly differently? As described in chapter 4, we see a strong cellular response of cells to surface topographies at a basic physiological level: cell size, proliferation, and metabolism were all affected. Here, cells adapted their phenotype to their new microenvironment by reducing their volume together with the availability of less mitochondria which led to a lower metabolism. Furthermore, in chapter 6 we observed distinct differences in secretion profiles of cells exposed to a variety of unique topographies. Principal component analysis visualized these differences between topographies based on their effect on the secretome, and showed a similar distance between several topographies and the flat samples compared to some topographies among each other. So, even though the flat surface is often seen as an outlier in the spectrum of topographies, the phenotypical distance between cellular reactions to different topographies can be of a similar magnitude.

What do we measure?

There are many examples of potent small molecules and growth factors that induce specific and strong cellular responses in term of elevated gene and protein expression. In hMSCs for example, addition of phenanthroline increases VEGF secretion significantly, and the addition of cAMP in combination with dexamethasone can potently increase the fraction of the alkaline phosphatase positive MSC population[14,15]. Quantification of topography-induced differentiation marker expression often showed smaller fold-changes. Typically observed differential protein and gene expression are similar to e.g. dexamethasone or bone morphogenetic protein induced alkaline phosphatase expression. As seen in the potent combination of dexamethasone and cAMP, two different stimuli can synergistically increase the strength of the final outcome. One can hypothesize the same for a combination of physical and chemical stimulation. Here, the physical stimulation might change e.g. the distribution of membrane receptors, creating an optimal environment for cells to react to the stimulation of chemical nature.

It may sound obvious, but it is important that the biological system one wants to manipulate needs to be able to respond to the introduced triggers and subsequently induce the desired phenotype. As described in chapter 2, many mechanobiological systems found in nature are "ready-to-react". For example, in previous work, we used embryonic stem cells for bone tissue engineering, but noticed that the cells failed to form bone tissue, even though we successfully differentiated them into osteoblast. However, when we differentiated embryonic stem cells into chondrocytes *in vitro* prior to implantation, the construct was able to induce bone formation. In this case, the cells needed a tweak – chondrogenesis – before they were able to execute the rest of their morphogenetic program[16]. Taking a cell from a very complex three dimensional environment *in vivo*, and placing it on flat plastic (attaching to materials orders of magnitude stiffer) and surrounded by a cocktail of proteins (serum), might very well create a system which is far from ideal. Perhaps the transformation of the microenvironment – by using topographical features – results in a cellular system which has a significantly higher potential to react to stimuli.

To quantify phenotypical changes, there is a need for parameters which remain constant across the different conditions. Since surface topographies were found to affect many basic functions of cells, it has been a challenge to correctly quantify topography-induced differences in phenotypes. Often we could overcome this by adding more biological references to the outcome measures. For example, a fairly easy assay as Presto Blue (or similar) is typically used to quantify relative differences in population expansion between different conditions, as the mitochondrial activity is hypothesized to remain constant. However, we found that cells cultured on topographies have a significantly lower mitochondrial metabolism after normalizing the data according to the number of cells measured. This showed the potential mismatch between what a very commonly used assay actually measures and the biological read-out for which it is typically used.

Furthermore, additional reference material will increase the quality of both gene and protein expression quantifications. For example, we observed strong fluctuations in "household" genes which are used as references in qPCR. For Western blot we hypothesized that levels of cytoskeletal-based reference proteins – such as β-actin and α-tubulin – were disturbed due to dramatic changes in cytoskeletal protein distribution, state and abundance. This does not mean that there is a need for an increase of reagents needed for experimental controls, but it is important to look critically at the data being produced. Small differences between conditions can easily show false trends. To overcome this, one could e.g. include multiple reference genes or proteins, or confirm the data using different techniques, and additionally assessing downstream targets as well.

Comparing differences in cellular state, of cells cultured on flat and topographically enhanced substrates, is also an important factor when assessing imaging-based read-outs. Showing extremely deformed cells and hypothesizing changes in cell behavior is intuitively easy to follow. Such changes in cell behavior can be quantified, for example, by the abundance of the protein of interest or its localization. However, when studying these aspects there are many details to take into consideration. For example, the total volume of the cells is smaller in cells grown on topography compared to flat. It is hypothesized that such a shrinkage of cells can be achieved by efflux of water, regulated by aquaporins[10]. Following this line of thought, smaller cells will have a lower water content and consequently a higher concentration of intracellular molecules. This means an elevated level of average signal intensity when measuring two dimensional micrographs, when using both epifluorescence as well as confocal imaging. The cellular confinement causes in many occasions subcellular branches. These strongly elongated "arms" seem to be compressed, but previous work demonstrated an increase in the z-direction[13]. To correctly address the protein abundance in these cells, confocal imaging is needed in which only thin slices of the cells are assessed instead of a poorly added-up intensity over this longer z-axis in epifluorescence. The same principles are true for imaging nuclei. To overcome these difficulties when using microscopy, it should be standard procedure to include confocality while imaging. Assessing thin slices of the complete cell will allow for a better quantification of protein distribution and abundancy.

Taken together, we have to keep in mind that there is a need to update the ways we use analytical tools for these new applications in order to ensure that we are still measuring what we want to measure. This hurdle is of course not new in research, and is found in all disciplines across science. With technology advancing quicker than ever before, the limits of what we can measure continues to shift as well.

Implementing analytical tools in biomaterial research

Besides pushing the detection limits of analytical tools, the field of its application can change as well. This opens up new opportunities for cell-biomaterial research. A great example here

is to use an advanced technique like mass spectrometry to study cell-surface topography interactions. In short, mass spectrometry can very precisely measure the weight of molecular fractions which can subsequently be used to identify the exact molecular composition of the cells' material. Using state-of-the-art mass spectra databases, it becomes possible to derive protein data from measured peptides. Cell derived samples – in which peptides can be measured – might therefore give a wealth of information on the proteins which are present in those cells, which represent the cellular state and reveal ongoing processes[17]. High resolution mass spectrometry based proteomics has been used for quantitative analysis of the cellular and/or organellar proteomes[18]. For example, mass spectrometry can be used to identify the differences in protein levels between similar cells isolated from different sides within the human body from which differential functionality is known. In this way, lung-derived and bone marrow-derived MSCs were compared which led to the identification of 352 differentially presented proteins that can affect clinical outcome when used in cell therapy[19].

As mentioned before, surface topography can be a potent way to control cell behavior, and the TopoChip contains a large collection of them. Obtaining mass spectra of cells exposed to these surface topographies allows us to study the cellular responses in more depth. Additionally, using these spectra, we can cluster surface topographies based on cellular protein composition, which can give more insights in the effects of topographical feature parameters on cell behavior. Current developments in the mass spectrometry field allow the generation of mass spectra retrieved from small surface areas of the sample. Using this approach one can create a so called mass spectrometry image. This can be used to assess protein compositions at a sub-cellular resolution, exploiting the full wealth of information hidden in there. This approach is quite similar to currently developed mass spectrometry based imaging of tissue sections to identify tumor cells. The spectra obtained from a certain cell type may resemble more closely that of e.g. cancerous cells. Using a clustering approach, one will be able to identify the variety in cells types within the prepared samples, and machine learning approaches will be able to recognize unwanted cells[20]. Mass spectrometry-based imaging of the TopoChip is approached in the same way. Clustering of the TopoUnits will reveal similarities in cellular responses to topographies, and additionally, they can be compared to known spectra from different cell types.

Implementation of this research line has already started in the form of a collaboration between cBITE and the division of imaging mass spectrometry from M4I (Institute of Maastricht MultiModal Molecular Imaging). In pilot experiments, we compared the lipids in cells exposed to a small selection of surface topographies and we detected changes in lipid composition (lipodomics). The next step here will be to standardize sample preparation and detection methods in order to obtain reproducible data. Furthermore, there is again a need for proper molecular reference molecules in order to be able to place the measured differences in molecular compositions of cells in the proper context. In the case of assessing lipodomics, a compound manipulating the cell membrane's lipid composition would be a valuable reference condition.

The use of mass spectrometry will introduce a new source of big data for cell-material interactions, on top of the datasets already being obtained using image analysis and transcriptomics. Furthermore, additional analytical tools can be used to obtain big data that can help to elucidate the mechanisms underlying cell-material interaction. A good example is three dimensional time-lapse imaging of living cells cultured on topographies. Such videos will be of great value for understanding what cellular confinement means. Observing the interaction between cells and topographical features, and how they adapt over time, will help us understand and interpret the other results much better. At this moment, it is still a challenge to quantify specific cellular functions in such movies and describe their scientific value. Fluorescent labeling of proteins relevant in mechanobiology would be a valuable addition here. For example, it would be interesting to compare translocation and activation of the mechanosensitive proteins YAP (yes associated protein) or EGR1 (early growth response) between cells cultured on flat and topographically enhanced substrates. Capturing protein distribution dynamics might identify the components involved in topography-induced changes in cellular state. The output of such experiments, which is currently being implemented in modelling approaches in our lab, can create a synergistic effect in terms of validation and quantification of additional parameters for the models.

Besides the development of analytical tools to study cell-material interaction, there is also a continuous need for developing the biomaterials itself as highlighted in chapter 2. So far for the TopoChip platform, this meant the introduction of the TopoWellPlate and the NanoTopoChip. Even though the implemented novelties might not sound revolutionary (e.g. using larger TopoUnits in a well plate format (TopoWellPlate) and scaling the topographical feature size down (NanoTopoChip)) their added value for the platform became evident immediately in terms of additional types of data (cell culture metabolites and secreted factors, red. chapter 5 and 6), and new insights in cell-material interactions (filopodium and podosome formation, chapter 7).

Development of novel systems for biomaterials research

Even though the newly developed tools were suitable to be used for the experimental work in this thesis, improvements can still be made to the current production methods. The NanoTopoChip is quite similar to the TopoChip in terms of production protocol, however, the imprint quality control requires closer monitoring. Where the topographical features on the TopoChip (between 10 and 28 µm in diameter) are clearly visible in great detail using regular light microscopy, the sub-micrometer-sized topographical features on the NanoTopoChip are harder to assess using this method. Consequently, in order to guarantee high-quality imprints, visual inspection using the regular light microscope will not be conclusive. Tightly controlled imprint procedures therefore need to be followed in order to ensure a high level of reproducibility. Additionally, samples should be tested regularly using scanning electron

microscopy to assess the topographical feature definitions in more detail. This quality control of the actual topographical feature shape is important since it is also the basis of many machine learning approaches that assess the influence of topography parameters on cell behavior. Often encountered problems in imprinting are tearing of topographical features and smoothing of the designed shapes. With the tearing, the pillars are separated from the imprinted substrates during demolding and remain in the mould, resulting in topographically enhanced substrates on which unpatterned regions appear. This problem is solely encountered by topographical features with a high aspect ratio (long and thin pillars). The smoothing of the *in silico* design during fabrication is due to the resolution of the used techniques.

The details lost in translation from the *in silico* design towards the imprinted topographical feature are also important to consider for the micrometer-scale topographies. Where the algorithm generated topographical features are built by pixels, the actual polymer imprint will always be slightly different due to its resolution. When using the observed changes in cell phenotype to draw correlations with topographical feature design parameters, these differences are not taken into account. Obviously, larger descriptors, such as spacing between the topographical features, are similar between the design and actual imprint. But to be able to create better predictive models for topography-induced cell behavior, it can be of great importance to include the actual material parameters. To achieve this, one can start by excluding parameters which are likely to differ from the imprinted topographical features. These parameters will be mostly based on the shape descriptions of high resolution. For example, describing the shape of topographical feature designs can differ from the resulting imprints in term of smoothed edges and smaller objects which are fused together. This will reduce the amount of parameters available to build the predictive models for cellular phenotype, however, the models will be based on true data instead of partly on (wrong) assumptions. Furthermore, the TopoChip can be imaged using electron microscopy to describe the true imprinted topographical features with proper measurements. For this, CellProfiler-derived object measurements can be used to define topography characteristics, such as circularity and spacing.

Within the TopoChip platform we have explored micrometer and nanometer-scale topographies and found, in line with literature, that both scales of surface structure can strongly influence cell behavior[6,21]. Where micrometer-scale structures might lead to cellular confinement induced responses (e.g. by addressing the cytoskeleton or stretch-activated channels), the nanometer-scale structures might act more on focal adhesion complex formation (e.g. integrin clustering or cell membrane receptor interaction). In search of further development of the TopoChip platform (besides the currently explored use of various chemistries (e.g. development of the ChemoTopoChip) and material stiffness (e.g. using hydrogels)), a combination of micrometer and nanometer-scale topographical features might be of interest. Of course, such a material design will be accompanied by both pros and cons. The biggest advantage of the combined design parameter approach will be its possible impact on cell behavior. Finding the ideal combinations of cellular confinement and receptor

interaction might potentially lead to very strong cellular reactions which should be easy to quantify during validation studies both *in vitro* and *in vivo*. Obviously, strong and consistent data of *in vivo* experiments will significantly increase the success rate of clinical trials as the last step needed to reach clinical application.

Creating the described complex surface structures will be technically challenging at the moment. Applying a nanometer-scale structure on top of micrometer-scale topographical features, but also on their side walls and the space between the features will not be possible using the current lithography approaches. An easier method to create nanometer-scale structures on top of the topographical features might be by using established approaches like acid-etching and sandblasting. These surface treatments are proven to be biologically active, as shown for example by an increase in osseo-integration of titanium substrates *in vivo*[22]. Currently, there already is a degree of (un)wanted nanometer-scale structures as a result of the used microfabrication protocol (e.g. O_2-treatment to enhance hydrophilicity is a mild etching process itself, able to etch away the polymer film). Together with the previously discussed parameters which are lost in translation, we can state that certain material properties are introduced in the manufacturing process, but may be not identified yet. Having full control over the production outcome might not be possible in the current production pipeline, but to what degree do we need to control the outcome of substrate microfabrication if we want to induce desired cellular phenotypes?

The desirable level of control over produced TopoChip-based materials.

All afore mentioned analytical tools are described to detect biomaterial induced changes in cellular phenotypes, such as: cell shape, metabolism, gene expression, protein translocation, etc. But what do we actually know about our materials, and how important are the known and unknown material properties in cell material interaction? Being introduced to the cleanroom production of the TopoChip platform meant, in the first place, repeating an existing protocol[23]. Proudly using these produced materials for cell culture opened my eyes for all the little tweaks which are important to successfully complete the production pipeline.

Based on visual assessment, topography induced changes in cell morphology appear to be similar across various chemistries. This is not surprising, since the changes are largely dictated by the physical boundaries created by the topographical features. However, the substrate chemistry is known to greatly influence other aspects of the induced phenotype. For example, in previous work we compared the effect of the osteogenic titanium-coated hit topography with a replica in polystyrene. The differences were striking. Where on titanium osteogenesis was higher on topography compared to flat substrates, on polystyrene this effect was found to be vice versa[24]. Therefore, we assume that the combination of cell type, substrate chemistry and defined surface topography creates a unique cellular response.

The level of homogeneity within cell populations is known for different cell sources, and can range from identical selected copies in a specific cell lines towards a quite heterogeneous cell population as in e.g. human bone marrow derived mesenchymal stromal cells. Besides this, there is a certain degree of heterogeneity in the material part as well. At this moment, speculation exists on five poorly defined material properties which are introduced during the production pipeline that are possibly influencing the behavior of cells cultured on them: (1) the effect of the O_2-treatment (increase in hydrophilicity to promote protein adsorption needed for cell attachment) and the change of its efficacy over time; (2) traces of PDMS (intermediate mould in the production pipeline) and FOTS (anti sticking layer to improve detachment) transferred along the imprint process; (3) the composition, nucleation, and distribution of the sputter-coated titanium; (4) the used template material on which the coating is applied (e.g. acidic degradation product of polylactic acid); and (5) a decrease in imprint quality due to re-use of Ormostamp. Stabilizing these parameters by standard operating procedures for material fabrication and preparation for cell culture will increase reproducibility in terms of material properties. Most certainly, it will also eliminate possible inconsistencies in material induced cellular responses. It is even more desirable to rule out afore mentioned five points. In order to achieve this, specialized analytic tools – operated by expert research groups – need to be used for material analysis. Even though establishment of such collaborations and subsequent analysis will take time, it will always be beneficial for science to work together in order to solve research questions.

The total sum of all material properties that are introduced to cells defines the effect of the biomaterial on the resulting cell behavior. Besides the strong effects from material chemistry and stiffness, the equation includes also numerous factors that define the full design space of the surface structure. The aim to fully control cell behavior using biomaterials creates the need to largely solve this very complex equation, or at least get as close to the desired outcomes as possible. Therefore, it is desirable to eliminate all uncontrolled or unanticipated artifacts of which we are aware, which can create heterogeneity in the produced materials.

Concluding remarks

Taken together, during the past years I was part of a research team which accomplished some important milestones within cBITE. First of all, the introduction of two novel cell culture tools in the TopoChip platform, the TopoWellPlate and the NanoTopoChip. The NanoTopoChip was introduced using a proof of principle study and is currently implemented in various new research lines. The TopoWellPlate, on the other hand, will need a production upgrade which will increase its status from a prototype towards an industrial-level product. Once this is achieved, there will be great opportunities for the TopoWellPlate as a tool to elucidate the canonical pathway of mechanotransduction. Within the context of this thesis, we were able to touch upon the underlying mechanisms of mechanotransduction in terms of

differentiation-related cell behavior as well as more basal cellular functions. Finally, the effect of surface topography on cell function has been beautifully demonstrated by the observation of cell morphology-guided cytokine secretion profiles. Using the TopoChip platform, one can potentially study any mechanobiological model of interest, ranging from fundamental research towards applicable material properties.

References

1. Rabelink, T. J. & Little, M. H. Stromal cells in tissue homeostasis: balancing regeneration and fibrosis. *Nat. Rev. Nephrol.* **9,** 747–53 (2013).

2. Unadkat, H. V *et al.* An algorithm-based topographical biomaterials library to instruct cell fate. *Proc. Natl. Acad. Sci.* **109,** 5905–5905 (2012).

3. Chen, C., Dubin, R. & Kim, M. C. Emerging trends and new developments in regenerative medicine: a scientometric update (2000 – 2014). *Expert Opin. Biol. Ther.* **14,** 1295–1317 (2014).

4. Engler, A. J., Sen, S., Sweeney, H. L. & Discher, D. E. Matrix Elasticity Directs Stem Cell Lineage Specification. *Cell* **126,** 677–689 (2006).

5. Mcbeath, R., Pirone, D. M., Nelson, C. M., Bhadriraju, K. & Chen, C. S. Cell Shape , Cytoskeletal Tension , and RhoA Regulate Stem Cell Lineage Commitment. *Dev. Cell* **6,** 483–495 (2004).

6. Dalby, M. J. *et al.* The control of human mesenchymal cell differentiation using nanoscale symmetry and disorder. *Nat. Mater.* 997–1003 (2007). doi:10.1038/nmat2013

7. Sutton, A. *et al.* Photothermally triggered actuation of hybrid materials as a new platform for in vitro cell manipulation. *Nat. Commun.* **8,** 14700 (2017).

8. Totaro, A. *et al.* YAP/TAZ link cell mechanics to Notch signalling to control epidermal stem cell fate. *Nat. Commun.* **8,** 15206 (2017).

9. Tsimbouri, P. M. *et al.* Stimulation of 3D osteogenesis by mesenchymal stem cells using a nanovibrational bioreactor. *Nat. Biomed. Eng.* **1,** 758–770 (2017).

10. Guo, M. *et al.* Cell volume change through water efflux impacts cell stiffness and stem cell fate. *Proc. Natl. Acad. Sci.* **c,** 201705179 (2017).

11. Nilius, B. & Honoré, E. Sensing pressure with ion channels. *Trends Neurosci.* **35,** 477–486 (2012).

12. Dalby, M. J., Gadegaard, N. & Oreffo, R. O. C. Harnessing nanotopography and integrin-matrix interactions to influence stem cell fate. *Nat. Mater.* **13,** 558–69 (2014).

13. Hulshof, F. F. B. *et al.* Mining for osteogenic surface topographies: In silico design to in vivo osseo-integration. *Biomaterials* **137,** 49–60 (2017).

14. Siddappa, R. *et al.* cAMP / PKA pathway activation in human mesenchymal stem cells in vitro results in robust bone formation in vivo. **105,** (2008).

15. Doorn, J. *et al.* A small molecule approach to engineering vascularized tissue. *Biomaterials* **34,** 3053–3063 (2013).

16. Jukes, J. M. *et al.* Endochondral bone tissue engineering using embryonic stem cells. *Proc. Natl. Acad. Sci.* **105,** 6840–6845 (2008).

17. Woolley, J. F. & Al-Rubeai, M. The application of SELDI-TOF mass spectrometry to mammalian cell culture. *Biotechnol. Adv.* **27,** 177–184 (2009).

18. Walther, T. C. & Mann, M. Mass spectrometry-based proteomics in cell biology. *J. Cell Biol.* **190,** 491–500 (2010).

19. Rolandsson Enes, S. *et al.* Quantitative proteomic characterization of lung-MSC and bone marrow-MSC using DIA-mass spectrometry. *Sci. Rep.* **7,** 1–12 (2017).

20. Abdelmoula, W. M. *et al.* Data-driven identification of prognostic tumor subpopulations using spatially mapped t-SNE of mass spectrometry imaging data. *Proc. Natl. Acad. Sci.* **113,** 12244–12249 (2016).

21. Downing, T. L. *et al.* Biophysical regulation of epigenetic state and cell reprogramming. *Nat. Mater.* **12,** 1154–1162 (2013).

22. Cochran, D. L. The scientific basis for and clinical experiences with Straumann implants including the ITI Dental Implant System: a consensus report. *Clin. Oral Implants Res.* **11 Suppl 1,** 33–58 (2000).

23. Zhao, Y. *et al.* High-definition micropatterning method for hard, stiff and brittle polymers. *Mater. Sci. Eng. C* **71,** 558–564 (2017).

24. Hulshof, F., de Boer, J. & Stamatialis, D. F. TopoChip: technology for instructing cell fate and morphology via designed surface topography. (2016).

⠞⠕⠏⠕⠛⠗⠁⠏⠓⠊⠉⠁⠇⠇⠽ ⠑⠝⠓⠁⠝⠉⠑⠙ ⠉⠑⠇⠇ ⠉⠥⠇⠞⠥⠗⠑ ⠎⠽⠎⠞⠑⠍⠎ ⠞

⠕⠏⠕⠛⠗⠁⠏⠓⠊⠉⠁⠇⠇⠽ ⠑⠝⠓⠁⠝⠉⠑⠙ ⠉⠑⠇⠇ ⠉⠥⠇⠞⠥⠗⠑ ⠎⠽⠎⠞⠑⠍⠎ ⠞⠕

⠕⠛⠗⠁⠏⠓⠊⠉⠁⠇⠇⠽ ⠑⠝⠓⠁⠝⠉⠑⠙ ⠉⠑⠇⠇ ⠉⠥⠇⠞⠥⠗⠑ ⠎⠽⠎⠞⠑⠍⠎ ⠞⠕ ⠊⠝

⠗⠁⠏⠓⠊⠉⠁⠇⠇⠽ ⠑⠝⠓⠁⠝⠉⠑⠙ ⠉⠑⠇⠇ ⠉⠥⠇⠞⠥⠗⠑ ⠎⠽⠎⠞⠑⠍⠎ ⠞⠕ ⠊⠝⠙

⠁⠏⠓⠊⠉⠁⠇⠇⠽ ⠑⠝⠓⠁⠝⠉⠑⠙ ⠉⠑⠇⠇ ⠉⠥⠇⠞⠥⠗⠑ ⠎⠽⠎⠞⠑⠍⠎ ⠞⠕ ⠊⠝⠙⠥⠉

⠓⠊⠉⠁⠇⠇⠽ ⠑⠝⠓⠁⠝⠉⠑⠙ ⠉⠑⠇⠇ ⠉⠥⠇⠞⠥⠗⠑ ⠎⠽⠎⠞⠑⠍⠎ ⠞⠕ ⠊⠝⠙⠥⠉⠑

⠉⠁⠇⠇⠽ ⠑⠝⠓⠁⠝⠉⠑⠙ ⠉⠑⠇⠇ ⠉⠥⠇⠞⠥⠗⠑ ⠎⠽⠎⠞⠑⠍⠎ ⠞⠕ ⠊⠝⠙⠥⠉⠑ ⠁⠝

⠇⠇⠽ ⠑⠝⠓⠁⠝⠉⠑⠙ ⠉⠑⠇⠇ ⠉⠥⠇⠞⠥⠗⠑ ⠎⠽⠎⠞⠑⠍⠎ ⠞⠕ ⠊⠝⠙⠥⠉⠑ ⠁⠝⠙

⠇⠽ ⠑⠝⠓⠁⠝⠉⠑⠙ ⠉⠑⠇⠇ ⠉⠥⠇⠞⠥⠗⠑ ⠎⠽⠎⠞⠑⠍⠎ ⠞⠕ ⠊⠝⠙⠥⠉⠑ ⠁⠝⠙ ⠍

⠑⠝⠓⠁⠝⠉⠑⠙ ⠉⠑⠇⠇ ⠉⠥⠇⠞⠥⠗⠑ ⠎⠽⠎⠞⠑⠍⠎ ⠞⠕ ⠊⠝⠙⠥⠉⠑ ⠁⠝⠙ ⠍⠕⠝

⠝⠓⠁⠝⠉⠑⠙ ⠉⠑⠇⠇ ⠉⠥⠇⠞⠥⠗⠑ ⠎⠽⠎⠞⠑⠍⠎ ⠞⠕ ⠊⠝⠙⠥⠉⠑ ⠁⠝⠙ ⠍⠕⠝⠊⠞

⠁⠝⠉⠑⠙ ⠉⠑⠇⠇ ⠉⠥⠇⠞⠥⠗⠑ ⠎⠽⠎⠞⠑⠍⠎ ⠞⠕ ⠊⠝⠙⠥⠉⠑ ⠁⠝⠙ ⠍⠕⠝⠊⠞⠕⠗

⠝⠉⠑⠙ ⠉⠑⠇⠇ ⠉⠥⠇⠞⠥⠗⠑ ⠎⠽⠎⠞⠑⠍⠎ ⠞⠕ ⠊⠝⠙⠥⠉⠑ ⠁⠝⠙ ⠍⠕⠝⠊⠞⠕⠗

⠑⠙ ⠉⠑⠇⠇ ⠉⠥⠇⠞⠥⠗⠑ ⠎⠽⠎⠞⠑⠍⠎ ⠞⠕ ⠊⠝⠙⠥⠉⠑ ⠁⠝⠙ ⠍⠕⠝⠊⠞⠕⠗ ⠍⠑

⠉⠑⠇⠇ ⠉⠥⠇⠞⠥⠗⠑ ⠎⠽⠎⠞⠑⠍⠎ ⠞⠕ ⠊⠝⠙⠥⠉⠑ ⠁⠝⠙ ⠍⠕⠝⠊⠞⠕⠗ ⠍⠑⠉⠓

⠑⠇⠇ ⠉⠥⠇⠞⠥⠗⠑ ⠎⠽⠎⠞⠑⠍⠎ ⠞⠕ ⠊⠝⠙⠥⠉⠑ ⠁⠝⠙ ⠍⠕⠝⠊⠞⠕⠗ ⠍⠑⠉⠓⠁⠝

⠇ ⠉⠥⠇⠞⠥⠗⠑ ⠎⠽⠎⠞⠑⠍⠎ ⠞⠕ ⠊⠝⠙⠥⠉⠑ ⠁⠝⠙ ⠍⠕⠝⠊⠞⠕⠗ ⠍⠑⠉⠓⠁⠝⠕

⠉⠥⠇⠞⠥⠗⠑ ⠎⠽⠎⠞⠑⠍⠎ ⠞⠕ ⠊⠝⠙⠥⠉⠑ ⠁⠝⠙ ⠍⠕⠝⠊⠞⠕⠗ ⠍⠑⠉⠓⠁⠝⠕⠃⠊

⠥⠇⠞⠥⠗⠑ ⠎⠽⠎⠞⠑⠍⠎ ⠞⠕ ⠊⠝⠙⠥⠉⠑ ⠁⠝⠙ ⠍⠕⠝⠊⠞⠕⠗ ⠍⠑⠉⠓⠁⠝⠕⠃⠊⠕⠇

⠞⠥⠗⠑ ⠎⠽⠎⠞⠑⠍⠎ ⠞⠕ ⠊⠝⠙⠥⠉⠑ ⠁⠝⠙ ⠍⠕⠝⠊⠞⠕⠗ ⠍⠑⠉⠓⠁⠝⠕⠃⠊⠕⠇⠕⠛

⠗⠑ ⠎⠽⠎⠞⠑⠍⠎ ⠞⠕ ⠊⠝⠙⠥⠉⠑ ⠁⠝⠙ ⠍⠕⠝⠊⠞⠕⠗ ⠍⠑⠉⠓⠁⠝⠕⠃⠊⠕⠇⠕⠛⠽

Chapter 9

Valorization

Introducing the TopoWellPlate in cell culture laboratories

Introduction

In this chapter, we discuss the valorization opportunities for the results obtained in this thesis. The definition of valorization, as provided by the National Valorization Committee (2011:8), stated that: "With knowledge valorization one creates value from knowledge. For this, knowledge needs to be suitable and/or available for social and/or economic use"[1].

Valorization has been an often encountered topic throughout the course of my PhD-trajectory. Both the laboratory of Cell Biology Inspired Tissue Engineering (cBITE) and Materiomics BV use the TopoChip platform, which repeatedly highlighted our differences in priorities. Materiomics aims to commercialize the TopoChip platform via patented surface topographies which can improve the interaction between implanted materials and the human body. In contrast, within cBITE we focus on unravelling the underlying mechanisms of mechanotransduction by which surface topography enhanced biomaterials control cell behavior. This results in a great conflict of interest. Where cBITE wants to share its scientific findings as broad as possible, Materiomics needs to keep all its findings secret till a patent has been filed. Moreover, cBITE's output model consists of publications in scientific journals, whereas Materiomics' output model involves filing patents and the major issue is the difference in lag time and the impact of publishing on novelty claims. A scientist who hinted at a certain molecular mechanism of surface topography-induced cell signaling in the discussion section of a minor article can still publish a Nature paper on that topic years later. In contrast, a correlation on topography design and functionality presented at the obscurest of conferences can block the protection of a block buster application of that correlation years later. Therefore, Materiomics is more cautious with disclosing information in the form of patents or scientific publications than cBITE, resulting in a longer lag time. Nevertheless, Materiomics and cBITE can benefit from one another, in terms of methods development, data analysis and obtained results. However, such a relationship should follow certain rules in order to protect the intellectual property of the TopoChip platform. As a consequence, obtained results were – without exception – handled as confidential. Using images that revealed material details and its accompanying data were not to be presented, and some of the chapters in this thesis could only be published after the patents were filed. To supervise this confidentiality, a strict procedure was followed for all output coming from cBITE before it was published in any way. This included revision by the cBITE chair first, followed by strategic considerations about the presented findings by Materiomics' business development team and CEO. Altogether, it is evident that valorization and scientific research can go hand-in-hand but one needs to know the rules that apply to both become successful.

Societal impact of this thesis

Scientists try to gain knowledge and spread this knowledge in the public domain. Between researchers, scientific communication occurs mainly via publications in peer-reviewed journals or at conferences and symposia. However, in order to create societal awareness around research topics and findings, there is a need to reach out via different routes as well.

The work presented in this thesis was largely financed by European Union, as the STELLAR project (Grant Agreement No. 305436) under the Seventh Framework Program (FP7/2007-2013). Within the STELLAR consortium – coordinated by the Nephrology department of the Leiden University Medical Centre (LUMC) – we strived for kidney function regeneration for patients suffering from chronic kidney diseases. In order to create societal awareness, significant energy was put in the communication of our work towards the public. Besides a regular website (http://www.stellarproject.eu/), the consortium invested in their visibility using social media (https://nl-nl.facebook.com/StellarStemCellsInKidneyDisease/). Via these routes, a follower base of hundreds of interested people (scientists and non-scientists) was created (October 2017), which led to many interesting discussions and collaborations in science as well as in art. Furthermore, the head of the STELLAR consortium (prof. Rabelink, LUMC Nephrology) appeared in a public television show on January 20 2015, (Tijd voor MAX) to elaborate on the latest progress made in kidney regeneration research (https://www.omroepmax.nl/pers/persberichten/september/tijd-voor-max-goede-doelenspecial-de-nierstichting/). This resulted in an information flow from our international research consortium towards the public domain, where many patients and their surroundings were reached, as well as our peers. The content of chapter 6, in which we identified conditions to optimise kidney stromal cell biology, particularly fitted this outreach strategy.

Chapters 3 and 4 comprise a more fundamental type of research, and the societal impact of this work seems to be less prominent. These chapters are in a sense more focussed on gaining knowledge. This knowledge can be useful in future research to elucidate the mechanism of action in biomaterials-controlled cell behaviour. Subsequently, we can design biomaterials rationally to perform specific tasks at the site of implantation. This could potentially result in additional positive effects of the biomaterials on their direct environment, and at the same time, diminished influence of negative side effects. Although the knowledge gained in chapter 3 and 4 does not directly create societal impact at this moment, it could be the basis of future discoveries with more impact since it contributes to the development of a platform technology.

The TopoWellPlate platform developed in chapter 5 did already progress along the Technology Readiness Level (TRL) scale (table 1). To assess technological development, this guideline was introduced by the NASA in 1974. More recently, the guidelines were adapted by the European Union, where it is now part of the Horizon 2020 guidelines[2]. The TRL-scale reaches from basic technology research (TRL1) towards full testing of an operation (TRL9).

The TopoWellPlate is a platform with potential to be further developed into an industrial product. Besides the prototype fabrication and proof of principle as presented in chapter 5 (TRL1/2), chapter 6 adds a more mature feasibility study for the TopoWellPlate concept (TRL2/3). However, full maturation (TRL9) of this product is needed in order to obtain its potential economic value.

Table 1: Technology Readiness Level definitions as published by the European Union. (Horizon2020 – Work Programme 2014-2015, General Annexes G)

Technology Readiness Level	Description
TRL 1	Basic principles observed
TRL 2	Technology concept formulated
TRL 3	Experimental proof of concept
TRL 4	Technology validated in lab
TRL 5	Technology validated in relevant environment
TRL 6	Technology demonstrated in relevant environment
TRL 7	System prototype demonstration in operational environment
TRL 8	System complete and qualified
TRL 9	Actual system proven in operational environment

Opportunities for the TopoWellPlate

In previous work using the TopoChip platform, we showed the beneficial properties of surface topographies over unpatterned tissue culture plastics for multiple biological models. For example, a prolonged hepatocyte viability *in vitro*[3], xeno-free IPSC stemness maintenance and self-renewal[4], and morphology specific secretion profiles of kidney-derived stromal cells (chapter 6 of this thesis).

Hepatocytes are the major cell type in the liver and account for more than 70% of its total tissue weight. Due to the detoxification activity of the liver, hepatocytes are used in drug development screening experiments by pharmaceutical companies. Currently, the golden standard for culturing hepatocytes only allows for an 8 day period to perform experiments, after which cell viability significantly reduces and cells detach. However, Materiomics identified surface topographies which increased the lifespan of hepatocytes for up to 30 days. Providing pharmaceutical companies with TopoWellPlates which are optimized for hepatocyte culture might therefore be of great interest to both parties. To be able to provide such a platform to these companies, Materiomics needs to further progress along the TRL-ladder with the TopoWellPlate platform. In order to do so, they assessed the current production method of the TopoWellPlate prototype and started exploring alternative production methods, which will be discussed in the next paragraph.

The need for the TopoWellPlate in drug development is based on the poor translation between the studied disease model and the current *in vitro* experimental set-up. Cells which are isolated from the human body experience a dramatic change in microenvironment when cultured on tissue culture plastic. The cells' new environment causes changes in cellular

phenotype, and alters functionality and potency. In drug development, testing of novel compounds is preferably performed on human primary cells in order to create a biological model as close as possible to the *in vivo* situation. However, due to afore mentioned reasons, the *in vitro* models are often far from ideal. Furthermore, the use of primary cells can be accompanied by more difficulties, as seen by the decrease in viability in the hepatocyte example. As an alternative, drug screening is typically performed on cell lines. And after the screening phase, the selected drugs need to be tested in animal models. Using topographies – which create an optimized culture environment for human primary cells – might help to overcome the need for animal studies, since the *in vitro* work takes up less time, and is performed in a more relevant biological system. Pharmaceutical companies are interested in the TopoWellPlate system since animal studies take up a large fraction of the total drug development budget (annually between 100 million and 1 billion)[5]. Reduction of these costs using TopoWellPlate technology might be very attractive in the pharmaceutical industry, where a total of approxamitely 55 billion dollars is spend on research and development for drug development[6].

Besides creating a product for the pharmaceutical industry, the TopoWellPlate can be also used in many other research facilities around the world. Of note, compared to the research and development budget in the pharma-industry, there is significantly less money spent in the academic world for the possible application of TopoWellPlate technology. As mentioned before, the TopoWellPlate can be used as a cell culture system to study models known to contain a mechanobiological component. More-and-more models are described to have a mechanosensitive mechanism. Let's highlight one example from this wealth of mechanoresponsive biological models, e.g. induced pluripotent stem cell (IPSC) culture. Since the introduction of IPSCs in 2006, many laboratories around the world used the Yamanaka factors to reprogram adult cells into pluripotent cells. Since IPSCs can potentially become every cell type of the human body and also divide infinitely, it is seen as an ideal cell source for tissue regeneration. One of the difficulties to overcome before these cells can be used for implantation is to eliminate the use of animal derived components in IPSC cultures. Fetal bovine serum as well as a protein coating is needed for successful IPSC cultures in which the cells proliferate while maintaining their pluripotency. In the search for a xeno-free cell culture system, we identified a specific surface topography on which IPSCs maintained their stemness markers for a prolonged period of time while continuing to proliferate. Obviously, implementing this surface topography as a standard in cell culture plastic for IPSC cultures could greatly reduce the difficulties in translating *in vitro* experiments to clinical application. Unfortunately, it was not possible to create value by valorization of this knowledge due to a conflict in novelty. Analysis of our findings as claimed in our manuscripts gives us: the identification of a surface structure which maintained the undifferentiated state of stem cells without the use of a feeder-layer. Prior to our observations, a Danish group published a paper with a similar scientific message: the identification of a distinct surface structure for undifferentiated expansion of stem cells[7]. Even though the details of the papers

differed greatly (e.g. human IPSCs vs. mouse embryonic stem cells, polystyrene substrates vs. coated silicon, and different defined surface structures) the novelty of our findings was affected. As a result, there was no ground to claim a novelty which could be patented and used for commercialization.

One can imagine that the TopoChip platform is an ideal starting point to explore many more biological models in which surface topography can improve cell culture. To improve our visibility as a platform in the field, we could perform more TopoChip or TopoWellPlate screens in order to identify ideal topographies for, and subsequently distribute TopoWellPlates to interested research groups. In terms of cell-material research, an additional benefit will be the extra amount of data produced as a result of using our defined surface topographies. This growing dataset on topography induced molecular processes can become valuable for compiling the canonical pathway of mechanotransduction (introduced in chapter 1), one of cBITE's main research topics.

The TopoWellPlate as a tissue culture plastic product

Regular 96-well plates cost around 2 euro per plate. However, in order to create an optimized cell culture environment there is also a need for defined culture medium, coatings, gels or a feeder layer, which makes the cell culture much more expensive. Regular tissue culture plates are typically produced using injection moulding. Here, liquid polystyrene (or other polymers) is poured into a mould, creating a multi-well plate once cooled down. Production of TopoWellPlates can be executed using a similar process, and requires in principle only an adjustment of the mould. Here, the cell culture surface area of the mould should be enhanced with the surface topography of interest. Obviously, collaborating with a tissue culture plastic producing company, such as Corning, Nunc, or Greiner, would greatly improve the know-how needed for translating the current more prototype-like state of the TopoWellPlate into a product of industrial quality. Such a collaboration would upgrade the TopoWellPlate as a product from its current TRL3 status towards TRL7/8 which is then ready for TRL9 implementation.

Creating topography enhanced moulds for injection moulding will have an initial cost prize, and per produced TopoWellPlate, a small additional volume of polystyrene to create the topography structure. However, once the production line is created for TopoWellPlates – containing e.g. a surface topography specifically defined for 1 cell type – the production price per TopoWellPlate will approach a traditional well plate production price. And as mentioned above, it will be relatively easy to perform a TopoChip screen to find a surface topography which can be implemented in new biological models. Using this strategy, we will be able to develop optimized TopoWellPlates for any research line.

Introducing a variety of cell type-specific well plates to the market will be revolutionary for *in vitro* cell biology[8]. Since standard cell culturing has already been well-established for decennia – e.g. using regular unpatterned tissue culture plastics – it will take some effort to convince researchers to implement the TopoWellPlate into their protocols. To achieve this, it will be necessary to show the beneficial properties of surface topographies in significant scientific journals, and building a portfolio of topography induced phenotypes. Furthermore, we need to create a network of collaborators in different fields of research which we provide with topographically enhanced cell culture plastics. This will allow them to familiarize themselves with the TopoWellPlate system, and subsequently, share results and experiences among peers. Since the TopoWellPlate is not the first innovation for cell cultureware which aims to become an integral part of the cell cultureware market, we can use previous success stories, such as the one described below, to design a potential market strategy for the TopoWellPlate as well.

In late 2005, a research group led by Sally Meiners published a paper on synthetic electrospun fibers which enhanced neural growth *in vitro*[9]. In this work, the authors emphasized the need for a three-dimensional microenvironment for neural cells *in vitro* to facilitate cell adhesion and neural outgrowth. Their electrospun nanofibers were shown to create such an environment, and furthermore, the synthetic nature of the material and lack of animal derived components made it applicable in a clinical setting. Within a year a second paper was published using this material, in which the authors demonstrated the beneficial effect of the nanofibers for self-renewal of mouse embryonic stem cells[10]. To commercialize this scientific finding and create a cell culture product of industrial quality, Donaldson Co., Surmodics, Inc., and Corning Inc. collaborated in the product development in 2006. Next, in 2008, an application note was released by Corning Inc. on a novel cell culture system – Ultra-Web – in which the benefits of the electrospun nanofibers over collagen coatings was described for hepatocytes[11]. Corning inc. is a leading company in the production of cell cultureware with yearly total expenses for all research and development of approximately 750 million euros. In 2016, Corning's revenues from external costumers for cell culture products were 327 million US dollars[12]. Currently, Ultra-Web multi-well plates are commercially available for € 31.50 per plate (Corning® 96 Well Flat Clear Bottom Black Polystyrene Ultra-Web™ Synthetic Surface Microplates, with Lid, Sterile (Product #3872XX1)) in the corning catalogue. Unfortunately, no detailed information is available about the percentage of revenues for Corning Inc. that is coming from the sales of Ultra-Web cell culture plates.

Once the TopoWellPlate is developed into a cell culture plate of industrial quality, it can probably enter the market for a similar price per plate as the Ultra-Web plates, e.g. € 30.00. Since we estimated the production costs of our plates to be only slightly higher than regular 96-well plates, the profit per well plate could be around 30 – 2 = € 28.00 per plate. A PubMed query revealed that over the last 5 years 2133 papers were published related to primary hepatocytes and drugs. For each of these papers, it can be expected that cells were maintained in culture for multiple weeks during which the experiments were executed. If we assume that

the total cell culture time is 2 months, in which 3 plates are used per week, a publication would typically require 8 × 3 = 24 plates. Following this hypothesis, the profit of the TopoWellPlate could have reached 24 (TopoWellPlates) × 2133 (published papers) × 28 (€ profit per plate) = € 1,433,376 over the last 5 years. This is solely based on published results from academic institutions using primary hepatocytes for drug development or the unravelling of molecular mechanisms. Obviously, similar figures could be applied for other cell types and research lines, and the use of TopoWellPlates in the pharmaceutical industry should give rise to even bigger numbers due to their high experimental capacity.

Conclusion

The TopoWellPlate system has a great potential for economical valorization. It is a cell culture tool which can be potentially implemented in the majority of cell biology laboratories around the world. We can offer those laboratories optimized cell culture plates which can overcome many types of difficulties that researchers are faced with when culturing all these different cell types. Furthermore, as a positive side-effect, all the data generated on the TopoChip-derived defined surface topographies can be used to create a fitting canonical pathway of mechanotransduction.

References

1. Landelijke Commissie Valorisatie. in *Waardevol: Indicatoren voor Valorisatie* 1–40 (2011).

2. European Commission. in *HORIZON 2020 WORK PROGRAMME 2014/2015 European research infrastructures - General Annexes* **2015,** (2015).

3. Materiomics. Designed Topographies Enable Long-term In Vitro Hepatocyte Culture Model. 1–5 (2015).

4. Reimer, A. *et al.* Scalable topographies to support proliferation and Oct4 expression by human induced pluripotent stem cells. *Sci. Rep.* **6,** 18948 (2016).

5. Morgan, S., Grootendorst, P., Lexchin, J., Cunningham, C. & Greyson, D. The cost of drug development: A systematic review. *Health Policy (New. York).* **100,** 4–17 (2011).

6. CSDD. Tufts Center for the Study of Drug Development. *Briefing Cost of Developing a New Drug Innovation in the Pharmaceutical Industry : New Estimates of R & D Costs* 617–636 (2014).

7. Markert, L. D. *et al.* Identification of distinct topographical surface microstructures favoring either undifferentiated expansion or differentiation of murine embryonic stem cells. *Stem Cells Dev.* **18,** 1331–1342 (2009).

8. Ryan, J. A. Evolution of Cell Culture Surfaces. *BioFiles* 8–11 (2008).

9. Ahmed, I. *et al.* Three-dimensional nanofibrillar surfaces covalently modified with tenascin-C-derived peptides enhance neuronal growth in vitro. *J. Biomed. Mater. Res. - Part A* **76,** 851–860 (2006).

10. Nur-E-Kamal, A., Ahmed, I., Kamal, J., Schindler, M. & Meiners, S. Three-Dimensional Nanofibrillar Surfaces Promote Self-Renewal in Mouse Embryonic Stem Cells. *Stem Cells* **24,** 426–433 (2006).

11. Rothenberg, M., Bryhan, M., Faruqi, F., Briggs, M. W. & Upton, T. *Human and Rat Hepatocytes Cultured on Ultra-Web™ and Ultra-Web Polyamine Synthetic Matrices show Enhanced Physiologic Activity When Compared to Collagen*. (2008).

12. Corning. *Corning Inc. Annual report 2016*. (2016).

⠠⠞⠓⠑ ⠠⠟⠥⠊⠉⠅ ⠃⠗⠕⠺⠝ ⠋⠭ ⠚⠥⠍⠏⠎ ⠕⠧⠑⠗ ⠞⠓⠑ ⠇⠁⠵⠽ ⠙⠕⠛

Epilogue

⠠⠞⠓⠑ ⠠⠟⠥⠊⠉⠅ ⠃⠗⠕⠺⠝ ⠋⠭ ⠚⠥⠍⠏⠎ ⠕⠧⠑⠗ ⠞⠓⠑ ⠇⠁⠵⠽ ⠙⠕⠛

Summary

Regenerative medicine solutions become increasingly interesting for solving health problems of patients. Here, the patient's own cells can be used in combination with a biomaterial in order to regenerate the function of a damaged tissue. Such a biomaterial is preferably able to support cells as a biocompatible carrier and additionally able to control the behavior of the cells which are in direct contact. To develop functional biomaterials able to control cell behavior in desired ways, there is a need to understand the mechanisms underlying cell-material interactions. In **chapter 1,** we introduced these interactions and compared the native environment of cells *in vivo* with the engineered environment we introduce cells to *in vitro*. Here, we were especially interested in physical stimuli coming from those biomaterials, and how these stimuli trigger cell-material interaction via mechanotransduction. Furthermore, we introduced the research aims of this thesis, the development of novel tools to induce and monitor mechanobiology and touched upon the involved molecular signaling.

Before starting the experimental work, we reviewed the literature to learn about the wonderful ways nature has found to deal with mechanobiological problems. In **chapter 2,** we explored what is needed to create a biological system 'ready-to-react' to physical stimuli, and hypothesized ways to use this knowledge for designing new instructive biomaterials.

In **chapter 3,** we used a holistic approach to explore the molecular mechanisms underlying mechanobiological osteogenic differentiation. For this, we selected a TopoChip-derived surface topography which was proven to induce osteogenesis solely by physical stimuli from the surface structure. We found a strong correlation between cytoskeletal organization and alkaline phosphatase expression, a marker for osteogenesis. Furthermore, we found pronounced differences in focal adhesion complex formation on topographically enhanced substrates compared to cells cultured on flat substrates. Using a candidate approach, we observed the early activation of mechanosensitive proteins YAP, ERG1, and SRF, which diminished after 24 hours when cell adhesion was completed. Transcriptomics analysis revealed a clear role for HIF-induced gene expression in cells cultured on the osteogenic topographies. Interestingly, a non-canonical HIF-signaling must have been initiating this gene expression since we did not observe a hypoxia-like response. Finally, we also found a pronounced role for epigenetics based on gene expression profiles which matched the epigenetic affecting drug trichostatin A and dramatically deformed nuclei.

Besides differentiation, we also explored the influence of surface topography on basic cell physiology. In **chapter 4,** we described the adaptation of cells to topographically enhanced substrates which takes place during the first hours after attachment. Here, we observed a quick cellular response that led to a reduction of cell and nucleus volumes. Furthermore, these cells also lowered their metabolism and inhibited cell cycle progression. Interestingly, cells cultured on topographically enhanced substrates – with a lower metabolism and proliferation rate – were less affected by anti-cancer drugs.

To study cell-topography interaction in high-throughput using assays other than imaging-based, we developed the TopoWellPlate. In **chapter 5,** we introduced this topographically enhanced 96-well plate and described the cleanroom production pipeline to produce these plates. Furthermore, we measured the metabolic activity via metabolized culture medium as a proof of principle experiment to show the potential of the TopoWellPlate as a cell culture tool. We observed that our surface topographies all resulted in a reduction of mitochondrial activity (as a measure of the cellular metabolism) with a maximum of a 2.5-fold difference in this screen. The use of the TopoWellPlate was further explored in **chapter 6**, and this time in a clinically more relevant context. Here, we screened surface topographies for their influence on the secretome fingerprints of kidney-derived perivascular stromal cells and bone marrow-derived mesenchymal stromal cells. We observed a strong correlation between cell shape and secretion fingerprint for the kidney-derived cells, however, this correlation was less pronounced in bone marrow-derived cells.

In the final experimental chapter, **chapter 7**, we introduced the NanoTopoChip. This TopoChip-sibling has topographical features at the nanometer scale which caused a completely different interaction with cells compared to micrometer scale topographical features. Using the NanoTopoChip we were able to induce a wide variety of cell-topography interactions, ranging from very strong cell attachment with many filopodia, towards a lack of focal adhesion complex formation and resulting in a diffuse g-actin organization.

In sum, this thesis provides new evidence on specific cellular responses to, and initiated molecular signaling by surface topography, and thereby contributes to elucidation of underlying mechanisms of mechanotransduction. Additionally, two novel topographically-enhanced cell culture systems are introduced proven to useful to induce and monitor mechanobiology. These conclusion are discussed in **chapter 8**, were we carefully place notice on (dis)advantages of the used read-outs and the meaning of the results. Furthermore, we suggested development of novel materials and analytic tools as envisioned future directions for cell-surface topography research. Finally, in **chapter 9**, we commented on the potential societal and economic impact of this thesis, and in particular the development of the TopoWellPlate as an optimized cell culture tool ideal for many research laboratories and pharmaceutical companies.

⠠⠞⠓⠑ ⠠⠟⠥⠊⠉⠅ ⠃⠗⠕⠺⠝ ⠋⠭ ⠚⠥⠍⠏⠎ ⠕⠧⠑⠗ ⠞⠓⠑ ⠇⠁⠵⠽ ⠙⠕⠛

Samenvatting

Tijdens ons leven kunnen verschillende functies in ons lichaam verminderen in kwaliteit of zelfs helemaal weg vallen. Denk hierbij aan chronische nierziekten of diabetes, maar ook bijvoorbeeld aan grote gaten in botten na het verwijderen van tumoren of versleten gewrichten. Momenteel zijn er voor veel van deze problemen oplossingen beschikbaar waarmee de functie (deels) wordt hersteld. Zo kan de nierfunctie deels over worden genomen door het dyaliseren van het bloed, het bloedsuikergehalte van diabetespatiënten gecontroleerd met het spuiten van insuline, en een versleten gewricht worden vervangen met een orthopedisch implantaat. Maar in plaats van een volledige functieovername zou het in veel gevallen eigenlijk meer gewenst zijn om het oude weefsel weer functioneel te herstellen. Dit is dan ook precies het doel van de regeneratieve geneeskunde.

In het wetenschapsveld van de regeneratieve geneeskunde worden talrijke van deze gezondheids-gerelateerde problemen onderzocht. Karakteristiek voor de oplossingen die via regeneratieve geneeskunde worden aangedragen is het gebruik van lichaamseigen cellen in combinatie met biomaterialen. Onder de verzamelnaam ‘biomaterialen’ vallen vele verschillende materialen, allemaal met unieke eigenschappen. Het idee achter het gebruik van biomaterialen in de regeneratieve geneeskunde is tweeledig: (1) zijn ze geschikt als dragermateriaal voor de cellen die moeten worden geïmplanteerd, en (2) er is de laatste 20 jaar steeds meer bewijs voor de mogelijkheden om cellen instructies te geven via deze biomaterialen. Waar een medicijn een specifieke chemische prikkel kan geven aan bijna alle cellen in het lichaam, kunnen biomaterialen ook juist heel specifiek de direct aangrenzende cellen stimuleren. Op deze manier kan bijvoorbeeld heel gericht de afgifte van medicijnen gereguleerd worden, en dat precies op de plaats in het lichaam waar de functie van het weefsel hersteld moet worden.

Bij het regenereren van weefsels is het ook van belang dat het weefsel kan groeien en dat oude cellen vervangen kunnen worden door nieuwe. Als bron voor deze groei en vernieuwing worden vaak volwassen stamcellen gebruikt. Deze kunnen uit de patiënt zelf worden gehaald. Het huidige onderzoek waarin biomaterialen gebruikt worden om weefselfuncties te herstellen richt zich met name op de interactie tussen de materialen en stamcellen. Via deze communicatie kunnen biomaterialen door hun chemische samenstelling stamcellen instructies geven. De mogelijkheden van dergelijke interacties worden momenteel veel onderzocht, en de bewijzen voor het gebruik stapelt zich op. Zo zijn er voorbeelden van biomaterialen die stamcellen kunnen laten delen, of kunnen laten differentiëren naar een meer gespecialiseerde cel die de functie kan overnemen van het beschadigde originele weefsel.

Naast de effecten van de chemische samenstelling zien we ook steeds meer voorbeelden waarin de fysieke eigenschappen van biomaterialen cellen instructies kunnen geven. Factoren die hierbij een rol spelen zijn bijvoorbeeld hoe hard of zacht het materiaal is, en de oppervlaktestructuur van het materiaal op micrometer- of zelfs de nanometerschaal. Het effect van materiaaloppervlaktestructuren op stamcellen is het thema van dit proefschrift. Hierin is geprobeerd om zoveel mogelijk te weten te komen over wat die fysieke prikkels nu precies

doen met stamcellen en waarom de cellen hierop reageren. Wanneer we de biologische mechanismes namelijk snappen kunnen we deze kennis gebruiken om heel gericht betere biomaterialen te ontwikkelen, en deze in te zetten om specifieke weefsels en functies te ondersteunen.

Om inzicht te krijgen in de invloed van fysieke prikkels op het functioneren van cellen hebben we in onze groep sinds een aantal jaar een door ons ontwikkeld speciaal celkweeksysteem. Op een stukje plastic van 2 bij 2 centimeter hebben we 66 bij 66 minuscule bakjes gecreëerd, elke met zijn eigen unieke oppervlaktestructuur op de bodem. Dit vernuftige hulpstuk noemen we de *TopoChip*, en wordt gebruikt om in één oogopslag 2176 unieke oppervlaktestructuren te bestuderen. (Notabene: 66 x 66 = 4356 bakjes, waarvan 4 bakjes zonder structuur (vlak): 4356 – 4 = 4352, en voor de zekerheid hebben we elke oppervlaktestructuur 2 keer opgenomen in het ontwerp: 4352 / 2 = 2176 unieke oppervlakte structuren) De oppervlaktestructuren die gebruikt zijn op de *TopoChip* zijn rijen van pilaren die door het repeterende gebruik een homogene structuur maken. De unieke vorm van deze pilaren geeft dus het unieke karakter aan de oppervlaktestructuur. Deze vorm vorm is gecreëerd door een computerprogramma wat driehoeken, cirkels en vierkanten heeft gecombineerd in willekeurige hoeveelheden, van willekeurige formaten en op willekeurige posities. Door 2176 verschillende oppervlaktestructuurontwerpen tegelijkertijd te bekijken kunnen we gaan uitrekenen welke eigenschappen van de structuur zorgen voor welke reactie van cellen. Met deze kennis kunnen we vervolgens ook gaan proberen te voorspellen hoe een oppervlaktestructuur eruit moet gaan zien om cellen te beïnvloeden, precies zoals wij dat willen. Op de experimenten in hoofdstuk 7 na, gebruiken we altijd oppervlaktestructuren afkomstig van de *TopoChip* op micrometer schaal.

In **hoofdstuk 1** wordt de vergelijking gemaakt tussen de directe omgeving van cellen in het menselijke lichaam en de manier waarop we deze omgeving na kunnen bootsen in het laboratorium. Welke chemische- en fysieke prikkels ontvangen cellen in het lichaam normaal gesproken, en welke prikkels willen wij namaken om precies de goede instructies te geven met behulp van biomaterialen. Momenteel is de kennis nog niet toereikend om alle mogelijke prikkels na te maken, maar de technologische ontwikkelingen die momenteel in volle vaart zijn maken dat er steeds nieuwe biomaterialen ontwikkeld kunnen worden. In **hoofdstuk 2** stellen we voor om naar de natuur om ons heen te kijken om daar naar voorbeelden te zoeken van biologische systemen die op fysieke prikkels reageren. Waarom zouden we zelf iets nieuws verzinnen als de natuur het in miljoenen jaren al tot in perfectie ontwikkeld heeft. Zo vinden we in de wonderlijke wereld om ons heen bijvoorbeeld planten die dicht gaan als ze worden aangeraakt ter bescherming tegen dieren die ze op willen eten, kleine propellers van zwemmende bacteriën die een functie hebben tijdens de aanhechting aan oppervlaktes, en de formatie van een laagje eelt op de huid van onze handen om onderliggende cellen te beschermen tegen herhaaldelijke wrijving.

In **hoofdstuk 3** richten we ons dan vervolgens op de mechanismen die cellen opstarten wanneer ze een fysieke prikkel krijgen die aanzet tot het vormen van bot. Door proeven uit te voeren hebben we geprobeerd te achterhalen wat er precies in cellen gebeurd wanneer ze aan een oppervlaktestructuur hechten waarvan we weten dat ze aanzetten tot het vormen van bot. We hebben gevonden dat cellen heel anders aanhechten aan deze materialen en vervolgens hun skelet ook anders organiseren. Verder hebben we gevonden dat ze vanaf het eerste moment van aanhechting al andere genen gaan gebruiken, en dus andere eiwitten aan gaan maken die dan door de cellen kunnen worden gebruikt. We hebben ook geobserveerd dat deze cellen sterk vervormde celkernen hebben, wat kan betekenen dat het gebruiken van het DNA in deze celkernen anders is dan in de conditie met een vlakke ondergrond. Wanneer we een compleet overzicht hebben van alle veranderingen in cellen die oppervlaktestructuren kunnen veroorzaken, kunnen we deze kennis gebruiken om vervolgens slimmere materiaaloppervlaktestructuren te ontwerpen. Met deze kennis kunnen we dan bijvoorbeeld oppervlaktes van orthopedische implantaten verbeteren, zodat hun levensduur in het lichaam verlengd zou kunnen worden.

Volledig geïntrigeerd door het effect dat oppervlaktestructuren op cellen kunnen hebben, zijn we in **hoofdstuk 4** dieper ingegaan op een tal van basale cellulaire processen die veranderen door fysieke prikkels. Zo hebben we waargenomen dat cellen hun volume snel kunnen verkleinen wanneer ze in aanraking komen met onze oppervlaktestructuren. Tegelijkertijd verkleinen ze ook het volume van de kern tot een derde, verlagen ze hun energieverbruik tot een derde en delen ze langzamer. We noemen dit ‘de aanpassing van cellen aan hun nieuwe omgeving’, waarin ze dus fysiek begrensd worden door de oppervlaktestructuur van het materiaal. Door deze aanpassingen in basale cellulaire processen bleken de cellen op oppervlaktestructuren bijvoorbeeld ook minder vatbaar voor medicijnen tegen kanker.

Om heel veel verschillende oppervlaktestructuren los van elkaar – maar op het zelfde moment – te kunnen testen, hebben we vervolgens een nieuw celkweeksysteem ontwikkeld. Deze celkweekplaat, de *TopoWellPlate*, wordt geïntroduceerd in **hoofdstuk 5**. Om te onderzoeken of deze nieuw ontwikkelde techniek werkt, hebben we het energieverbruik van de blootgestelde cellen tegelijkertijd voor 87 verschillende oppervlaktestructuren gemeten. In **hoofdstuk 6** pakken we vervolgens een klinisch meer relevant probleem aan met de *TopoWellPlate*. Hier onderzoeken we hoe oppervlaktestructuren stamcellen uit de nieren en uit het beenmerg kunnen beïnvloeden. Daarbij zijn we vooral geïnteresseerd in de stofjes die deze cellen uitscheiden, en of we controle kunnen krijgen over de samenstelling van het uitgescheidingsprofiel. Vooral in niercellen bleek er een sterke samenhang te zijn tussen de vorm van de cellen (welke afhangt van de onderliggende oppervlaktestructuur) en de kwantiteit waarin de verschillende stofjes worden uitgescheiden.

Waar de oppervlaktestructuren in de voorgaande hoofdstukken 10 micrometer hoog waren en tussen de 10 en 28 micrometer in doorsnede (1 micrometer = 0,001 millimeter), verkleinen we in **hoofdstuk 7** de oppervlaktestructuren naar de nanometerschaal (1 nanometer = 0,000001

millimeter). Het celkweeksysteem wat we hiervoor hebben ontwikkeld hebben we dan ook toepasselijk de *NanoTopoChip* genoemd. In vergelijking met de fysieke begrenzingen die cellen ervaren op de micrometerschaal-oppervlaktestructuren, zagen we dat nanometerschaal-oppervlaktestructuren vooral invloed had op de hechting van cellen en de daaruit volgende organisatie van het skelet.

In **hoofdstuk 8** plaatsen we al onze bevindingen in een overkoepelende context, en proberen we lering te trekken uit alles wat we hebben geobserveerd. Daarin komen vragen aan bod over wat we nu precies gemeten hebben met onze meetmethodes, wat de uitkomsten ons nu precies vertellen, wat we kunnen vertrouwen, en waar we nog vraagtekens bij moeten plaatsen. Verder formuleren we ideeën over toekomstige onderzoeksmogelijkheden, en zaken waarmee we verder moeten gaan om ze goed in kaart te brengen. Hier dekken we zowel onze ideeën over de cellen alsmede over de materialen die we ontwikkeld hebben.

Tot slot, in **hoofdstuk 9**, schetsen we wat de sociale en economische waarde kan zijn van de resultaten uit dit proefschrift. Hierin geven we aan wat we voor de maatschappij kunnen betekenen en hoe we bijvoorbeeld patiënten en geïnteresseerde kunnen bereiken. Verder hebben we een voorbeeld uitgewerkt waarin we stellen dat we de *TopoWellPlate* als commercieel verkrijgbaar product kunnen introduceren, en wat hiervan de financiële mogelijkheden zijn wanneer we de markten van de medicijnenindustrie en de wetenschap op de universiteiten aanboren.

⠠⠞⠓⠑ ⠠⠟⠥⠊⠉⠅ ⠃⠗⠕⠺⠝ ⠋⠭ ⠚⠥⠍⠏⠎ ⠕⠧⠑⠗ ⠞⠓⠑ ⠇⠁⠵⠽ ⠙⠕⠛

List of publications

Scientific publications

SL Vega, A Dhaliwal, V Arvind, PJ Patel, **NRM Beijer**, J de Boer, NS Murthy, J Kohn, PV Moghe. Organizational metrics of interchromatin speckle factor domains: integrative classifier for stem cell adhesion & lineage signaling. Integrative Biology (2015)

NRM Beijer, AS Vasilevich, B Pilavci, RK Truckenmüller, Y Zhao, S Singh, BJ Papenburg, J de Boer. TopoWellPlate: a well-plate-based screening platform to study cell–surface Topography interactions. Advanced Biosystems (2017)

GFB Hulshof, BJ Papenburg, AS Vasilevich, M Hulsman, Y Zhao, M Levers, N Fekete, M de Boer, H Yuan, S Singh, **NRM Beijer**, MA Bray, DJ Logan, M Reinders, AE Carpenter, C van Blitterswijk, D Stamatialis, J de Boer. Mining for osteogenic surface topographies: In silico design to in vivo osseo-integration. Biomaterials (2017)

GFB Hulshof, Y Zhao, AS Vasilevich, **NRM Beijer**, M de Boer, BJ Papenburg, C van Blitterswijk, D Stamatialis, J de Boer. NanoTopoChip: high-throughput nanotopographical cell instruction. Acta Biomaterialia (2017)

DG Leuning [ǂ], **NRM Beijer** [ǂ], NA du Fossé, S Vermeulen, E Lievers, C van Kooten, TJ Rabelink, J de Boer. The cytokine secretion profile of mesenchymal stromal cells is determined by surface structure of the microenvironment. [ǂ] Shared first author. (Under review)

AS Vasilevich, F Mourcin, A Mentink-Leusink, GFB Hulshof, **NRM Beijer**, Y Zhao, M Levers, BJ Papenburg, S Singh, AE Carpenter, D Stamatialis, C van Blitterswijk, K Tarte, J de Boer. Designed surface topographies control ICAM-1 expression in tonsil-derived human stromal cells. (Submitted)

S Zijl, AS Vasilevich, P Viswanathan, AL Helling, **NRM Beijer**, G Walko, C Chiappini, J de Boer, FM Watt. Micro-scaled topographies direct differentiation of human epidermal stem cells. (Submitted)

NRM Beijer, ZM Nauryzgaliyeva, EM Arteaga, L Pieuchot, K Anselme, J van de Peppel, AS Vasilevich, N Groen, N Roumans, DGAJ Hebels, J de Boer. Dynamic adaptation of mesenchymal stem cell physiology upon exposure to surface micropatterns. (In preparation)

NRM Beijer, A Dede-Eren, R Reihs, DGAJ Hebels, J van der Peppel, ZM Nauryzgaliyeva, S Vermeulen, MMJ Kamphuis, D Pereira, AS Vasilevich, S Singh, J de Boer. The mechanobiological fingerprint of osteogenesis. (In preparation)

Scientific communications related to this thesis

2013 Oral presentation at the 2nd Belgian Symposium on Tissue Engineering, Leuven, Belgium.

2013 Poster presentation at the 22nd Annual Conference of the Netherlands Society for Biomaterials and Tissue Engineering, Lunteren, the Netherlands.

2014 Oral presentation at the 23rd Annual Conference of the Netherlands Society for Biomaterials and Tissue Engineering, Lunteren, the Netherlands.

2015 Introducing the MERLN institute for regenerative medicine cBITE department to King Willem-Alexander, Maastricht, the Netherlands.

2015 Poster presentation at the NanoBioTech conference, Montreux, Switzerland.

2015 Poster presentation at the 24th Annual Conference of the Netherlands Society for Biomaterials and Tissue Engineering, Lunteren, the Netherlands.

2016 Pitched cBITE at the LINK opening cat-walk sessions elevated pitches, Maastricht, the Netherlands.

2016 Poster presentation at the Gordon Conference series on Signal Transduction by Engineered Extracellular Matrices, University of New England, Maine, United States.

2016 Oral presentation at the Dutch Society for Calcium and Bone Metabolism, Zeist, the Netherlands.

2017 Presented a workshop at the NanoBio Surfaces and Interfaces in Healthcare and Science meeting, Leuven, Belgium.

Awards

2013 ESF travel grant, Belgian symposium on Tissue Engineering, Leuven, Belgium

2015 Best poster presentation, NanoBioTech Conference, Montreux, Switzerland

2016 Best oral presentation, NVCB annual meeting, Zeist, the Netherlands

⠠⠞⠓⠑ ⠠⠟⠥⠊⠉⠅ ⠃⠗⠕⠺⠝ ⠋⠭ ⠚⠥⠍⠏⠎ ⠕⠧⠑⠗ ⠞⠓⠑ ⠇⠁⠵⠽ ⠙⠕⠛

Acknowledgements

Momenten om mensen te bedanken zijn er vaak, maar worden zeker wel eens voorbijgelopen zonder te gebruiken. De momenten om aan een groter publiek voor iemand je dank uit te spreken zijn daarentegen schaarster, maar daar kan je je wel beter op voorbereiden.

Jan, na een aantal jaar onder je hoede te hebben gestaan wil ik je bedanken voor al je begeleiding. Naast je prominente rol in mijn opleiding tot biomedisch technoloog, wil ik je ook zeker bedanken voor de leiding die je mij hebt gegeven tijdens mijn ontwikkeling als persoon, en natuurlijk voor het duwtje richting de toekomst. Dank voor alles, en ook zeker voor het feit dat dit proefschrift hier nu ligt!

Roman, even though your official role as co-promotor had not been established until recently, looking back at my trajectory you fit this perfectly! I attended various courses you are teaching, we had many interesting discussions throughout the last years and worked together on different projects, and shared multiple other nice moments! Thank you!

During my quest, I have had many many wonderful colleagues who helped me tremendously. Starting in Twente, in the department of Tissue Regeneration. I am grateful for everyone who spent time with me, both during and outside lab hours! Nathalie, Vanessa, Frits as part of Jan's group, but also Corina, Ana, Niloofar, Erik, Ziryan, Ivan, Carlos, Ravi, David, Paul, Feb, Angad, Joao, Lorenzo, Pamela, Tom and Anouk, Audrey and Carola. Furthermore, of course, the team of Materiomics with whom I have worked together for this entire period: Bernke, Marloes, Natalie, Yiping, Joris, Wei-Shu, James, Sandra and Donato.

And during my extended stay in Twente where I was warmly hosted by the Dirk's BST. Thank you Dimitrios, Ilaria, Natalia, Kasia, Denys and Lydia, I enjoyed my stay in your group very much and I really appreciate all the energy you all gave me! Uiteraard ook alle waardevolle momenten die ik heb gedeeld met Mike en Bas op kantoor, but also with the others from the department: Jos, Karin, Mark, Hetty, Pia, Jonas, Tony and Zhengchou.

Within the MERLN facilities I was able the finish the biggest part of my thesis, and I am very grateful for the opportunities I have gotten there. The enormous group of inspiring people I have worked with there is too big to name every person individually, but believe me, I am happy I have met all of you! In particular, Romina, Angelique, Pascal, Daniel, David, Afonso, Danielle, Timo, Denis, Andrea, Fiona, Jip, and Khadija. Keep up the good work!

Moving to Maastricht gave me the opportunity to work closely together with my team again, and I very much appreciated the great team spirit within cBITE! Speciale dank gaat uit naar Christine die mijn verhuizing heeft kunnen bewerkstelligen, mij heeft laten landen in Maastricht, en waar ik een goede vriend aan over houd. Dennie, naast alle humor die wij hebben kunnen delen, lunchmomenten en borreltjes, wil ik je ook zeker bedanken voor de enorme hulp tijdens de laatste maanden! Steven, het was heel fijn om jou bij mij in hetzelfde materiaalproductie-schuitje te hebben, en vooral de reisjes naar Twente steken erboven uit! Alex, we started together in Jan's group 5 years ago, and I want to thank you for all the nice

collaborations, and cool projects we worked on together. Furthermore, I am grateful to have worked with all the other bright people within cBITE: Pascal, Aurélie, Nadia, Ayşegül, Urnaa, Linfeng, Saïd and Jasia.

Without a doubt, I would not have been able to finish this thesis without the help of my great students! Heel erg bedankt voor je tomeloze inzet Bayram, samen hebben we prachtige resultaten behaald! Jéré, dank voor je ongelofelijk goede werk! Iedereen kon wel al zien dat jij succesvol een PhD-project aan zou kunnen. Estela, thank you so much for the happiness you brought into the team! Adapting so quickly to the other side of the world, and always with passion in the lab! And Zarina, you came in as an unexperienced young bachelor student, and walked out as a proud and independent researcher. Thank you very very much for all your energy the last year!

Marloes, wat fijn dat jij mijn paranimf bent! Ik kan bij het afronden van mijn promotie wel iemand gebruiken waarbij ik er altijd op vertrouw dat het wel goed komt! Wij verschillen zo erg op zoveel vlakken, maar ik denk ook dat dat juist maakt dat wij zo een goed team zijn! Heel erg bedankt voor alle steun en hulp!

Emo, waar moet ik beginnen! Bedankt dat jij mijn paranimf bent! Ons verhaal gaat echt al meer dan twintig jaar terug, en daarin hebben we echt alles samen meegemaakt! Als ik al onze mooie herinneringen op zou schrijven, zou het boekje dikker worden dan dit proefschrift! Ik kan je hiervoor niet genoeg bedanken!

En natuurlijk ook mijn andere vrienden, die door dik en dun altijd aan mijn zijde stonden! Ook al heb ik lang ver weg van jullie gewoond, stonden jullie altijd voor mij klaar. Ik ben heel erg dankbaar dat ik zulke fijne vrienden mag hebben als jullie! Tom, onze tijd in Enschede was heel bijzonder, en heeft ons voor het leven gevormd! Bedankt dat wij dit samen door hebben mogen maken! Jordi, ik weet niet waar jij de tijd en energie vandaan haalt, maar jij was echt altijd en overal bij wat ik me kan herinneren! Bedankt voor al je steun op de moeilijke, maar het meeste van de tijd natuurlijk op de gezellige momenten!

Maaike en Ata, heel erg bedankt voor jullie steun tijdens dit hele traject! Ook al zagen we elkaar door de afstand minder vaak dan mij lief was, heb ik jullie steun altijd gevoeld! Mede door het doorzettingsvermogen wat ik bij jullie heb gezien, heb ik dit proefschrift af kunnen ronden! Papa en Mama, zonder jullie vorming, steun, energie, enthousiasme, medeleven, laten blijken van trots, geloof in mij en liefde was dit proefschrift er niet geweest! Ik ben jullie heel erg dankbaar voor alles wat jullie voor mij hebben gedaan! Ik hou van jullie!

En tot slot, liebe Annelie! Met jou aan mijn zijde schijnt altijd de zon! Bedankt dat jij er altijd voor mij bent, en ook de laatste maanden mij erdoorheen hebt gesleept. Het is heel bijzonder geweest dat wij samen onze proefschriften tegelijkertijd af hebben kunnen ronden, en jouw steun hierin is onmeetbaar groot. Ik kijk heel erg uit naar onze toekomst! Ik hou van jou!

⠞⠕⠏⠕⠛⠗⠁⠏⠓⠊⠉⠁⠇⠇⠽ ⠑⠝⠓⠁⠝⠉⠑⠙ ⠉⠑⠇⠇ ⠉⠥⠇⠞⠥⠗⠑ ⠎⠽⠎⠞⠑⠍⠎ ⠞

⠕⠏⠕⠛⠗⠁⠏⠓⠊⠉⠁⠇⠇⠽ ⠑⠝⠓⠁⠝⠉⠑⠙ ⠉⠑⠇⠇ ⠉⠥⠇⠞⠥⠗⠑ ⠎⠽⠎⠞⠑⠍⠎ ⠞⠕

⠕⠛⠗⠁⠏⠓⠊⠉⠁⠇⠇⠽ ⠑⠝⠓⠁⠝⠉⠑⠙ ⠉⠑⠇⠇ ⠉⠥⠇⠞⠥⠗⠑ ⠎⠽⠎⠞⠑⠍⠎ ⠞⠕ ⠊

⠗⠁⠏⠓⠊⠉⠁⠇⠇⠽ ⠑⠝⠓⠁⠝⠉⠑⠙ ⠉⠑⠇⠇ ⠉⠥⠇⠞⠥⠗⠑ ⠎⠽⠎⠞⠑⠍⠎ ⠞⠕ ⠊⠝⠙

⠏⠓⠊⠉⠁⠇⠇⠽ ⠑⠝⠓⠁⠝⠉⠑⠙ ⠉⠑⠇⠇ ⠉⠥⠇⠞⠥⠗⠑ ⠎⠽⠎⠞⠑⠍⠎ ⠞⠕ ⠊⠝⠙⠥⠉

⠓⠊⠉⠁⠇⠇⠽ ⠑⠝⠓⠁⠝⠉⠑⠙ ⠉⠑⠇⠇ ⠉⠥⠇⠞⠥⠗⠑ ⠎⠽⠎⠞⠑⠍⠎ ⠞⠕ ⠊⠝⠙⠥⠉⠑

⠉⠁⠇⠇⠽ ⠑⠝⠓⠁⠝⠉⠑⠙ ⠉⠑⠇⠇ ⠉⠥⠇⠞⠥⠗⠑ ⠎⠽⠎⠞⠑⠍⠎ ⠞⠕ ⠊⠝⠙⠥⠉⠑ ⠁

⠇⠇⠽ ⠑⠝⠓⠁⠝⠉⠑⠙ ⠉⠑⠇⠇ ⠉⠥⠇⠞⠥⠗⠑ ⠎⠽⠎⠞⠑⠍⠎ ⠞⠕ ⠊⠝⠙⠥⠉⠑ ⠁⠝⠙

⠽ ⠑⠝⠓⠁⠝⠉⠑⠙ ⠉⠑⠇⠇ ⠉⠥⠇⠞⠥⠗⠑ ⠎⠽⠎⠞⠑⠍⠎ ⠞⠕ ⠊⠝⠙⠥⠉⠑ ⠁⠝⠙ ⠍

⠑⠝⠓⠁⠝⠉⠑⠙ ⠉⠑⠇⠇ ⠉⠥⠇⠞⠥⠗⠑ ⠎⠽⠎⠞⠑⠍⠎ ⠞⠕ ⠊⠝⠙⠥⠉⠑ ⠁⠝⠙ ⠍⠕⠝

⠝⠓⠁⠝⠉⠑⠙ ⠉⠑⠇⠇ ⠉⠥⠇⠞⠥⠗⠑ ⠎⠽⠎⠞⠑⠍⠎ ⠞⠕ ⠊⠝⠙⠥⠉⠑ ⠁⠝⠙ ⠍⠕⠝⠊

⠁⠝⠉⠑⠙ ⠉⠑⠇⠇ ⠉⠥⠇⠞⠥⠗⠑ ⠎⠽⠎⠞⠑⠍⠎ ⠞⠕ ⠊⠝⠙⠥⠉⠑ ⠁⠝⠙ ⠍⠕⠝⠊⠞⠕

⠉⠑⠙ ⠉⠑⠇⠇ ⠉⠥⠇⠞⠥⠗⠑ ⠎⠽⠎⠞⠑⠍⠎ ⠞⠕ ⠊⠝⠙⠥⠉⠑ ⠁⠝⠙ ⠍⠕⠝⠊⠞⠕⠗

⠙ ⠉⠑⠇⠇ ⠉⠥⠇⠞⠥⠗⠑ ⠎⠽⠎⠞⠑⠍⠎ ⠞⠕ ⠊⠝⠙⠥⠉⠑ ⠁⠝⠙ ⠍⠕⠝⠊⠞⠕⠗ ⠍⠑

⠉⠑⠇⠇ ⠉⠥⠇⠞⠥⠗⠑ ⠎⠽⠎⠞⠑⠍⠎ ⠞⠕ ⠊⠝⠙⠥⠉⠑ ⠁⠝⠙ ⠍⠕⠝⠊⠞⠕⠗ ⠍⠑⠉⠓

⠑⠇⠇ ⠉⠥⠇⠞⠥⠗⠑ ⠎⠽⠎⠞⠑⠍⠎ ⠞⠕ ⠊⠝⠙⠥⠉⠑ ⠁⠝⠙ ⠍⠕⠝⠊⠞⠕⠗ ⠍⠑⠉⠓⠁

⠇ ⠉⠥⠇⠞⠥⠗⠑ ⠎⠽⠎⠞⠑⠍⠎ ⠞⠕ ⠊⠝⠙⠥⠉⠑ ⠁⠝⠙ ⠍⠕⠝⠊⠞⠕⠗ ⠍⠑⠉⠓⠁⠝⠕

⠉⠥⠇⠞⠥⠗⠑ ⠎⠽⠎⠞⠑⠍⠎ ⠞⠕ ⠊⠝⠙⠥⠉⠑ ⠁⠝⠙ ⠍⠕⠝⠊⠞⠕⠗ ⠍⠑⠉⠓⠁⠝⠕⠃⠊

⠇⠞⠥⠗⠑ ⠎⠽⠎⠞⠑⠍⠎ ⠞⠕ ⠊⠝⠙⠥⠉⠑ ⠁⠝⠙ ⠍⠕⠝⠊⠞⠕⠗ ⠍⠑⠉⠓⠁⠝⠕⠃⠊⠕⠇

⠞⠥⠗⠑ ⠎⠽⠎⠞⠑⠍⠎ ⠞⠕ ⠊⠝⠙⠥⠉⠑ ⠁⠝⠙ ⠍⠕⠝⠊⠞⠕⠗ ⠍⠑⠉⠓⠁⠝⠕⠃⠊⠕⠇⠕

⠗⠑ ⠎⠽⠎⠞⠑⠍⠎ ⠞⠕ ⠊⠝⠙⠥⠉⠑ ⠁⠝⠙ ⠍⠕⠝⠊⠞⠕⠗ ⠍⠑⠉⠓⠁⠝⠕⠃⠊⠕⠇⠕⠛⠽

Biography

Nick Beijer was born on the 10th of April 1989 in Zaanstad, the Netherlands. During his youth, he developed a great interest in the wonderful world around him, and wanted to learn everything about the ongoing processes in nature. At the St. Michael College he majored in Biology, Physics and Mathematics, and spent many hours on the football pitch or behind the piano. In September 2007 Nick moved to Enschede to study Biomedical Engineering at the University of Twente. Here, he was able to gain more knowledge on the wonders of the human body, from an engineering perspective.

During his master he specialized in 'Molecular, Cellular and Tissue Engineering', and as part of this program he did an internship at Glasgow University, Scotland. He obtained his Master's degree in August 2013 after finishing a project on 'The molecular mechanisms of mechanotransduction caused by algorithm generated micro-topographies', at the department of Tissue Regeneration (MIRA Institute, University of Twente).

Subsequently, in September 2013, he started as a PhD student in the same group under supervision of Professor Jan de Boer on the STELLAR project aiming for kidney regeneration solutions. Along the way, the group moved from the University of Twente to Maastricht University, where the department of Tissue Regeneration became the MERLN Institute for Technology-Inspired Regenerative Medicine, and deBoer's lab became department of Cell Biology-Inspired Tissue Engineering (cBITE). During his 4.5 years at cBITE, Nick was highly involved in many projects and collaborations which focused on the underlying mechanisms of mechanotransduction in cell-material interactions. In this context, he worked on the development of multiple topographically enhanced cell culture systems to induce and monitor mechanobiology.